

SECOND ORDER NUMERICAL METHODS FOR NAVIER-STOKES AND  
DARCY-BRINKMAN EQUATIONS

A THESIS SUBMITTED TO  
THE GRADUATE SCHOOL OF NATURAL AND APPLIED SCIENCES  
OF  
MIDDLE EAST TECHNICAL UNIVERSITY

BY

MEDİNE DEMİR

IN PARTIAL FULFILLMENT OF THE REQUIREMENTS  
FOR  
THE DEGREE OF DOCTOR OF PHILOSOPHY  
IN  
MATHEMATICS

JUNE 2022



Approval of the thesis:

**SECOND ORDER NUMERICAL METHODS FOR NAVIER-STOKES AND  
DARCY-BRINKMAN EQUATIONS**

submitted by **MEDİNE DEMİR** in partial fulfillment of the requirements for the degree of **Doctor of Philosophy in Mathematics Department, Middle East Technical University** by,

Prof. Dr. Halil KALIPÇILAR  
Dean, Graduate School of **Natural and Applied Sciences** \_\_\_\_\_

Prof. Dr. Yıldırım OZAN  
Head of Department, **Mathematics** \_\_\_\_\_

Prof. Dr. Songül KAYA MERDAN  
Supervisor, **Mathematics, METU** \_\_\_\_\_

Assoc. Prof. Dr. Aytekin Bayram ÇIBİK  
Co-supervisor, **Mathematics Department, Gazi University** \_\_\_\_\_

**Examining Committee Members:**

Prof. Dr. Canan BOZKAYA  
Mathematics Department, METU \_\_\_\_\_

Prof. Dr. Songül KAYA MERDAN  
Mathematics Department, METU \_\_\_\_\_

Prof. Dr. Ömür UĞUR  
Institute of Applied Mathematics, METU \_\_\_\_\_

Assoc. Prof. Dr. Fikriye Nuray YILMAZ  
Mathematics Department, Gazi University \_\_\_\_\_

Assoc. Prof. Dr. Mustafa AĞGÜL  
Mathematics Department, Hacettepe University \_\_\_\_\_

Date:

**I hereby declare that all information in this document has been obtained and presented in accordance with academic rules and ethical conduct. I also declare that, as required by these rules and conduct, I have fully cited and referenced all material and results that are not original to this work.**

Name, Surname: Medine Demir

Signature :



## ABSTRACT

### SECOND ORDER NUMERICAL METHODS FOR NAVIER-STOKES AND DARCY-BRINKMAN EQUATIONS

Demir, Medine  
Ph.D., Department of Mathematics  
Supervisor: Prof. Dr. Songül KAYA MERDAN  
Co-Supervisor: Assoc. Prof. Dr. Aytekin Bayram ÇIBIK

June 2022, 145 pages

In this thesis, second-order, efficient and reliable numerical stabilization methods are considered for approximating solutions to the incompressible, viscous fluid flow driven by the Navier-Stokes equations and for the Darcy-Brinkman equations driven by double-diffusive convection. The standard Galerkin finite element method remains insufficient for accurately solving these complex nonlinear equations that creates some problems such as numerical instabilities and unphysical oscillations in the solution. A good numerical algorithm should resolve all the scales in the solution to avoid these problems which requires too much computational effort. Thus, developing proper and efficient numerical algorithm that exhibits correct physical behaviour of the flow and accurately approximates solutions over a finite time interval remains a great challenge in computational fluid dynamics.

First, this thesis proposes a numerical scheme which tests and analyzes a subgrid artificial viscosity method to model the incompressible Navier-Stokes equations along a linearly extrapolated BDF2 time discretization method. The method considers the viscous term as a combination of the vorticity and the grad-div stabilization term. The method introduces global stabilization by adding a term, then antidiffuses through the

extra mixed variables. A detailed analysis of conservation laws, including both energy and helicity balance of the method is presented. It is shown that the approximate solutions of the method are unconditionally stable and optimally convergent. Several numerical tests are presented for validating the support of the derived theoretical results.

Second, this thesis considers the backward Euler based linear time filtering method for the developed energy-momentum-angular momentum conserving formulation of the time dependent, incompressible Navier-Stokes equations in the case of weakly enforced divergence constraint. The method adds time filtering as a post-processing step to the energy-momentum-angular momentum conserving formulation to enhance the accuracy and to improve the approximate solutions. It is shown that in comparison with the backward-Euler based energy-momentum-angular momentum conserving formulation without any filter, the proposed method not only leads to a 2-step, unconditionally stable and second order accurate method but also increases numerical accuracy of solutions. Numerical studies verify the theoretical findings and demonstrate preeminence of the proposed method over the unfiltered case.

Third, this thesis studies an efficient, accurate, effective and unconditionally stable time stepping scheme for the Darcy-Brinkman equations in double-diffusive convection. The stabilization within the proposed method uses the idea of stabilizing the curvature for velocity, temperature and concentration equations. Accuracy in time is proven and the convergence results for the fully discrete solution of problem variables is given. Several numerical examples including a convergence study are provided that support the derived theoretical results and demonstrate the efficiency and the accuracy of the method.

**Keywords:** Subgrid artificial viscosity model, Navier-Stokes equations, linearly extrapolated BDF2, energy-momentum-angular momentum conserving formulation, time filter, Darcy-Brinkman equations, curvature stabilization, finite element method.

## ÖZ

### NAVIER-STOKES VE DARCY-BRINKMAN DENKLEMLERİ İÇİN İKİNCİ DERECEDEDEN SAYISAL YÖNTEMLER

Demir, Medine  
Doktora, Matematik Bölümü  
Tez Yöneticisi: Prof. Dr. Songül KAYA MERDAN  
Ortak Tez Yöneticisi: Doç. Dr. Aytekin Bayram ÇIBIK

Haziran 2022 , 145 sayfa

Bu tezde, Navier-Stokes denklemleri tarafından yönlendirilen sıkıştırılmaz, viskoz akışkan akışına ve çift-yayımlı taşınım tarafından yönlendirilen Darcy-Brinkman denklemlerine yaklaşık çözümler bulmak için ikinci mertebeden, verimli ve güvenilir sayısal stabilizasyon yöntemleri ele alınmıştır. Standart Galerkin sonlu elemanlar yöntemi, çözümde sayısal kararsızlıklar ve fiziksel olmayan salınımlar gibi bazı problemler yarattığı için bu karmaşık doğrusal olmayan denklemleri doğru bir şekilde çözmek için yetersiz kalmaktadır. İyi bir sayısal algoritma, çok fazla hesaplama çabası gerektiren bu problemlerden kaçınmak için çözümdeki tüm ölçekleri çözmelidir. Bu nedenle, akışın doğru fiziksel davranışını sergileyen ve sonlu bir zaman aralığında çözümlere doğru şekilde yaklaşan uygun ve verimli sayısal algoritma geliştirmek, hesaplamalı akışkanlar dinamiğinde büyük bir zorluk olarak devam etmektedir.

İlk olarak, bu tez sıkıştırılmaz Navier-Stokes denklemlerini modellemek için bir alt ızgara yapay viskozite yöntemini doğrusal ekstrapolasyonlu BDF2 zaman ayrıklaştırması ile birlikte kullanarak sayısal bir şema önerir, test eder ve analizini yapar. Yöntem, viskoz terimini, girdap ve grad-div stabilizasyon terimlerinin birleşimi ola-

arak ele alır. Bu alt ızgara yapay viskozite yöntemi, bir terim ekleyerek global stabilizasyonu tanıtır, ardından ekstra karışık değişkenler aracılığıyla yayılmayı önler. Yöntemin hem enerji hem de sarmallık dengesi dahil olmak üzere koruma yasalarının ayrıntılı analizini gösterilir. Ayrıca yöntemin ürettiği yaklaşık çözümlerin koşulsuz, kararlı ve optimal yakınsak olduğu da gösterilir. Elde edilen teorik sonuçları desteklemek ve doğrulamak için çeşitli sayısal testler sunulmuştur.

İkinci olarak, bu tez zayıf zorlanmış divergens kısıtlaması durumunda, sıkıştırılmaz, zamana bağlı Navier-Stokes denklemlerinin enerji-momentum-açısal momentum koruyucu (EMAC) formülasyonu geliştirilen model için geri-Euler tabanlı doğrusal zaman filtreleme yöntemini ele alır. Yöntem ile bu formülasyona doğruluğu artırmak ve yaklaşık çözümleri geliştirmek için bir işlem sonrası adım olarak zaman filtreleme ekler. Geri-Euler tabanlı EMAC formülasyonu ile herhangi bir filtre içermeyen formülasyon karşılaştırmalı olarak gösterilir, önerilen yöntem yalnızca 2 adımlı, koşulsuz kararlı ve ikinci dereceden doğru yöntem değil, aynı zamanda çözümlerin sayısal doğruluğunu da arttıran bir yöntemdir. Sayısal çalışmalar teorik bulguları doğrular ve önerilen yöntemin filtrelenmemiş duruma göre üstünlüğünü gösterir.

Üçüncü olarak, bu tez verimli, doğru, etkili ve koşulsuz olarak kararlı bir zaman adımı şemasını çift yayımlı taşınmada Darcy-Brinkman denklemleri için çalışır. Önerilen yöntemdeki stabilizasyon hız, sıcaklık ve konsantrasyon denklemleri için eğriliği stabilize etme fikrini kullanır. Zamandaki doğruluğu kanıtlanmıştır ve problem değişkenlerinin tamamen ayrık çözümleri için yakınsama sonuçları verilmiştir. Elde edilen teorik sonuçları destekleyen ve yöntemin etkinliği ve doğruluğunu ortaya koyan, yakınsama çalışması dahil olmak üzere çeşitli sayısal örnekler sunulmuştur.

Anahtar Kelimeler: Alt ızgara yapay viskozite modeli, Navier-Stokes denklemleri, lineer ekstrapolasyonlu BDF2, enerji-itme-açısal itme formülasyonu, zaman filtresi, Darcy-Brinkman denklemleri, eğrilik stabilizasyonu, sonlu eleman yöntemi.

To my beloved family

## ACKNOWLEDGMENTS

First and foremost, I would like to express my immense gratitude to my supervisor Prof. Dr. Songül Kaya Merdan for her precious guidance, encouragement and continuous support and endless patience during my thesis. It was a great honor to work with her and her valuable ideas and suggestions will always be a guide in my academic world.

I am also deeply grateful to my co-supervisor Assoc. Prof. Dr. Aytekin Çıbık for his constant help and support for the coding part of this work. A special thanks goes to Prof. Dr. Canan Bozkaya for her valuable comments and kindly approach during my thesis and Ph. D courses. I would also like to thank my defense committee members Prof. Dr. Ömür Uğur, Assoc. Dr. Fikriye Nuray Yılmaz, and Assoc. Dr. Mustafa Ağgöl for their constitutive criticisms.

I would like to thank to my colleagues in the math department especially Fatma Güler Eroğlu and Sinem Arslan for their support and help. I am also deeply indebted to my friend Merve Karataş for her kind friendship and for always supporting me throughout my life.

Last but not least, my special and sincerest thanks belong to my mother Ayten Demir and my father Aslan Demir for their endless love and motivation through all my life. I would not have achieved any success in my life without their support and belief in me. I also wish to express heartfelt thanks to my lovely sisters Kezban Demir and Merve Demir and to my dear brothers Bülent Demir and Kadir Demir for their continuous support and encouragement through all my life.

## TABLE OF CONTENTS

ABSTRACT . . . . .	v
ÖZ . . . . .	vii
ACKNOWLEDGMENTS . . . . .	x
TABLE OF CONTENTS . . . . .	xi
LIST OF TABLES . . . . .	xiv
LIST OF FIGURES . . . . .	xv
CHAPTERS	
1 INTRODUCTION . . . . .	1
2 MATHEMATICAL PRELIMINARIES AND NOTATIONS . . . . .	11
3 AN ANALYSIS OF A LINEARLY EXTRAPOLATED BDF2 SUBGRID ARTIFICIAL VISCOSITY METHOD FOR INCOMPRESSIBLE FLOWS . . . . .	23
3.1 Notations and Mathematical Preliminaries . . . . .	27
3.2 Numerical Scheme . . . . .	32
3.3 Conservation Laws for BDF2LE Based SAV Solution . . . . .	33
3.4 Numerical Analysis . . . . .	37
3.5 Numerical Experiments . . . . .	45
3.5.1 Convergence Rates . . . . .	46
3.5.2 Flow Around a Cylinder . . . . .	47

3.5.3	Flow Between Two Offset Circles . . . . .	50
3.5.4	Poiseuille's Flow . . . . .	53
4	TIME FILTERED SECOND ORDER BACKWARD EULER METHOD FOR EMAC FORMULATION OF NAVIER-STOKES EQUATIONS . . . . .	57
4.1	Notations and Mathematical Preliminaries . . . . .	60
4.2	Numerical Scheme . . . . .	65
4.3	Conservation Laws . . . . .	66
4.4	Numerical Analysis . . . . .	69
4.5	Numerical Experiments . . . . .	76
4.5.1	Convergence Rates . . . . .	77
4.5.2	Gresho Problem . . . . .	78
4.5.3	Flow Around a Cylinder . . . . .	80
4.5.4	Flow Over a Flat Plate . . . . .	84
5	A FAMILY OF SECOND ORDER TIME STEPPING METHODS FOR THE DARCY-BRINKMAN EQUATIONS . . . . .	87
5.1	Mathematical Preliminaries . . . . .	90
5.2	Numerical Scheme . . . . .	93
5.3	Numerical Analysis . . . . .	95
5.4	Numerical Experiments . . . . .	115
5.4.1	Numerical convergence study . . . . .	116
5.4.2	Buoyancy Driven Cavity Test . . . . .	118
5.4.2.1	The effect of buoyancy ratio $N$ . . . . .	119
5.4.2.2	The effect of Lewis number $Le$ . . . . .	120
5.4.2.3	The effect of Rayleigh number $Ra$ . . . . .	121



5.4.2.4	Thermal and Mass Distributions in Buoyancy Driven Cavity . . . . .	122
6	CONCLUSION . . . . .	125
	REFERENCES . . . . .	127
	CURRICULUM VITAE . . . . .	145

## LIST OF TABLES

### TABLES

Table 3.1 Errors and convergence rates for the Scheme (3.2.1)-(3.2.3). . . . .	46
Table 3.2 Comparison of maximum drag and lift coefficients and the times at which they occur. . . . .	49
Table 4.1 Spatial errors and rates . . . . .	78
Table 4.2 Temporal errors and rates . . . . .	78
Table 4.3 Comparison of maximum drag and lift coefficients and the times at which they occur. . . . .	83
Table 4.4 The average drag coefficients and the Strouhal number. . . . .	85
Table 5.1 Spatial errors and rates of convergence for $\epsilon = \epsilon_1 = \epsilon_2 = 0$ . . . . .	117
Table 5.2 Spatial errors and rates of convergence for $\epsilon = \epsilon_1 = \epsilon_2 = 1$ . . . . .	117
Table 5.3 Temporal errors and rates of convergence for $\epsilon = \epsilon_1 = \epsilon_2 = 0$ . . . . .	117
Table 5.4 Temporal errors and rates of convergence for $\epsilon = \epsilon_1 = \epsilon_2 = 1$ . . . . .	118
Table 5.5 Comparison of average Nusselt numbers on the vertical boundary of the cavity at $x = 0$ (hot wall) for $Pr = 1, Le = 2, N = 0.8$ with mesh size used in computation for varying Rayleigh Numbers . . . . .	123
Table 5.6 Comparison of average Sherwood numbers on the vertical boundary of the cavity at $x = 0$ (hot wall) for $Pr = 1, Le = 2, N = 0.8$ with mesh size used in computation for varying Rayleigh Numbers . . . . .	123

## LIST OF FIGURES

### FIGURES

Figure 3.1	Domain $\Omega$ of the test problem . . . . .	47
Figure 3.2	The velocity contours of the scheme (3.2.1)-(3.2.3) at $t = 2, 4, 5, 6, 7, 8$ (from up to down). . . . .	48
Figure 3.3	Evolution of maximum value of drag values, lift values and pres- sure differences obtained when using the scheme (3.2.1)-(3.2.3) with $\Delta t = 0.01$ . . . . .	50
Figure 3.4	The domain of the test problem . . . . .	50
Figure 3.5	Velocity contours for $Re = 200$ . . . . .	51
Figure 3.6	Time evolutions of energy for $Re = 200, 800, 1200$ from left to right. . . . .	52
Figure 3.7	Time evolutions of enstrophy for $Re = 200, 800, 1200$ from left to right. . . . .	52
Figure 3.8	Velocity field for CN-SAV. . . . .	53
Figure 3.9	Velocity field for BDF2LE-SAV. . . . .	54
Figure 3.10	Time evolutions of relative velocity error and energy . . . . .	55
Figure 4.1	Speed contours of true solution of the Gresho prolem at all times.	79
Figure 4.2	Plots of time versus $L^2$ error, energy, momentum and angular momentum. . . . .	80

Figure 4.3	Numerical and physical dissipation versus time for our scheme . . .	80
Figure 4.4	Domain $\Omega$ of the test problem . . . . .	81
Figure 4.5	The velocity of the BE-EMAC scheme at $t = 2, 4, 6, 8$ (from up to down). . . . .	82
Figure 4.6	The velocity of the EMAC-FILTERED scheme at $t = 2, 4, 6, 8$ (from up to down). . . . .	82
Figure 4.7	Domain $\Omega$ of the test problem . . . . .	84
Figure 5.1	The physical domain with its boundary conditions . . . . .	119
Figure 5.2	Velocity streamlines, Temperature contours and Concentration contours(from left to right) for $Pr = 1, Ra = 10^5, Le = 2$ with $N =$ $1.3$ (up) and $N = 0.8$ (down) . . . . .	120
Figure 5.3	Velocity streamlines, Temperature contours and Concentration contours (from left to right) for $Pr = 1, Ra = 10^5, N = 1$ with $Le =$ $0.2$ (up) and $Le = 1.0$ (down) . . . . .	121
Figure 5.4	Velocity streamlines, Temperature contours and Concentration contours (from left to right) for $Pr = 1, Le = 2, N = 0.8$ with $Ra =$ $10^4$ (up), $Ra = 10^5$ (middle) and $Ra = 10^6$ (down) . . . . .	122

## CHAPTER 1

### INTRODUCTION

Mathematical modeling is the process of expressing a real-life problem by using mathematical concepts and language, particularly used in natural sciences such as physics, biology, earth science, chemistry, and engineering disciplines such as computer science and electrical engineering and also in social science like sociology, economics, and psychology. Mathematical models can take a variety of forms such as in dynamical systems, statistical models, differential equations, or game-theoretic models. Numerous models in natural and applied sciences describe the interaction of several distinct physical fields including structural deformation, fluid flow, electric field, temperature, pore-pressure, etc. In this thesis, we consider the mathematical models that include fluid flows. The mathematical formulation of these fluid flow problems consists of systems of coupled partial differential equations subject to suitable boundary conditions. Due to their complex structures, it is generally impossible or extremely difficult to obtain analytical or closed-form solutions for partial differential equations, except for some basic problems in simple geometries. Also, finding solutions from some laboratory experiments requires a very realistic experimental setup which is not easily applicable and results in scaling problems, measurement difficulties, and operating costs. Hence, numerical methods are the most attractive methods for solving these complex nonlinear equations thanks to the rapid increase in computer speed day by day.

Computational fluid dynamics (CFD) is the field of numerically solving these problems using computational power, applied to a wide range of fields such as aerodynamics, hypersonics, weather simulation, natural science, and environmental engineering, industrial system design and analysis, biological engineering, fluid flows, and

heat transfer, engine and combustion analysis, and visual effects for film and games. There are two numerical approaches in CFD, namely Eulerian and Lagrangian. The basic idea in the Eulerian approach is to discretize the computational space with a finite set of points called the grid (or mesh) and compute the approximate solution at these grid points [34]. On the other hand, the Lagrangian approach discretizes the computational region by a series of particles moving at the local flow rate and calculates approximate solutions at each particle's position at each separate time [34]. Some of Lagrangian techniques include the discrete element method [40], immersed particle method [137], smoothed particle hydrodynamics [85] and finite volume particle method [110]. In addition to these, there are some other numerical methods to solve fluid flow problems such as the Boundary Element Method (BEM) and Dual Reciprocity Boundary Element method (DRBEM) which also gives very promising results. The Eulerian approach to compute approximate solutions to fluid flow problems which can be accomplished using several different ways includes the Finite Difference Method (FDM), Finite Volume Method (FVM) and Finite Element Method (FEM). The main differences among these numerical methods are the type of approach to the variables, discretization of the problem domain and the computational cost of the technique.

The finite difference method approximates the unknown solutions in the governing differential equation by using the finite differences for the derivatives of the unknowns and inserting the given boundary conditions. FDM methods transform the governing nonlinear differential equation into a system of linear equations which can be solved by matrix algebra techniques. FDM methods are one of the commonly used numerical methods due to their simplicity, efficiency, and low computational cost. The major disadvantage is the difficulty of discretizing curved boundaries and adding boundary conditions involving derivatives.

The basic idea of the finite volume method is to divide the domain into a number of control volumes (elements) whose centroid consists of the variable of interest and to integrate the differential forms of the governing equation over each control volume which results in the conservation equations for the variable inside the control volume. The primary advantage of this method is that it is conservative, i.e. its solution satisfies the conservation laws for the quantities like mass, momentum, energy

etc. Another advantage is that, unlike finite difference methods, it is easily applied for irregular or complex domains. Also, it produces more accurate and stable solutions, especially for the problems with interfaces and strong shocks. Moreover, it is preferable for calculating discontinuous solutions of compressible flows and partial differential equations containing discontinuous coefficients since the local continuity property does not need to be retained. However, obtaining higher-order accurate solutions is difficult which is the main drawback of this method.

The finite element method, which is used in this thesis, is the most commonly used and popular numerical method in engineering designed in the 1980s to fix the discretization problem in complex geometry and facilitates the addition of boundary conditions. The main idea is to discretize the domain into small portions called as elements and interpolating the solution by using polynomial interpolation functions over this finite domain which are then combined into a larger system of equations that models the entire problem. Then, a solution is approximated by minimizing an associated error function [100, 106, 122]. It is commonly used in computer and industrial applications [20, 48, 80], biomedical, thermal and fluid flows, structural analysis, solid mechanics, thermal and electrical analysis, mechanical engineering disciplines like aeronautical (design of aircraft) and biomechanical etc.

The accurate and fast approximation to the solutions to fluid flow problems is vital for many applications in engineering, power generation, chemical manufacturing, polymer processing, petroleum exploration, medical research, meteorology, astrophysics, etc. In this thesis, we consider two types of fluid flow problems, namely the incompressible, viscous fluid flow and the fluid flow driven by double-diffusive convection. The motion of incompressible, viscous fluid flow is governed by Navier Stokes equations (NSE) which are given as follows:

$$\begin{aligned}
\mathbf{u}_t - \nu \Delta \mathbf{u} + \mathbf{u} \cdot \nabla \mathbf{u} + \nabla p &= \mathbf{f} && \text{in } \Omega \times (0, T), \\
\nabla \cdot \mathbf{u} &= 0 && \text{in } \Omega \times (0, T], \\
\mathbf{u} &= \mathbf{0} && \text{on } \partial\Omega \times [0, T], \\
\mathbf{u}(\mathbf{x}, 0) &= \mathbf{u}_0(\mathbf{x}) && \text{for } \mathbf{x} \in \Omega, \\
\int_{\Omega} p d\mathbf{x} &= \mathbf{0} && \text{in } (0, T].
\end{aligned} \tag{1.0.1}$$

Here,  $\Omega$  denotes a bounded and regular flow domain in  $\mathbb{R}^d$  ( $d = 2$  or  $3$ ),  $\mathbf{u}(x, t)$  represents the velocity,  $p(x, t)$  the zero-mean pressure,  $\mathbf{f}(x, t)$  an external force,  $\nu$

the kinematic viscosity and  $\mathbf{u}_0$  is a weakly divergence-free initial condition. The first equation in (1.0.1) describes the conservation of momentum in which  $\mathbf{u}_t$  is the rate of change in velocity, the term  $\mathbf{u} \cdot (\nabla \cdot \mathbf{u})$  is the convective term that governs the inertial effects, the term  $-\nu \Delta \mathbf{u}$  is the diffusive term describing the process of the relative motion of different components in a mixture and the term  $\nabla p$  is the pressure describes the forces acting on the surface of each fluid volume. The control parameter in (1.0.1) is Reynolds number  $Re$  and is given as

$$Re = \frac{UL}{\nu}$$

where  $L$  and  $U$  are the characteristic length and velocity scales of the flow respectively and  $\nu$  are the kinematic viscosity of the flow. The second equation in (1.0.1) is the incompressibility constraint describing the conservation of mass. Furthermore, the last equation in (1.0.1) is the usual normalization condition on pressure meaning that the pressure has zero mean value. The reader is referred to [8] for the derivation of these equations.

Since NSE is the broadly applied set of mathematical models and are based on the conservation of mass and the conservation of momentum laws. They describe the physics of many important phenomena of scientific and engineering interest such as weather forecasts [15, 136], ocean currents, flow in pipes [32, 33, 125] and channels, blood flow [25, 90, 163], pollution analysis [39, 107], the design of aircraft and cars. These equations are extensions of famous Euler's equations in the 18th century that describe the flow of incompressible and frictionless fluids, i.e.  $\nu = 0$ . In 1822, Claude-Louis Navier introduced the notion of a Newton viscous term for a more realistic and more difficult problem of viscous fluids [22]. Later, in 1845, George Gabriel Stokes enhanced the NSE analysis with a different definition of internal friction in the fluids, making the equation more convincing [47].

The NSE is so complex equations that, despite great efforts of more than a century ago, it still seems far away to exactly predict their solutions and understand their consequences. There are several difficulties in solving NSE. Firstly, the reduction of the physical problems defined in continuous space and time to a large system of equations in discrete and finite space and time naturally creates some undesirable effects such as numerical instability and unphysical oscillations in the solution. As a result,



it causes loss of important physically conserved quantities like energy, momentum, angular momentum, enstrophy, helicity, etc. Moreover, the NSE is a set of coupled nonlinear equations that can not be solved analytically, except for some very basic flows and boundary conditions.

The mathematical theory starts with the Leray's paper [62] which describes NSE's solutions using weak solutions. Within that study, he proved the existence and uniqueness of the weak solutions for NSE for all cases in two dimensions but the existence and uniqueness of the solutions in three dimensions is still unknown and is a one million dollar Clay prize problem [21]. Also, it is well known that at high  $Re$  numbers, the convective term becomes dominant which leads to complex, turbulent fluid flow requiring high computer capacity in simulations. The application of a direct numerical simulation (DNS) of equation (1.0.1) such as by the Galerkin finite element method both in time and space remains incapable to cope with these difficulties and simulating turbulent flows determined by the Kolmogorov theory which reported that a resolved DNS requires  $O(Re^{9/4})$  mesh points [74] which exceeds the limits of computing power available today. Furthermore, the DNS of the NSE creates more problems such as truncation errors, boundary condition problems, convergence, accuracy, and stability problems and violation of many important conservation laws including energy, momentum, angular momentum and others. Thus, stabilization methods are required to obtain high-fidelity solutions. Hence, designing a cost-effective, accurate and reliable numerical algorithm with high-fidelity solutions remains a great challenge in the computational fluid dynamics community.

Double-diffusive convection models describe convection phenomena in fluid driven by the combination of different density temperature and concentration gradients in the porous medium. A detailed derivation of the model can be found in [29]. The physical model includes the momentum forced by the combined heat and mass transfer which causes natural convection. Double diffusive convection plays a significant role in many scientific, engineering and industrial applications such as, metallurgy, oceanography, geology, biology, chemical processes, the heating, and cooling processes in solid oxide fuel cells, petroleum drilling, contaminant transport in groundwater, etc [66, 69, 127, 135]. Moreover, the model incorporates the velocity fields and pressure fields as well as contains the temperature and concentration fields, which are

often used in the industry [7, 19], astrophysics [49], the oceanography [43, 121], and so on. A common example describing double-diffusive convection is certain motions in the ocean. The flow of saltwater in the ocean occurs due to the changes in temperature and salt concentration gradients and diffusivity. The temperature dissipates faster than the concentration (salinity). Double-diffusive convection in oceanography is a vertical motion and there are two modes as salt fingers and diffusive. These salt fingers of rising water occur when warm, saltwater lies over higher density, cold freshwater. As the diffusion of heat is faster than salt, the water loses its heat faster than its salinity. Since the water becomes cooler but remains salty, it becomes denser. This causes the downward motion of the salt fingers. On the other hand, diffusive convection occurs when cold and freshwater lies over salty and warmer water.

Under the assumption of Boussinesq approximation that ignores density variations in fluid except in the buoyancy term including the thermal expansion coefficient [51], the governing equations of double-diffusive convection phenomena in a confined porous enclosure are given by the Darcy-Brinkman system (see [16]),

$$\begin{aligned}
\mathbf{u}_t - \nu \Delta \mathbf{u} + (\mathbf{u} \cdot \nabla) \mathbf{u} + Da^{-1} \mathbf{u} + \nabla p &= (\beta_T T + \beta_S S) \mathbf{g} \quad \text{in } (0, t] \times \Omega, \\
\nabla \cdot \mathbf{u} &= 0 \quad \text{in } (0, t] \times \Omega, \\
\mathbf{u} &= \mathbf{0} \quad \text{on } (0, t] \times \partial\Omega, \\
T_t - \gamma \Delta T + \mathbf{u} \cdot \nabla T &= 0 \quad \text{in } (0, t] \times \partial\Omega, \\
S_t - D_c \Delta S + \mathbf{u} \cdot \nabla S &= 0 \quad \text{in } (0, t] \times \partial\Omega, \\
T, S &= 0 \quad \text{on } \Gamma_D, \\
\frac{\partial T}{\partial n} &= 0, \quad \frac{\partial S}{\partial n} = 0 \quad \text{on } \Gamma_N, \\
\mathbf{u}(0, \mathbf{x}) &= \mathbf{u}_0, \quad T(0, \mathbf{x}) = T_0, \quad S(0, \mathbf{x}) = S_0 \quad \text{in } \Omega.
\end{aligned} \tag{1.0.2}$$

Here  $\mathbf{u}$  is the fluid velocity,  $\mathbf{u}_0$ , the initial velocity,  $p$  the pressure,  $T$  the temperature,  $T_0$ , the initial temperature,  $S$  the concentration,  $S_0$ , the initial concentration. We also have the kinematic viscosity  $\nu > 0$ , the Darcy number  $Da$ , the thermal diffusivity  $\gamma > 0$ , the mass diffusivity  $D_c > 0$ , the gravitational acceleration vector  $\mathbf{g}$  and the thermal and solutal expansion coefficients are  $\beta_T, \beta_S$ , respectively. The dimensionless parameters are the buoyancy ratio  $N = \frac{\beta_S \Delta S}{\beta_T \Delta T}$ , the Schmidt number  $Sc = \frac{\nu}{D_c}$ , Prandtl number  $Pr = \frac{\nu}{\gamma}$ , the Darcy number  $Da = \frac{K}{H^2}$ , the Lewis number  $Le = \frac{Sc}{Pr}$

and the thermal Rayleigh number  $Ra = \frac{\mathbf{g}\beta_T\Delta TH^3}{\nu\gamma}$ .  $\Gamma_D$  be a regular open subset and  $\Gamma_D = \partial\Omega \setminus \Gamma_N$ .  $H$  is the cavity height,  $K$  is the permeability,  $\Delta T$  and  $\Delta S$  are the temperature and concentration differences, respectively.

Several works are studying the physical mechanism of double-diffusive convection, e.g., [9, 86]. Darcy-Brinkman equations (1.0.2) are difficult to solve due to both its physical mechanism and the structure of its modeling equation. First of all, since Darcy-Brinkman equations (1.0.2) includes the NSE, it inherits the same difficulties as the NSE. After that, this model has different boundary layers formed due to the coupling between fluid flow, and the heat and mass transfer equations which makes the system very difficult to solve analytically. Thus, many researchers tried to solve Darcy-Brinkman equations numerically by using different types of numerical techniques such as the finite volume method (FVM) [64, 68, 82] and the boundary element method (BEM) [59, 60] as well as the FEM in different flow configurations in a cavity [72] and a porous medium [13, 67, 88]. Besides the coupling of multiple physical fields, the system expresses heat transfer with Rayleigh number ( $Ra$ ) which is defined as

$$Ra = \frac{\mathbf{g}\beta_T(T_{\text{bottom}} - T_{\text{top}})L^3}{\nu\gamma}$$

where  $\mathbf{g}$  denotes gravitational acceleration vector,  $\beta_T$  denotes thermal expansion coefficient,  $L$  denotes the vertical length,  $\nu$  denotes kinematic viscosity,  $\gamma$  denotes thermal diffusivity,  $T_{\text{bottom}}$  and  $T_{\text{top}}$  denote the temperature in the bottom and in the top, respectively. The size of  $Ra$  determines whether the flow is laminar or turbulent. High  $Ra$  numbers lead to numerical instabilities due to the dominance of the convective term. As a result, the flow behaves turbulent. All these obstacles have prompted scientists to seek efficient and reliable stabilization methods for the standard finite element discretization to get physically correct solutions of the Darcy-Brinkman equations.

This thesis aims to develop second-order, efficient and reliable numerical algorithms for two-fluid flow problems: the incompressible, Newtonian fluid flow driven by the NSE and Darcy-Brinkman equations with double-diffusive convection. The first goal is to extend the mathematical support of a subgrid artificial viscosity (SAV) method of [73] to simulate the incompressible NSE to better perform a linearly extrapolated BDF2 (BDF2LE) time discretization. The method considers the viscous term as a

combination of the vorticity and the grad-div stabilization term. SAV method introduces global stabilization by adding a term, then anti-diffuses through the extra mixed variables. As a result, a successful stabilization method is obtained with optimal accuracy in time without choosing computationally inefficient time steps in case of small viscosity. The second goal is to investigate the effect of the backward Euler-based linear time filtering method of [140] for the developed energy-momentum-angular momentum conserving (EMAC) formulation of the time-dependent incompressible Navier-Stokes equations in the case of weakly enforced divergence constraint. The proposed method yields a two-step time filtered Backward Euler method which is efficient, optimally accurate in both space and time, A-stable and easy to adapt into any existing code. The third goal is to study the idea of curvature stabilization of [94] for a family of second-order time-stepping methods for the Darcy-Brinkman system. The main idea of the method is to incorporate linearizations and stabilization terms such that the discrete curvature solution in velocity, temperature, concentration, and pressure are proportional to this combination. This leads to sufficient stabilization along with optimal accuracy in time.

**Chapter 2** presents some necessary mathematical preliminaries and notations used in the analysis of the NSE and the double-diffusive Darcy-Brinkman system.

**Chapter 3** provides the numerical analysis of the subgrid artificial viscosity (SAV) method for the incompressible NSE equipped with BDF2LE temporal discretization. A detailed analysis of conservation laws, including both the energy and helicity balance of the method, is presented. A complete numerical analysis of SAV method along with the proofs of unconditional stability and convergence is provided. The derived theoretical results are validated with some numerical experiments.

**Chapter 4** focuses on the backward Euler based linear time filtering method for the EMAC formulation of the time-dependent incompressible NSE in the case of weakly enforced divergence constraint. The time filtering is added as a modular step to the standard backward Euler code leading to a two-step method that can be easily implemented into any existing legacy code. Conservation properties are studied and a complete stability and convergence analysis of the method is presented. Several numerical experiments are provided that both verify the theoretical findings and demonstrate the

preeminence of the proposed method over the unfiltered case.

**Chapter 5** studies the numerical approximation of a family of second-order time-stepping methods for the Darcy-Brinkman system. The proposed algorithm is constructed by using the idea of stabilizing the curvature for velocity, temperature and concentration equations. The stability and convergence analysis of the method are provided. Several numerical examples are performed to support the derived theoretical results and demonstrate the efficiency and accuracy of the method.

**Chapter 6** is devoted to the conclusions of this dissertation and the discussion for possible future research directions.



## CHAPTER 2

### MATHEMATICAL PRELIMINARIES AND NOTATIONS

In this chapter, we present some mathematical preliminaries and notations frequently used throughout this thesis. Additionally,  $C$  stands for generic constants independent of all flow parameters and also from meshsize  $h$  and time-step size  $\Delta t$ .

Standard notations of [109] for function spaces with their definitions will be used throughout the thesis. We also introduce some important definitions and theorems from [122, 143].

Assume that  $\Omega$  in  $\mathbb{R}^d$ , ( $d = 2, 3$ ) is a convex polygonal or polyhedral domain with a boundary  $\partial\Omega$ . For a function  $g : \Omega \rightarrow \mathbb{R}^d$ , define the partial derivative of order  $|\alpha|$  by

$$D^\alpha g = \frac{\partial^{|\alpha|} g}{\partial x_1^{\alpha_1} \partial x_2^{\alpha_2} \dots \partial x_d^{\alpha_d}} \quad (2.0.1)$$

where  $\alpha = (\alpha_1, \alpha_2, \dots, \alpha_d)$  is a multi-index of non-negative integer numbers and its length is defined by  $|\alpha| = \alpha_1 + \alpha_2 + \dots + \alpha_d$ .

**Definition 2.0.1** *A measurable function  $f$  defined on  $\Omega$  is said to be essentially bounded if there exists a constant  $M$  such that*

$$|f(x)| \leq M, \quad \text{for almost everywhere (a.e.) on } \Omega .$$

*The essential supremum of  $\Omega$  is the greatest lower bound of such constants  $M$  and is denoted by*

$$\|f\|_{L^\infty} := \operatorname{ess\,sup}_{x \in \Omega} |f(x)|,$$

**Definition 2.0.2** Let  $g \in C(\Omega)$ .

- Then the support of  $g$  is defined as follows:

$$\text{supp}(g) = \overline{\{x \in \Omega : g(x) \neq 0\}}. \quad (2.0.2)$$

- $\mathbf{u}$  is said to have a compact support in  $\Omega$  if  $\text{supp}(g) \subset \Omega$  is compact in  $\mathbb{R}^d$ . This means that  $\mathbf{u}$  vanishes on the boundary  $\partial\Omega$ .
- $C_0^\infty(\Omega) := \{g \in C^\infty(\Omega) : g \text{ has a compact support in } \Omega\}$ .

**Definition 2.0.3 ( The Lebesgue Spaces )** The Lebesgue spaces are the class of all measurable functions whose  $p$ -th powers are integrable and are denoted by

$$L^p(\Omega) := \{g : g \text{ is also a measurable function and } \int_{\Omega} |g(x)|^p dx < \infty\} \quad (2.0.3)$$

for all  $1 \leq p \leq \infty$ .

$L^p(\Omega)$ -norm is defined by

$$\|g\|_{L^p} = \left( \int_{\Omega} |g(x)|^p dx \right)^{1/p}, \quad 1 \leq p < \infty \quad (2.0.4)$$

$$\|g\|_{L^\infty} = \text{ess sup}_{x \in \Omega} |g(x)|, \quad p = \infty. \quad (2.0.5)$$

The special case  $p = 2$  gives  $L^2(\Omega)$ , a Hilbert space equipped with the following inner product

$$(g, h) = \int_{\Omega} g(x)h(x)dx, \quad \|\mathbf{u}\| = \sqrt{(g, g)}.$$

The zero-mean subspace of  $L^2(\Omega)$  is defined by

$$L_0^2(\Omega) := \{g \in L^2(\Omega) : \int_{\Omega} g(x)dx = 0\}.$$

**Definition 2.0.4 ( The Sobolev Spaces )** Sobolev spaces are defined as

$$W^{k,p}(\Omega) := \{g \in L^p(\Omega) : D^\alpha g \in L^p(\Omega) \text{ for } |\alpha| \leq k\} \quad (2.0.6)$$

for any  $k \in \mathbb{N}, 1 \leq p \leq \infty$ .



The Sobolev spaces are Banach spaces with the following norms:

$$\|g\|_{W^{k,p}(\Omega)} = \left( \sum_{|\alpha| \leq k} \int_{\Omega} \|D^{\alpha} g\|_{L^p}^p \right)^{1/p}, \quad 1 \leq p \leq \infty \quad (2.0.7)$$

$$\|g\|_{W^{k,\infty}(\Omega)} = \sum_{|\alpha| \leq k} \operatorname{ess\,sup}_{x \in \Omega} |D^{\alpha} g|. \quad (2.0.8)$$

- For  $k = 0$ ,  $W^{0,p}(\Omega) = L^p(\Omega)$ .
- For  $p = 2$ ,  $W^{k,2}(\Omega) = H^k(\Omega)$  are Hilbert spaces equipped with the norm  $\|\cdot\|_k$  and the semi-norm  $|\cdot|_k$ .
- The most important Sobolev space used in this thesis is the closed subspace of  $H^1(\Omega)$ , defined by

$$H_0^1(\Omega) := \{v \in H^1(\Omega) : v = 0 \in \partial\Omega\}.$$

The dual space of  $H_0^1(\Omega)$  is denoted by  $H^{-1}$  with norm

$$\|f\|_{-1} = \sup_{v \in H_0^1(\Omega)} \frac{|(f, v)|}{\|\nabla v\|}.$$

**Definition 2.0.5** For any (scalar or vector valued) function  $v(x, t)$  defined on  $\Omega \times (0, T]$ , the following norms are used

$$\|v\|_{\infty, k} := \operatorname{ess\,sup}_{0 \leq t \leq T} \|v(\cdot, t)\|_k, \quad \|v\|_{p, k} = \left( \int_0^T \|v(\cdot, t)\|_p^k dx \right)^{1/p}$$

where  $T > 0$  is a given finite last time. Discrete norms are defined with the following notations

$$\|v\|_{\infty, k} := \operatorname{ess\,sup}_{0 \leq n \leq N} \|v^n\|_k, \quad \|v\|_{p, k} = \left( \Delta t \sum_{n=0}^N \|v^n\|_p^k dx \right)^{1/p}$$

where  $\Delta t$  is the time step such that  $t^n = n\Delta t$  with  $n = 0, 1, \dots, N$  and we denote  $v(t^n) = v^n$ .

**Lemma 2.0.1** If  $\frac{1}{p} + \frac{1}{q} = 1$ , then

$$1 \leq \frac{x}{p} + \frac{x^{1-q}}{q}$$

holds for all real  $x > 0$ .

**Proof.** Consider the function

$$f(x) = \frac{x}{p} + \frac{x^{1-q}}{q}$$

which satisfies

$$f(1) = \frac{1}{p} + \frac{1^{1-q}}{q} = \frac{1}{p} + \frac{1}{q} = 1.$$

The proof follows by showing that  $f$  takes its minimum value of 1 at  $x = 1$ . Taking the derivative of  $f$

$$\begin{aligned} f'(x) &= \frac{1}{p} + \frac{1 - qx^{-q}}{q} = \frac{q + p(1 - q)x^{-q}}{pq} \\ &= \frac{q + (p - pq)x^{-q}}{pq} = \frac{q + (p - (p + q))x^{-q}}{pq} \\ &= \frac{q - qx^{-q}}{pq} = \frac{1 - x^{-q}}{p}, \end{aligned}$$

it follows that the only critical point of  $f$  is  $x = 1$ . Then, as

$$f''(x) = \frac{qx^{-q-1}}{p} > 0$$

for all  $x > 0$ , the function  $f$  attains its minimum value of 1 at the critical point  $x = 1$ .  $\square$

**Lemma 2.0.2 (Young's Inequality)** For  $a, b \geq 0$ , the following inequality holds

$$ab \leq \frac{\varepsilon}{p}a^p + \frac{\varepsilon^{-\frac{q}{p}}}{q}b^q$$

for any  $\varepsilon > 0$ ,  $p, q \leq 1$  and  $\frac{1}{p} + \frac{1}{q} = 1$ .

**Proof.** The proof is trivial, if either of  $a = 0$  or  $b = 0$  holds. For the case  $a > 0$  and  $b > 0$ , use the inequality in Lemma 2.0.1 for  $x = \frac{a^{p-1}}{b} > 0$  to get,

$$\begin{aligned} 1 &\leq \frac{1}{p} \left( \frac{a^{p-1}}{b} \right) + \frac{1}{q} \left( \frac{a^{p-1} 1^{-q}}{b} \right) = \frac{a^{p-1}}{pb} + \frac{a^{p+q-pq-1}}{qb^{1-q}} \\ &= \frac{a^{p-1}}{pb} + \frac{b^{1-q}}{qa} = \frac{1}{ab} \left( \frac{a^p}{p} + \frac{b^q}{q} \right) \end{aligned} \quad (2.0.9)$$

Multiplying both sides of (2.0.9) with  $ab$  yields the result.  $\square$

**Lemma 2.0.3 (The Hölder's Inequality)** Let  $f \in L^p(\Omega)$  and  $g \in L^q(\Omega)$  for  $\frac{1}{p} + \frac{1}{q} = 1$  with  $p, q \in [1, \infty]$ . Then  $fg \in L^1(\Omega)$  and

$$\|fg\|_{L^1} \leq \|f\|_{L^p} \|g\|_{L^q}. \quad (2.0.10)$$

**Proof.** If either  $\|f\|_{L^p} = 0$  or  $\|g\|_{L^q} = 0$ , then (2.0.10) holds trivially. Otherwise, setting  $\varepsilon = 1$ ,  $a = \frac{|f(x)|}{\|f\|_{L^p}}$  and  $b = \frac{|g(x)|}{\|g\|_{L^q}}$  in (2.0.2) and integrating over  $\Omega$  yields

$$\frac{1}{\|f\|_{L^p} \|g\|_{L^q}} \int_{\Omega} |f(x)g(x)| dx < \frac{1}{p \|f\|_{L^p}^p} \int_{\Omega} |f(x)| dx + \frac{1}{q \|g\|_{L^q}^q} \int_{\Omega} |g(x)| dx. \quad (2.0.11)$$

Using the definition of Lebesgue integral (2.0.4), one writes

$$\frac{1}{\|f\|_{L^p} \|g\|_{L^q}} \int_{\Omega} |f(x)g(x)| dx < \frac{1}{p} + \frac{1}{q} = 1. \quad (2.0.12)$$

Then, multiplying the above inequality by  $\|f\|_{L^p} \|g\|_{L^q}$  immediately gives the result.

□

**Lemma 2.0.4 (Cauchy-Schwarz Inequality)** Let  $f, g \in L^2(\Omega)$ , then the Cauchy-Schwarz inequality holds

$$|(f, g)| \leq \|f\| \|g\|. \quad (2.0.13)$$

**Proof.** The special case for  $p = q = 2$  in Lemma 2.0.3 directly yields the result. □

**Lemma 2.0.5** The following inequality is satisfied,

$$\int_{\Omega} fgh \leq \|f\|_{L^p} \|g\|_{L^q} \|h\|_{L^r}$$

where  $1 \leq p, q, r \leq \infty$  with  $\frac{1}{p} + \frac{1}{q} + \frac{1}{h} = 1$ .

**Proof.** Apply (2.0.10) to get

$$\int_{\Omega} fgh \leq \left( \int_{\Omega} f^p \right)^{\frac{1}{p}} \left( \int_{\Omega} (gh)^m \right)^{\frac{1}{m}} dx$$

where  $\frac{1}{p} + \frac{1}{m} = 1$ . Apply the (2.0.10) again for the second term of the right hand side of (2) to obtain

$$\int_{\Omega} fgh \leq \left( \int_{\Omega} f^p \right)^{\frac{1}{p}} \left( \int_{\Omega} g^{mn} \right)^{\frac{1}{mn}} \left( \int_{\Omega} h^{mr} \right)^{\frac{1}{mr}} dx.$$

Taking  $mn = q$  and  $mn = r$  in (2) yields (2.0.5) with  $\frac{1}{p} + \frac{1}{q} + \frac{1}{h} = 1$ . □

**Lemma 2.0.6 (Poincaré-Friedrichs' Inequality [31])** Let  $\Omega \subset F = \{(x_1, x_2, \dots, x_n) : 0 < x_i < C_{PF}\}$ . Then, for  $f \in H_0^1(\Omega)$ ,

$$\|f\| \leq C_{PF} \|\nabla f\|, \quad \forall f \in \mathbf{X},$$

where  $C_{PF} = C_{PF}(\Omega)$  is a positive constant depends on the size of the domain only.

**Proof.** To prove (2.0.6), it is enough to show that  $f \in C_0^\infty(\Omega)$  since  $C_0^\infty(\Omega)$  is dense in  $H_0^1(\Omega)$ . One can write

$$f(x_1, x_2, \dots, x_n) = f(x_1, x_2, \dots, 0) + \int_0^{x_n} \frac{\partial f(x_1, x_2, \dots, a)}{\partial a} da. \quad (2.0.14)$$

Then, set  $f = 0$  on  $F \setminus \Omega$  and apply (2.0.13) for (2.0.14) to get

$$\begin{aligned} |f(x)| &\leq \left( \int_0^{x_n} 1^2 da \right)^{1/2} \cdot \left( \int_0^{x_n} |\nabla f(x_1, x_2, \dots, a)|^2 da \right)^{1/2} \\ &\leq \left( \int_0^{C_{PF}} |\nabla f(x_1, x_2, \dots, a)|^2 da \right)^{1/2} \end{aligned} \quad (2.0.15)$$

Integrating over the  $x_n$  coordinates, one has

$$\int_0^{x_n} |f(x)| dx_n \leq \left( \int_0^{C_{PF}} |\nabla f(x)|^2 dx_n \right)^{1/2} \quad (2.0.16)$$

Lastly, integrating over the other coordinates results in

$$\int_F |f| dx \leq (C_{PF} \int_F |\nabla f|^2 dx)^{1/2} \quad (2.0.17)$$

□

**Lemma 2.0.7 (Inverse Estimate [141])** Let  $T_h$  be a quasi-uniform family of triangulation of  $\Omega$ . Then, for  $f \in H_0^1(\Omega)$ ,

$$\|\nabla f\| \leq Ch^{-1} \|f\|. \quad (2.0.18)$$

**Lemma 2.0.8** For any  $f \in H^1(\Omega)$ , the following relation is satisfied:

$$\|\nabla \cdot f\| \leq \sqrt{d} \|\nabla f\|,$$

where  $d$  is the dimension of the domain  $\Omega$ .

**Proof.** We prove the estimate only for  $d = 3$ , the proof for  $d = 2$  can be done by using similar arguments. Take  $f = (u(x, y, z), v(x, y, z), w(x, y, z))$  in  $H^1(\Omega)$ . Then, using the definition of the divergence operator and

$$\nabla \cdot f = \frac{\partial u}{\partial x} + \frac{\partial v}{\partial y} + \frac{\partial w}{\partial z} =: u_x + v_y + w_z$$

and using Young's inequality gives

$$\begin{aligned} \|\nabla \cdot f\|^2 &= \int_{\Omega} (u_x + v_y + w_z + 2u_x v_y + 2u_x w_z + 2v_y w_z) dx \\ &\leq \int_{\Omega} 3(u_x^2 + v_y^2 + w_z^2) dx = (\sqrt{3} \|\nabla f\|)^2 \end{aligned}$$

Taking the square root of both sides of the inequality yields the estimate.  $\square$

**Lemma 2.0.9 (Ladyzhenskaya inequality [95]) (2d)** For any  $\nabla f \in L^2(\Omega)$  and  $f \in L^4(\Omega)$  with compact support, there is a constant  $C$  satisfying for  $\Omega \subset \mathbb{R}^2$

$$\|f\|_{L^4(\Omega)} \leq C \sqrt{\|f\| \|\nabla f\|}. \quad (2.0.19)$$

**Proof.** We prove the inequality only for  $\Omega = \mathbb{R}^2$ . Using (2.0.4), we write

$$\|f\|_{L^4(\mathbb{R}^2)}^4 = \int_{\Omega} f^4 dx \leq \int_{-\infty}^{\infty} \max_{x_1} f^2 dx_2 \int_{-\infty}^{\infty} \max_{x_2} f^2 dx_1. \quad (2.0.20)$$

Note also that

$$\max_{x_k} f^2(x_1, x_2) = 2 \int_{-\infty}^{\infty} |f f_{x_k}| dx_k. \quad (2.0.21)$$

Using (2.0.21), we obtain

$$\begin{aligned} \|f\|_{L^4(\mathbb{R}^2)}^4 &\leq 4 \int_{-\infty}^{\infty} \int_{-\infty}^{\infty} |f f_{x_1}| dx_1 dx_2 \int_{-\infty}^{\infty} \int_{-\infty}^{\infty} |f f_{x_2}| dx_1 dx_2 \\ &\leq 4 \int_{\Omega} f^2 dx \int_{\Omega} f_{x_1} f_{x_2} dx. \end{aligned} \quad (2.0.22)$$

Applying Young's inequality to the second factor in (2.0.22), we have

$$\begin{aligned} \|f\|_{L^4(\mathbb{R}^2)}^4 &\leq 2 \int_{\Omega} f^2 dx \int_{\Omega} (f_{x_1}^2 + f_{x_2}^2) dx \\ &\leq 2 \int_{\Omega} f^2 dx \int_{\Omega} (\nabla f)^2 dx \end{aligned} \quad (2.0.23)$$

Lastly, taking the fourth root of both sides in (2.0.23) gives (2.0.19).  $\square$

**Theorem 2.0.1** (The Sobolev Embedding Theorem [109]) Let  $\Omega \in \mathbb{R}^d$  be a bounded domain with a locally Lipschitz boundary. Let  $k$  be a non-negative integer and let  $p$  satisfies  $1 \leq p \leq \infty$ . For  $kp = d$ ,

$$W^{k,p}(\Omega) \hookrightarrow L^q(\Omega), \quad p < q \leq \infty.$$

**Remark 2.0.1** In this thesis, we use Theorem (2.0.1) for the case  $k = 1, p = 2$  and  $q = 4$  such that

$$H^1(\Omega) \hookrightarrow L^4(\Omega),$$

which means

$$\|f\|_{L^4} \leq \|f\|_{H^1}.$$

**Lemma 2.0.10** The norms on  $H^1(\Omega)$  and  $H_0^1(\Omega)$  are equivalent.

**Proof.** The norms on  $H^1(\Omega)$  and  $H_0^1(\Omega)$  are given by, respectively

$$\|f\|_1 = (\|f\|^2 + \|\nabla f\|^2)^{1/2}, \quad \|f\|_0 = \|\nabla f\|.$$

Choose  $f \in H_0^1(\Omega)$ . Then, the application of the Poincaré-Friedrichs' inequality gives

$$\|f\|_1^2 \leq (1 + C_{PF}^2) \|\nabla f\|^2,$$

and taking the square root of both sides yields

$$\|f\|_1 \leq \sqrt{(1 + C_{PF}^2)} \|\nabla f\|. \quad (2.0.24)$$

Also,

$$\|f\|_1 \geq \|\nabla f\|. \quad (2.0.25)$$

(2.0.24) and (2.0.25) show the equivalence of these norms.  $\square$

The analysis of the methods in Chapter 4 and Chapter 5 requires the definition of  $G$ -norm and  $F$ -norm.

**Definition 2.0.6** Let  $I \in \mathbb{R}^{n \times n}$  be an identity matrix and  $\begin{bmatrix} \mathbf{u} \\ \mathbf{v} \end{bmatrix}$  is a  $2n$  vector. Following notation of [27, 94],  $G \in \mathbb{R}^{2n \times 2n}$  symmetric matrix is defined by

$$G = \begin{pmatrix} g_{11} & g_{12} \\ g_{21} & g_{22} \end{pmatrix}$$

where

$$\begin{aligned}
g_{11} &= \frac{\theta(2\theta + 3)}{4} \frac{\nu + \epsilon}{\nu} I - \frac{\theta(2\theta + 1)}{4} \frac{\epsilon}{\nu} I, \\
g_{12} = g_{21} &= -\left( \frac{(\theta + 1)(2\theta - 1)}{4} \frac{\nu + \epsilon}{\nu} I + \frac{(1 - \theta)(2\theta + 1)}{4} \frac{\epsilon}{\nu} I \right), \\
g_{22} &= \frac{\theta(2\theta - 1)}{4} \frac{\nu + \epsilon}{\nu} I - \frac{\theta(-2\theta + 3)}{4} \frac{\epsilon}{\nu} I.
\end{aligned}$$

with  $G$ -norm is defined by

$$\left\| \begin{bmatrix} \mathbf{u} \\ \mathbf{v} \end{bmatrix} \right\|_G^2 = \left( \begin{bmatrix} \mathbf{u} \\ \mathbf{v} \end{bmatrix}, G \begin{bmatrix} \mathbf{u} \\ \mathbf{v} \end{bmatrix} \right) \quad (2.0.26)$$

which can be negative. The form of  $G$ -matrix is common in BDF2 analysis, see e.g., [36] and references therein.

Additionally,  $F \in \mathbb{R}^{n \times n}$  symmetric positive definite matrix is defined by

$$F = \theta(2\theta - 1)I + \frac{4\theta^2\epsilon}{\nu}I \quad (2.0.27)$$

and for any  $\mathbf{u} \in \mathbb{R}^n$ ,  $F$  norm of the  $n$  vector  $\mathbf{u}$  is defined by

$$\|\mathbf{u}\|_F = (\mathbf{u}, F\mathbf{u}). \quad (2.0.28)$$

The following equality is useful for the error analysis in Chapter 4 and Chapter 5.

**Lemma 2.0.11** *The symmetric positive definite matrix  $F \in \mathbb{R}^{n \times n}$  and the symmetric matrix  $G \in \mathbb{R}^{2n \times 2n}$  which are given above satisfy the following equality:*

$$\begin{aligned}
&\left( \frac{(\theta + \frac{1}{2})w^{n+1} - 2\theta w^n + (\theta - \frac{1}{2})w^{n-1}}{\Delta t}, \theta \frac{(\nu + \epsilon)}{\nu} w^{n+1} + \left(1 - \theta \frac{\nu + 2\epsilon}{\nu}\right) w^n + \theta \frac{\epsilon}{\nu} w^{n-1} \right) \\
&= \left\| \begin{bmatrix} w^{n+1} \\ w^n \end{bmatrix} \right\|_G^2 - \left\| \begin{bmatrix} w^n \\ w^{n-1} \end{bmatrix} \right\|_G^2 + \frac{1}{4} \|w^{n+1} - 2w^n + w^{n-1}\|_F^2.
\end{aligned}$$

**Proof.** First, extending the inner product in the left hand side of the equality gives

$$\begin{aligned}
& \left( \frac{(\theta + \frac{1}{2})w^{n+1} - 2\theta w^n + (\theta - \frac{1}{2})w^{n-1}}{\Delta t}, \theta \frac{(\nu + \epsilon)}{\nu} w^{n+1} - \left(1 - \theta \frac{\nu + 2\epsilon}{\nu}\right) w^n + \theta \frac{\epsilon}{\nu} w^{n-1} \right) \\
&= \frac{1}{\Delta t} \left[ (w^{n+1})^T \left(\theta + \frac{1}{2}\right) \theta \frac{\nu + \epsilon}{\nu} w^{n+1} - (w^{n+1})^T \left(\theta + \frac{1}{2}\right) \left(1 - \theta \frac{\nu + 2\epsilon}{\nu}\right) w^n \right. \\
&\quad + (w^{n+1})^T \left(\theta + \frac{1}{2}\right) \theta \frac{\epsilon}{\nu} w^{n-1} - 2(w^n)^T \theta^2 \frac{\nu + \epsilon}{\nu} w^{n+1} + 2(w^n)^T \theta \left(1 - \theta \frac{\nu + 2\epsilon}{\nu}\right) w^n \\
&\quad - 2(w^n)^T \theta^2 \frac{\epsilon}{\nu} w^{n-1} + (w^{n-1})^T \left(\theta - \frac{1}{2}\right) \theta \frac{\nu + \epsilon}{\nu} w^{n+1} \\
&\quad \left. - (w^{n-1})^T \left(\theta + \frac{1}{2}\right) \left(1 - \theta \frac{\nu + 2\epsilon}{\nu}\right) w^n + (w^{n-1})^T \left(\theta - \frac{1}{2}\right) \theta \frac{\epsilon}{\nu} w^{n-1} \right]. \quad (2.0.29)
\end{aligned}$$

Then, extending each term on the right-hand side of the equality using definitions of the  $G$ -norm and  $F$ -norm yields

$$\begin{aligned}
\left\| \begin{bmatrix} w^{n+1} \\ w^n \end{bmatrix} \right\|_G^2 &= (w^{n+1})^T \frac{\theta(2\theta + 3)}{4} \frac{\nu + \epsilon}{\nu} w^{n+1} - (w^{n+1})^T \frac{\theta(2\theta + 1)}{4} \frac{\epsilon}{\nu} w^{n+1} \\
&\quad - (w^{n+1})^T \frac{(\theta + 1)(2\theta - 1)}{4} \frac{\nu + \epsilon}{\nu} w^n - (w^{n+1})^T \frac{(1 - \theta)(2\theta + 1)}{4} \frac{\epsilon}{\nu} w^n \\
&\quad - (w^n)^T \frac{(\theta + 1)(2\theta - 1)}{4} \frac{\nu + \epsilon}{\nu} w^{n+1} - (w^n)^T \frac{(1 - \theta)(2\theta + 1)}{4} \frac{\epsilon}{\nu} w^{n+1} \\
&\quad + (w^n)^T \frac{\theta(2\theta - 1)}{4} \frac{\nu + \epsilon}{\nu} w^n - (w^n)^T \frac{\theta(-2\theta + 3)}{4} \frac{\epsilon}{\nu} w^n \quad (2.0.30)
\end{aligned}$$

$$\begin{aligned}
\left\| \begin{bmatrix} w^n \\ w^{n-1} \end{bmatrix} \right\|_G^2 &= (w^n)^T \frac{\theta(2\theta + 3)}{4} \frac{\nu + \epsilon}{\nu} w^n - (w^n)^T \frac{\theta(2\theta + 1)}{4} \frac{\epsilon}{\nu} w^n \\
&\quad - (w^n)^T \frac{(\theta + 1)(2\theta - 1)}{4} \frac{\nu + \epsilon}{\nu} w^{n-1} - (w^n)^T \frac{(1 - \theta)(2\theta + 1)}{4} \frac{\epsilon}{\nu} w^{n-1} \\
&\quad - (w^{n-1})^T \frac{(\theta + 1)(2\theta - 1)}{4} \frac{\nu + \epsilon}{\nu} w^n - (w^{n-1})^T \frac{(1 - \theta)(2\theta + 1)}{4} \frac{\epsilon}{\nu} w^n \\
&\quad + (w^{n-1})^T \frac{\theta(2\theta - 1)}{4} \frac{\nu + \epsilon}{\nu} w^{n-1} - (w^{n-1})^T \frac{\theta(-2\theta + 3)}{4} \frac{\epsilon}{\nu} w^{n-1} \quad (2.0.31)
\end{aligned}$$



$$\begin{aligned}
\|w^{n+1} - 2w^n + w^{n-1}\|_F^2 &= (w^{n+1})^T \theta(2\theta - 1)w^{n+1} + (w^{n+1})^T \frac{4\theta^2 \epsilon}{\nu} w^{n+1} \\
&\quad - 4(w^{n+1})^T \theta(2\theta - 1)w^n + (w^{n+1})^T \frac{4\theta^2 \epsilon}{\nu} w^n - 4(w^n)^T \theta(2\theta - 1)w^n \\
&\quad + (w^n)^T \frac{4\theta^2 \epsilon}{\nu} w^n + 2(w^{n+1})^T \theta(2\theta - 1)w^{n-1} + (w^{n+1})^T \frac{4\theta^2 \epsilon}{\nu} w^{n-1} \\
&\quad + 4(w^n)^T \theta(2\theta - 1)w^n + (w^n)^T \frac{4\theta^2 \epsilon}{\nu} w^n \\
&\quad + (w^{n-1})^T \theta(2\theta - 1)w^{n-1} + (w^{n-1})^T \frac{4\theta^2 \epsilon}{\nu} w^{n-1}. \tag{2.0.32}
\end{aligned}$$

Lastly, multiplying (2.0.30) by 1, (2.0.31) by -1 and (2.0.32) by  $\frac{1}{4}$  and summing them gives the terms in the left hand side of (2.0.29), which proves the result.  $\square$

In the analysis in Chapter 4 and Chapter 5, we also use the following well-known properties of  $G$ -norm stated in [27, 36].

**Lemma 2.0.12** *For any  $\mathbf{u}, \mathbf{v} \in \mathbb{R}^n$ , we have*

$$\begin{aligned}
\left( \begin{bmatrix} \mathbf{u} \\ \mathbf{v} \end{bmatrix}, G \begin{bmatrix} \mathbf{u} \\ \mathbf{v} \end{bmatrix} \right) &= \frac{2\theta + 1}{4} \|\mathbf{u}\|^2 - \frac{2\theta - 1}{4} \|\mathbf{v}\|^2 \\
&\quad + \frac{(\theta + 1)(2\theta - 1)}{4} \|\mathbf{u} - \mathbf{v}\|^2 + \frac{\theta \epsilon}{2\nu} \|\mathbf{u} - \mathbf{v}\|^2 \\
&\geq \frac{2\theta + 1}{4} \|\mathbf{u}\|^2 - \frac{2\theta - 1}{4} \|\mathbf{v}\|^2, \tag{2.0.33}
\end{aligned}$$

$$\begin{aligned}
\left( \begin{bmatrix} \mathbf{u} \\ \mathbf{v} \end{bmatrix}, G \begin{bmatrix} \mathbf{u} \\ \mathbf{v} \end{bmatrix} \right) &\leq \frac{2\theta + 1}{4} \|\mathbf{u}\|^2 + \frac{(\theta + 1)(2\theta - 1)}{2} \|\mathbf{u} - \mathbf{v}\|^2 + \frac{\theta \epsilon}{2\nu} \|\mathbf{u} - \mathbf{v}\|^2 \\
&\leq \left( \frac{2\theta + 1}{4} + (\theta + 1)(2\theta - 1) + \frac{\theta \epsilon}{\nu} \right) \|\mathbf{u}\|^2 \\
&\quad + \left( (\theta + 1)(2\theta - 1) + \frac{\theta \epsilon}{\nu} \right) \|\mathbf{v}\|^2. \tag{2.0.34}
\end{aligned}$$

**Proof.** Using the  $G$  matrix (2.0.6), we have

$$\begin{aligned}
\left( \begin{bmatrix} \mathbf{u} \\ \mathbf{v} \end{bmatrix}, G \begin{bmatrix} \mathbf{u} \\ \mathbf{v} \end{bmatrix} \right) &= \frac{\theta(2\theta + 3)}{4} \frac{\nu + \epsilon}{\nu} \mathbf{u}^2 - \frac{\theta(2\theta + 1)}{4} \frac{\epsilon}{\nu} \mathbf{u}^2 \\
&\quad - \frac{(\theta + 1)(2\theta - 1)}{4} \frac{\nu + \epsilon}{\nu} \mathbf{u}\mathbf{v} - \frac{(1 - \theta)(2\theta + 1)}{4} \frac{\epsilon}{\nu} \mathbf{u}\mathbf{v} \\
&\quad - \frac{(\theta + 1)(2\theta - 1)}{4} \frac{\nu + \epsilon}{\nu} \mathbf{u}\mathbf{v} - \frac{(1 - \theta)(2\theta + 1)}{4} \frac{\epsilon}{\nu} \mathbf{u}\mathbf{v} \\
&\quad + \frac{\theta(2\theta - 1)}{4} \frac{\nu + \epsilon}{\nu} \mathbf{v}^2 - \frac{\theta(-2\theta + 3)}{4} \frac{\epsilon}{\nu} \mathbf{v}^2
\end{aligned}$$

$$\begin{aligned}
&= \frac{2\theta + 1}{4} \|\mathbf{u}\|^2 - \frac{2\theta - 1}{4} \|\mathbf{v}\|^2 \\
&\quad + \frac{(\theta + 1)(2\theta - 1)}{4} \|\mathbf{u} - \mathbf{v}\|^2 + \frac{\theta \epsilon}{2\nu} \|\mathbf{u} - \mathbf{v}\|^2
\end{aligned} \tag{2.0.35}$$

$$\geq \frac{2\theta + 1}{4} \|\mathbf{u}\|^2 - \frac{2\theta - 1}{4} \|\mathbf{v}\|^2. \tag{2.0.36}$$

Dropping the positive terms in (2.0.35) gives the result (2.0.33).

Then, eliminating the negative term in (2.0.35) and using the inequality

$\|\mathbf{u} - \mathbf{v}\| \leq 2(\|\mathbf{u}\|^2 + \|\mathbf{v}\|^2)$ , we obtain

$$\begin{aligned}
\left( \begin{bmatrix} \mathbf{u} \\ \mathbf{v} \end{bmatrix}, G \begin{bmatrix} \mathbf{u} \\ \mathbf{v} \end{bmatrix} \right) &\leq \frac{2\theta + 1}{4} \|\mathbf{u}\|^2 + \frac{(\theta + 1)(2\theta - 1)}{2} \|\mathbf{u} - \mathbf{v}\|^2 + \frac{\theta \epsilon}{2\nu} \|\mathbf{u} - \mathbf{v}\|^2 \\
&\leq \frac{2\theta + 1}{4} \|\mathbf{u}\|^2 + (\theta + 1)(2\theta - 1) \|\mathbf{u}\|^2 + \frac{\theta \epsilon}{\nu} \|\mathbf{u}\|^2 \\
&\quad + (\theta + 1)(2\theta - 1) \|\mathbf{u}\|^2 + \frac{\theta \epsilon}{\nu} \|\mathbf{v}\|^2
\end{aligned} \tag{2.0.37}$$

which yields the estimate (2.0.34).  $\square$

**Lemma 2.0.13 (Discrete Gronwall's Lemma)** *Assume that  $\Delta t$ ,  $B$ , and  $a_n, b_n, c_n, d_n$  (for integers  $n \geq 0$ ) be non-negative numbers such that if*

$$a_N + \Delta t \sum_{n=0}^N b_n \leq \Delta t \sum_{n=0}^{N-1} d_n a_n + \Delta t \sum_{n=0}^N c_n + B \quad \forall N \geq 0 \tag{2.0.38}$$

then for  $\Delta t > 0$ ,

$$a_N + \Delta t \sum_{n=0}^N b_n \leq \exp\left(\Delta t \sum_{n=0}^{N-1} d_n\right) \left(\Delta t \sum_{n=0}^N c_n + B\right) \quad \text{for } N \geq 0. \tag{2.0.39}$$

**Proof.** For the proof, see reference [57].  $\square$

## CHAPTER 3

### AN ANALYSIS OF A LINEARLY EXTRAPOLATED BDF2 SUBGRID ARTIFICIAL VISCOSITY METHOD FOR INCOMPRESSIBLE FLOWS

In this chapter, we consider an efficient and accurate numerical approximation of the Navier-Stokes equations (NSE). Recall from Chapter 1, the governing equations of NSE are given by

$$\begin{aligned} \mathbf{u}_t - \nu \Delta \mathbf{u} + \mathbf{u} \cdot \nabla \mathbf{u} + \nabla p &= \mathbf{f} && \text{in } \Omega \times (0, T), \\ \nabla \cdot \mathbf{u} &= 0 && \text{in } \Omega \times (0, T], \\ \mathbf{u} &= \mathbf{0} && \text{on } \partial\Omega \times [0, T], \\ \mathbf{u}(\mathbf{x}, 0) &= \mathbf{u}_0(\mathbf{x}) && \text{for } \mathbf{x} \in \Omega, \\ \int_{\Omega} p d\mathbf{x} &= \mathbf{0} && \text{in } (0, T]. \end{aligned} \tag{3.0.1}$$

Here,  $\Omega$  denotes a bounded and regular flow domain in  $\mathbb{R}^d$  ( $d = 2$  or  $3$ ),  $\mathbf{u}(x, t)$  represents the velocity,  $p(x, t)$  the zero-mean pressure,  $\mathbf{f}(x, t)$  an external force,  $\nu$  the kinematic viscosity and  $\mathbf{u}_0$  is a weakly divergence-free initial condition. In the literature, there are different stabilization techniques used to accurately approximate the NSE solutions, the Large eddy simulation (LES) method and the variational multiscale (VMS) method, which is based on the LES method are two of common approaches among them. In the LES method, the principal idea is to directly compute large flow scales (resolved scales) by averaging solutions in space via a convolution filter while modeling the effects of the small flow scales (unresolved scales) [17]. However, there are some challenges in applying the LES method. One of the biggest challenges is the necessity of choosing an appropriate filter function. Also, the LES method produces commutation errors arising from limiting the LES method theory from the unbounded domain to bounded domain. Moreover, instead of incorporating the effects of unresolved scales into all resolved scales via a turbulence model, adding its effects to only a portion of the resolved scales would physically indicate

more real flow characteristics. For further details of the LES method, one can refer to [61, 101, 105, 117]. An alternative to the LES method is the variational multiscale (VMS) method which also simulates only large flow scales with some fundamental differences from the LES method. VMS methods have been proposed by Hughes in 1995, [134] which separates the solution scales as large and small scales and developed by Guermond [58] in which an artificial diffusion term is added acting only on small scales. Then, Layton [156] developed a method based on [58] by adding and then subtracting artificial viscosity terms to reduce instabilities due to extra terms. Later, Collis [129] introduced the VMS method for turbulent flows which separate the flow field into three scales (large, small, and unresolved small scales). There have been a huge number of studies on the framework of VMS method such as for NSE [150, 151] and convection-diffusion equations [152]. Unlike the LES method, the VMS method defines large scales with projection into appropriate function spaces. Also, the VMS method considers a variational formulation of NSE in contrast to the LES method which is derived from the strong form of NSE. In addition, unlike to the LES methods, in the VMS method, the turbulence model directly influences the small flow scales while indirectly affecting the large scales by the subgrid-scale model due to the intrinsic matching of all scales. Moreover, the VMS method naturally enables to inclusion of boundary domains and boundary conditions in the mathematical analysis.

There are various classes and realizations of VMS for different types of fluid problems, see [149] for an overview. Among them, the popular and commonly applied VMS methods are residual-based VMS method and projection-based VMS method. The principal idea in residual-based VMS is to look for the solution of Galerkin discretization of (3.0.1) by adding control of strong residuals of both momentum and continuity equation which acts on all scales. The classical residual-based VMS stabilization techniques seen in the literature are the streamline-upwind/Petrov-Galerkin (SUPG), pressure-stabilizing Petrov-Galerkin (PSPG) and grad-div stabilization. Although there have been a considerable number of studies of such methods [12, 111, 158, 159], these residual-based VMS methods have some drawbacks. One of the main drawbacks of these methods is that they introduce an artificial nonsymmetric term. Also, they produce a strong coupling of velocity and pressure. This becomes par-

ticularly challenging for some complex flows with compressible properties or with additional variables. In addition, all residual-based stabilizations change the right-hand side  $f$  of the NSE problem and this change complicates the application of these schemes for time-dependent problems. Moreover, the number of matrix blocks that need to be stored and combined for these methods is quite large. As a remedy to all these drawbacks, scientists have introduced the projection-based VMS method.

In recent years, the projection-based VMS method has become one of the popular stabilizations method to obtain more stable approximations. In this method, large scales are defined by projection into suitable function spaces, and the function spaces satisfying the Ladyzenskaya-Brezzi-Babuska (LBB) condition are chosen for both large and small scales. The choice of large-scale space is important for this method. This choice can be done in two different ways. The first choice is to define large scale space on the same grid as small scale space using lower degree polynomials than the standard finite element spaces which is called as one level VMS method, see [151] for a discussion. The second choice is to define large-scale space on a coarser grid than the standard finite element spaces which are called two-level VMS method, see [152]. There are various studies of this method in the literature. The VMS method is applied to the NSE in [150], to the non-isothermal free convection problems in [63], to the MHD in [81], and to the steady-state natural convection in [5], and the Darcy-Brinkman equations in [4]. All these studies reveal that this VMS method gives more accurate approximations on coarse meshes, can be easily applied to any existing code, and reduces the need for high computation power.

Due to the proven good theoretical and practical properties of VMS methods, it is natural to broaden its understanding by developing efficient, accurate, and stable numerical algorithms. The method we consider in this study is first proposed in [156] which is VMS method, for finding solutions to the convection-dominated convection-diffusion equation. The VMS method of [156] introduces global stabilization by adding a term, then anti-diffuses through the extra mixed variables which are chosen as the large scales of solution. In this way the effective artificial viscosity type stabilization influences only the small scales, thus the method we considered herein can be thought of as a subgrid artificial viscosity (SAV) method. Based on these ideas, on page 156 of [156], the new formulation of SAV has been proposed without any

numerical analysis. In this formulation, the stability process is applied to the viscous term by using the vector identity  $\Delta \mathbf{u} = -\nabla \times (\nabla \times \mathbf{u}) + \nabla(\nabla \cdot \mathbf{u})$  to reduce the extra storage in  $3D$ . As a result, a two-level method is obtained that combines both vorticity and the grad-div stabilization in the viscous term. This SAV method greatly reduces extra storage compared to velocity and its gradient. SAV method was first analyzed in the study of [73] by using Crank-Nicholson (CN) scheme without any linearization. As noted in [73], the system is improved in a better way without choosing computationally inefficient time step, that is, the system of method includes just three variables with the use of a coarse grid of vorticity instead of nine variables for the full velocity gradient. Thus, the method significantly improves the solution of the system in case of a small viscosity without choosing a computationally inefficient time step. The current study extends the mathematical idea of the mixed, conforming SAV finite element method to the multistep the second-order backward-difference (BDF2) time discretization. Since it exhibits strong stability and damping properties that are better than those of CN time discretization for the simulation of underresolved regimes, BDF2 is one of the most popular choices of time-stepping schemes [83]. We note that the backward differentiation formula is a class of time-stepping schemes that has been commonly used and studied for the time-dependent ordinary and partial differential equations [36, 44, 65, 130–132, 142, 154, 157]. In light of the previous literature, herein we consider a successful SAV stabilization scheme to be used with linearly extrapolated BDF2 (BDF2LE) formula in time without affecting accuracy.

This chapter carefully considers several physical and mathematical questions concerning SAV solutions, and it is arranged as follows. Section 3.2 presents the SAV algorithm based on the BDF2LE time-stepping method. In Section 3.3, we first investigate the conservation of the fundamental integral variants of fluid flow energy and helicity for SAV solutions. It is well known these quantities are important for the physical fidelity of the model, but many models do not conserve them. In many Galerkin finite element discretization for incompressible flow problems, energy conservation is lost. In typical discretization, for example, by using Taylor-Hood finite elements, the conservation of mass is only weakly enforced. However, on practical meshes, the divergence error can still be significant. To preserve the conservation of energy, the skew-symmetric or rotational formulations of the nonlinear term

are used, [118]. A finite element formulation of [84] and [77] preserves energy and helicity with a slightly altered definition of discrete helicity together with the skew-symmetric formulation of the nonlinear term. In this report, by using underlying ideas of [77, 84], we show that without viscous or external forces, the energy and helicity will remain constant in time and they will be correctly balanced when these forces are present.

Section 3.4 gives a complete numerical analysis of the SAV method along with the proofs of unconditional stability and convergence. In our scheme, overall accuracy and mass conservation in the discrete solution depends on the carefully chosen stabilization parameters, namely the artificial viscosity and the grad-div stabilization. Standard error analysis for the SAV method predicts that the optimal choice for the artificial viscosity parameter should be  $O(h^2)$  and the grad-div stabilization parameter should be  $O(1)$ .

Section 3.5 presents several numerical examples to present evidence of optimal accuracy for an analytical test problem, and also demonstrate the ability of SAV method to give good results on the flow around a cylinder, flow between two offset circles and Poiseuille's Flow.

### 3.1 Notations and Mathematical Preliminaries

In this section, we present some definitions and inequalities which are necessary for our numerical analysis. Throughout this thesis, we consider a convex polygonal or polyhedral simply connected domain  $\Omega$  in  $\mathbb{R}^d$ , ( $d = 2, 3$ ) with smooth boundary  $\partial\Omega$ . We use bold letters to denote the vector-valued functions and their spaces. To define the method precisely, we will approximate the solution of (3.0.1) by using the finite element method. We consider the standard function spaces for the continuous velocity field and pressure spaces defined respectively by

$$\begin{aligned} \mathbf{X} &:= (\mathbf{H}_0^1(\Omega))^d, \\ Q &:= L_0^2(\Omega). \end{aligned} \tag{3.1.1}$$

The set of weakly divergence-free functions in  $\mathbf{X}$  is defined by

$$\mathbf{V} := \{\mathbf{v} \in \mathbf{X} : (\nabla \cdot \mathbf{v}, q) = 0, \forall q \in Q\}.$$

The variational formulation of (3.0.1) reads as follows: Find  $\mathbf{u} : (0, T] \rightarrow \mathbf{X}$ ,  $p : (0, T] \rightarrow Q$  satisfying

$$(\mathbf{u}_t, \mathbf{v}) + \nu(\nabla \mathbf{u}, \nabla \mathbf{v}) + b(\mathbf{u}, \mathbf{u}, \mathbf{v}) - (p, \nabla \cdot \mathbf{v}) = (\mathbf{f}, \mathbf{v}) \quad \forall \mathbf{v} \in \mathbf{X}, \quad (3.1.2)$$

$$(q, \nabla \cdot \mathbf{u}) = 0 \quad \forall q \in Q, \quad (3.1.3)$$

For a spatial discretization, we need to take the conforming finite element spaces  $\mathbf{X}_h \subset \mathbf{X}$ ,  $Q_h \subset Q$  defined on a regular, admissible triangulation  $\pi_h$  of the domain  $\Omega$  with maximum diameter  $h$ . It is assumed that the conforming finite element spaces of the velocity and pressure spaces satisfy the discrete inf-sup condition (or LBB condition [142]), e.g., there is a constant  $\beta$  independent of the mesh size  $h$  such that

$$\inf_{q_h \in Q_h} \sup_{\mathbf{v}_h \in \mathbf{X}_h} \frac{(q_h, \nabla \cdot \mathbf{v}_h)}{\|\nabla \mathbf{v}_h\| \|q_h\|} \geq \beta > 0. \quad (3.1.4)$$

We introduce the discretely divergence-free subspace  $\mathbf{V}_h \subset \mathbf{X}_h$  given by

$$\mathbf{V}_h := \{\mathbf{v}_h \in \mathbf{X}_h : (q_h, \nabla \cdot \mathbf{v}_h) = 0, \forall q_h \in Q_h\}.$$

Under the inf-sup condition (3.1.4),  $\mathbf{V}_h$  is a nonempty, closed subspace of  $\mathbf{X}_h$  and the formulation in  $\mathbf{X}_h$  is equivalent to  $\mathbf{V}_h$ . Note that in general  $\mathbf{V}_h \not\subset \mathbf{V}$ , see [141]. In this thesis, we use the Taylor-Hood element pair  $(\mathbf{X}_h; Q_h) = (P_k^d; P_{k-1})$  which are defined as

$$\mathbf{X}_h = \{\mathbf{u}_h \in \mathbf{X} : u_h|_K \in P_k^d(K), \forall K \in \pi_h\},$$

$$Q_h = \{q_h \in Q : q_h|_K \in P_{k-1}(K), \forall K \in \pi_h\}.$$

As noted in [38, 141], for  $k \geq 2$ , Taylor-Hood finite element pair satisfies LBB-condition (3.1.4). Additionally, following [122, 143], it is assumed that the finite element spaces  $(\mathbf{X}_h, Q_h)$  satisfy the following well-known approximation properties

$$\inf_{\mathbf{v}_h \in \mathbf{X}_h} (\|\mathbf{u} - \mathbf{v}_h\| + h\|\nabla(\mathbf{u} - \mathbf{v}_h)\|) \leq Ch^{k+1}\|\mathbf{u}\|_{k+1} \quad \mathbf{u} \in H^{k+1}(\Omega), \quad (3.1.5)$$

$$\inf_{q_h \in Q_h} \|p - q_h\| \leq Ch^k\|p\|_k \quad p \in H^k(\Omega). \quad (3.1.6)$$



We define skew-symmetric trilinear form for the convective term in (3.0.1)

$$b^*(\mathbf{u}, \mathbf{v}, \mathbf{w}) = \frac{1}{2}(\mathbf{u} \cdot \nabla \mathbf{v}, \mathbf{w}) - \frac{1}{2}(\mathbf{u} \cdot \nabla \mathbf{w}, \mathbf{v}) \quad (3.1.7)$$

From the definition of the skew-symmetric trilinear form, it immediately follows that

$$b^*(\mathbf{u}, \mathbf{v}, \mathbf{w}) = -b^*(\mathbf{u}, \mathbf{w}, \mathbf{v}), \quad b^*(\mathbf{u}, \mathbf{u}, \mathbf{u}) = 0. \quad (3.1.8)$$

Error analysis will require the following upper bounds for the skew-symmetric trilinear form (3.1.7).

**Lemma 3.1.1** *For  $\mathbf{u}, \mathbf{v}, \mathbf{w} \in \mathbf{X}$ , the skew-symmetric trilinear form satisfies the following bounds*

$$b^*(\mathbf{u}, \mathbf{v}, \mathbf{w}) \leq C_1 \|\nabla \mathbf{u}\| \|\nabla \mathbf{v}\| \|\nabla \mathbf{w}\| \quad (3.1.9)$$

where  $C_1 := C_1(\Omega)$  is a constant depending only on the domain  $\Omega$ .

Furthermore, it will be assumed that if  $\mathbf{v}, \nabla \mathbf{v} \in L^\infty(\Omega)$ , the following bound holds

$$b^*(\mathbf{u}, \mathbf{v}, \mathbf{w}) \leq \frac{1}{2} \left( \|\mathbf{u}\| \|\nabla \mathbf{v}\|_\infty \|\mathbf{w}\| + \|\mathbf{u}\| \|\mathbf{v}\|_\infty \|\nabla \mathbf{w}\| \right). \quad (3.1.10)$$

**Proof.** For the proof of the first estimate, we start with the triangle inequality

$$|b^*(\mathbf{u}, \mathbf{v}, \mathbf{w})| \leq \frac{1}{2} (|(\mathbf{u} \cdot \nabla) \mathbf{v}, \mathbf{w}| + |(\mathbf{u} \cdot \nabla) \mathbf{w}, \mathbf{v}|) \quad (3.1.11)$$

Then, we apply the inequality (2.0.5) to the first convective term in (3.1.11) with  $p = r = 4$  and  $q = 2$

$$|(\mathbf{u} \cdot \nabla) \mathbf{v}, \mathbf{w}| \leq \|\mathbf{u}\|_{L^4(\Omega)} \|\nabla \mathbf{v}\|_{L^2(\Omega)} \|\mathbf{w}\|_{L^4(\Omega)}. \quad (3.1.12)$$

Similarly, the application of (2.0.5) to the second convective term in (3.1.11) with  $p = r = 4$  and  $q = 2$  gives

$$|(\mathbf{u} \cdot \nabla) \mathbf{w}, \mathbf{v}| \leq \|\mathbf{u}\|_{L^4(\Omega)} \|\nabla \mathbf{w}\|_{L^2(\Omega)} \|\mathbf{v}\|_{L^4(\Omega)} \quad (3.1.13)$$

Lastly, inserting (3.1.12) and (3.1.13) to (3.1.11), applications of the Ladyzhenskaya (2.0.19) inequality and the Sobolev imbedding theorem gives the estimate (3.1.9).

To prove the second estimate, apply (2.0.5) inequality to the first convective term in (3.1.11) with  $p = r = 2$  and  $q = \infty$  and to the second convective term with  $p = q = 2$  and  $r = \infty$  to get

$$b^*(\mathbf{u}, \mathbf{v}, \mathbf{w}) \leq \frac{1}{2} (\|\mathbf{u}\| \|\nabla \mathbf{v}\|_{L^\infty(\Omega)} \|\mathbf{w}\| + \|\mathbf{u}\| \|\nabla \mathbf{w}\| \|\mathbf{v}\|_{L^\infty(\Omega)}) \quad (3.1.14)$$

Finally, by applying the Poincaré-Friedrichs inequality we get the estimate (3.1.10).

□

We define the discretely divergence-free function space by

$$\mathbf{V}_h := \{\mathbf{v}_h \in \mathbf{X}_h \mid (\nabla \cdot \mathbf{v}_h, q_h) = 0, \forall q_h \in Q_h\}.$$

Under the inf-sup condition (3.1.4), the variational formulation of NSE (1.0.1) in  $(\mathbf{X}_h, Q_h)$  is equivalent to in  $(\mathbf{V}_h, Q_h)$ , see, e.g., [141]. We also assume that  $(\mathbf{X}_h, Q_h)$  satisfy the well-known approximation properties (3.1.5)-(3.1.6) for the choice of typical piecewise polynomials of degree  $(k, k - 1)$ . To formulate the SAV discretization method, we need some further notations. Let  $\pi^H$  be a family of triangulations of  $\Omega$  and let  $\pi^h$  be a refinement of  $\pi^H$ . We also introduce a coarse or large scale space  $L_H \subset L^2(\Omega)^d$  on a regular mesh  $\pi^H$ . We define  $L_H$  on the same grid as  $(X_h, Q_h)$  by using lower degree polynomials in the case of  $(X_h, Q_h)$  being a higher-order finite element spaces. Specifically, we consider piecewise polynomials with degree  $k$  for velocity space  $L_H$  on the coarse mesh, we use piecewise polynomials with degree  $k - 1$  for discretization.

In addition, for the proposed method, the size of coarse mesh  $H$ , connected with  $L_H$ , must be balanced between efficiency and accuracy. The larger  $H$  reduces storage and yields more efficient projections into  $L_H$ . However, in this case accuracy decreases. In our case, as a result of error analysis, one has  $H = O(h^{1/2})$  in the case of  $k = 2$  for not spoiling the asymptotic convergence rate. This choice has been used through numerical experiments. Another common choice is to use a single mesh i.e.,  $H = h$ , which is also a very convenient way of programming to strike a good balance but it requires computational resources.

**Definition 3.1.1** *The  $L^2$  projection  $P_{L_H} : (L^2(\Omega))^d \longrightarrow L_H$  is also defined by*

$$(P_{L_H} \phi - \phi, l_H) = 0 \quad \forall l_H \in L_H. \quad (3.1.15)$$

In addition, approximation on coarse mesh space  $L_H$  is given by

$$\|\phi - P_{L_H}\phi\| \leq CH^k|\phi|_{k+1}, \quad \phi \in L^2(\Omega) \cap (H^{k+1}(\Omega))^d. \quad (3.1.16)$$

**Lemma 3.1.2** *There exists  $C > 0$  such that*

$$\left\| \frac{3w^{n+1} - 4w^n + w^{n-1}}{2\Delta t} \right\| \leq \frac{1}{\Delta t} \int_{t^{n+1}}^{t^{n-1}} \|w_t\|^2 dt \quad (3.1.17)$$

$$\left\| \frac{3w(t^{n+1}) - 4w(t^n) + w(t^{n-1})}{2\Delta t} - w_t(t^{n+1}) \right\| \leq C\Delta t^3 \int_{t^{n-1}}^{t^{n+1}} \|w_{ttt}\|^2 dt \quad (3.1.18)$$

$$\|2w^n - w^{n-1} - w^{n+1}\| \leq C\Delta t^3 \int_{t^{n-1}}^{t^{n+1}} \|w_{tt}\|^2 dt \quad (3.1.19)$$

**Proof.** For the first estimate, we expand each term in BDF2 around  $t^{n+1}$  using the fundamental theorem of calculus

$$w^{n+1} = w^{n+1} \quad (3.1.20)$$

$$w^n = w^{n+1} + \int_{t^{n+1}}^{t^n} w_t(t) dt \quad (3.1.21)$$

$$w^{n-1} = w^{n+1} + \int_{t^{n+1}}^{t^{n-1}} w_t(t) dt \quad (3.1.22)$$

Then, multiplying (3.1.20) with  $\frac{3}{2\Delta t}$ , (3.1.21) with  $\frac{-4}{2\Delta t}$ , and (3.1.22) with  $\frac{1}{2\Delta t}$  and sum them gives the remainder term of BDF2:

$$\frac{3w^{n+1} - 4w^n + w^{n-1}}{2\Delta t} \leq \frac{1}{\Delta t} \int_{t^{n-1}}^{t^{n+1}} w_t^2(t) dt \quad (3.1.23)$$

Integrating (3.1.23) yields the estimate (3.1.17). The second estimate is proved in a similar manner using the Taylor's theorem with integral remainders

$$w_t(t^{n+1}) = w_t(t^{n+1}) \quad (3.1.24)$$

$$w^{n+1} = w^{n+1} \quad (3.1.25)$$

$$w^n = w^{n+1} - w_t(t^{n+1})\Delta t + w_{tt}(t^{n+1})\frac{\Delta t^2}{2} + \int_{t^{n+1}}^{t^n} w_{ttt}(t)\frac{(t^n - t)^2}{2} dt \quad (3.1.26)$$

$$w^{n-1} = w^{n+1} - 2w_t(t^{n+1})\Delta t + 2w_{tt}(t^{n+1})\Delta t^2 + \int_{t^{n+1}}^{t^{n-1}} w_{ttt}(t)\frac{(t^{n-1} - t)^2}{2} dt \quad (3.1.27)$$

Then, multiplying (3.1.24) with  $-1$ , (3.1.25) with  $\frac{3}{2\Delta t}$ , (3.1.26) with  $\frac{-4}{2\Delta t}$  and (3.1.27) with  $\frac{1}{2\Delta t}$  and adding them we obtain

$$\begin{aligned} & \left( \frac{3w^{n+1} - 4w^n + w^{n-1}}{2\Delta t} - w_t(t^{n+1}) \right) \\ & \leq \frac{1}{4\Delta t} \left( \int_{t^{n+1}}^{t^{n-1}} \|w_{ttt}\|^2 (t^{n-1} - t)^2 dt - 4 \int_{t^n}^{t^{n+1}} \|w_{ttt}\|^2 (t^n - t)^2 dt \right) \end{aligned} \quad (3.1.28)$$

Integrating (3.1.28) yields the estimate (3.1.18).

For the proof of the last estimation, we utilize the Taylor's theorem with integral remainders for each term in the linear extrapolation around  $t^{n+1}$

$$w(t^{n+1}) = w^{n+1} \quad (3.1.29)$$

$$w^n = w^{n+1} - w_t(t^{n+1})\Delta t + \int_{t^{n+1}}^{t^n} w_{tt}(t)(t^n - t)dt \quad (3.1.30)$$

$$w^{n-1} = w^{n+1} - 2w_t(t^{n+1})\Delta t + \int_{t^{n+1}}^{t^{n-1}} w_{tt}(t)(t^{n-1} - t)dt \quad (3.1.31)$$

Then, multiply (3.1.29) and (3.1.31) by  $-1$ , (3.1.30) with 2, and add them gives

$$\begin{aligned} & (2w^n - w^{n-1}) - w(t^{n+1}) \\ & \leq 2 \int_{t^{n+1}}^{t^n} w_{tt}(t)(t^n - t)dt - \int_{t^{n+1}}^{t^{n-1}} w_{tt}(t)(t^{n-1} - t)dt \end{aligned} \quad (3.1.32)$$

Integrating (3.1.32), the estimate (3.1.19) is obtained.  $\square$

## 3.2 Numerical Scheme

We approximate the solution of the NSE (3.0.1) by a second-order accurate SAV algorithm based on BDF2LE by the following algorithm. In this method, for the linear term, implicit time discretization and for the nonlinear term, two-step linear extrapolation have been used. Let a positive number  $N$  be given and define the step size  $\Delta t = T/n$ ,  $n = 1, \dots, N$  with given at time  $t^n = n\Delta t$  as follows.

**Scheme(BDF2LE Based SAV Method):** Let  $S_H$  be the new coarse mesh variable and the initial condition  $\mathbf{u}_0$  be given. Define  $\mathbf{u}_h^0, \mathbf{u}_h^{-1}$  as the nodal interpolants of  $\mathbf{u}^0$ .

Then, given  $\mathbf{u}_h^n, \mathbf{u}_h^{n-1}$ , find  $(\mathbf{u}_h^{n+1}, p_h^{n+1}, S_H^{n+1}) \in (\mathbf{X}_h, Q_h, L_H)$  satisfying  $\forall (\mathbf{v}_h, q_h, l_H) \in (\mathbf{X}_h, Q_h, L_H)$

$$\begin{aligned} & \left( \frac{3\mathbf{u}_h^{n+1} - 4\mathbf{u}_h^n + \mathbf{u}_h^{n-1}}{2\Delta t}, \mathbf{v}_h \right) + \nu(\nabla \mathbf{u}_h^{n+1}, \nabla \mathbf{v}_h) + b^*(2\mathbf{u}_h^n - \mathbf{u}_h^{n-1}, \mathbf{u}_h^{n+1}, \mathbf{v}_h) \\ & - (p_h^{n+1}, \nabla \cdot \mathbf{v}_h) + \alpha_1(\nabla \times \mathbf{u}_h^{n+1}, \nabla \times \mathbf{v}_h) - \alpha_1(S_H^{n+1}, \nabla \times \mathbf{v}_h) \\ & + \alpha_2(\nabla \cdot \mathbf{u}_h^{n+1}, \nabla \cdot \mathbf{v}_h) = (\mathbf{f}(t^{n+1}), \mathbf{v}_h), \quad (3.2.1) \end{aligned}$$

$$(\nabla \cdot \mathbf{u}_h^{n+1}, q_h) = 0, \quad (3.2.2)$$

$$(S_H^{n+1} - \nabla \times \mathbf{u}_h^n, l_H) = 0. \quad (3.2.3)$$

Herein,  $\alpha_1 = \alpha_1(\mathbf{x}, h)$  is the user-selected artificial (subgrid) viscosity parameter and  $\alpha_2$  is the grad-div stabilization parameter.

**Remark 3.2.1** *In this thesis, we assume that  $\alpha_1$  and  $\alpha_2$  are known positive constants.*

**Remark 3.2.2** *In (3.2.1)-(3.2.3), the application of  $\alpha_1$  can be thought of as follows. The first term in (3.2.1) adds stabilization via artificial viscosity to all scales and the second term in (3.2.1) via (3.2.3) subtracts the stabilization for the large scales. In this way, the effective stabilization in the scheme acts only on small scales.*

**Remark 3.2.3** *As it is mentioned in [73], Scheme (3.2.1)-(3.2.3) requires coarse grid storage of vorticity with three variables, instead of the full velocity gradient with nine variables of projection-based VMS, see [156]. In addition, the method adds and subtracts the stabilization for consistency but the subtracted term is treated as extra variable in a mixed method. BDF2LE-based SAV method is augmented with the grad-div stabilization term adding such term improves the conservation of mass in finite element approximation, [76].*

### 3.3 Conservation Laws for BDF2LE Based SAV Solution

This section studies the discrete conservation laws of Scheme (3.2.1)-(3.2.3). We present both the energy and helicity balance of the algorithm. In general, helicity is not generally preserved for usual boundary conditions, see [78]. An alternative

discrete helicity definition, proposed in [84], uses the solution of the discrete vorticity equation instead of being the curl of the velocity. In this way, helicity balance is recovered up to the boundary effect. Following the underlying ideas of [84], we choose  $\tilde{\mathbf{X}}_h$  to be the vorticity space which is the same as velocity discrete space but without imposing homogeneous Dirichlet boundary conditions. Herein, discrete helicity definition for Galerkin discretization of the NSE which is denoted by  $H_h(t)$  and computed as

$$H_h(t) = \int_{\Omega} \mathbf{u}_h(t) \cdot \mathbf{w}_h(t).$$

Herein  $\mathbf{w}_h = \nabla \times \mathbf{u}_h$  denotes the solution of a discrete vorticity equation which is obtained by applying the rotation operator to Scheme (3.2.1)-(3.2.3). The discrete vorticity equation is as follows: For given  $\mathbf{u}_h(t)$ , for all  $t > 0$ , find  $(\mathbf{w}_h(t), \lambda_h, D_H) \in (\tilde{\mathbf{X}}_h, Q_h, L_H)$  satisfying  $\forall (\chi_h, \tau_h, \rho_H) \in (\mathbf{X}_h, Q_h, L_H)$

$$\begin{aligned} & \left( \frac{3\mathbf{w}_h^{n+1} - 4\mathbf{w}_h^n + \mathbf{w}_h^{n-1}}{2\Delta t}, \chi_h \right) + \nu(\nabla \mathbf{w}_h^{n+1}, \nabla \chi_h) - b^*(2\mathbf{w}_h^n - \mathbf{w}_h^{n-1}, \mathbf{u}_h^{n+1}, \chi_h) \\ & + b^*(2\mathbf{u}_h^n - \mathbf{u}_h^{n-1}, \mathbf{w}_h^{n+1}, \chi_h) - (\lambda_h^{n+1}, \nabla \cdot \chi_h) + \alpha_1(\nabla \times \mathbf{w}_h^{n+1}, \nabla \times \chi_h) \\ & - \alpha_1(D_H^{n+1}, \nabla \times \chi_h) + \alpha_2(\nabla \cdot \mathbf{w}_h^{n+1}, \nabla \cdot \chi_h) = (\nabla \times \mathbf{f}(t^{n+1}), \chi_h), \end{aligned} \quad (3.3.1)$$

$$(\nabla \cdot \mathbf{w}_h^{n+1}, \tau_h) = 0, \quad (3.3.2)$$

$$(D_H^{n+1} - \nabla \times \mathbf{w}_h^n, \rho_H) = 0, \quad (3.3.3)$$

$$\mathbf{w}_h^{n+1} = I_h(\nabla \times \mathbf{u}_h^{n+1}) \quad \text{on} \quad \partial\Omega, \quad (3.3.4)$$

$$\mathbf{w}_h^{n+1} = I_h(\nabla \times \mathbf{u}_h^0) \quad \text{for} \quad t = 0, \quad (3.3.5)$$

where  $I_h : \nabla \times \mathbf{X}_h \rightarrow \tilde{\mathbf{X}}_h$  is an interpolation operator and  $\lambda_h$  is a multiplier which stands for the discrete divergence-free condition for vorticity. Note that due to (3.3.2),  $\mathbf{w}_h$  is also in  $\mathbf{X}_h$ .

We first state the energy balance of the SAV method.

**Theorem 3.3.1** *Solutions of Scheme (3.2.1)-(3.2.3) satisfy the discrete energy balance:*

$$\begin{aligned} & \|\mathbf{u}_h^N\|^2 + \|2\mathbf{u}_h^N - \mathbf{u}_h^{N-1}\|^2 \\ & + \Delta t \sum_{n=1}^{N-1} \left( \nu \|\nabla \mathbf{u}_h^{n+1}\|^2 + \alpha_1(\nabla \times (\mathbf{u}_h^{n+1} - \mathbf{u}_h^n), \nabla \times \mathbf{u}_h^{n+1}) + \alpha_2 \|\nabla \cdot \mathbf{u}_h^{n+1}\|^2 \right) \\ & = \|\mathbf{u}_h^1\|^2 + \|2\mathbf{u}_h^1 - \mathbf{u}_h^0\|^2 + (\mathbf{f}(t^{n+1}), \mathbf{u}_h^{n+1}). \end{aligned} \quad (3.3.6)$$

**Proof.** Set  $\mathbf{v}_h = \mathbf{u}_h^{n+1}$  in (3.2.1) and  $q_h = p_h^{n+1}$  in (3.2.2), and use the identity

$$a(3a - 4b + c) = \frac{1}{2}((a^2 - b^2) + (2a - b)^2 - (2b - c)^2 + (a - 2b + c)^2).$$

This yields

$$\begin{aligned} & \frac{1}{4\Delta t} \|\mathbf{u}_h^{n+1}\|^2 - \frac{1}{4\Delta t} \|\mathbf{u}_h^n\|^2 + \frac{1}{2\Delta t} \|2\mathbf{u}_h^{n+1} - \mathbf{u}_h^n\|^2 - \frac{1}{2\Delta t} \|2\mathbf{u}_h^n - \mathbf{u}_h^{n-1}\|^2 \\ & + \frac{1}{2\Delta t} \|\mathbf{u}_h^{n+1} - 2\mathbf{u}_h^n + \mathbf{u}_h^{n-1}\|^2 + \alpha_1(\nabla \times (\mathbf{u}_h^{n+1} - \mathbf{u}_h^n), \nabla \times \mathbf{u}_h^{n+1}) \\ & + \nu \|\nabla \mathbf{u}_h^{n+1}\|^2 + \alpha_2 \|\nabla \cdot \mathbf{u}_h^{n+1}\|^2 = (\mathbf{f}(t^{n+1}), \mathbf{u}_h^{n+1}), \end{aligned} \quad (3.3.7)$$

Now, summing from  $n = 1$  to  $N - 1$  and multiplying each term by  $4\Delta t$  proves the stated result.  $\square$

We give the helicity balance of the scheme by using (3.3.1) – (3.3.5).

**Theorem 3.3.2** *Solutions of Scheme (3.2.1)-(3.2.3) satisfy the following discrete helicity balance:*

$$\begin{aligned} & (\mathbf{w}_h^N, \mathbf{u}_h^N) + (2\mathbf{w}_h^N - \mathbf{w}_h^{N-1}, 2\mathbf{u}_h^N - \mathbf{u}_h^{N-1}) \\ & + \sum_{n=1}^{N-1} (\mathbf{w}_h^{n+1} - 2\mathbf{w}_h^n + \mathbf{w}_h^{n-1}, \mathbf{u}_h^{n+1} - 2\mathbf{u}_h^n + \mathbf{u}_h^{n-1}) \\ & + \Delta t \nu \sum_{n=1}^{N-1} (\nabla \mathbf{w}_h^{n+1}, \nabla \mathbf{u}_h^{n+1}) + \Delta t \alpha_1 \sum_{n=1}^{N-1} (\nabla \times \mathbf{w}_h^{n+1}, \nabla \times (\mathbf{u}_h^{n+1} - \mathbf{u}_h^n)) \\ & + \Delta t \alpha_2 \sum_{n=1}^{N-1} (\nabla \cdot \mathbf{w}_h^{n+1}, \nabla \cdot \mathbf{u}_h^{n+1}) = (\mathbf{w}_h^1, \mathbf{u}_h^1) + (2\mathbf{w}_h^1 - \mathbf{w}_h^0, 2\mathbf{u}_h^1 - \mathbf{u}_h^0) \\ & + 2\Delta t \sum_{n=1}^{N-1} \left( (\mathbf{f}(t^{n+1}), \mathbf{w}_h^{n+1}) + (\nabla \times \mathbf{f}(t^{n+1}), \mathbf{u}_h^{n+1}) \right). \end{aligned} \quad (3.3.8)$$

**Proof.** Choose  $\mathbf{v}_h = \mathbf{w}_h^{n+1}$  in (3.2.1) and  $\chi_h = \mathbf{u}_h^{n+1}$  in (3.3.1). Then, the pressure term and one of the nonlinear terms in (3.3.1) vanish and we get

$$\begin{aligned} & \left( \frac{3\mathbf{u}_h^{n+1} - 4\mathbf{u}_h^n + \mathbf{u}_h^{n-1}}{2\Delta t}, \mathbf{w}_h^{n+1} \right) + \nu (\nabla \mathbf{u}_h^{n+1}, \nabla \mathbf{w}_h^{n+1}) + b^*(2\mathbf{u}_h^n - \mathbf{u}_h^{n-1}, \mathbf{u}_h^{n+1}, \mathbf{w}_h^{n+1}) \\ & + \alpha_1 (\nabla \times \mathbf{u}_h^{n+1}, \nabla \times \mathbf{w}_h^{n+1}) - \alpha_1 (S_H^{n+1}, \nabla \times \mathbf{w}_h^{n+1}) \\ & + \alpha_2 (\nabla \cdot \mathbf{u}_h^{n+1}, \nabla \cdot \mathbf{w}_h^{n+1}) = (\mathbf{f}(t^{n+1}), \mathbf{w}_h^{n+1}) \end{aligned} \quad (3.3.9)$$

and

$$\begin{aligned}
& \left( \frac{3\mathbf{w}_h^{n+1} - 4\mathbf{w}_h^n + \mathbf{w}_h^{n-1}}{2\Delta t}, \mathbf{u}_h \right) + \nu(\nabla \mathbf{w}_h^{n+1}, \nabla \mathbf{u}_h^{n+1}) + b^*(2\mathbf{u}_h^n - \mathbf{u}_h^{n-1}, \mathbf{w}_h^{n+1}, \mathbf{u}_h^{n+1}) \\
& \quad + \alpha_1(\nabla \times \mathbf{w}_h^{n+1}, \nabla \times \mathbf{u}_h^{n+1}) - \alpha_1(D_H^{n+1}, \nabla \times \mathbf{u}_h^{n+1}) \\
& \quad + \alpha_2(\nabla \cdot \mathbf{w}_h^{n+1}, \nabla \cdot \mathbf{u}_h^{n+1}) = (\nabla \times \mathbf{f}(t^{n+1}), \mathbf{u}_h^{n+1}). \quad (3.3.10)
\end{aligned}$$

Now, setting  $l_H = \nabla \times \mathbf{w}_h^{n+1}$  in (3.2.3) and  $\rho_H = \nabla \times \mathbf{u}_h^{n+1}$  in (3.3.3) we get

$$(S_H^{n+1}, \nabla \times \mathbf{w}_h^{n+1}) = (\nabla \times \mathbf{u}_h^n, \nabla \times \mathbf{w}_h^{n+1}), \quad (3.3.11)$$

and

$$(D_H^{n+1}, \nabla \times \mathbf{u}_h^{n+1}) = (\nabla \times \mathbf{w}_h^n, \nabla \times \mathbf{u}_h^{n+1}). \quad (3.3.12)$$

Then, substituting (3.3.11) into the equation (3.3.9) and (3.3.12) into the equation (3.3.10) leads to

$$\begin{aligned}
& \left( \frac{3\mathbf{u}_h^{n+1} - 4\mathbf{u}_h^n + \mathbf{u}_h^{n-1}}{2\Delta t}, \mathbf{w}_h^{n+1} \right) + \nu(\nabla \mathbf{u}_h^{n+1}, \nabla \mathbf{w}_h^{n+1}) \\
& \quad + b^*(2\mathbf{u}_h^n - \mathbf{u}_h^{n-1}, \mathbf{u}_h^{n+1}, \mathbf{w}_h^{n+1}) + \alpha_1(\nabla \times (\mathbf{u}_h^{n+1} - \mathbf{u}_h^n), \nabla \times \mathbf{w}_h^{n+1}) \\
& \quad + \alpha_2(\nabla \cdot \mathbf{u}_h^{n+1}, \nabla \cdot \mathbf{w}_h^{n+1}) = (\mathbf{f}(t^{n+1}), \mathbf{w}_h^{n+1}), \quad (3.3.13)
\end{aligned}$$

and

$$\begin{aligned}
& \left( \frac{3\mathbf{w}_h^{n+1} - 4\mathbf{w}_h^n + \mathbf{w}_h^{n-1}}{2\Delta t}, \mathbf{u}_h \right) + \nu(\nabla \mathbf{w}_h^{n+1}, \nabla \mathbf{u}_h^{n+1}) \\
& \quad + b^*(2\mathbf{u}_h^n - \mathbf{u}_h^{n-1}, \mathbf{w}_h^{n+1}, \mathbf{u}_h^{n+1}) + \alpha_1(\nabla \times (\mathbf{w}_h^{n+1} - \mathbf{w}_h^n), \nabla \times \mathbf{u}_h^{n+1}) \\
& \quad + \alpha_2(\nabla \cdot \mathbf{w}_h^{n+1}, \nabla \cdot \mathbf{u}_h^{n+1}) = (\nabla \times \mathbf{f}(t^{n+1}), \mathbf{u}_h^{n+1}). \quad (3.3.14)
\end{aligned}$$

Next, rewriting the first terms on the left hand sides of (3.3.13) and (3.3.14) yields

$$\begin{aligned}
& \frac{1}{4\Delta t}(\mathbf{u}_h^{n+1}, \mathbf{w}_h^{n+1}) - \frac{1}{4\Delta t}(\mathbf{u}_h^n, \mathbf{w}_h^n) \\
& \quad + \frac{1}{4\Delta t}(2\mathbf{u}_h^{n+1} - \mathbf{u}_h^n, \mathbf{w}_h^{n+1} - \mathbf{w}_h^n) - \frac{1}{4\Delta t}(2\mathbf{u}_h^n - \mathbf{u}_h^{n-1}, \mathbf{w}_h^n - \mathbf{w}_h^{n-1}) \\
& \quad + \frac{1}{4\Delta t}(\mathbf{u}_h^{n+1} - 2\mathbf{u}_h^n + \mathbf{u}_h^{n-1}, \mathbf{w}_h^{n+1} - 2\mathbf{w}_h^n + \mathbf{w}_h^{n-1}) \\
& \quad + \nu(\nabla \mathbf{u}_h^{n+1}, \nabla \mathbf{w}_h^{n+1}) + b^*(2\mathbf{u}_h^n - \mathbf{u}_h^{n-1}, \mathbf{u}_h^{n+1}, \mathbf{w}_h^{n+1}) \\
& \quad + \alpha_1(\nabla \times (\mathbf{u}_h^{n+1} - \mathbf{u}_h^n), \nabla \times \mathbf{w}_h^{n+1}) + \alpha_2(\nabla \cdot \mathbf{u}_h^{n+1}, \nabla \cdot \mathbf{w}_h^{n+1}) = (\mathbf{f}(t^{n+1}), \mathbf{w}_h^{n+1}),
\end{aligned}$$



and

$$\begin{aligned}
& \frac{1}{4\Delta t}(\mathbf{w}_h^{n+1}, \mathbf{u}_h^{n+1}) - \frac{1}{4\Delta t}(\mathbf{w}_h^n, \mathbf{u}_h^n) \\
& + \frac{1}{4\Delta t}(2\mathbf{w}_h^{n+1} - \mathbf{w}_h^n, \mathbf{u}_h^{n+1} - \mathbf{u}_h^n) - \frac{1}{4\Delta t}(2\mathbf{w}_h^n - \mathbf{w}_h^{n-1}, \mathbf{u}_h^n - \mathbf{u}_h^{n-1}) \\
& + \frac{1}{4\Delta t}(\mathbf{w}_h^{n+1} - 2\mathbf{w}_h^n + \mathbf{w}_h^{n-1}, \mathbf{u}_h^{n+1} - 2\mathbf{u}_h^n + \mathbf{u}_h^{n-1}) \\
& + \nu(\nabla \mathbf{w}_h^{n+1}, \nabla \mathbf{u}_h^{n+1}) + b^*(2\mathbf{u}_h^n - \mathbf{u}_h^{n-1}, \mathbf{w}_h^{n+1}, \mathbf{u}_h^{n+1}) \\
& + \alpha_1(\nabla \times (\mathbf{w}_h^{n+1} - \mathbf{w}_h^n), \nabla \times \mathbf{u}_h^{n+1}) + \alpha_2(\nabla \cdot \mathbf{w}_h^{n+1}, \nabla \cdot \mathbf{u}_h^{n+1}) \\
& = (\nabla \times \mathbf{f}(t^{n+1}), \mathbf{u}_h^{n+1}).
\end{aligned}$$

Add these two equations and use (3.1.8) to obtain

$$\begin{aligned}
& \frac{1}{2\Delta t}(\mathbf{u}_h^{n+1}, \mathbf{w}_h^{n+1}) - \frac{1}{2\Delta t}(\mathbf{u}_h^n, \mathbf{w}_h^n) + \frac{1}{2\Delta t}(2\mathbf{u}_h^{n+1} - \mathbf{u}_h^n, \mathbf{w}_h^{n+1} - \mathbf{w}_h^n) \\
& - \frac{1}{2\Delta t}(2\mathbf{u}_h^n - \mathbf{u}_h^{n-1}, \mathbf{w}_h^n - \mathbf{w}_h^{n-1}) \\
& + \frac{1}{2\Delta t}(\mathbf{u}_h^{n+1} - 2\mathbf{u}_h^n + \mathbf{u}_h^{n-1}, \mathbf{w}_h^{n+1} - 2\mathbf{w}_h^n + \mathbf{w}_h^{n-1}) \\
& + 2\alpha_1(\nabla \times (\mathbf{u}_h^{n+1} - \mathbf{u}_h^n), \nabla \times \mathbf{w}_h^{n+1}) + 2\nu(\nabla \mathbf{u}_h^{n+1}, \nabla \mathbf{w}_h^{n+1}) \\
& + 2\alpha_2(\nabla \cdot \mathbf{u}_h^{n+1}, \nabla \cdot \mathbf{w}_h^{n+1}) = (\mathbf{f}(t^{n+1}), \mathbf{w}_h^{n+1}) + (\nabla \times \mathbf{f}(t^{n+1}), \mathbf{u}_h^{n+1}).
\end{aligned}$$

Finally, summing over time steps and multiplying both sides by  $2\Delta t$  gives the required helicity balance.  $\square$

### 3.4 Numerical Analysis

This section provides unconditional stability results and convergence analysis of the proposed Algorithm 3.2. To do this, for theoretical analysis we present the finite element discretization in  $\mathbf{V}_h$ .

Then, BDF2LE based SAV method in  $\mathbf{V}_h$  reads as follows: Find  $(\mathbf{u}_h^{n+1}, S_H^{n+1}) \in (\mathbf{V}_h, L_H)$  satisfying  $\forall (\mathbf{v}_h, l_H) \in (\mathbf{V}_h, L_H)$ .

$$\begin{aligned}
& \left( \frac{3\mathbf{u}_h^{n+1} - 4\mathbf{u}_h^n + \mathbf{u}_h^{n-1}}{2\Delta t}, \mathbf{v}_h \right) + \nu(\nabla \mathbf{u}_h^{n+1}, \nabla \mathbf{v}_h) + b^*(2\mathbf{u}_h^n - \mathbf{u}_h^{n-1}, \mathbf{u}_h^{n+1}, \mathbf{v}_h) \\
& + \alpha_1(\nabla \times \mathbf{u}_h^{n+1}, \nabla \times \mathbf{v}_h) - \alpha_1(S_H^{n+1}, \nabla \times \mathbf{v}_h) \\
& + \alpha_2(\nabla \cdot \mathbf{u}_h^{n+1}, \nabla \cdot \mathbf{v}_h) = (\mathbf{f}(t^{n+1}), \mathbf{v}_h) \quad (3.4.1)
\end{aligned}$$

$$(S_H^{n+1} - \nabla \times \mathbf{u}_h^n, l_H) = 0 \quad (3.4.2)$$

The following lemma is required for proving the existence of discrete solutions to (3.4.1)-(3.4.2), see [155]. This motivates the more detailed error analysis that follows.

**Lemma 3.4.1** *Let  $\mathbf{f} \in L^\infty(0, T; H^{-1}(\Omega))$  and  $\mathbf{u}_h$  be a solution of Scheme (3.2.1)-(3.2.3). Then, for any  $\Delta t > 0$  and  $N \geq 1$*

$$\begin{aligned} \|\mathbf{u}_h^N\|^2 + \|2\mathbf{u}_h^N - \mathbf{u}_h^{N-1}\|^2 + 2\Delta t \sum_{n=1}^{N-1} (\nu \|\nabla \mathbf{u}_h^{n+1}\|^2 + 2\alpha_2 \|\nabla \cdot \mathbf{u}_h^{n+1}\|^2) \\ + 2\alpha_1 \Delta t \|\nabla \times \mathbf{u}_h^N\|^2 \leq \|\mathbf{u}_h^1\|^2 + \|2\mathbf{u}_h^1 - \mathbf{u}_h^0\|^2 \\ + 2\alpha_1 \Delta t \|\nabla \times \mathbf{u}_h^1\|^2 + 2\Delta t \sum_{n=1}^{N-1} \nu^{-1} \|\mathbf{f}(t^{n+1})\|_{-1}^2. \end{aligned} \quad (3.4.3)$$

**Proof.** To start the proof, we first choose  $\mathbf{v}_h = \mathbf{u}_h^{n+1}$  in (3.4.1), vanishing the skew-symmetric trilinear term to obtain

$$\begin{aligned} \left( \frac{3\mathbf{u}_h^{n+1} - 4\mathbf{u}_h^n + \mathbf{u}_h^{n-1}}{2\Delta t}, \mathbf{u}_h^{n+1} \right) + v(\nabla \mathbf{u}_h^{n+1}, \nabla \mathbf{u}_h^{n+1}) + \alpha_1(\nabla \times \mathbf{u}_h^{n+1}, \nabla \times \mathbf{u}_h^{n+1}) \\ + \alpha_2(\nabla \cdot \mathbf{u}_h^{n+1}, \nabla \cdot \mathbf{u}_h^{n+1}) = \alpha_1(S_H^{n+1}, \nabla \times \mathbf{u}_h^{n+1}) + (\mathbf{f}(t^{n+1}), \mathbf{u}_h^{n+1}). \end{aligned} \quad (3.4.4)$$

Next, for the first term in the left-hand side of (3.4.4), we use the identity;

$$\frac{1}{2}(3a - 4b + c)a = \frac{1}{4}[a^2 + (2a - b)^2] - \frac{1}{4}[b^2 + (2b - c)^2] + \frac{1}{4}(a - 2b + c)^2 \quad (3.4.5)$$

Then, one has

$$\begin{aligned} \frac{1}{4\Delta t} \left[ \|\mathbf{u}_h^{n+1}\|^2 + \|2\mathbf{u}_h^{n+1} - \mathbf{u}_h^n\|^2 \right] - \frac{1}{4\Delta t} \left[ \|\mathbf{u}_h^n\|^2 + \|2\mathbf{u}_h^n - \mathbf{u}_h^{n-1}\|^2 \right] \\ + \frac{1}{4\Delta t} \|\mathbf{u}_h^{n+1} - 2\mathbf{u}_h^n + \mathbf{u}_h^{n-1}\|^2 + \nu \|\nabla \mathbf{u}_h^{n+1}\|^2 + \alpha_1 \|\nabla \times \mathbf{u}_h^{n+1}\|^2 \\ + \alpha_2 \|\nabla \cdot \mathbf{u}_h^{n+1}\|^2 = \alpha_1(S_H^{n+1}, \nabla \times \mathbf{u}_h^{n+1}) + (\mathbf{f}(t^{n+1}), \mathbf{u}_h^{n+1}) \end{aligned} \quad (3.4.6)$$

The application of Cauchy-Schwarz inequality, Young's inequality, and the dual norm on the right-hand side terms of (5.3.5) gives

$$\begin{aligned} \frac{1}{4\Delta t} \left[ \|\mathbf{u}_h^{n+1}\|^2 + \|2\mathbf{u}_h^{n+1} - \mathbf{u}_h^n\|^2 \right] - \frac{1}{4\Delta t} \left[ \|\mathbf{u}_h^n\|^2 + \|2\mathbf{u}_h^n - \mathbf{u}_h^{n-1}\|^2 \right] \\ + \frac{1}{4\Delta t} \|\mathbf{u}_h^{n+1} - 2\mathbf{u}_h^n + \mathbf{u}_h^{n-1}\|^2 + \frac{\nu}{2} \|\nabla \mathbf{u}_h^{n+1}\|^2 + \frac{\alpha_1}{2} \|\nabla \times \mathbf{u}_h^{n+1}\|^2 \\ + \alpha_2 \|\nabla \cdot \mathbf{u}_h^{n+1}\|^2 \leq \frac{\alpha_1}{2} \|S_H^{n+1}\|^2 + \frac{1}{2\nu} \|\mathbf{f}(t^{n+1})\|_{-1}^2 \end{aligned} \quad (3.4.7)$$

Note that choosing  $l_H = S_H^{n+1}$  in (3.4.2) and using the Cauchy-Schwarz and Young's inequalities, we obtain the following bound for the first term on the right-hand side of (3.4.7)

$$\|S_H^{n+1}\|^2 = (S_H^{n+1}, \nabla \times \mathbf{u}_h^n) \leq \|\nabla \times \mathbf{u}_h^n\| \|S_H^{n+1}\| \leq \frac{1}{2} \|\nabla \times \mathbf{u}_h^n\|^2 + \frac{1}{2} \|S_H^{n+1}\|^2,$$

so that

$$\|S_H^{n+1}\| \leq \|\nabla \times \mathbf{u}_h^n\|. \quad (3.4.8)$$

Using the above inequality, dropping the non-negative term  $\frac{1}{4\Delta t} \|\mathbf{u}_h^{n+1} - 2\mathbf{u}_h^n + \mathbf{u}_h^{n-1}\|^2$  and rearranging terms in (3.4.7), we obtain

$$\begin{aligned} \frac{1}{4\Delta t} \left[ \|\mathbf{u}_h^{n+1}\|^2 - \|\mathbf{u}_h^n\|^2 \right] + \frac{1}{4\Delta t} \left[ \|2\mathbf{u}_h^{n+1} - \mathbf{u}_h^n\|^2 - \|2\mathbf{u}_h^n - \mathbf{u}_h^{n-1}\|^2 \right] + \frac{\nu}{2} \|\nabla \mathbf{u}_h^{n+1}\|^2 \\ + \frac{\alpha_1}{2} \|\nabla \times \mathbf{u}_h^{n+1}\|^2 + \alpha_2 \|\nabla \cdot \mathbf{u}_h^{n+1}\|^2 \leq \frac{\alpha_1}{2} \|\nabla \times \mathbf{u}_h^n\|^2 + \frac{\nu^{-1}}{2} \|\mathbf{f}(t^{n+1})\|_{-1}^2. \end{aligned}$$

Multiplying both sides of the inequality by  $4\Delta t$  and taking the sum from  $n = 1$  to  $n = N - 1$  yields the required stability bound.  $\square$

We proceed to present an error analysis of our method. To obtain the optimal error estimations, we assume that the following regularity assumptions are satisfied by the analytical solution:

$$\begin{aligned} \mathbf{u} \in L^\infty(0, T; H^1(\Omega)) \cap H^1(0, T; H^{k+1}(\Omega)) \cap H^3(0, T; L^2(\Omega)) \cap H^2(0, T; H^1(\Omega)), \\ p \in L^2(0, T; H^k(\Omega)). \end{aligned} \quad (3.4.9)$$

**Theorem 3.4.1** *Let  $(\mathbf{u}, p)$  be the solution of the NSE such that the regularity assumptions (3.4.9) are satisfied. Then, for any  $N$ , the following bound holds for the difference  $\mathbf{e}^n = \mathbf{u}^n - \mathbf{u}_h^n$ :*

$$\begin{aligned}
& \|e^N\|^2 + \|2e^N - e^{N-1}\|^2 + \sum_{n=1}^{N-1} \|e^{n+1} - 2e^n + e^{n-1}\|^2 + \nu\Delta t \sum_{n=1}^{N-1} \|\nabla e^{n+1}\|^2 \\
& \leq \exp(C\nu^{-1}T) \left[ \|e^1\|^2 + \|2e^1 - e^0\|^2 + \nu^{-1}h^{2k+2} \|\mathbf{u}_t\|_{2,k+1}^2 \right. \\
& \quad + \nu^{-1}h^{2k} \|\mathbf{u}\|_{2,k+1}^2 \|\nabla \mathbf{u}\|_{\infty,0}^2 + (\nu + \nu^{-1}\alpha_1^2 + \alpha_2 + \nu^{-2})h^{2k} \|\mathbf{u}\|_{2,k+1}^2 \\
& \quad + \alpha_2^{-1}h^{2k+2} \|p\|_{2,k+1}^2 + \alpha_1 h^{2k} \|\mathbf{u}\|_{2,k+1}^2 + \alpha_1 H^{2k} \|\mathbf{u}\|_{2,k+1}^2 \\
& \quad + \alpha_1 \Delta t^2 \|\mathbf{u}_t\|_{\infty,0}^2 + \nu^{-1} \Delta t^4 \|\mathbf{u}_{ttt}\|_{2,0}^2 \\
& \quad \left. + \nu^{-1} \Delta t^4 \|\nabla \mathbf{u}\|_{\infty,0}^2 \|\nabla \mathbf{u}_{tt}\|_{2,0}^2 \right] \tag{3.4.10}
\end{aligned}$$

**Proof.** To obtain the error equation, denote  $\mathbf{u}(t^n) = \mathbf{u}^n$ . Then, the true solutions  $(\mathbf{u}_h^{n+1}, p_h^{n+1}, S_H^{n+1})$  at time level  $t^{n+1}$  satisfy

$$\begin{aligned}
& \left( \frac{3\mathbf{u}^{n+1} - 4\mathbf{u}^n + \mathbf{u}^{n-1}}{2\Delta t}, \mathbf{v}_h \right) + \nu(\nabla \mathbf{u}^{n+1}, \nabla \mathbf{v}_h) + b^*(2\mathbf{u}^n - \mathbf{u}^{n-1}, \mathbf{u}^{n+1}, \mathbf{v}_h) \\
& \quad + \alpha_1(\nabla \times \mathbf{u}^{n+1}, \nabla \times \mathbf{v}_h) - \alpha_1(\nabla \times \mathbf{u}^{n+1}, \nabla \times \mathbf{v}_h) + \alpha_2(\nabla \cdot \mathbf{u}^{n+1}, \nabla \cdot \mathbf{v}_h) \\
& \quad - (p^{n+1}, \nabla \cdot \mathbf{v}_h) = (f^{n+1}, \mathbf{v}_h) + \text{Intp}(\mathbf{u}^{n+1}; \mathbf{v}_h) \tag{3.4.11}
\end{aligned}$$

where the local truncation error is

$$\begin{aligned}
\text{Intp}(\mathbf{u}^{n+1}, \mathbf{v}_h) &= \left( \frac{3\mathbf{u}^{n+1} - 4\mathbf{u}^n + \mathbf{u}^{n-1}}{2\Delta t} - \mathbf{u}_t^{n+1}, \mathbf{v}_h \right) \\
& \quad + b^*(2\mathbf{u}^n - \mathbf{u}^{n-1}, \mathbf{u}^{n+1}, \mathbf{v}_h) - b^*(\mathbf{u}^{n+1}, \mathbf{u}^{n+1}, \mathbf{v}_h).
\end{aligned}$$

Subtracting the equation (3.4.1) from (3.4.11) yields

$$\begin{aligned}
& \left( \frac{3e^{n+1} - 4e^n + e^{n-1}}{2\Delta t}, \mathbf{v}_h \right) + \nu(\nabla e^{n+1}, \nabla \mathbf{v}_h) + b^*(2\mathbf{u}^n - \mathbf{u}^{n-1}, \mathbf{u}^{n+1}, \mathbf{v}_h) \\
& \quad - b^*(2\mathbf{u}_h^n - \mathbf{u}_h^{n-1}, \mathbf{u}_h^{n+1}, \mathbf{v}_h) + \alpha_1(\nabla \times e^{n+1}, \nabla \times \mathbf{v}_h) + \alpha_2(\nabla \cdot e^{n+1}, \nabla \cdot \mathbf{v}_h) \\
& \quad = \alpha_1(\nabla \times \mathbf{u}^{n+1} - S_H^{n+1}, \nabla \times \mathbf{v}_h) + (p^{n+1}, \nabla \cdot \mathbf{v}_h) + \text{Intp}(\mathbf{u}^{n+1}; \mathbf{v}_h) \tag{3.4.12}
\end{aligned}$$

Adding and subtracting terms for the convective terms, by using the properties (3.1.8), one gets

$$\begin{aligned}
& b^*(2\mathbf{u}^n - \mathbf{u}^{n-1}, \mathbf{u}^{n+1}, \mathbf{v}_h) - b^*(2\mathbf{u}_h^n - \mathbf{u}_h^{n-1}, \mathbf{u}_h^{n+1}, \mathbf{v}_h) \\
& = b^*(2\mathbf{u}^n - \mathbf{u}^{n-1}, \mathbf{u}^{n+1}, \mathbf{v}_h) - b^*(2\mathbf{u}_h^n - \mathbf{u}_h^{n-1}, \mathbf{u}_h^{n+1}, \mathbf{v}_h) \\
& \quad + b^*(2\mathbf{u}_h^n - \mathbf{u}_h^{n-1}, \mathbf{u}^{n+1}, \mathbf{v}_h) - b^*(2\mathbf{u}_h^n - \mathbf{u}_h^{n-1}, \mathbf{u}_h^{n+1}, \mathbf{v}_h) \\
& = b^*(2e^n - e^{n-1}, \mathbf{u}^{n+1}, \mathbf{v}_h) + b^*(2\mathbf{u}_h^n - \mathbf{u}_h^{n-1}, e^{n+1}, \mathbf{v}_h). \tag{3.4.13}
\end{aligned}$$

Decompose the velocity error in the usual way:

$$\mathbf{e}^n = (\mathbf{u}^n - I_{\mathbf{u}}(\mathbf{u}^n)) + (I_{\mathbf{u}}(\mathbf{u}^n) - \mathbf{u}_h^n) = \boldsymbol{\eta}^n + \boldsymbol{\phi}_h^n, \quad (3.4.14)$$

where  $I_{\mathbf{u}}(\mathbf{u}^n)$  is an interpolant of  $\mathbf{u}^n$  in  $V_h$ .

Using error decomposition,  $\mathbf{v}_h = \boldsymbol{\phi}_h^{n+1}$  in the (3.1.8) yields

$$\begin{aligned} & \frac{1}{4\Delta t} \left[ \|\boldsymbol{\phi}_h^{n+1}\|^2 + \|2\boldsymbol{\phi}_h^{n+1} - \boldsymbol{\phi}_h^n\|^2 \right] - \frac{1}{4\Delta t} \left[ \|\boldsymbol{\phi}_h^n\|^2 + \|2\boldsymbol{\phi}_h^n - \boldsymbol{\phi}_h^{n-1}\|^2 \right] \\ & + \frac{1}{4\Delta t} \|\boldsymbol{\phi}_h^{n+1} - 2\boldsymbol{\phi}_h^n + \boldsymbol{\phi}_h^{n-1}\|^2 + \nu \|\nabla \boldsymbol{\phi}_h^{n+1}\|^2 \\ & + \alpha_1 \|\nabla \times \boldsymbol{\phi}_h^{n+1}\|^2 + \alpha_2 \|\nabla \cdot \boldsymbol{\phi}_h^{n+1}\|^2 \\ = & - \left( \frac{3\boldsymbol{\eta}^{n+1} - 4\boldsymbol{\eta}^n + \boldsymbol{\eta}^{n-1}}{2\Delta t}, \boldsymbol{\phi}_h^{n+1} \right) - \nu (\nabla \boldsymbol{\eta}^{n+1}, \nabla \boldsymbol{\phi}_h^{n+1}) \\ & - b^*(2\mathbf{u}_h^n - \mathbf{u}_h^{n-1}, \boldsymbol{\eta}^{n+1}, \boldsymbol{\phi}_h^{n+1}) - b^*(2\boldsymbol{\eta}^n - \boldsymbol{\eta}^{n-1}, \mathbf{u}^{n+1}, \boldsymbol{\phi}_h^{n+1}) \\ & - b^*(2\boldsymbol{\phi}_h^n - \boldsymbol{\phi}_h^{n-1}, \mathbf{u}^{n+1}, \boldsymbol{\phi}_h^{n+1}) - \alpha_1 (\nabla \times \boldsymbol{\eta}^{n+1}, \nabla \times \boldsymbol{\phi}_h^{n+1}) \\ & + \alpha_1 (\nabla \times \mathbf{u}^{n+1} - S_H^{n+1}, \nabla \times \boldsymbol{\phi}_h^{n+1}) - \alpha_2 (\nabla \cdot \boldsymbol{\eta}^{n+1}, \nabla \cdot \boldsymbol{\phi}_h^{n+1}) \\ & + (p^{n+1} - q_h, \nabla \cdot \boldsymbol{\phi}_h^{n+1}) + \text{Intp}(\mathbf{u}^{n+1}; \boldsymbol{\phi}_h^{n+1}) \end{aligned} \quad (3.4.15)$$

The terms on the right-hand side of (3.4.15) have to be bounded. For the first term, applying Cauchy-Schwarz, Poincaré-Friedrichs inequalities, the estimation (3.1.17) and Young's inequality, one gets

$$\begin{aligned} \left| - \left( \frac{3\boldsymbol{\eta}^{n+1} - 4\boldsymbol{\eta}^n + \boldsymbol{\eta}^{n-1}}{2\Delta t}, \boldsymbol{\phi}_h^{n+1} \right) \right| & \leq \left\| \frac{3\boldsymbol{\eta}^{n+1} - 4\boldsymbol{\eta}^n + \boldsymbol{\eta}^{n-1}}{2\Delta t} \right\| \|\nabla \boldsymbol{\phi}_h^{n+1}\| \\ & \leq \frac{C\nu^{-1}}{\Delta t} \int_{t^{n-1}}^{t^{n+1}} \|\boldsymbol{\eta}_t\|^2 dt \\ & \quad + \frac{\nu}{16} \|\nabla \boldsymbol{\phi}_h^{n+1}\|^2. \end{aligned} \quad (3.4.16)$$

The viscosity term is bounded by using Cauchy-Schwarz and Young's inequalities:

$$\begin{aligned} \left| -\nu (\nabla \boldsymbol{\eta}^{n+1}, \nabla \boldsymbol{\phi}_h^{n+1}) \right| & \leq \nu \|\nabla \boldsymbol{\eta}^{n+1}\| \|\nabla \boldsymbol{\phi}_h^{n+1}\| \\ & \leq C\nu \|\nabla \boldsymbol{\eta}^{n+1}\|^2 + \frac{\nu}{16} \|\nabla \boldsymbol{\phi}_h^{n+1}\|^2. \end{aligned} \quad (3.4.17)$$

We proceed to bound the convective terms using Cauchy-Schwarz, Poincaré-Friedrichs, Young's inequalities and the estimation (3.1.9):

$$\begin{aligned} \left| -b^*(2\mathbf{u}_h^n - \mathbf{u}_h^{n-1}, \boldsymbol{\eta}^{n+1}, \boldsymbol{\phi}_h^{n+1}) \right| & \leq C (\|\nabla \mathbf{u}_h^n\| + \|\nabla \mathbf{u}_h^{n-1}\|) \|\nabla \boldsymbol{\eta}^{n+1}\| \|\nabla \boldsymbol{\phi}_h^{n+1}\| \\ & \leq C\nu^{-1} \|\nabla \boldsymbol{\eta}^{n+1}\|^2 (\|\nabla \mathbf{u}_h^n\|^2 + \|\nabla \mathbf{u}_h^{n-1}\|^2) \\ & \quad + \frac{\nu}{16} \|\nabla \boldsymbol{\phi}_h^{n+1}\|^2, \end{aligned} \quad (3.4.18)$$

and

$$\begin{aligned}
| -b^*(2\boldsymbol{\eta}^n - \boldsymbol{\eta}^{n-1}, \mathbf{u}^{n+1}, \boldsymbol{\phi}_h^{n+1}) | &\leq C(\|\nabla\boldsymbol{\eta}^n\| + \|\nabla\boldsymbol{\eta}^{n-1}\|)\|\nabla\mathbf{u}_h^{n+1}\|\|\nabla\boldsymbol{\phi}_h^{n+1}\| \\
&\leq C\nu^{-1}\|\nabla\mathbf{u}^{n+1}\|^2(\|\nabla\boldsymbol{\eta}^n\|^2 + \|\nabla\boldsymbol{\eta}^{n-1}\|^2) \\
&\quad + \frac{\nu}{16}\|\nabla\boldsymbol{\phi}_h^{n+1}\|^2. \tag{3.4.19}
\end{aligned}$$

Using (3.1.10), one gets for the last convective term

$$\begin{aligned}
| -b^*(2\boldsymbol{\phi}_h^n - \boldsymbol{\phi}_h^{n-1}, \mathbf{u}^{n+1}, \boldsymbol{\phi}_h^{n+1}) | &\leq \frac{1}{2}\left(\|2\boldsymbol{\phi}_h^n - \boldsymbol{\phi}_h^{n-1}\|\|\nabla\mathbf{u}^{n+1}\|_\infty\|\boldsymbol{\phi}_h^{n+1}\| + \|2\boldsymbol{\phi}_h^n - \boldsymbol{\phi}_h^{n-1}\|\|\mathbf{u}^{n+1}\|_\infty\|\nabla\boldsymbol{\phi}_h^{n+1}\|\right) \\
&\leq C(\|\boldsymbol{\phi}_h^n\| + \|\boldsymbol{\phi}_h^{n-1}\|)\|\nabla\boldsymbol{\phi}_h^{n+1}\|(\|\nabla\mathbf{u}^{n+1}\|_\infty + \|\mathbf{u}^{n+1}\|_\infty) \\
&\leq C\nu^{-1}(\|\boldsymbol{\phi}_h^n\|^2 + \|\boldsymbol{\phi}_h^{n-1}\|^2)(\|\nabla\mathbf{u}^{n+1}\|_\infty^2 + \|\mathbf{u}^{n+1}\|_\infty^2) + \frac{\nu}{16}\|\nabla\boldsymbol{\phi}_h^{n+1}\|^2. \tag{3.4.20}
\end{aligned}$$

The next couple of estimates will use Cauchy-Schwarz and Young's inequalities and they will also contribute to the error bound. One obtains in a straightforward way

$$| -\alpha_1(\nabla \times \boldsymbol{\eta}^{n+1}, \nabla \times \boldsymbol{\phi}_h^{n+1}) | \leq C\nu^{-1}\alpha_1^2\|\nabla\boldsymbol{\eta}^{n+1}\|^2 + \frac{\nu}{16}\|\nabla\boldsymbol{\phi}_h^{n+1}\|^2 \tag{3.4.21}$$

$$| -\alpha_2(\nabla \cdot \boldsymbol{\eta}^{n+1}, \nabla \cdot \boldsymbol{\phi}_h^{n+1}) | \leq \alpha_2\|\nabla \cdot \boldsymbol{\eta}^{n+1}\|\|\nabla \cdot \boldsymbol{\phi}_h^{n+1}\|$$

$$| -\nu(\nabla\boldsymbol{\eta}^{n+1}, \nabla\boldsymbol{\phi}_h^{n+1}) | \leq C\alpha_2\|\nabla\boldsymbol{\eta}^{n+1}\|^2 + \frac{\alpha_2}{2}\|\nabla \cdot \boldsymbol{\phi}_h^{n+1}\|^2. \tag{3.4.22}$$

Next, we bound the coarse mesh projection term. Using the definition of the  $L^2$ -projection operator  $P_{L_H}$  (3.1.15) and from (3.4.2), one can write  $S_H^{n+1} = P_{L_H}(\nabla \times \mathbf{u}_h^n)$ . Then, we add and subtract  $P_{L_H}(\nabla \times \mathbf{u}^n)$  and  $\nabla \times \mathbf{u}^n$  to the coarse mesh projection term and use error definition, one gets

$$\begin{aligned}
| \alpha_1(\nabla \times \mathbf{u}^{n+1} - S_H^{n+1}, \nabla \times \boldsymbol{\phi}_h^{n+1}) | &= | \alpha_1(P_{L_H}(\nabla \times \mathbf{e}^n) + (I - P_{L_H})(\nabla \times \mathbf{u}^n) + (\nabla \times (\mathbf{u}^{n+1} - \mathbf{u}^n)), \nabla \times \boldsymbol{\phi}_h^{n+1}) |.
\end{aligned}$$

Using error decomposition (3.4.14), Cauchy-Schwarz, and Young's inequalities, inverse estimation and (3.4.8) yields

$$\begin{aligned}
& |\alpha_1(P_{L_H}(\nabla \times \mathbf{e}^n) + (I - P_{L_H})(\nabla \times \mathbf{u}^n) + (\nabla \times (\mathbf{u}^{n+1} - \mathbf{u}^n))), \nabla \times \phi_h^{n+1}| \\
&= \alpha_1(P_{L_H}(\nabla \times \mathbf{e}^n) + (I - P_{L_H})(\nabla \times \mathbf{u}^n) + (\nabla \times \mathbf{u}^{n+1} - \nabla \times \mathbf{u}^n), \nabla \times \phi_h^{n+1}) \\
&= \alpha_1(P_{L_H}(\nabla \times \boldsymbol{\eta}^n), \nabla \times \phi_h^{n+1}) + \alpha_1(P_{L_H}(\nabla \times \phi_h^n), \nabla \times \phi_h^{n+1}) \\
&+ \alpha_1((I - P_{L_H})(\nabla \times \mathbf{u}^n), \nabla \times \phi_h^{n+1}) + \alpha_1((\nabla \times \mathbf{u}^{n+1} - \nabla \times \mathbf{u}^n), \nabla \times \phi_h^{n+1}) \\
&\leq C\alpha_1\|P_{L_H}(\nabla \times \boldsymbol{\eta}^n)\|^2 + C\alpha_1\|P_{L_H}(\nabla \times \phi_h^n)\|^2 \\
&+ C\alpha_1\|(I - P_{L_H})(\nabla \times \mathbf{u}^n)\|^2 + C\alpha_1\|\nabla \times (\mathbf{u}^{n+1} - \mathbf{u}^n)\|^2 + \frac{\alpha_1}{2}\|\nabla \times \phi_h^{n+1}\|^2 \\
&\leq C\alpha_1\|\nabla \boldsymbol{\eta}^n\|^2 + C\alpha_1 h^{-2}\|\phi_h^n\|^2 + C\alpha_1\|(I - P_{L_H})(\nabla \times \mathbf{u}^n)\|^2 \\
&+ C\alpha_1\|\nabla \times (\mathbf{u}^{n+1} - \mathbf{u}^n)\|^2 + \frac{\alpha_1}{2}\|\nabla \times \phi_h^{n+1}\|^2. \tag{3.4.23}
\end{aligned}$$

To bound the pressure term, we use the fact that  $(\nabla \cdot \phi_h, q_h) = 0, \forall q_h \in \mathbf{V}_h$  together with Cauchy-Schwarz and Young's inequalities:

$$|(p(t^{n+1}), \nabla \cdot \phi_h^{n+1})| \leq C\alpha_2^{-1}\|p(t^{n+1}) - q_h\|^2 + \frac{\alpha_2}{4}\|\nabla \cdot \phi_h^{n+1}\|^2. \tag{3.4.24}$$

Finally, the local truncation error  $Intp(\mathbf{u}^{n+1}; \phi_h^{n+1})$  can be bounded as follows. The first term of  $Intp(\mathbf{u}^{n+1}; \phi_h^{n+1})$  is estimated by using Cauchy-Schwarz, Poincaré Friedrichs, Young's, and Hölder's inequalities together with the estimation (3.1.18)

$$\begin{aligned}
& \left| - \left( \mathbf{u}_t(t^{n+1}) - \frac{3\mathbf{u}(t^{n+1}) - 4\mathbf{u}(t^n) + \mathbf{u}(t^{n-1})}{2\Delta t}, \phi_h^{n+1} \right) \right| \\
&\leq \left\| \frac{3\mathbf{u}(t^{n+1}) - 4\mathbf{u}(t^n) + \mathbf{u}(t^{n-1})}{2\Delta t} - \mathbf{u}_t(t^{n+1}) \right\| \|\phi_h^{n+1}\| \\
&\leq C\Delta t^3 \nu^{-1} \int_{t^{n-1}}^{t^{n+1}} \|\mathbf{u}_{ttt}\|^2 dt + \frac{\nu}{16} \|\nabla \phi_h^{n+1}\|^2. \tag{3.4.25}
\end{aligned}$$

To bound the convective terms in  $Intp(\mathbf{u}^{n+1}; \phi_h^{n+1})$ , we first rearrange the terms. Using the bound (3.1.9) and applying Cauchy-Schwarz, Young's and Hölder's inequalities together with the the estimation (3.1.19), we get

$$\begin{aligned}
& b^*(2\mathbf{u}^n - \mathbf{u}^{n-1}, \mathbf{u}^{n+1}, \mathbf{v}_h) - b^*(\mathbf{u}^{n+1}, \mathbf{u}^{n+1}, \mathbf{v}_h) \\
&= b^*(2\mathbf{u}^n - \mathbf{u}^{n-1} - \mathbf{u}^{n+1}, \mathbf{u}^{n+1}, \mathbf{v}_h) \\
&\leq C \|\nabla(2\mathbf{u}^n - \mathbf{u}^{n-1} - \mathbf{u}^{n+1})\| \|\nabla \mathbf{u}^{n+1}\| \|\phi_h^{n+1}\| \\
&\leq C\Delta t^3 \nu^{-1} \|\nabla \mathbf{u}^{n+1}\|^2 \int_{t^{n-1}}^{t^{n+1}} \|\nabla \mathbf{u}_{tt}\|^2 dt \\
&+ \frac{\nu}{16} \|\nabla \phi_h^{n+1}\|^2. \tag{3.4.26}
\end{aligned}$$

Collecting all estimates (3.4.16)-(3.4.26) and the equality (3.4.15) simplifies to

$$\begin{aligned}
& \frac{1}{4\Delta t} \left[ \|\phi_h^{n+1}\|^2 - \|\phi_h^n\|^2 \right] + \frac{1}{4\Delta t} \left[ \|2\phi_h^{n+1} - \phi_h^n\|^2 - \|2\phi_h^n - \phi_h^{n-1}\|^2 \right] \\
& + \frac{1}{4\Delta t} \|\phi_h^{n+1} - 2\phi_h^n + \phi_h^{n-1}\|^2 + \frac{7\nu}{16} \|\nabla \phi_h^{n+1}\|^2 \\
& + \frac{\alpha_1}{2} \|\nabla \times \phi_h^{n+1}\|^2 + \frac{\alpha_2}{4} \|\nabla \cdot \phi_h^{n+1}\|^2 \\
\leq & \frac{C\nu^{-1}}{\Delta t} \int_{t^{n-1}}^{t^{n+1}} \|\eta_t\|^2 dt \\
& + C\nu^{-1} \|\nabla \eta^{n+1}\|^2 (\|\nabla \mathbf{u}_h^n\|^2 + \|\nabla \mathbf{u}_h^{n-1}\|^2) \\
& + C\nu^{-1} \|\nabla \mathbf{u}^{n+1}\|^2 (\|\nabla \eta^n\|^2 + \|\nabla \eta^{n-1}\|^2) \\
& + C\nu^{-1} (\|\phi_h^n\|^2 + \|\phi_h^{n-1}\|^2) (\|\nabla \mathbf{u}^{n+1}\|_\infty^2 + \|\mathbf{u}^{n+1}\|_\infty^2) \\
& + C(\nu + \nu^{-1}\alpha_1^2 + \alpha_2 + \nu^{-2}) \|\nabla \eta^{n+1}\|^2 + C\alpha_2^{-1} \left\| \inf_{q_h \in Q_h} \|p(t^{n+1}) - q_h\| \right\|^2 \\
& + C\alpha_1 \|\nabla \eta^n\|^2 + C\alpha_1 h^{-2} \|\phi_h^n\|^2 + C\alpha_1 \|(I - P_{L_H})(\nabla \times \mathbf{u}^n)\|^2 \\
& + C\alpha_1 \|\nabla \times (\mathbf{u}^{n+1} - \mathbf{u}^n)\|^2 + C\Delta t^3 \nu^{-1} \int_{t^{n-1}}^{t^{n+1}} \|\mathbf{u}_{ttt}\|^2 dt \\
& + C\Delta t^3 \nu^{-1} \|\nabla \mathbf{u}^{n+1}\|^2 \int_{t^{n-1}}^{t^{n+1}} \|\nabla \mathbf{u}_{tt}\|^2 dt. \tag{3.4.27}
\end{aligned}$$

Multiplication of each term by  $4\Delta t$ , summation from  $n = 1$  to  $n = N - 1$ , Lemma 3.4.1 and the approximation properties along with (3.1.5)-(3.1.6) and (3.1.16) yields

$$\begin{aligned}
& \|\phi_h^N\|^2 + \|2\phi_h^N - \phi_h^{N-1}\|^2 + \sum_{n=1}^{N-1} \|\phi_h^{n+1} - 2\phi_h^n + \phi_h^{n-1}\|^2 \\
& + \Delta t \sum_{n=1}^{N-1} (\nu \|\nabla \phi_h^{n+1}\|^2 + \alpha_1 \|\nabla \times \phi_h^{n+1}\|^2 + \alpha_2 \|\nabla \cdot \phi_h^{n+1}\|^2) \\
\leq & \|\phi_h^1\|^2 + \|2\phi_h^1 - \phi_h^0\|^2 + C \left( \nu^{-1} h^{2k+2} \|\mathbf{u}_t\|_{2,k+1}^2 \right. \\
& + \nu^{-1} h^{2k} \|\mathbf{u}\|_{2,k+1}^2 \|\nabla \mathbf{u}\|_{\infty,0}^2 + (\nu + \nu^{-1}\alpha_1^2 + \alpha_2 + \nu^{-2}) h^{2k} \|\mathbf{u}\|_{2,k+1}^2 \\
& + \alpha_2^{-1} h^{2k+2} \|p\|_{2,k+1}^2 + \alpha_1 h^{2k} \|\mathbf{u}\|_{2,k+1}^2 + \alpha_1 H^{2k} \|\mathbf{u}\|_{2,k+1}^2 + \alpha_1 \Delta t^2 \|\mathbf{u}_t\|_{\infty,0}^2 \\
& \left. + \nu^{-1} \Delta t^4 \|\mathbf{u}_{ttt}\|_{2,0}^2 + \nu^{-1} \Delta t^4 \|\nabla \mathbf{u}\|_{\infty,0}^2 \|\nabla \mathbf{u}_{tt}\|^2 \right) \\
& + C\Delta t (\nu^{-1} + \alpha_1 h^{-2}) \sum_{n=1}^{N-1} \|\phi_h^n\|^2. \tag{3.4.28}
\end{aligned}$$

□

Theorem 3.4.1 and the estimation (3.1.16) immediately yield the following Corollary, proving second-order accuracy both in time and space.



**Corollary 3.4.1** *In addition to the regularity assumptions of (3.4.9), consider the Taylor-Hood finite element spaces  $(\mathbf{X}_h, Q_h) = (P_2, P_1)$ , the coarse mesh size  $H = O(\sqrt{h})$ , the artificial viscosity parameter  $\alpha_1 = O(h^2)$  and the grad-div stabilization parameter  $\alpha_2 \leq O(1)$ . Then, the error in velocity satisfies second order accuracy both in space and time such that for all  $\Delta t > 0$*

$$\begin{aligned} \|\mathbf{e}^N\|^2 + \|2\mathbf{e}^N - \mathbf{e}^{N-1}\|^2 + \sum_{n=1}^{N-1} \|\mathbf{e}^{n+1} - 2\mathbf{e}^n + \mathbf{e}^{n-1}\|^2 + \nu\Delta t \sum_{n=1}^{N-1} \|\nabla \mathbf{e}^{n+1}\|^2 \\ \leq C \left( \|\mathbf{e}^1\|^2 + \|\mathbf{e}^0\|^2 + h^4 + \Delta t^4 \right). \end{aligned}$$

**Remark 3.4.1** *The initial approximation of velocity  $\mathbf{u}_h^0$  has to be weakly divergence-free for the method to be stable. Moreover, to obtain optimal order of accuracy, it needs to be suitably interpolated in  $\mathbf{V}_h$  in such a way that  $\|\mathbf{e}^0\|$  is optimal, that is  $\|\mathbf{e}^0\| \leq Ch^2\|\mathbf{u}\|_2$ . Since we use a two-step method in this study, two initial conditions  $\mathbf{u}_h^0$  and  $\mathbf{u}_h^1$  are needed. Herein, for simplicity, we consider  $\mathbf{u}_h^0 = \mathbf{u}_h^1 = I_{\mathbf{u}}(\mathbf{u}^0)$  for some interpolation  $I_{\mathbf{u}}$  in  $\mathbf{V}_h$ , which guarantees second-order accuracy both in space and time. Alternatively,  $\mathbf{u}_h^1$  can be obtained from the Crank-Nicolson method by using  $\mathbf{u}_h^0$  as described in [87, 164].*

### 3.5 Numerical Experiments

In this part, we provide four numerical illustrations testing a numerical solution of (3.2.1)-(3.2.3), namely the BDF2LE-SAV method. The first test verifies the order of the convergence rates which are obtained in Corollary 3.4.1. In addition, we demonstrate the efficiency of the BDF2LE-SAV method on the flow around a cylinder, two-dimensional flow between two offset circles problems, and Poiseuille's Flow. All solutions are compared with the CN-SAV method of [73]. Simulations are carried out by considering Taylor-Hood finite element spaces  $(P_2, P_1)$  to approximate velocity and pressure and  $P_1$  for the large scale space  $L_H$ . All the numerical experiments are implemented with the finite element software package *Freefem++*, [42].

### 3.5.1 Convergence Rates

This subsection verifies the predicted convergence rates of our numerical scheme (3.2.1)-(3.2.3). For this purpose, we consider (3.0.1) with the prescribed solution given by

$$\mathbf{u} = \begin{bmatrix} (1 + 0.01t)\sin(2\pi y) \\ (1 + 0.01t)\cos(2\pi x) \end{bmatrix}, \quad p = x + y \quad (3.5.1)$$

which satisfies (3.0.1). Simulations are performed in a unit square  $\Omega := [0, 1]^2$  with  $\nu = 1$  and the last time  $T = 0.01$ . The coarse mesh size  $H = \sqrt{h}$ , the parameters  $\alpha_1 = h^2$  and  $\alpha_2 = 1$  are chosen. The external force  $\mathbf{f}$  is determined by the true solution (3.5.1). Boundary conditions are set to be true solutions on  $\partial\Omega$ . We compute approximate solutions on successive mesh refinements and the velocity errors are computed in the discrete norm  $L^2(0, T; H^1(\Omega))$

$$\|\mathbf{u} - \mathbf{u}_h\|_{2,1} = \left\{ \Delta t \sum_{n=1}^N \|\mathbf{u}(t^n) - \mathbf{u}_h^n\|^2 \right\}^{1/2}.$$

Results for errors are shown in Table 3.1 and second order accuracy is observed, exactly as the theory predicts.

Table 3.1: Errors and convergence rates for the Scheme (3.2.1)-(3.2.3).

$h$	$\Delta t$	$\ \mathbf{u} - \mathbf{u}_h\ _{2,1}$	Rate
1/4	0.01	5.25977e-1	–
1/8	0.005	1.3403e-1	1.96
1/16	0.0025	3.397e-2	1.98
1/32	0.00125	8.50843e-3	1.99
1/64	0.000625	2.13204e-3	1.99
1/128	0.0003125	5.32992e-4	2.00

### 3.5.2 Flow Around a Cylinder

The second example is considered to verify the efficiency of our scheme (3.2.1)-(3.2.3) on two-dimensional flow along a rectangular channel in which a cylinder is depicted as seen in Figure 3.1 ([92]). This famous benchmark problem is highly preferable since it exhibits real flow characteristics and provides highly reliable data that allows measuring the accuracy of codes. In addition, simulating this flow accurately is critical to observing the behavior of eddies. The study [92] has addressed this problem and presented the computational results to define the reference values. The accuracy of these reference values has been significantly improved in [144].

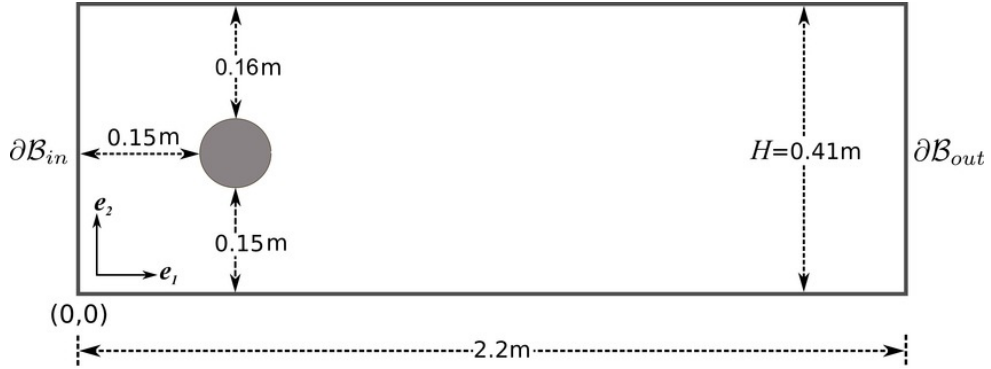


Figure 3.1: Domain  $\Omega$  of the test problem

The inflow and outflow velocities are presented as

$$u_1(0, y, t) = u_1(2.2, y, t) = \frac{6}{0.41^2} \sin\left(\frac{\pi t}{8}\right) y(0.41 - y),$$

$$u_2(0, y, t) = u_2(2.2, y, t) = 0.$$

We enforce no-slip boundary conditions at the cylinder and walls. We choose zero initial condition  $\mathbf{u}(x, y, t) = 0$ , the kinematic viscosity  $\nu = 10^{-3}$  and the forcing  $\mathbf{f} = 0$ . Also, we choose artificial viscosity parameters as  $\alpha_1 = h^2$  and  $\alpha_2 = 0.001$  for regular mesh size  $h$  and the coarse mesh size  $H = \sqrt{h}$ . In all computations, we use a very coarse mesh consisting of only 10210 total degrees of freedom with the last time  $T = 8$  and time-step  $\Delta t = 0.01$ . We first present the flow development in Figure 3.2 which matches with the results of [92, 144]. With increasing inflow, we observe the

appearance of two vortices behind the cylinder, see  $t = 2$  and  $t = 4$ . Then vortices leave the cylinder and the formation of a vortex street is clearly seen, which lasts until  $t = 8$ . The most frequently monitored quantities of interest that are considered in

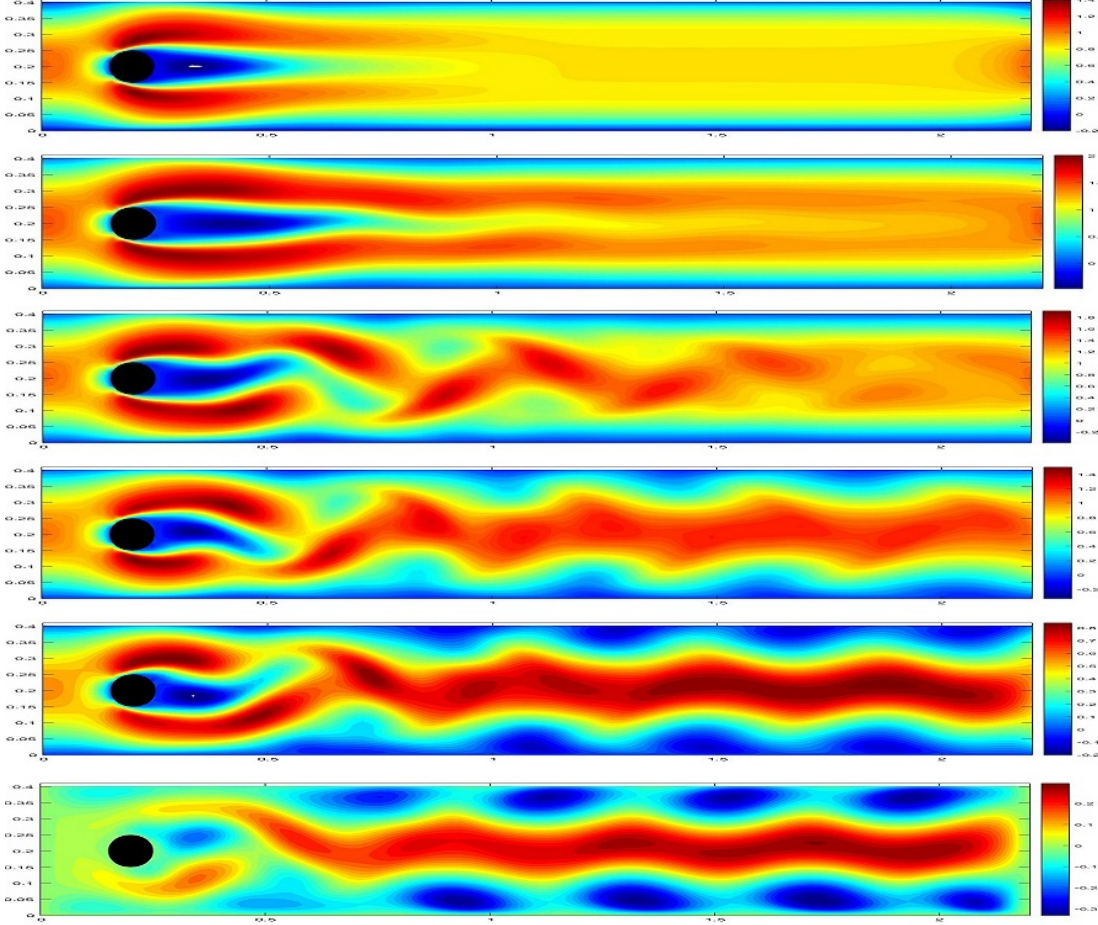


Figure 3.2: The velocity contours of the scheme (3.2.1)-(3.2.3) at  $t = 2, 4, 5, 6, 7, 8$  (from up to down).

the literature for this flow are the drag  $c_d(t)$ , the lift coefficient  $c_l(t)$ , and pressure drop across the object  $\Delta p(t)$ . These values are defined in [92] as follows:

$$c_d(t) = \frac{2}{\rho LU_{max}^2} \int_S (\rho \nu \frac{\partial \mathbf{u}_{t_S}}{\partial n} n_y - p(t) n_x) dS$$

$$c_l(t) = -\frac{2}{\rho LU_{max}^2} \int_S (\rho \nu \frac{\partial \mathbf{u}_{t_S}}{\partial n} n_x + p(t) n_y) dS$$

$$\Delta p(t) = p(t; 0.15, 0.2) - p(t; 0.25, 0.2)$$

where  $S$  is the boundary of the cylinder,  $U_{max}$  is the maximum mean flow,  $L$  is the diameter of the cylinder,  $n = (n_x, n_y)^T$  is the normal vector on the circular boundary  $S$  and  $\mathbf{u}_{t_S}$  is the tangential velocity for  $t_S = (n_y, -n_x)^T$  the tangential vector. The plots of evolution of the drag and lift coefficient and the pressure difference are also presented in Figure 3.3 and the graphs are consistent with DNS results of [92, 144]. Note that in Table 3.2, we take only the maximum drag  $c_{d,max}$  and maximum lift  $c_{l,max}$  values behind the cylinder together with the times at which they occur. The following reference intervals are given in [92, 144]:

$$c_{d,max}^{ref} \in [2.93, 2.97], \quad c_{l,max}^{ref} \in [0.47, 0.49].$$

We compare drag and lift coefficients of the CN-SAV method which provides 10239 degrees of freedom with time step size  $\Delta t = 0.001$ . The computed coefficients of Scheme (3.2.1)-(3.2.3) (BDF2LE-SAV) and CN-SAV are compared with reference values in [144] that are provided by using about 500000 degrees of freedom in space and time step size  $\Delta t = 0.00125$ . In Table 3.2, we observe that in each case, the

Table 3.2: Comparison of maximum drag and lift coefficients and the times at which they occur.

Method	$c_{d,max}$	$t(c_{d,max})$	$c_{l,max}$	$t(c_{l,max})$
CN-SAV(Ref [73])	2.87198	3.685	0.436564	5.784
Ref [144]	2.95092	3.93	0.47795	5.69
BDF2LE-SAV	2.96523	3.93	0.452956	5.78

BDF2LE-SAV method provides the best prediction of the maximum drag coefficient compared with [73]. Also, the proposed method predicts the maximum lift coefficient better than the CN-SAV method. In each case, the results are much closer to the reference values of [144]. Thus, it is fair to say with the BDF2LE-SAV method more accurate results are obtained with a relatively small number of degrees of freedom.

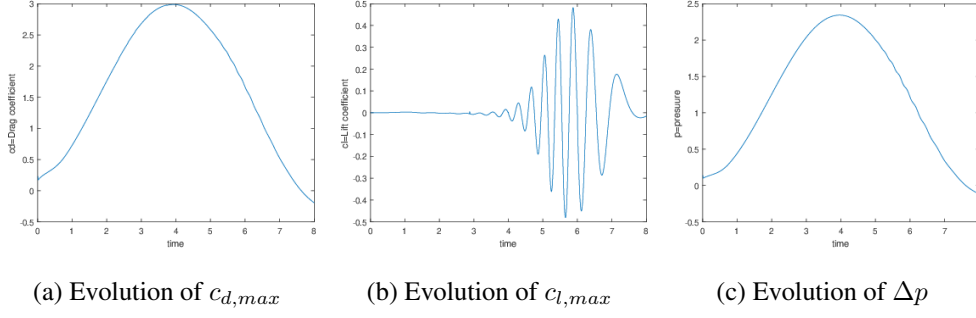


Figure 3.3: Evolution of maximum value of drag values, lift values and pressure differences obtained when using the scheme (3.2.1)-(3.2.3) with  $\Delta t = 0.01$

### 3.5.3 Flow Between Two Offset Circles

The third experiment demonstrates the stability of SAV with BDF2LE method on two dimensional flow in annular region between two offset circles. The domain we use is a circle with an interior decentralized circle inside. Pick  $r_1 = 1$ ,  $r_2 = 0.1$  and  $c = (c_1, c_2) = (\frac{1}{2}, 0)$ . The domain is then given by

$$\Omega = \{(x, y) : x^2 + y^2 \leq r_1^2\} \cap \{(x, y) : (x - c_1)^2 + (y - c_2)^2 \geq r_2^2\}.$$

The numerical solutions are computed on a Delunay-generated triangular mesh and an example mesh can be seen in Figure 3.4. Zero initial conditions have been used

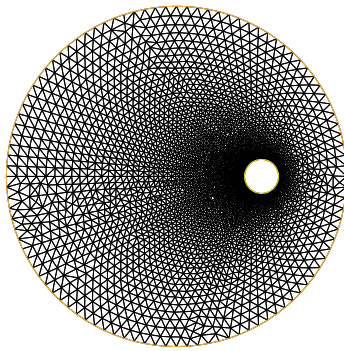


Figure 3.4: The domain of the test problem

and no-slip boundary conditions are considered on both circles. We choose time step size  $\Delta t = 0.025$  and the last time  $T = 5$ . The flow is generated by the body force

rotating in the counterclockwise direction

$$f(x, y, t) = (-4y(1 - x^2 - y^2), 4x(1 - x^2 - y^2))^T.$$

In this problem, the rotational force  $\mathbf{f} = 0$  at the outer circle and thus the flow motion is due to the interaction of the flow with the inner circle. Under the influence of the body force, the flow interacts with the inside disk. Then, we observe the formation of a vortex street called von Kármán which re-interacts with the inner circle creating more complex structures. Figure 3.5 shows this behavior, in which some snapshots of velocity streamlines are presented for  $Re = 200$ . Further studies on this flow can be found in [93, 128, 145, 148].

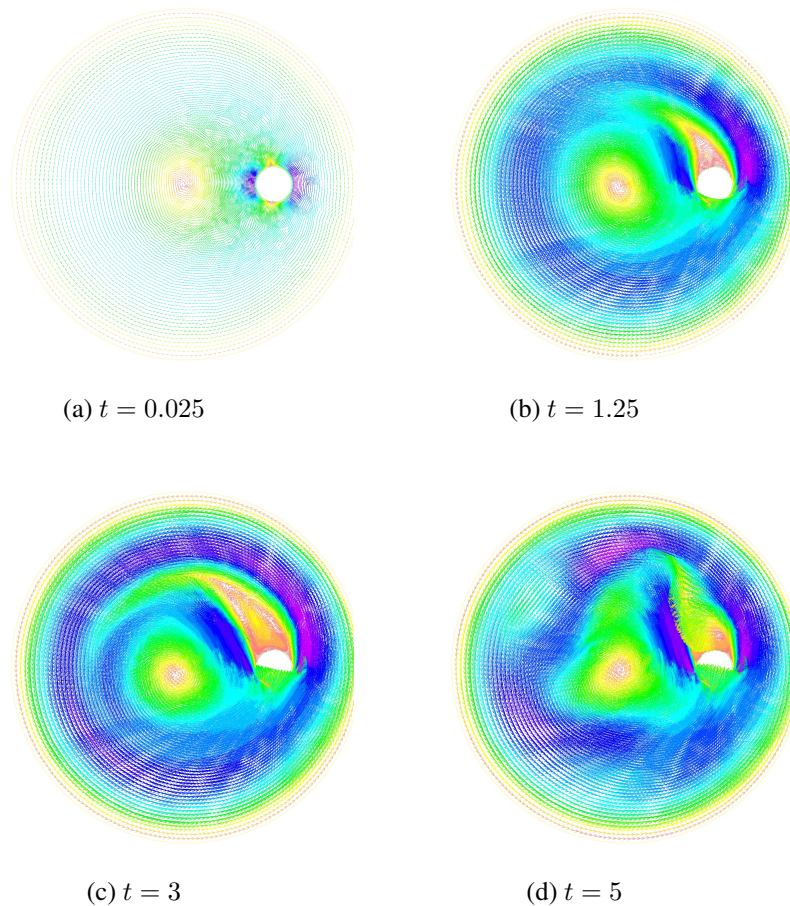


Figure 3.5: Velocity contours for  $Re = 200$

Popular quantities of interest in this experiment are the kinetic energy and the enstrophy values for  $0 \leq t \leq 5$ , defined by

$$Energy = \frac{1}{2} \|\mathbf{u}\|^2, \quad Enstrophy = \frac{1}{2} \nu \|\nabla \times \mathbf{u}\|^2.$$

Figure 3.6 and Figure 3.7 show kinetic energy and enstrophy statistics for different Reynolds numbers. The curves marked with ‘NSE-BDF2LE’ denote the computation of the flow problem by using BDF2LE method without SAV. Figures show that while all three methods’ energy and enstrophy are stable for  $Re = 200$ , energy and enstrophy values of the CN-SAV increase with increasing values of  $Re$ . However, time evolutions of energy and enstrophy of BDF2LE-SAV remain constant and the graphs of the BDF2LE-SAV stay close to the approximation of NSE-BDF2LE. Observe also that with the proposed scheme, energy and enstrophy oscillate less and stay stable in comparison with NSE-BDF2LE. This verifies the greater stability properties of the BDF2LE-SAV method.

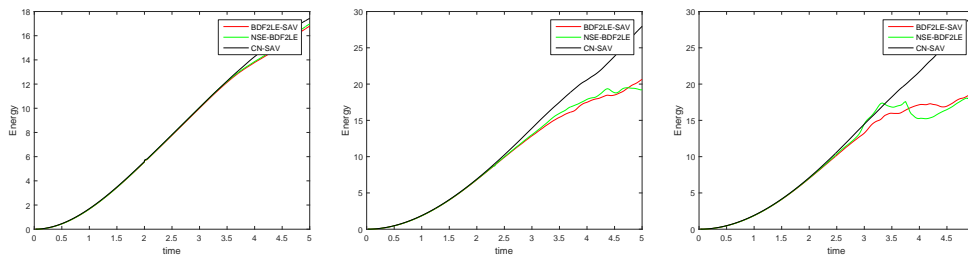


Figure 3.6: Time evolutions of energy for  $Re = 200, 800, 1200$  from left to right.

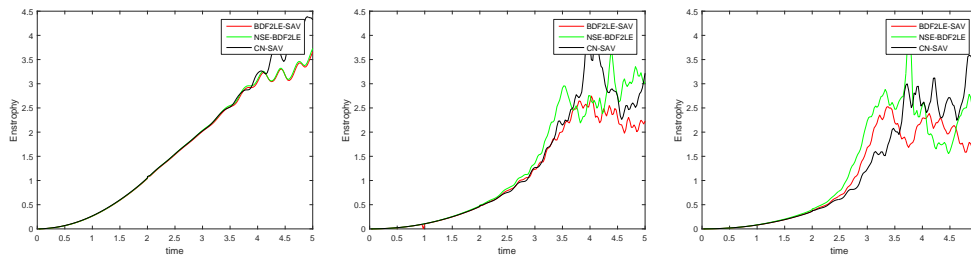


Figure 3.7: Time evolutions of enstrophy for  $Re = 200, 800, 1200$  from left to right.



### 3.5.4 Poiseuille's Flow

In the last experiment, our goal is to test the contribution of Scheme (3.2.1)-(3.2.3) and again to compare CN-SAV method for Poiseuille's flow. This test, discussed in [18], is a well-known academic example having numerical instabilities in the case of small viscosity. The computations are performed in  $[0, 4] \times [0, 1]$  rectangular domain with  $\nu = 10^{-4}$ ,  $\Delta t = 1$ ,  $f = 0$ ,  $h = 0.1$ , and  $T = 1500$ . Numerical results for  $\alpha_1 = h^2$ ,  $\alpha_2 = 0.001$ , and the coarse mesh size  $H = \sqrt{h}$  are presented. We take the parabolic inflow and outflow velocity profiles as

$$\mathbf{u} = \begin{pmatrix} 4y(1-y) \\ 0 \end{pmatrix} \quad (3.5.2)$$

and use it also for initial conditions and enforce the no-slip boundary conditions on the top and bottom of the boundary.

We first provide plots of velocity fields obtained from CN-SAV and BDF2LE-SAV methods given in Figure 3.8 and Figure 3.9, respectively. During the computation of this result, it is observed that after  $t = 15$ , while the flow computed by the CN-SAV method loses its features, the velocity fields computed by the BDF2LE-SAV method are appropriately simulated and stay stable even at the final time, see Figure 3.9.

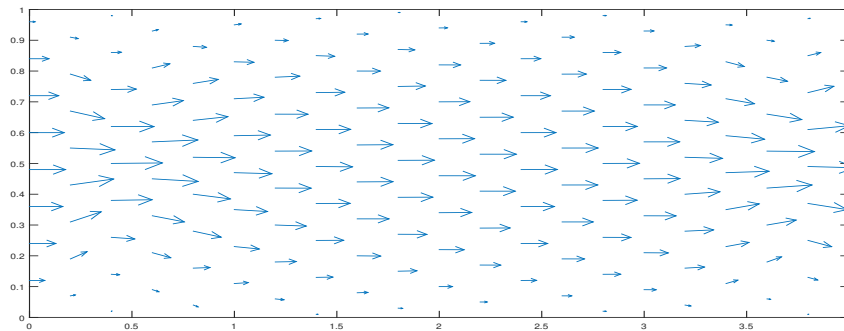


Figure 3.8: Velocity field for CN-SAV.

Results of the numerical studies of relative velocity error and energy versus time are presented in Figure 3.10. It can be seen from part (a) of Figure 3.10 that the velocity

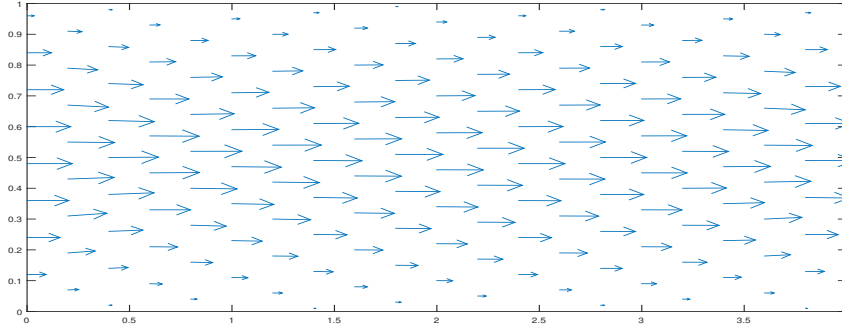
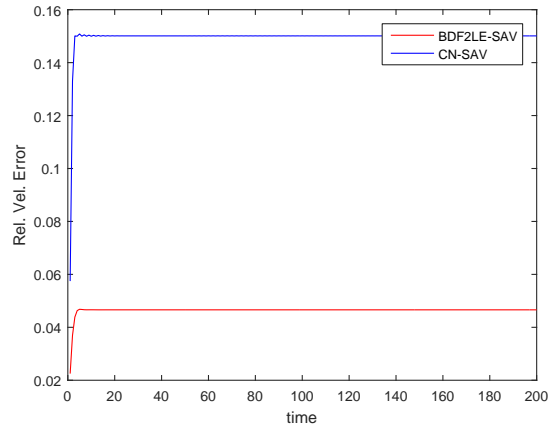
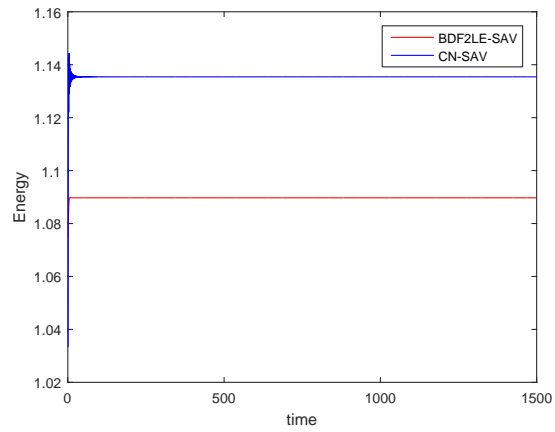


Figure 3.9: Velocity field for BDF2LE-SAV.

errors of the CN-SAV method are larger than the ones with the BDF2LE-SAV method. In part (b) of Figure 3.10, from the simulations, we observe that solution of the CN-SAV starts to oscillate from  $t = 160$  and continues till  $t = 580$  with small oscillations, which is hard to observe from the figure, then it reaches its equilibrium position. Unlike the CN-SAV method, the solution of the BDF2LE-SAV method reaches its equilibrium position in a very short time at  $t = 10$ , and then maintains the same energy throughout the simulation as seen in part (b) of Figure 3.10.



(a) Relative velocity error for BDF2LE-SAV and CN-SAV.



(b) Energy for BDF2LE-SAV and CN-SAV.

Figure 3.10: Time evolutions of relative velocity error and energy



## CHAPTER 4

### TIME FILTERED SECOND ORDER BACKWARD EULER METHOD FOR EMAC FORMULATION OF NAVIER-STOKES EQUATIONS

This chapter studies an efficient and accurate numerical approximation of the Navier-Stokes equations (NSE) which are given by

$$\begin{aligned}\mathbf{u}_t - \nu \Delta \mathbf{u} + \mathbf{u} \cdot \nabla \mathbf{u} + \nabla p &= \mathbf{f} && \text{in } \Omega \times (0, T), \\ \nabla \cdot \mathbf{u} &= 0 && \text{in } \Omega \times (0, T], \\ \mathbf{u} &= \mathbf{0} && \text{on } \partial\Omega \times [0, T], \\ \mathbf{u}(\mathbf{x}, 0) &= \mathbf{u}_0(\mathbf{x}) && \text{for } \mathbf{x} \in \Omega, \\ \int_{\Omega} p d\mathbf{x} &= \mathbf{0} && \text{in } (0, T].\end{aligned}\tag{4.0.1}$$

Here,  $\Omega$  denotes a bounded and regular flow domain in  $\mathbb{R}^d$  ( $d = 2$  or  $3$ ),  $\mathbf{u}(x, t)$  represents the velocity,  $p(x, t)$  the zero-mean pressure,  $\mathbf{f}(x, t)$  an external force,  $\nu$  the kinematic viscosity and  $\mathbf{u}_0$  is a weakly divergence-free initial condition.

It is known that, in classical  $H$ -conforming methods, the divergence constraint is only weakly enforced [146] leading to some divergence error and this results in loss of numerical accuracy as well as many important conservation laws, including energy, momentum, angular momentum, and others. It is well-known that a good way to measure the accuracy of a model is by how much physical balance it retains. This idea was recognized by Arakawa, Fix, Lam, and others in [1] by constructing energy and enstrophy conserving scheme for the 2D NSE, for ocean circulation models in [46], for the shallow water equations in [2] and for many many different equations from physics, e.g. [14, 26, 53, 55, 77, 116, 120]. The success of numerical simulation of NSEs depends on physically motivated discretization schemes. For this purpose, practitioners have developed many numerical methods with the typical formulations of the nonlinearity such as convective, conservative, rotational, and skew-symmetric

formulations, see e.g. [55, 77, 84]. Among them, the skew-symmetric form of nonlinearity conserves energy and helicity [77, 84, 119] while it fails to conserve momentum and angular momentum shown in [123]. It was also shown in [123] that the rotational form only conserves energy, the conservative form only conserves momentum and angular momentum and the convective form conserves neither energy, momentum and angular momentum. Hence, none of them conserve all the balances of physical quantities such as energy-momentum-angular momentum conserving (EMAC) at the same time. To handle this issue, in the study [123], the authors introduce a new formulation of NSE by reformulating the nonlinear term, named the EMAC formulation which is the first scheme conserving all of these mentioned quantities even under the weakly enforced divergence constraint as well as properly defined vorticity, helicity, and 2D enstrophy. It is worth noting that, utilizing pointwise divergence-free approximations such as those newly developed in [30, 53, 56, 133] makes all of these formulations equivalent and each of them will conserve all of these quantities in a suitable sense. However, the choice of such particular elements is not so practical due to the need of non-standard meshing, approximating polynomial degrees, and not included in open source FE software for large scale computing [153]. Following the original paper [123], there have been a considerable number of studies of the EMAC formulation for various problems such as vortex-induced vibration [35], turbulent ow simulation [97], cardiovascular simulations and hemodynamics [98, 99], noise radiated by an open cavity [114] and others e.g. [35, 50, 96, 124]. In the light of these studies, the EMAC formulation has proven to exhibit superior performance, especially over longer periods [91] compared to traditionally used schemes based on skew-symmetric formulations. All these studies agree with the opinion that the EMAC formulation reduces numerical dissipation and significantly increases numerical accuracy compared to previously studied ones thanks to its ability to conserve all the physical quantities.

The central challenge in the CFD community is time accuracy to reflect important physical features of solutions. From the practical point of view, incorporating minimum complexity into existing codes and increasing numerical accuracy are critical for many purposes. In general, backward Euler (BE) time discretization is well-known to be one of the most commonly used methods to approximate the time-dependent vis-

cous flow problems, [54, 147]. BE is the basis for the construction of more complex methods due to its stability, rapid convergence to analytical solutions, and easy implementation. However, it causes spurious oscillations in flow physics [115] for larger time step sizes even if the method is stable. The way to increase numerical accuracy and enhance physical features for fully implicit and BE methods was first proposed in the study [6] for the ODEs.

As stated in [115], by adding only one additional line of code to BE scheme, it is possible to reduce numerical dissipation, increase accuracy from the first order to the second-order, and obtain an  $A$ -stable method with a useful error estimator. Besides constant time steps, the methods could be extended also to variable time step sizes. The method, called time filtering, is extended to the incompressible NSE in [140], to MHD equations in [3] and to the Boussinesq equations in [79]. The common theme in these studies is to apply the linear time filtering method to BE scheme with constant time step resulting in two uncoupled steps at each time level. In the first step, the required equation is solved by using BE time-stepping method and in the second step, the approximate solutions obtained in the first step are post processed with a second-order, linear time filtering. The resulting algorithm achieves a second-order, more accurate, and an  $A$ -stable method. Moreover, combining the second step with the first step yields a second-order accurate method akin to the backward differentiation (BDF2) formula and performs a consistent and simple stability/convergence analysis. While a family of general variable step size time filter algorithms is investigated by [138], general linear methods by using pre-filter or post-filter by using constant step size have been considered in [139]. Such filtering processes yield embedded higher-order methods with minimum complexity, see [139].

The purpose of this chapter is to investigate the effect of this novel idea from [140] on the EMAC formulation of time-dependent, incompressible fluid flows for constant time steps. Herein, based on the success of EMAC formulation in [123] and time filtering on BE for constant time step in [140], we naturally took the step of combining these two ideas to see whether the time filtering method will improve the accuracy of solutions of NSE with EMAC formulation. The proposed numerical scheme is a two-step time filtered BE method which is efficient,  $O(\Delta t^2)$ ,  $A$ -stable and easy to adapt into any existing code. In the first step, velocity solutions of the EMAC scheme

are calculated with the usual BE finite element discretization, which we call BE-EMAC. The second step post proceeds this velocity approximation by using a second-order time filtering under constant step size. Thus, by combining the BE discretized EMAC formulation of NSE with time filtering, one benefits from the simplicity of BE method and does not suffer from its mentioned drawbacks. The EMAC treatment of non-linearity uses the Newton method. Although the BE time-stepping scheme does not conserve energy exactly as the Crank-Nicolson scheme does, our aim here is to show the improvement which has been done due to the addition of time filter post-processing. We do not assert the superiority of the scheme over Crank-Nicolson-based time stepping schemes in terms of conservation of total kinetic energy. We show the conservation of the physically conserved quantities such as (a modified) energy, momentum, and angular momentum and we refer to it as energy, momentum, and angular momentum conserving time filtered formulation (EMAC-FILTERED). Additionally, we provide that the method is both stable and optimally accurate. To the best of the authors' knowledge, this is the first attempt to combine EMAC formulation with a time filtering post-processing for solving NSE numerically.

The presentation of this chapter is as follows. Section 4.1 provides some notations and mathematical preliminaries needed for a smooth analysis to follow. In Section 4.2, EMAC-FILTERED method is described. Conservation properties are studied in Section 4.3. Section 4.4 is devoted to a complete stability and convergence analysis of the EMAC-FILTERED method. In Section 4.5, several numerical experiments are performed which test the conservation properties, the accuracy, and the efficiency of the method and compares it with BE-EMAC solutions.

#### 4.1 Notations and Mathematical Preliminaries

We consider the same function spaces and their properties as in Section 3.1 of the Chapter 3. The variational formulation of (4.0.1) reads as follows: Find  $\mathbf{u} : (0, T] \longrightarrow \mathbf{X}$ ,  $p : (0, T] \longrightarrow Q$  satisfying

$$(\mathbf{u}_t, \mathbf{v}) + \nu(\nabla \mathbf{u}, \nabla \mathbf{v}) + b(\mathbf{u}, \mathbf{u}, \mathbf{v}) - (p, \nabla \cdot \mathbf{v}) = (\mathbf{f}, \mathbf{v}) \quad \forall \mathbf{v} \in \mathbf{X}, \quad (4.1.1)$$

$$(q, \nabla \cdot \mathbf{u}) = 0 \quad \forall q \in Q, \quad (4.1.2)$$



In this chapter, we use a different trilinear form called EMAC formulation for the nonlinear term in NSE. To obtain EMAC formulation, let the symmetric part of  $\nabla \mathbf{u}$  be denoted by  $\mathbb{D}(\mathbf{u}) = \frac{\nabla \mathbf{u} + \nabla \mathbf{u}^T}{2}$  and the skew-symmetric part by  $\nabla_n \mathbf{u} := \frac{\nabla \mathbf{u} - \nabla \mathbf{u}^T}{2}$ . Also note that for any  $\mathbf{u}, \mathbf{v} \in \mathbf{H}^1(\Omega)$  the following holds

$$(\nabla_n \mathbf{u})\mathbf{v} = \frac{1}{2}(\nabla \times \mathbf{u}) \times \mathbf{v} \quad (4.1.3)$$

Then, for any  $\mathbf{u}, \mathbf{v} \in \mathbf{H}^1(\Omega)$  the following vector identities are obtained by straightforward calculations

$$(\mathbf{u} \cdot \nabla \mathbf{u})\mathbf{u} = (\nabla \times \mathbf{u}) \times \mathbf{u} + \nabla \frac{1}{2}|\mathbf{u}|^2 =: (\nabla \times \mathbf{u}) \times \mathbf{u} + \nabla \mathbf{q}, \quad (4.1.4)$$

$$(\nabla \mathbf{u})\mathbf{u} = \mathbb{D}(\mathbf{u})\mathbf{u} + (\nabla_n \mathbf{u})\mathbf{u} = \mathbb{D}(\mathbf{u})\mathbf{u} + \frac{1}{2}(\nabla \times \mathbf{u}) \times \mathbf{u} \quad (4.1.5)$$

where  $\mathbf{q} := \frac{|\mathbf{u}|^2}{2}$ . Then, identities (4.1.3)-(4.1.5) yields the following identity which is the key idea for the EMAC formulation

$$(\mathbf{u} \cdot \nabla)\mathbf{u} = 2\mathbb{D}(\mathbf{u})\mathbf{u} - \frac{1}{2}\nabla|\mathbf{u}|^2 \quad (4.1.6)$$

for which the inertia term is split into the acceleration driven by  $2\mathbb{D}(\mathbf{u})$  and the potential term further absorbed by redefined pressure. Following [123], the trilinear form for EMAC formulation is defined by

$$c(\mathbf{u}, \mathbf{v}, \mathbf{w}) = 2(\mathbb{D}(\mathbf{u})\mathbf{v}, \mathbf{w}) + ((\nabla \cdot \mathbf{u})\mathbf{v}, \mathbf{w}) \quad (4.1.7)$$

For purpose, it is important to assume that  $\mathbf{u}, \mathbf{v}, \mathbf{w} \in \mathbf{X}$ , i.e. no divergence free condition is assumed for any of  $\mathbf{u}, \mathbf{v}, \mathbf{w}$ . It is critical to add the divergence term in the definition of  $c(\cdot, \cdot, \cdot)$  to satisfy the cancellation property,  $c(\mathbf{v}, \mathbf{v}, \mathbf{v}) = 0$ .

The following lemma is useful in the analysis.

**Lemma 4.1.1** *For  $\mathbf{u}, \mathbf{v}, \mathbf{w} \in \mathbf{X}$ , the following identities hold:*

$$(\mathbf{u} \cdot \nabla \mathbf{v}, \mathbf{w}) = -(\mathbf{u} \cdot \nabla \mathbf{w}, \mathbf{v}) - ((\nabla \cdot \mathbf{u})\mathbf{v}, \mathbf{w}), \quad (4.1.8)$$

$$(\mathbf{u} \cdot \nabla \mathbf{w}, \mathbf{w}) = -\frac{1}{2}((\nabla \cdot \mathbf{u})\mathbf{w}, \mathbf{w}), \quad (4.1.9)$$

$$(\mathbf{u} \cdot \nabla \mathbf{v}, \mathbf{w}) = ((\nabla \mathbf{v})\mathbf{u}, \mathbf{w}) = ((\nabla \mathbf{v})^T \mathbf{w}, \mathbf{u}). \quad (4.1.10)$$

**Proof.** The first follows from the integration by parts:

$$\int_{\Omega} (\mathbf{u} \cdot \nabla)\mathbf{v} \cdot \mathbf{w} + \int_{\Omega} (\mathbf{u} \cdot \nabla \mathbf{w})\mathbf{v} + \int_{\Omega} (\nabla \cdot \mathbf{u})(\mathbf{v} \cdot \mathbf{w}) = \int_{\partial\Omega} (\mathbf{u} \cdot \mathbf{n})(\mathbf{v} \cdot \mathbf{w}) \quad (4.1.11)$$

Then, the fact that  $\mathbf{u} = 0$  on  $\partial\Omega$  vanishes the right-hand side term in (4.1.11) which yields the equation (4.1.8).

The second is obtained by choosing  $\mathbf{v} = \mathbf{w}$  in (4.1.8). To prove the third identity, take  $\mathbf{u} = [\mathbf{u}_1, \mathbf{u}_2, \mathbf{u}_3]$ ,  $\mathbf{v} = [\mathbf{v}_1, \mathbf{v}_2, \mathbf{v}_3]$ ,  $\mathbf{w} = [\mathbf{w}_1, \mathbf{w}_2, \mathbf{w}_3] \in \mathbf{X}$ . Then, extending the first inner product gives

$$\begin{aligned}
(\mathbf{u} \cdot \nabla \mathbf{v}, \mathbf{w}) &= [\mathbf{u}_1 \mathbf{u}_2 \mathbf{u}_3] \begin{bmatrix} \partial_x(\mathbf{v}_1) & \partial_x(\mathbf{v}_2) & \partial_x(\mathbf{v}_3) \\ \partial_y(\mathbf{v}_1) & \partial_y(\mathbf{v}_2) & \partial_y(\mathbf{v}_3) \\ \partial_z(\mathbf{v}_1) & \partial_z(\mathbf{v}_2) & \partial_z(\mathbf{v}_3) \end{bmatrix} \begin{bmatrix} \mathbf{w}_1 \\ \mathbf{w}_2 \\ \mathbf{w}_3 \end{bmatrix} \\
&= \begin{bmatrix} \mathbf{u}_1 \partial_x(\mathbf{v}_1) + \mathbf{u}_2 \partial_y(\mathbf{v}_1) + \mathbf{u}_3 \partial_z(\mathbf{v}_1) \\ \mathbf{u}_1 \partial_x(\mathbf{v}_2) + \mathbf{u}_2 \partial_y(\mathbf{v}_2) + \mathbf{u}_3 \partial_z(\mathbf{v}_2) \\ \mathbf{u}_1 \partial_x(\mathbf{v}_3) + \mathbf{u}_2 \partial_y(\mathbf{v}_3) + \mathbf{u}_3 \partial_z(\mathbf{v}_3) \end{bmatrix}^T \begin{bmatrix} \mathbf{w}_1 \\ \mathbf{w}_2 \\ \mathbf{w}_3 \end{bmatrix} \\
&= \mathbf{u}_1 \partial_x(\mathbf{v}_1) \mathbf{w}_1 + \mathbf{u}_2 \partial_y(\mathbf{v}_1) \mathbf{w}_1 + \mathbf{u}_3 \partial_z(\mathbf{v}_1) \mathbf{w}_1 \\
&\quad + \mathbf{u}_1 \partial_x(\mathbf{v}_2) \mathbf{w}_2 + \mathbf{u}_2 \partial_y(\mathbf{v}_2) \mathbf{w}_2 + \mathbf{u}_3 \partial_z(\mathbf{v}_2) \mathbf{w}_2 \\
&\quad + \mathbf{u}_1 \partial_x(\mathbf{v}_3) \mathbf{w}_3 + \mathbf{u}_2 \partial_y(\mathbf{v}_3) \mathbf{w}_3 + \mathbf{u}_3 \partial_z(\mathbf{v}_3) \mathbf{w}_3 \quad (4.1.12)
\end{aligned}$$

Next, extending the inner product  $((\nabla \mathbf{v}) \mathbf{u}, \mathbf{w})$  we have

$$\begin{aligned}
((\nabla \mathbf{v}) \mathbf{u}, \mathbf{w}) &= \begin{bmatrix} \partial_x(\mathbf{v}_1) \mathbf{u}_1 + \partial_y(\mathbf{v}_1) \mathbf{u}_2 + \partial_z(\mathbf{v}_1) \mathbf{u}_3 \\ \partial_x(\mathbf{v}_2) \mathbf{u}_1 + \partial_y(\mathbf{v}_2) \mathbf{u}_2 + \partial_z(\mathbf{v}_2) \mathbf{u}_3 \\ \partial_x(\mathbf{v}_3) \mathbf{u}_1 + \partial_y(\mathbf{v}_3) \mathbf{u}_2 + \partial_z(\mathbf{v}_3) \mathbf{u}_3 \end{bmatrix}^T \begin{bmatrix} \mathbf{w}_1 \\ \mathbf{w}_2 \\ \mathbf{w}_3 \end{bmatrix} \\
&= \partial_x(\mathbf{v}_1) \mathbf{u}_1 \mathbf{w}_1 + \partial_y(\mathbf{v}_1) \mathbf{u}_2 \mathbf{w}_1 + \partial_z(\mathbf{v}_1) \mathbf{u}_3 \mathbf{w}_1 \\
&\quad + \partial_x(\mathbf{v}_2) \mathbf{u}_1 \mathbf{w}_2 + \partial_y(\mathbf{v}_2) \mathbf{u}_2 \mathbf{w}_2 + \partial_z(\mathbf{v}_2) \mathbf{u}_3 \mathbf{w}_2 \\
&\quad + \partial_x(\mathbf{v}_3) \mathbf{u}_1 \mathbf{w}_3 + \partial_y(\mathbf{v}_3) \mathbf{u}_2 \mathbf{w}_3 + \mathbf{u}_3 \partial_z(\mathbf{v}_3) \mathbf{u}_2 \mathbf{w}_3 \quad (4.1.13)
\end{aligned}$$

Similarly, the last inner product  $((\nabla \mathbf{v})^T \mathbf{w}, \mathbf{u})$  is extended as

$$((\nabla \mathbf{v})^T \mathbf{w}, \mathbf{u}) = [\mathbf{w}_1 \mathbf{w}_2 \mathbf{w}_3] \begin{bmatrix} \partial_x(\mathbf{v}_1) & \partial_y(\mathbf{v}_1) & \partial_z(\mathbf{v}_1) \\ \partial_x(\mathbf{v}_2) & \partial_y(\mathbf{v}_2) & \partial_z(\mathbf{v}_2) \\ \partial_x(\mathbf{v}_3) & \partial_y(\mathbf{v}_3) & \partial_z(\mathbf{v}_3) \end{bmatrix} \begin{bmatrix} \mathbf{u}_1 \\ \mathbf{u}_2 \\ \mathbf{u}_3 \end{bmatrix}$$

$$\begin{aligned}
&= \begin{bmatrix} \mathbf{w}_1 \partial_x(\mathbf{v}_1) + \mathbf{w}_2 \partial_x(\mathbf{v}_2) + \mathbf{w}_3 \partial_x(\mathbf{v}_3) \\ \mathbf{w}_1 \partial_y(\mathbf{v}_1) + \mathbf{w}_2 \partial_y(\mathbf{v}_2) + \mathbf{w}_3 \partial_y(\mathbf{v}_3) \\ \mathbf{w}_1 \partial_z(\mathbf{v}_1) + \mathbf{w}_2 \partial_z(\mathbf{v}_2) + \mathbf{w}_3 \partial_z(\mathbf{v}_3) \end{bmatrix}^T \begin{bmatrix} \mathbf{u}_1 \\ \mathbf{u}_2 \\ \mathbf{u}_3 \end{bmatrix} \\
&= \mathbf{w}_1 \partial_x(\mathbf{v}_1) \mathbf{u}_1 + \mathbf{w}_2 \partial_y(\mathbf{v}_1) \mathbf{u}_1 + \mathbf{w}_3 \partial_z(\mathbf{v}_1) \mathbf{u}_1 \\
&\quad + \mathbf{w}_1 \partial_x(\mathbf{v}_2) \mathbf{u}_2 + \mathbf{w}_2 \partial_y(\mathbf{v}_2) \mathbf{u}_2 + \mathbf{w}_3 \partial_z(\mathbf{v}_2) \mathbf{u}_2 \\
&\quad + \mathbf{w}_1 \partial_x(\mathbf{v}_3) \mathbf{u}_3 + \mathbf{w}_2 \partial_y(\mathbf{v}_3) \mathbf{u}_3 + \mathbf{w}_3 \partial_z(\mathbf{v}_3) \mathbf{u}_3 \tag{4.1.14}
\end{aligned}$$

It is clearly seen that the extensions of the inner products have the same terms.  $\square$

To introduce the time filtering method, we need some further definitions and inequalities. For preliminaries related to time filtering, we first start with  $G$ -norm. Since  $G$ -stability refers to  $A$ -stability, the  $G$ -matrix is often used in BDF2 analysis. Concerning the  $G$ -matrix defined in Chapter 2, with the choices of  $\theta = 1$  and  $\nu = 2\epsilon$ ,  $G$ -matrix of the described method is as follows:

$$G = \begin{pmatrix} \frac{3}{2} & -\frac{3}{4} \\ -\frac{3}{4} & \frac{1}{2} \end{pmatrix}$$

with the  $G$ -norm and  $F$ -norm defined in Chapter 2.

**Lemma 4.1.2** *The symmetric positive matrix  $F \in \mathbb{R}^{n \times n}$  and the symmetric matrix  $G \in \mathbb{R}^{2n \times 2n}$  satisfy the following equality:*

$$\begin{aligned}
&\left( \frac{\frac{3}{2}w^{n+1} - 2w^n + \frac{1}{2}w^{n-1}}{\Delta t}, \frac{3}{2}w^{n+1} - w^n + \frac{1}{2}w^{n-1} \right) \\
&= \frac{1}{\Delta t} \left\| \begin{bmatrix} w^{n+1} \\ w^n \end{bmatrix} \right\|_G^2 - \frac{1}{\Delta t} \left\| \begin{bmatrix} w^n \\ w^{n-1} \end{bmatrix} \right\|_G^2 \\
&\quad + \frac{1}{4\Delta t} \left\| w^{n+1} - 2w^n + w^{n-1} \right\|_F^2 \tag{4.1.15}
\end{aligned}$$

**Proof.** Taking  $\theta = 1$  and  $\nu = 2\epsilon$  in Lemma 2.0.11 in Chapter 2 gives the result.  $\square$

**Lemma 4.1.3** *For any  $\mathbf{u}, \mathbf{v} \in \mathbb{R}^n$ , we have*

$$\left( \begin{bmatrix} \mathbf{u} \\ \mathbf{v} \end{bmatrix}, G \begin{bmatrix} \mathbf{u} \\ \mathbf{v} \end{bmatrix} \right) \geq \frac{3}{4} \|\mathbf{u}\|^2 - \frac{1}{4} \|\mathbf{v}\|^2, \tag{4.1.16}$$

$$\left( \begin{bmatrix} \mathbf{u} \\ \mathbf{v} \end{bmatrix}, G \begin{bmatrix} \mathbf{u} \\ \mathbf{v} \end{bmatrix} \right) \leq \frac{3}{2} \|\mathbf{u}\|^2 + \frac{3}{4} \|\mathbf{v}\|^2. \quad (4.1.17)$$

**Proof.** Taking  $\theta = 1$  and  $\nu = 2\epsilon$  in Lemma 2.0.12 in Chapter 2 yields the estimates.

□

To formulate the method, we use the following interpolation operator  $F$

$$F[\mathbf{w}^{n+1}] = \frac{3}{2} \mathbf{w}^{n+1} - \mathbf{w}^n + \frac{1}{2} \mathbf{w}^{n-1}. \quad (4.1.18)$$

In the analysis, we also need the following consistency error estimations.

**Lemma 4.1.4** *There exists  $C > 0$  such that*

$$\|F[w^{n+1}] - w^{n+1}\|^2 \leq C \Delta t^3 \int_{t^{n-1}}^{t^{n+1}} \|w_{tt}\|^2 \quad (4.1.19)$$

**Proof.** *Using Taylor's theorem with integral remainder, we have*

$$\begin{aligned} F[w^{n+1}] - w^{n+1} &= \frac{1}{2} w^{n+1} - w^n + \frac{1}{2} w^{n-1} \\ &= \frac{1}{2} \left( w^n + \Delta t w_t^n + \int_{t^n}^{t^{n+1}} w_{tt}(t^{n+1} - t) dt \right) - w^n \\ &\quad + \frac{1}{2} \left( w^n - \Delta t w_t^n + \int_{t^n}^{t^{n-1}} w_{tt}(t^{n-1} - t) dt \right) \\ &= C \left( \int_{t^n}^{t^{n+1}} w_{tt}(t^{n+1} - t) dt + \int_{t^n}^{t^{n-1}} w_{tt}(t^{n-1} - t) dt \right) \end{aligned}$$

*Thus, we have*

$$\begin{aligned} &(F[w^{n+1}] - w^{n+1})^2 \\ &\leq C \left( \int_{t^n}^{t^{n+1}} w_{tt}^2 (t^{n+1} - t)^2 dt + \int_{t^n}^{t^{n-1}} w_{tt}^2 (t^{n-1} - t)^2 dt \right) \\ &\leq C \Delta t^3 \int_{t^{n-1}}^{t^{n+1}} w_{tt}^2 dt \end{aligned} \quad (4.1.20)$$

*Integrating (4.1.20) with respect to  $x$  yields the result.*

□

## 4.2 Numerical Scheme

We consider the following weak formulation of the EMAC formulation of (1.0.1):  
Find  $\mathbf{u} : (0, T] \rightarrow \mathbf{X}$ ,  $P : (0, T] \rightarrow Q$  satisfying

$$(\mathbf{u}_t, \mathbf{v}) + \nu(\nabla \mathbf{u}, \nabla \mathbf{v}) + c(\mathbf{u}, \mathbf{u}, \mathbf{v}) - (P, \nabla \cdot \mathbf{v}) = (\mathbf{f}, \mathbf{v}) \quad \forall \mathbf{v} \in \mathbf{X} \quad (4.2.1)$$

$$(q, \nabla \cdot \mathbf{u}) = 0 \quad \forall q \in Q, \quad (4.2.2)$$

where  $P$  is defined as  $P = p - \frac{1}{2}|\mathbf{u}|^2$  and  $\mathbf{u}(0, \mathbf{x}) = \mathbf{u}_0(\mathbf{x}) \in \mathbf{X}$ . Here, we use the EMAC form of the nonlinear term. We now present the two-step time filtered numerical scheme of (4.2.1)-(4.2.2) for constant time step. In the first step, the velocity approximation of the scheme (4.2.1)-(4.2.2) is calculated with the usual BE finite element (fully implicit) discretization and the second step introduces a simple time filter which combines this velocity solution linearly with the solutions at previous time levels. The second step increases time accuracy remarkably although it does not significantly alter system complexity. The modular time filtered numerical scheme of (4.2.1)-(4.2.2) of the NSE with EMAC formulation reads as follows:

**Algorithm 4.2.1 (EMAC-FILTERED Scheme)** *Let external force  $f$  and the initial condition  $\mathbf{u}_0$  be given. Select  $T$  as the end time, and let  $N$  be the number of time steps to take the time step size  $\Delta t = T/N$ . Define  $\mathbf{u}_h^0, \mathbf{u}_h^{-1}$  as the nodal interpolants of  $\mathbf{u}_0$ , then for any  $n \geq 1$  ( $n = 1, \dots, N - 1$ ), find  $(\mathbf{u}_h^{n+1}, P_h^{n+1}) \in (\mathbf{X}_h, Q_h)$  via the following two steps:*

**Step 1:** Compute  $(\tilde{\mathbf{u}}_h^{n+1}, P_h^{n+1}) \in (\mathbf{X}_h, Q_h)$  such that

$$\begin{aligned} \left( \frac{\tilde{\mathbf{u}}_h^{n+1} - \mathbf{u}_h^n}{\Delta t}, \mathbf{v}_h \right) + \nu(\nabla \tilde{\mathbf{u}}_h^{n+1}, \nabla \mathbf{v}_h) + c(\tilde{\mathbf{u}}_h^{n+1}, \tilde{\mathbf{u}}_h^{n+1}, \mathbf{v}_h) \\ - (P_h^{n+1}, \nabla \cdot \mathbf{v}_h) = (\mathbf{f}(t^{n+1}), \mathbf{v}_h), \end{aligned} \quad (4.2.3)$$

$$(\nabla \cdot \tilde{\mathbf{u}}_h^{n+1}, q_h) = 0. \quad (4.2.4)$$

**Step 2:**

$$\mathbf{u}_h^{n+1} = \tilde{\mathbf{u}}_h^{n+1} - \frac{1}{3}(\tilde{\mathbf{u}}_h^{n+1} - 2\mathbf{u}_h^n + \mathbf{u}_h^{n-1}) \quad (4.2.5)$$

for all  $(\mathbf{v}_h, q_h) \in (\mathbf{X}_h, Q_h)$ .

**Remark 4.2.1** *One option in Algorithm 4.2.1 is that also filtering pressure as  $P_h^{n+1} = \tilde{P}_h^{n+1} - \frac{1}{3}(\tilde{P}_h^{n+1} - 2P_h^n + P_h^{n-1})$ . However, as noted in [3, 140], not filtering pressure yields better numerical results because of consistency terms arising from pressure equations. Based on these previous experiences in [3, 140], we choose not to filter pressure.*

We note that Step 1 is the standard backward Euler scheme for the NSE. Step 2 is just a postprocessing step and it can be easily applied into existing codes. This implemented linear time filter makes the method numerically efficient.

Rewriting (4.2.5) as  $\tilde{\mathbf{u}}_h^{n+1} = \frac{3}{2}\mathbf{u}_h^{n+1} - \mathbf{u}_h^n + \frac{1}{2}\mathbf{u}_h^{n-1}$  and inserting in (4.2.3)-(4.2.4) along with (4.1.18), the following equivalent method is obtained.

$$\begin{aligned} & \frac{1}{\Delta t} \left( \frac{3}{2}\mathbf{u}_h^{n+1} - 2\mathbf{u}_h^n + \frac{1}{2}\mathbf{u}_h^{n-1}, \mathbf{v}_h \right) + \nu (\nabla(F[\mathbf{u}_h^{n+1}]), \nabla \mathbf{v}_h) \\ & + c(F[\mathbf{u}_h^{n+1}], F[\mathbf{u}_h^{n+1}], \mathbf{v}_h) - (P_h^{n+1}, \nabla \cdot \mathbf{v}_h) = (\mathbf{f}(t^{n+1}), \mathbf{v}_h) \end{aligned} \quad (4.2.6)$$

$$(\nabla \cdot (F[\mathbf{u}_h^{n+1}]), q_h) = 0 \quad (4.2.7)$$

for all  $(\mathbf{v}_h, q_h) \in (\mathbf{X}_h, Q_h)$ . We note that to simplify the stability and convergence analysis, the equivalent formulation (4.2.6)-(4.2.7) will be used. However, the formulation (4.2.3)-(4.2.5) will be considered in the implementation of the method for computer simulations.

**Remark 4.2.2** *We emphasize here that although the time derivative is discretized by using the classical BDF2 time-stepping method, the other terms in (4.2.7) are not. Thus, the method should not be considered the standard BDF2 method. We refer to [140], for details of the time filtering approach.*

### 4.3 Conservation Laws

In this section, we investigate the conservation of the integral invariants of fluid flow energy, momentum, and angular momentum for Algorithm 4.2.1. It is well known that the physical accuracy of a model is measured by how well its solutions preserve these quantities. For NSE, energy, momentum, and angular momentum are defined by

$$\text{Kinetic Energy : } E = \frac{1}{2}(\mathbf{u}, \mathbf{u}) = \frac{1}{2} \int_{\Omega} |\mathbf{u}|^2, d\mathbf{x},$$

$$\text{Linear Momentum : } M = \int_{\Omega} \mathbf{u} d\mathbf{x},$$

$$\text{Angular Momentum : } AM = \int_{\Omega} \mathbf{u} \times \mathbf{x} d\mathbf{x}.$$

Let  $e_i$  be the  $i$ -th unit vector and  $\phi_i = x \times e_i$ . Then, momentum and angular momentum can be equivalently defined by

$$M_i = \int_{\Omega} \mathbf{u}_i d\mathbf{x} = (\mathbf{u}, e_i),$$

$$(AM)_i = \int_{\Omega} (\mathbf{u} \times x) \cdot e_i d\mathbf{x} = (\mathbf{u}, \phi_i).$$

Let  $\Omega_s$  be a strip around  $\partial\Omega$  and  $\Omega_i$  be such that  $\Omega = \Omega_s \cup \Omega_i$ . Based on [123], we assume that  $\mathbf{u}_h = 0$  and  $p_h = 0$  on  $\Omega_s$ . Thus, it is important to assume that the solutions  $\mathbf{u}, p$  have compact support in  $\Omega$  (e.g. consider an isolated vortex). We first state the energy balance of the EMAC-FILTERED scheme (4.2.6)-(4.2.7).

**Theorem 4.3.1** *EMAC-FILTERED scheme (4.2.6)-(4.2.7) conserves a modified kinetic energy for  $\nu = 0, \mathbf{f} = 0$ :*

$$\begin{aligned} & \left\| \begin{bmatrix} \mathbf{u}_h^N \\ \mathbf{u}_h^{N-1} \end{bmatrix} \right\|_G^2 + \Delta t \sum_{n=1}^{N-1} (\nu \|\nabla F[\mathbf{u}_h^{n+1}]\|^2) + \frac{1}{4} \sum_{n=1}^{N-1} \|\mathbf{u}_h^{n+1} - 2\mathbf{u}_h^n + \mathbf{u}_h^{n-1}\|_F^2 \\ & = \left\| \begin{bmatrix} \mathbf{u}_h^1 \\ \mathbf{u}_h^0 \end{bmatrix} \right\|_G^2 + \Delta t \sum_{n=1}^{N-1} (\mathbf{f}(t^{n+1}), F[\mathbf{u}_h^{n+1}]) \end{aligned} \quad (4.3.1)$$

**Remark 4.3.1** *We should point out here that, one can obtain exact energy conservation by making use of Crank-Nicolson time discretization along with an EMAC scheme. The aim here is to show the improvement of the classical BE-based scheme by adding simple time filter post-processing and obtaining second-order accuracy in terms of time. Also note that the numerical dissipation  $\frac{3}{4} \|\mathbf{u}_h^{n+1} - 2\mathbf{u}_h^n + \mathbf{u}_h^{n-1}\|^2 \approx \frac{3}{4} \Delta t^4 \|\mathbf{u}_{tt}(t^{n+1})\|^2$ , of the scheme is asymptotically smaller than the numerical dissipation of backward Euler method.*

**Proof.** Set  $\mathbf{v}_h = F[\mathbf{u}_h^{n+1}]$  in (4.2.6),  $q_h = p_h^{n+1}$  in (4.2.7), then the nonlinear term and pressure term vanishes. Then with the use of Lemma 4.1.2, one gets

$$\begin{aligned} \frac{1}{\Delta t} \left\| \begin{bmatrix} \mathbf{u}_h^{n+1} \\ \mathbf{u}_h^n \end{bmatrix} \right\|_G^2 - \frac{1}{\Delta t} \left\| \begin{bmatrix} \mathbf{u}_h^n \\ \mathbf{u}_h^{n-1} \end{bmatrix} \right\|_G^2 + \frac{1}{4\Delta t} \|\mathbf{u}_h^{n+1} - 2\mathbf{u}_h^n + \mathbf{u}_h^{n-1}\|_F^2 \\ + \nu \|\nabla F[\mathbf{u}_h^{n+1}]\|^2 = (\mathbf{f}(t^{n+1}), F[\mathbf{u}_h^{n+1}]). \end{aligned} \quad (4.3.2)$$

Multiplying both sides of (4.3.2) by  $\Delta t$  and taking sum from  $n = 1$  to  $N - 1$  proves the result.  $\square$

Next, we consider the conservation of momentum and angular momentum of Algorithm 4.2.1. Let us define  $\chi(g) \in \mathbf{X}$  to be the restriction of some arbitrary function  $g$  by setting  $\chi(g) = g$  in  $\Omega$  and arbitrarily defined elsewhere to meet the boundary conditions such that  $\chi(g) = g$  in  $\Omega_i$  but  $g|_{\partial\Omega} = 0$ .

**Theorem 4.3.2** For  $\nu = 0, \mathbf{f} = 0$ , *EMAC-FILTERED* scheme (4.2.6)-(4.2.7) conserves momentum and angular momentum for all  $t > 0$ , i.e.,

$$M_{Emac-Fil}(t) = M_{Emac-Fil}(0)$$

$$AM_{Emac-Fil}(t) = AM_{Emac-Fil}(0)$$

**Proof.** We start by showing momentum conservation. Choose  $\mathbf{v}_h = \chi(e_i)$  in (4.2.6) to get

$$((\mathbf{u}_h)_t, e_i) + \nu(\nabla F[\mathbf{u}_h^{n+1}], \nabla e_i) + c(F[\mathbf{u}_h^{n+1}], F[\mathbf{u}_h^{n+1}], e_i) = (\mathbf{f}(t^{n+1}), e_i). \quad (4.3.3)$$

For the nonlinear term in (4.3.3), expand the rate of deformation tensor and use the identity (4.1.8) along with the fact that  $e_i$  is divergence-free. This yields

$$\begin{aligned} & c(F[\mathbf{u}_h^{n+1}], F[\mathbf{u}_h^{n+1}], e_i) \\ &= 2(\mathbf{D}(F[\mathbf{u}_h^{n+1}])F[\mathbf{u}_h^{n+1}], e_i) + (\text{div}(F[\mathbf{u}_h^{n+1}])F[\mathbf{u}_h^{n+1}], e_i) \\ &= (F[\mathbf{u}_h^{n+1}] \cdot \nabla F[\mathbf{u}_h^{n+1}], e_i) + (e_i \cdot \nabla F[\mathbf{u}_h^{n+1}], F[\mathbf{u}_h^{n+1}]) \\ &\quad + ((\nabla \cdot F[\mathbf{u}_h^{n+1}])F[\mathbf{u}_h^{n+1}], e_i) \\ &= (e_i \cdot \nabla F[\mathbf{u}_h^{n+1}], F[\mathbf{u}_h^{n+1}]) \\ &= 0. \end{aligned}$$



Under the assumption  $\nu = 0, \mathbf{f} = 0$ , one gets

$$\frac{d}{dt}(\mathbf{u}_h, e_i) = 0$$

which is precisely the conservation of momentum.

For conservation of angular momentum, take  $\mathbf{v}_h = \chi(\phi_i)$  in (4.2.1) to get

$$((\mathbf{u}_h)_t, \phi_i) + \nu(\nabla F[\mathbf{u}_h^{n+1}], \nabla \phi_i) + c(F[\mathbf{u}_h^{n+1}], F[\mathbf{u}_h^{n+1}], \phi_i) = (\mathbf{f}(t^{n+1}), \phi_i)$$

In a similar manner, by using the identities (4.1.8) and (4.1.9) respectively along with  $\nabla \cdot \phi_i = 0$ , the nonlinear term reduces to

$$\begin{aligned} & c(F[\mathbf{u}_h^{n+1}], F[\mathbf{u}_h^{n+1}], \phi_i) \\ &= 2(\mathbf{D}(F[\mathbf{u}_h^{n+1}])F[\mathbf{u}_h^{n+1}], \phi_i) + (\text{div}(F[\mathbf{u}_h^{n+1}])F[\mathbf{u}_h^{n+1}], \phi_i) \\ &= (F[\mathbf{u}_h^{n+1}] \cdot \nabla F[\mathbf{u}_h^{n+1}], \phi_i) + (F[\mathbf{u}_h^{n+1}], \nabla F[\mathbf{u}_h^{n+1}], \phi_i) \\ &\quad + ((\nabla \cdot F[\mathbf{u}_h^{n+1}])F[\mathbf{u}_h^{n+1}], \phi_i) \\ &= (F[\mathbf{u}_h^{n+1}] \cdot \nabla F[\mathbf{u}_h^{n+1}], \phi_i) + ((\nabla F[\mathbf{u}_h^{n+1}])F[\mathbf{u}_h^{n+1}], \phi_i) \\ &= -(F[\mathbf{u}_h^{n+1}] \cdot \nabla \phi_i, F[\mathbf{u}_h^{n+1}]) \end{aligned}$$

Note that, expansion of the last term gives  $(F[\mathbf{u}_h^{n+1}] \cdot \nabla \phi_i, F[\mathbf{u}_h^{n+1}]) = 0$ , i.e., the non-linear term vanishes. The use of  $\nu = 0, \mathbf{f} = 0$  results in

$$\frac{d}{dt}(\mathbf{u}_h, \phi_i) = 0,$$

which is the required statement of angular momentum conservation.  $\square$

#### 4.4 Numerical Analysis

This section provides unconditional stability result and convergence analysis of the proposed Algorithm 4.2.1. We first provide the stability analysis of the method.

**Lemma 4.4.1** *Let  $\mathbf{f} \in L^\infty(0, T; H^{-1}(\Omega))$ . Then for all  $\Delta t > 0$  and  $N \geq 2$ , the solution of Algorithm 4.2.1 is unconditionally stable in the following sense:*

$$\begin{aligned} & \|\mathbf{u}_h^N\|^2 + \frac{1}{3} \sum_{n=1}^{N-1} \|\mathbf{u}_h^{n+1} - 2\mathbf{u}_h^n + \mathbf{u}_h^{n-1}\|_F^2 + \frac{2\Delta t\nu}{3} \sum_{n=1}^{N-1} \|\nabla F[\mathbf{u}_h^{n+1}]\|^2 \\ & \leq \left(\frac{1}{3}\right)^N \|\mathbf{u}_h^0\|^2 + 2N(\|\mathbf{u}_h^1\|^2 + \|\mathbf{u}_h^0\|^2) + \frac{2N\Delta t\nu^{-1}}{3} \sum_{n=1}^{N-1} \|\mathbf{f}(t^{n+1})\|^2 \end{aligned} \quad (4.4.1)$$

**Proof.** We start the proof by the global energy conservation (4.3.1). The application of Cauchy-Schwarz inequality, Young's inequality, and the dual norm on the forcing term gives

$$(\mathbf{f}(t^{n+1}), F[\mathbf{u}_h^{n+1}]) \leq \frac{\nu^{-1}\Delta t}{2} \|\mathbf{f}(t^{n+1})\|_{-1}^2 + \frac{\nu\Delta t}{2} \|\nabla F[\mathbf{u}_h^{n+1}]\|^2. \quad (4.4.2)$$

Inserting the estimate in (4.3.1) and applying Lemma 4.1.3 leads to

$$\begin{aligned} \frac{3}{4} \|\mathbf{u}_h^N\|^2 + \frac{1}{4} \sum_{n=1}^{N-1} \|\mathbf{u}_h^{n+1} - 2\mathbf{u}_h^n + \mathbf{u}_h^{n-1}\|_F^2 + \frac{\nu\Delta t}{2} \sum_{n=1}^{N-1} (\|\nabla F[\mathbf{u}_h^{n+1}]\|^2) \\ \leq \frac{1}{4} \|\mathbf{u}_h^{N-1}\|^2 + \frac{3}{2} \|\mathbf{u}_h^1\|^2 + \frac{3}{4} \|\mathbf{u}_h^0\|^2 + \frac{\nu^{-1}\Delta t}{2} \|\mathbf{f}(t^{n+1})\|_{-1}^2 \end{aligned} \quad (4.4.3)$$

Lastly, the proof is completed by multiplying by  $\frac{4}{3}$  and using the induction.  $\square$

We proceed to present a detailed convergence analysis of the proposed time filtered method for NSE equations with EMAC formulation. We use the following notations for the discrete norms. For  $\mathbf{v}^n \in H^p(\Omega)$ , we define :

$$\|\mathbf{v}\|_{\infty,p} := \max_{0 \leq n \leq N} \|\mathbf{v}^n\|_p, \quad \|\mathbf{v}\|_{m,p} := \left( \Delta t \sum_{n=0}^N \|\mathbf{v}^n\|_p^m \right)^{\frac{1}{m}}.$$

For the optimal asymptotic error estimation, assume that the following regularity assumptions hold for the exact solution of NSE (4.0.1):

$$\begin{aligned} \mathbf{u} &\in \mathbf{L}^\infty(0, T; (\mathbf{H}^{k+1}(\Omega))^d), \\ \mathbf{u}_t &\in \mathbf{L}^2(0, T; (\mathbf{H}^{k+1}(\Omega))^d), \\ \mathbf{u}_{tt} &\in \mathbf{L}^2(0, T; (\mathbf{H}^1(\Omega))^d), \\ \mathbf{u}_{ttt} &\in \mathbf{L}^2(0, T; (\mathbf{L}^2(\Omega))^d), \\ P &\in L^2(0, T; (H^k(\Omega))^d). \end{aligned} \quad (4.4.4)$$

**Theorem 4.4.1** *Let  $(\mathbf{u}, p)$  be the solution of NSE (4.0.1) such that the regularity assumptions (4.4.4) are satisfied. Then, the following bound holds for the error  $e_{\mathbf{u}}^n = \mathbf{u}^n - \mathbf{u}_h^n$*

$$\begin{aligned}
& \|e_{\mathbf{u}}^N\|^2 + \frac{1}{3} \sum_{n=1}^{N-1} \|e_{\mathbf{u}}^{n+1} - 2e_{\mathbf{u}}^n + e_{\mathbf{u}}^{n-1}\|_F^2 + \frac{2\Delta t\nu}{3} \sum_{n=1}^{N-1} \|\nabla F[e_{\mathbf{u}}^{n+1}]\|^2 \\
& \leq K \left[ \left(\frac{1}{3}\right)^N \|e_{\mathbf{u}}^0\|^2 + 2N(\|e_{\mathbf{u}}^1\|^2 + \|e_{\mathbf{u}}^0\|^2) + \nu^{-1}h^{2k+2} \|\mathbf{u}_t\|_{2,k+1}^2 \right. \\
& \quad + \nu h^{2k} \|\mathbf{u}\|_{2,k+1}^2 + \nu^{-1}h^{2k} \|P^{n+1}\|_{2,k}^2 + \nu^{-1}\Delta t^4 \|\mathbf{u}_{ttt}\|_{L^2(0,T;L^2(\Omega))}^2 \\
& \quad + \Delta t^4 (\nu + \nu^{-1}(\|\nabla F[\mathbf{u}^{n+1}]\|_{\infty,0} + \|\nabla \mathbf{u}^{n+1}\|_{\infty,0})) \|\nabla \mathbf{u}_{tt}\|_{L^2(0,T;L^2(\Omega))}^2 \\
& \quad + \nu^{-1} \|\nabla F[\mathbf{u}^{n+1}]\|_{\infty,0} h^{2k+1} \|\mathbf{u}\|_{2,k+1}^2 \\
& \quad \left. + \nu^{-1} \|\nabla F[\mathbf{u}^{n+1}]\|_{\infty,0} \|F[\mathbf{u}^{n+1}]\|_{\infty,0} h^{2k} \|\mathbf{u}\|_{2,k+1}^2 \right] \quad (4.4.5)
\end{aligned}$$

with  $K = \exp(C\nu^{-1} \|\mathbf{u}\|_{\infty,0})$ , where  $C$  is a generic constant independent of  $h$  and  $\Delta t$ .

Theorem 4.4.1 with the most common choice of inf-sup stable finite element spaces, like the Taylor-Hood element, for the velocity and pressure naturally leads to the following Corollary, proving second-order accuracy both in time and space.

**Proof.** The proof starts by deriving the error equations. Denote  $\mathbf{u}^{n+1} = \mathbf{u}(t^{n+1})$ . At time  $t^{n+1}$ , the true solution of the NSE (4.0.1) satisfies

$$\begin{aligned}
& \left( \frac{3\mathbf{u}^{n+1} - 4\mathbf{u}^n + \mathbf{u}^{n-1}}{2\Delta t}, \mathbf{v}_h \right) + \nu(\nabla F[\mathbf{u}^{n+1}], \nabla \mathbf{v}_h) + c(F[\mathbf{u}^{n+1}], F[\mathbf{u}^{n+1}], \mathbf{v}_h) \\
& \quad - (P^{n+1}, \nabla \cdot \mathbf{v}_h) = (\mathbf{f}^{n+1}, \mathbf{v}_h) + \text{Intp}(\mathbf{u}, \mathbf{v}_h) \quad (4.4.6)
\end{aligned}$$

for all  $\mathbf{v}_h \in \mathbf{V}_h$  where

$$\begin{aligned}
\text{Intp}(\mathbf{u}^{n+1}, \mathbf{v}_h) &= \left( \frac{3\mathbf{u}^{n+1} - 4\mathbf{u}^n + \mathbf{u}^{n-1}}{2\Delta t} - \mathbf{u}_t^{n+1}, \mathbf{v}_h \right) + \nu(\nabla F[\mathbf{u}^{n+1}] - \mathbf{u}^{n+1}, \nabla \mathbf{v}_h) \\
& \quad + c(F[\mathbf{u}^{n+1}], F[\mathbf{u}^{n+1}], \mathbf{v}_h) - c(\mathbf{u}^{n+1}, \mathbf{u}^{n+1}, \mathbf{v}_h)
\end{aligned}$$

denotes the local truncation error.

Subtracting (4.2.6) from (4.4.6) yields

$$\begin{aligned}
& \left( \frac{3e_{\mathbf{u}}^{n+1} - 4e_{\mathbf{u}}^n + e_{\mathbf{u}}^{n-1}}{2\Delta t}, \mathbf{v}_h \right) + \nu(\nabla F[e_{\mathbf{u}}^{n+1}], \nabla \mathbf{v}_h) + c(F[\mathbf{u}^{n+1}], F[\mathbf{u}^{n+1}], \mathbf{v}_h) \\
& \quad - c(F[\mathbf{u}_h^{n+1}], F[\mathbf{u}_h^{n+1}], \mathbf{v}_h) - (P^{n+1}, \nabla \cdot \mathbf{v}_h) = \text{Intp}(\mathbf{u}, \mathbf{v}_h) \quad (4.4.7)
\end{aligned}$$

Decompose the error as

$$e_{\mathbf{u}}^n = \mathbf{u}(t^n) - \mathbf{u}_h^n = (\mathbf{u}(t^n) - I^h \mathbf{u}^n) + (I^h \mathbf{u}^n - \mathbf{u}_h^n) = \eta^n + \phi_h^n. \quad (4.4.8)$$

where  $I^h \mathbf{u}^n$  is an interpolant of  $\mathbf{u}^n$  in  $\mathbf{V}_h$ . Choosing  $\mathbf{v}_h = F[\phi_h^{n+1}]$  in (4.4.7), using the error decomposition and Lemma 4.1.2, it follows that

$$\begin{aligned}
& \frac{1}{\Delta t} \left\| \begin{bmatrix} \phi_h^{n+1} \\ \phi_h^n \end{bmatrix} \right\|_G^2 - \frac{1}{\Delta t} \left\| \begin{bmatrix} \phi_h^n \\ \phi_h^{n-1} \end{bmatrix} \right\|_G^2 + \frac{1}{4\Delta t} \|\phi_h^{n+1} - 2\phi_h^n + \phi_h^{n-1}\|_F^2 \\
& + \nu \|\nabla F[\phi_h^{n+1}]\|^2 \\
& = \left( \frac{3\eta^{n+1} - 4\eta^n + \eta^{n-1}}{2\Delta t}, F[\phi_h^{n+1}] \right) + \nu (\nabla F[\eta^{n+1}], \nabla F[\phi_h^{n+1}]) \\
& - c(F[\mathbf{u}^{n+1}], F[\mathbf{u}^{n+1}], F[\phi_h^{n+1}]) + c(F[\mathbf{u}_h^{n+1}], F[\mathbf{u}_h^{n+1}], F[\phi_h^{n+1}]) \\
& - (P^{n+1}, \nabla \cdot F[\phi_h^{n+1}]) + \text{Intp}(\mathbf{u}, F[\phi_h^{n+1}]) \tag{4.4.9}
\end{aligned}$$

Next, estimate the terms on the right hand side of (4.4.9). The first two terms are bounded by applying Cauchy-Schwarz, the estimation (3.1.17) and Young's inequality:

$$\begin{aligned}
\left| - \left( \frac{3\eta^{n+1} - 4\eta^n + \eta^{n-1}}{2\Delta t}, F[\phi_h^{n+1}] \right) \right| & \leq \left\| \frac{3\eta^{n+1} - 4\eta^n + \eta^{n-1}}{2\Delta t} \right\| \|F[\phi_h^{n+1}]\|^2 \\
& \leq \frac{C\nu^{-1}}{\Delta t} \int_{t^{n-1}}^{t^{n+1}} \|\eta_t\|^2 dt \\
& \quad + \frac{\nu}{28} \|\nabla F[\phi_h^{n+1}]\|^2 \tag{4.4.10}
\end{aligned}$$

$$\begin{aligned}
|\nu (\nabla F[\eta^{n+1}], \nabla F[\phi_h^{n+1}])| & \leq \nu \|\nabla F[\eta^{n+1}]\| \|\nabla F[\phi_h^{n+1}]\| \\
& \leq C\nu^{-1} \|\nabla F[\eta^{n+1}]\|^2 \\
& \quad + \frac{\nu}{28} \|\nabla F[\phi_h^{n+1}]\|^2. \tag{4.4.11}
\end{aligned}$$

Following Theorem 3.2 in [91], the nonlinear terms are estimated as,

$$\begin{aligned}
& \left| -c(F[\mathbf{u}^{n+1}], F[\mathbf{u}^{n+1}], F[\phi_h^{n+1}]) + c(F[\mathbf{u}_h^{n+1}], F[\mathbf{u}_h^{n+1}], F[\phi_h^{n+1}]) \right| \\
& \leq C\nu^{-1} \left( \|\nabla F[\mathbf{u}^{n+1}]\|^2 \|F[\eta^{n+1}]\| \|\nabla F[\eta^{n+1}]\| \right. \\
& \quad \left. + \|\nabla F[\mathbf{u}^{n+1}]\| \|F[\mathbf{u}^{n+1}]\| \|\nabla F[\eta^{n+1}]\|^2 \right) \\
& \quad + C\nu^{-1} \|\nabla F[\mathbf{u}^{n+1}]\|^2 \|F[\phi_h^{n+1}]\|^2 + \frac{\nu}{28} \|\nabla F[\phi_h^{n+1}]\|^2. \tag{4.4.12}
\end{aligned}$$

For the pressure term, use the fact that  $(\nabla \cdot \phi_h, q_h) = 0, \forall \phi_h \in \mathbf{V}_h$  together with Cauchy-Schwarz and Young's inequalities to get

$$\begin{aligned}
|(P^{n+1}, \nabla \cdot \phi_h^{n+1})| & = |(P^{n+1} - q_h, \nabla \cdot \phi_h^{n+1})| \\
& \leq C\nu^{-1} \left\| \inf_{q_h \in Q_h} \|P^{n+1} - q_h\| \right\|^2 + \frac{\nu}{28} \|\nabla F[\phi_h^{n+1}]\|^2 \tag{4.4.13}
\end{aligned}$$

We proceed to bound the terms in the local truncation error  $Intp(\mathbf{u}, F[\phi_h^{n+1}])$ . For the first two terms of  $Intp(\mathbf{u}, F[\phi_h^{n+1}])$ , apply the Cauchy-Schwarz and Young's inequalities together with the estimations (3.1.18) and (4.1.19) to obtain

$$\begin{aligned}
& \left| \left( \frac{3\mathbf{u}^{n+1} - 4\mathbf{u}^n + \mathbf{u}^{n-1}}{2\Delta t} - \mathbf{u}_t^{n+1}, F[\phi_h^{n+1}] \right) \right| \\
& \leq \left\| \frac{3\mathbf{u}^{n+1} - 4\mathbf{u}^n + \mathbf{u}^{n-1}}{2\Delta t} - \mathbf{u}_t(t^{n+1}) \right\| \|F[\phi_h^{n+1}]\| \\
& \leq C\Delta t^3 \nu^{-1} \int_{t^{n-1}}^{t^{n+1}} \|\mathbf{u}_{ttt}\|^2 dt + \frac{\nu}{28} \|\nabla F[\phi_h^{n+1}]\| \quad (4.4.14)
\end{aligned}$$

$$\begin{aligned}
\nu(\nabla(F[\mathbf{u}^{n+1}] - \mathbf{u}^{n+1}), \nabla F[\phi_h^{n+1}]) & \leq C\nu \|\nabla(F[\mathbf{u}^{n+1}] - \mathbf{u}^{n+1})\|^2 + \frac{\nu}{28} \|\nabla F[\phi_h^{n+1}]\|^2 \\
& \leq C\nu\Delta t^3 \int_{t^{n-1}}^{t^{n+1}} \|\nabla \mathbf{u}_{tt}\|^2 dt + \frac{\nu}{28} \|\nabla F[\phi_h^{n+1}]\|^2.
\end{aligned}$$

To bound the convective terms in  $Intp(\mathbf{u}, F[\phi_h^{n+1}])$ , we first rearrange the terms. Adding and subtracting terms for the convective terms and using the definition of the EMAC formulation gives

$$\begin{aligned}
& c(F[\mathbf{u}^{n+1}], F[\mathbf{u}^{n+1}], F[\phi_h^{n+1}]) - c(\mathbf{u}^{n+1}, \mathbf{u}^{n+1}, F[\phi_h^{n+1}]) \\
& = c(F[\mathbf{u}^{n+1}] - \mathbf{u}^{n+1}, F[\mathbf{u}^{n+1}], F[\phi_h^{n+1}]) + c(\mathbf{u}^{n+1}, F[\mathbf{u}^{n+1}] - \mathbf{u}^{n+1}, F[\phi_h^{n+1}]) \\
& = (F[\mathbf{u}^{n+1}] \cdot \nabla(F[\mathbf{u}^{n+1}] - \mathbf{u}^{n+1}), F[\phi_h^{n+1}]) \\
& \quad + (F[\phi_h^{n+1}] \cdot \nabla(F[\mathbf{u}^{n+1}] - \mathbf{u}^{n+1}), F[\mathbf{u}^{n+1}]) - \\
& \quad ((F[\mathbf{u}^{n+1}] - \mathbf{u}^{n+1}) \cdot \nabla F[\mathbf{u}^{n+1}], F[\phi_h^{n+1}]) \\
& \quad - ((F[\mathbf{u}^{n+1}] - \mathbf{u}^{n+1}) \cdot \nabla F[\phi_h^{n+1}], F[\mathbf{u}^{n+1}]) \\
& \quad + ((F[\mathbf{u}^{n+1}] - \mathbf{u}^{n+1}) \cdot \nabla \mathbf{u}^{n+1}, F[\phi_h^{n+1}]) \\
& \quad + (F[\phi_h^{n+1}] \cdot \nabla \mathbf{u}^{n+1}, F[\mathbf{u}^{n+1}] - \mathbf{u}^{n+1}) \\
& \quad - (\mathbf{u}^{n+1} \cdot \nabla(F[\mathbf{u}^{n+1}] - \mathbf{u}^{n+1}), F[\phi_h^{n+1}]) \\
& \quad - (\mathbf{u}^{n+1} \cdot \nabla F[\phi_h^{n+1}], (F[\mathbf{u}^{n+1}] - \mathbf{u}^{n+1})). \quad (4.4.15)
\end{aligned}$$

Then, the convective terms in (4.4.15) are estimated by applying the Cauchy-Schwarz and Young's inequalities together with the estimation (4.1.19) as

$$\begin{aligned}
& |(F[\mathbf{u}^{n+1}] \cdot \nabla(F[\mathbf{u}^{n+1}] - \mathbf{u}^{n+1}), F[\phi_h^{n+1}])| \\
& \leq C\nu^{-1} \|\nabla F[\mathbf{u}^{n+1}]\|^2 \|\nabla(F[\mathbf{u}^{n+1}] - \mathbf{u}^{n+1})\|^2 + \frac{\nu}{28} \|\nabla F[\phi_h^{n+1}]\|^2 \\
& \leq C\nu^{-1}\Delta t^3 \|\nabla F[\mathbf{u}^{n+1}]\|^2 \int_{t_{3n-1}}^{t^{n+1}} \|\nabla \mathbf{u}_{tt}\|^2 dt + \frac{\nu}{28} \|\nabla F[\phi_h^{n+1}]\|^2, \quad (4.4.16)
\end{aligned}$$

$$\begin{aligned}
& |(F[\phi_h^{n+1}] \cdot \nabla F[\mathbf{u}^{n+1}] - \mathbf{u}^{n+1}), F[\mathbf{u}^{n+1}]| \\
& \leq C\nu^{-1} \|\nabla F[\mathbf{u}^{n+1}]\|^2 \|\nabla(F[\mathbf{u}^{n+1}] - \mathbf{u}^{n+1})\|^2 + \frac{\nu}{28} \|\nabla F[\phi_h^{n+1}]\|^2 \\
& \leq C\nu^{-1} \Delta t^3 \|\nabla F[\mathbf{u}^{n+1}]\|^2 \int_{t^{n-1}}^{t^{n+1}} \|\nabla \mathbf{u}_{tt}\|^2 dt + \frac{\nu}{28} \|\nabla F[\phi_h^{n+1}]\|^2, \quad (4.4.17)
\end{aligned}$$

$$\begin{aligned}
& | - ((F[\mathbf{u}^{n+1}] - \mathbf{u}^{n+1}) \cdot \nabla F[\mathbf{u}^{n+1}], F[\phi_h^{n+1}]) | \\
& \leq C\nu^{-1} \|\nabla F[\mathbf{u}^{n+1}]\|^2 \|\nabla(F[\mathbf{u}^{n+1}] - \mathbf{u}^{n+1})\|^2 + \frac{\nu}{28} \|\nabla F[\phi_h^{n+1}]\|^2 \\
& \leq C\nu^{-1} \Delta t^3 \|\nabla F[\mathbf{u}^{n+1}]\|^2 \int_{t^{n-1}}^{t^{n+1}} \|\nabla \mathbf{u}_{tt}\|^2 dt + \frac{\nu}{28} \|\nabla F[\phi_h^{n+1}]\|^2, \quad (4.4.18)
\end{aligned}$$

$$\begin{aligned}
& | - ((F[\mathbf{u}^{n+1}] - \mathbf{u}^{n+1}) \cdot \nabla F[\phi_h^{n+1}], F[\mathbf{u}^{n+1}]) | \\
& \leq C\nu^{-1} \|\nabla F[\mathbf{u}^{n+1}]\|^2 \|\nabla(F[\mathbf{u}^{n+1}] - \mathbf{u}^{n+1})\|^2 + \frac{\nu}{28} \|\nabla F[\phi_h^{n+1}]\|^2 \\
& \leq C\nu^{-1} \Delta t^3 \|\nabla F[\mathbf{u}^{n+1}]\|^2 \int_{t^{n-1}}^{t^{n+1}} \|\nabla \mathbf{u}_{tt}\|^2 dt + \frac{\nu}{28} \|\nabla F[\phi_h^{n+1}]\|^2, \quad (4.4.19)
\end{aligned}$$

$$\begin{aligned}
& | ((F[\mathbf{u}^{n+1}] - \mathbf{u}^{n+1}) \cdot \nabla \mathbf{u}^{n+1}, F[\phi_h^{n+1}]) | \\
& \leq C\nu^{-1} \|\nabla \mathbf{u}^{n+1}\|^2 \|\nabla(F[\mathbf{u}^{n+1}] - \mathbf{u}^{n+1})\|^2 + \frac{\nu}{28} \|\nabla F[\phi_h^{n+1}]\|^2 \\
& \leq C\nu^{-1} \Delta t^3 \|\nabla \mathbf{u}^{n+1}\|^2 \int_{t^{n-1}}^{t^{n+1}} \|\nabla \mathbf{u}_{tt}\|^2 dt + \frac{\nu}{28} \|\nabla F[\phi_h^{n+1}]\|^2, \quad (4.4.20)
\end{aligned}$$

$$\begin{aligned}
& | (F[\phi_h^{n+1}] \cdot \nabla \mathbf{u}^{n+1}, F[\mathbf{u}^{n+1}] - \mathbf{u}^{n+1}) | \\
& \leq C\nu^{-1} \|\nabla \mathbf{u}^{n+1}\|^2 \|\nabla(F[\mathbf{u}^{n+1}] - \mathbf{u}^{n+1})\|^2 + \frac{\nu}{28} \|\nabla F[\phi_h^{n+1}]\|^2 \\
& \leq C\nu^{-1} \Delta t^3 \|\nabla \mathbf{u}^{n+1}\|^2 \int_{t_{3n-1}}^{t^{n+1}} \|\nabla \mathbf{u}_{tt}\|^2 dt + \frac{\nu}{28} \|\nabla F[\phi_h^{n+1}]\|^2, \quad (4.4.21)
\end{aligned}$$

$$\begin{aligned}
& | - (\mathbf{u}^{n+1} \cdot \nabla(F[\mathbf{u}^{n+1}] - \mathbf{u}^{n+1}), F[\phi_h^{n+1}]) | \\
& \leq C\nu^{-1} \|\nabla \mathbf{u}^{n+1}\|^2 \|\nabla(F[\mathbf{u}^{n+1}] - \mathbf{u}^{n+1})\|^2 + \frac{\nu}{28} \|\nabla F[\phi_h^{n+1}]\|^2 \\
& \leq C\nu^{-1} \Delta t^3 \|\nabla \mathbf{u}^{n+1}\|^2 \int_{t^{n-1}}^{t^{n+1}} \|\nabla \mathbf{u}_{tt}\|^2 dt + \frac{\nu}{28} \|\nabla F[\phi_h^{n+1}]\|^2, \quad (4.4.22)
\end{aligned}$$

$$\begin{aligned}
& | - (\mathbf{u}^{n+1} \cdot \nabla F[\phi_h^{n+1}], (F[\mathbf{u}^{n+1}] - \mathbf{u}^{n+1})) | \\
& \leq C\nu^{-1} \|\nabla \mathbf{u}^{n+1}\|^2 \|\nabla(F[\mathbf{u}^{n+1}] - \mathbf{u}^{n+1})\|^2 + \frac{\nu}{28} \|\nabla F[\phi_h^{n+1}]\|^2 \\
& \leq C\nu^{-1} \Delta t^3 \|\nabla \mathbf{u}^{n+1}\|^2 \int_{t^{n-1}}^{t^{n+1}} \|\nabla \mathbf{u}_{tt}\|^2 dt + \frac{\nu}{28} \|\nabla F[\phi_h^{n+1}]\|^2. \quad (4.4.23)
\end{aligned}$$

Inserting (4.4.16)-(4.4.23) into (4.4.6) gives

$$\begin{aligned}
& \frac{1}{\Delta t} \left\| \begin{bmatrix} \phi_h^{n+1} \\ \phi_h^n \end{bmatrix} \right\|_G^2 - \frac{1}{\Delta t} \left\| \begin{bmatrix} \phi_h^n \\ \phi_h^{n-1} \end{bmatrix} \right\|_G^2 + \frac{1}{4\Delta t} \|\phi_h^{n+1} - 2\phi_h^n + \phi_h^{n-1}\|_F^2 \\
& \quad + \frac{\nu}{2} \|\nabla F[\phi_h^{n+1}]\|^2 \\
& \leq \frac{C\nu^{-1}}{\Delta t} \int_{t^{n-1}}^{t^{n+1}} \|\eta_t\|^2 dt + C\nu \|\nabla F[\eta^{n+1}]\|^2 + C\nu^{-1} \inf_{q_h \in Q_h} \|P^{n+1} - q_h\|^2 \\
& \quad + C\nu^{-1} \Delta t^3 \int_{t^{n-1}}^{t^{n+1}} \|\mathbf{u}_{ttt}\|^2 dt + C\nu \Delta t^3 \int_{t^{n-1}}^{t^{n+1}} \|\nabla \mathbf{u}_{tt}\|^2 dt \\
& \quad + C\nu^{-1} \Delta t^3 (\|\nabla F[\mathbf{u}^{n+1}]\|^2 + \|\nabla \mathbf{u}^{n+1}\|^2) \int_{t^{n-1}}^{t^{n+1}} \|\nabla \mathbf{u}_{tt}\|^2 dt \\
& \quad + C\nu^{-1} \left( \|\nabla F[\mathbf{u}^{n+1}]\|^2 \|F[\eta^{n+1}]\| \|\nabla F[\eta^{n+1}]\| \right. \\
& \quad \left. + \|\nabla F[\mathbf{u}^{n+1}]\| \|F[\mathbf{u}^{n+1}]\| \|\nabla F[\eta^{n+1}]\|^2 \right) \\
& \quad + C\nu^{-1} \|\nabla F[\mathbf{u}^{n+1}]\|^2 \|F[\phi_h^{n+1}]\|^2
\end{aligned}$$

Multiplying by  $\Delta t$ , summing from  $n = 1$  to  $n = N - 1$  and using approximation properties (3.1.5)-(3.1.6) yields

$$\begin{aligned}
& \left\| \begin{bmatrix} \phi_h^N \\ \phi_h^{N-1} \end{bmatrix} \right\|_G^2 + \frac{1}{4} \|\phi_h^{n+1} - 2\phi_h^n + \phi_h^{n-1}\|_F^2 + \frac{\nu\Delta t}{2} \|\nabla F[\phi_h^{n+1}]\|^2 \\
& \leq \left\| \begin{bmatrix} \phi_h^1 \\ \phi_h^0 \end{bmatrix} \right\|_G^2 + C \left( \nu^{-1} h^{2k+2} \|\mathbf{u}_t\|_{2,k+1}^2 + \nu h^{2k} \|\mathbf{u}\|_{2,k+1}^2 + \nu^{-1} h^{2k} \|P^{n+1}\|_{2,k}^2 \right) \\
& \quad + C\nu^{-1} \Delta t^4 \|\mathbf{u}_{ttt}\|_{L^2(0,T;L^2(\Omega))}^2 \\
& \quad + C\Delta t^4 (\nu + \nu^{-1} (\|\|\nabla F[\mathbf{u}^{n+1}]\|\|_{\infty,0} + \|\|\nabla \mathbf{u}^{n+1}\|\|_{\infty,0})) \|\nabla \mathbf{u}_{tt}\|_{L^2(0,T;L^2(\Omega))}^2 \\
& \quad + C\nu^{-1} \left( \|\|\nabla F[\mathbf{u}^{n+1}]\|\|_{\infty,0} h^{2k+1} \|\mathbf{u}\|_{2,k+1}^2 \right. \\
& \quad \left. + \|\|\nabla F[\mathbf{u}^{n+1}]\|\|_{\infty,0} \|F[\mathbf{u}^{n+1}]\|_{\infty,0} h^{2k} \|\mathbf{u}\|_{2,k+1}^2 \right) \\
& \quad + C\nu^{-1} \|\|\nabla F[\mathbf{u}^{n+1}]\|\|_{\infty,0} \Delta t \sum_{n=1}^{N-1} \|F[\phi_h^{n+1}]\|^2 \tag{4.4.24}
\end{aligned}$$

Applying the discrete Gronwall inequality with the assumption

$$\Delta t \leq C(\|\|\nabla F[\mathbf{u}^{n+1}]\|\|_{\infty,0})^{-1}$$

and using Lemma 4.1.3 produces

$$\begin{aligned}
& \|\phi_h^N\|^2 + \frac{1}{3} \sum_{n=1}^{N-1} \|\phi_h^{n+1} - 2\phi_h^n + \phi_h^{n-1}\|_F^2 + \frac{2\Delta t\nu}{3} \sum_{n=1}^{N-1} \|\nabla F[\phi_h^{n+1}]\|^2 \\
& \leq K \left[ \left(\frac{1}{3}\right)^N \|\phi_h^0\|^2 + 2N(\|\phi_h^1\|^2 + \|\phi_h^0\|^2) + \nu^{-1}h^{2k+2} \|\mathbf{u}_t\|_{2,k+1}^2 \right. \\
& \quad + \nu h^{2k} \|\mathbf{u}\|_{2,k+1}^2 + \nu^{-1}h^{2k} \|P^{n+1}\|_{2,k}^2 + \nu^{-1}\Delta t^4 \|\mathbf{u}_{ttt}\|_{L^2(0,T;L^2(\Omega))}^2 \\
& \quad + \Delta t^4 (\nu + \nu^{-1}(\|\nabla F[\mathbf{u}^{n+1}]\|_{\infty,0} + \|\nabla \mathbf{u}^{n+1}\|_{\infty,0})) \|\nabla \mathbf{u}_{tt}\|_{L^2(0,T;L^2(\Omega))}^2 \\
& \quad + \nu^{-1} \|\nabla F[\mathbf{u}^{n+1}]\|_{\infty,0} h^{2k+1} \|\mathbf{u}\|_{2,k+1}^2 \\
& \quad \left. + \nu^{-1} \|\nabla F[\mathbf{u}^{n+1}]\|_{\infty,0} \|F[\mathbf{u}^{n+1}]\|_{\infty,0} h^{2k} \|\mathbf{u}\|_{2,k+1}^2 \right] \quad (4.4.25)
\end{aligned}$$

where  $K = \exp(C\nu^{-1} \|\mathbf{u}\|_{\infty,0})$ , where  $C$  is a generic constant independent of  $h$  and  $\Delta t$ . The final result follows from the triangle inequality.  $\square$

**Corollary 4.4.1** *Under the assumptions of Theorem 4.4.1, let  $(\mathbf{X}_h, Q_h) = (P_2, P_1)$  be the Taylor-Hood finite element spaces for velocity and pressure. Then, the asymptotic error estimation satisfies, for all  $\Delta t > 0$*

$$\begin{aligned}
\|e_{\mathbf{u}}^N\|^2 + \frac{1}{3} \sum_{n=1}^{N-1} \|e_{\mathbf{u}}^{n+1} - 2e_{\mathbf{u}}^n + e_{\mathbf{u}}^{n-1}\|_F^2 + \frac{2\Delta t\nu}{3} \sum_{n=1}^{N-1} \|\nabla F[e_{\mathbf{u}}^{n+1}]\|^2 \\
\leq C \left( h^4 + \Delta t^4 + \|e^0\|^2 + \|e^1\|^2 \right).
\end{aligned}$$

**Proof.** Using the regularity assumption (4.4.4) gives the required result.  $\square$

## 4.5 Numerical Experiments

In this section, we perform four different numerical experiments to test the effectiveness of the proposed Algorithm (4.2.3)-(4.2.5) and compare the results with the non-filtered BE-EMAC scheme (step 1 without step 2). The first test confirms the order of convergence rates predicted in Corollary 4.4.1 for an analytic test problem with a known solution. In the second example, we check the energy, momentum, and angular momentum conservation of the EMAC-FILTERED scheme in a so-called Gresho problem. In the third test, we studied a typical benchmark problem of flow around a cylinder to demonstrate the superiority of the EMAC-FILTERED method over the



BE-EMAC scheme. In the last test, we tested the efficiency of the EMAC-FILTERED method on a channel flow problem over a flat plate. All simulations are carried out with the Taylor-Hood finite element pairs  $(\mathbf{X}_h, Q_h) = (P_2, P_1)$  for velocity and pressure on conforming triangular grids. The computations are performed with the public license finite element software package FreeFem++ [42].

#### 4.5.1 Convergence Rates

In this part, we verify the expected convergence rates of our numerical scheme (4.2.3)-(4.2.5) described by Corollary 4.4.1. For this purpose, we pick the analytical solution:

$$\mathbf{u} = \begin{pmatrix} \cos(y)e^t \\ \sin(x)e^t \end{pmatrix}, \quad p = (x - y)(1 + t)$$

with the kinematic viscosity  $\nu = 1$  and from which the external force is determined so that (4.0.1) is satisfied. Computations are performed in the unit square domain  $\Omega = [0, 1]^2$ . The boundary conditions are enforced to be the true solution. The approximate solutions are computed on successive mesh refinements and the velocity errors are measured in the discrete norm  $L^2(0, T; H^1(\Omega))$

$$\|\mathbf{u} - \mathbf{u}_h\|_{2,1} = \left\{ \Delta t \sum_{n=1}^N \|\nabla(\mathbf{u}(t^n) - \mathbf{u}_h^n)\|^2 \right\}^{1/2}.$$

To test the spatial convergence, we fixed the time step as  $\Delta t = 0.00001$  with an end time  $T = 10^{-4}$  to isolate the spatial error and calculate the errors for varying  $h$ . Results for errors and rates are shown in Table 4.1. Similarly, we fix the mesh size to  $h = 1/128$  to compute temporal errors and convergence rates by using different time steps with an end time of  $T = 1$ , see Table 4.2. One can observe second-order accuracy both in time and space, which is the optimal convergence rate found in Corollary 4.4.1. Thus we can conclude that the addition of time filtering not only increases the time accuracy but also does not degrade the spatial order of convergence.

Table 4.1: Spatial errors and rates

$h$	$\ u - u_h\ _{2,1}$	Rate
1/4	2.32618e-6	–
1/8	5.80867e-7	2.00209
1/16	1.44272e-7	2.00938
1/32	3.5518e-8	2.0221
1/64	9.56472e-9	1.89275

Table 4.2: Temporal errors and rates

$\Delta t$	$\ u - u_h\ _{2,1}$	Rate
1/4	0.0281784	–
1/8	0.00693954	2.02165
1/16	0.00124549	2.47811
1/32	0.000227284	2.45412
1/64	4.08335e-5	2.4767

#### 4.5.2 Gresho Problem

The second experiment we consider is the Gresho problem, which is a rotating vortex problem [102, 112] independent of time for the case of inviscid flow. Angular velocity depends only on radius and centrifugal force is balanced by pressure distributions. We aim here to numerically verify that the quantities mentioned in Section 4.3 are conserved by the EMAC-FILTERED scheme. The simulation starts with an initial condition  $\mathbf{u}_0$  that is an exact solution of the steady Euler equations. On the domain  $\Omega = (-0.5, 0.5)^2$  with  $r = \sqrt{x^2 + y^2}$ , the velocity and pressure solutions are defined by

$$\begin{aligned}
r \leq 0.2 & : \left\{ \mathbf{u} = \begin{pmatrix} -5y \\ 5x \end{pmatrix}, p = 12.5r^2 + C_1 \right. \\
0.2 \leq r \leq 0.4 & : \left\{ \mathbf{u} = \begin{pmatrix} \frac{2y}{r} + 5y \\ \frac{2x}{r} - 5x \end{pmatrix}, p = 12.5r^2 - 20r + 4\log(r) + C_2 \right. \\
r > 0.4 & : \left\{ \mathbf{u} = \begin{pmatrix} 0 \\ 0 \end{pmatrix}, p = 0 \right.
\end{aligned}$$

where

$$C_2 = (-12.5)(0.4)^2 + 20(0.4)^2 - 4\log(0.4), \quad C_1 = C_2 - 20(0.2) + 4\log(0.2).$$

The speed plot of this initial condition can be seen in Figure 4.1.

We compute solutions of the EMAC-FILTERED and BE-EMAC schemes by using

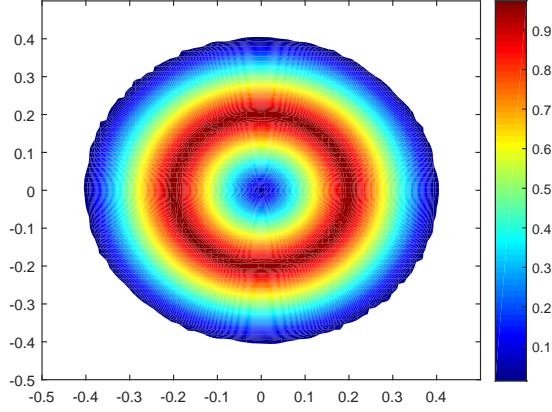


Figure 4.1: Speed contours of true solution of the Gresho problem at all times.

Newton iterations to solve the nonlinear term with  $\mathbf{f} = 0, \nu = 0$  and no penetration boundary conditions up to  $T = 8$ . The computations are run on a  $48 \times 48$  uniform mesh with a time step size  $\Delta t = 0.025$ . Since the initial condition is the solution of the steady Euler equation, the accuracy of the method depends on keeping this solution unchanged over time. In addition, since there are no viscosity and external force, the problem is highly suitable to test the conservation properties of a numerical method. Plots of energy, momentum, angular momentum, and  $L^2$  error versus time of both the EMAC-FILTERED and the BE-EMAC are shown in Figure 4.2. We can deduce from the figure that the EMAC-FILTERED scheme we consider conserves momentum, and angular momentum and is accurate as predicted in the theory. Making use of this scheme has no drawbacks in terms of preserving desired physical quantities when compared to BE-EMAC. For longer time intervals, the energy loss of the EMAC-FILTERED scheme is slightly better than the BE-EMAC scheme after  $t = 5$ .

In addition, we calculate and compare the physical dissipation and numerical dissipation to support the conservation properties of the scheme for the same test with  $Re = 1000$  over the time interval of  $[0, 10]$ . The results are presented in Figure 4.3. As seen, numerical dissipation, which is almost zero, is much smaller than the physical dissipation. This shows that the energy loss of the proposed scheme is very low. So we can deduce that, in terms of physical quantities, making use of the EMAC-FILTERED scheme has no disadvantage over the BE-EMAC scheme and is even

slightly advantageous in terms of energy loss.

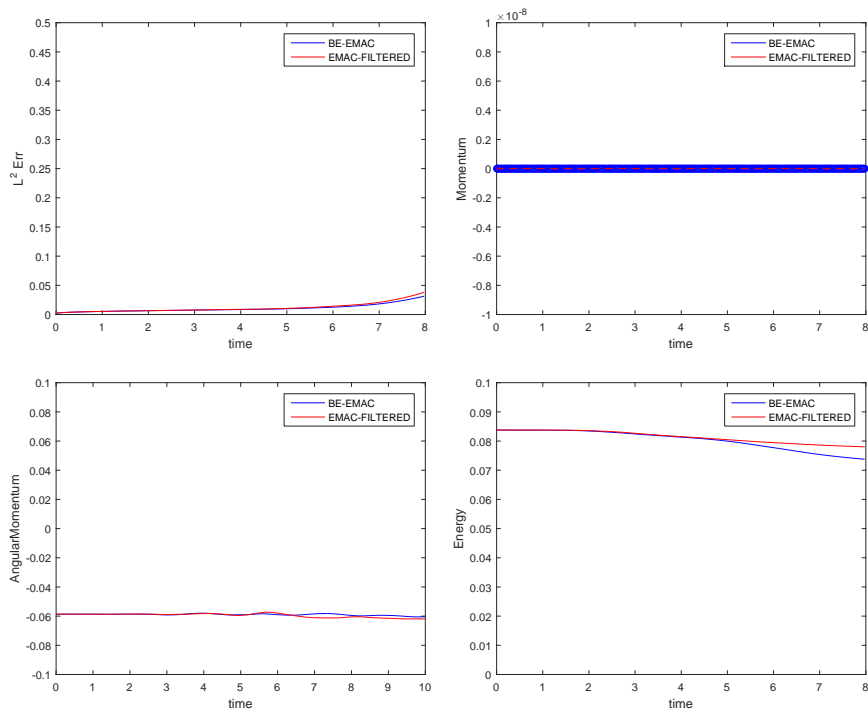


Figure 4.2: Plots of time versus  $L^2$  error, energy, momentum and angular momentum.

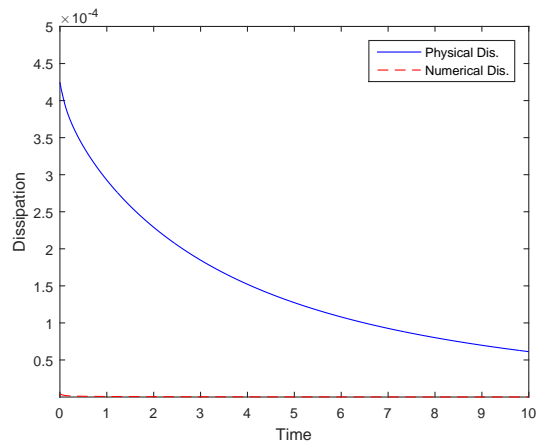


Figure 4.3: Numerical and physical dissipation versus time for our scheme

### 4.5.3 Flow Around a Cylinder

In the next experiment, we test the performance of the EMAC-FILTERED algorithm on a well-known benchmark problem taken from [92, 144], known as channel flow

around a cylinder, and compare the results with that of the BE-EMAC scheme. This problem has been widely studied for the simulation of fluid flows thanks to its real flow characteristics and highly reliable data to measure the accuracy of methods. For the problem set-up, we follow the paper [92]. The computational domain is a  $[0, 2.2] \times [0, 0.41]$  rectangular channel with a cylinder (circle) of radius 0.05 centered at  $(0.2, 0.2)$ , seen in Figure 4.4 ([92]).

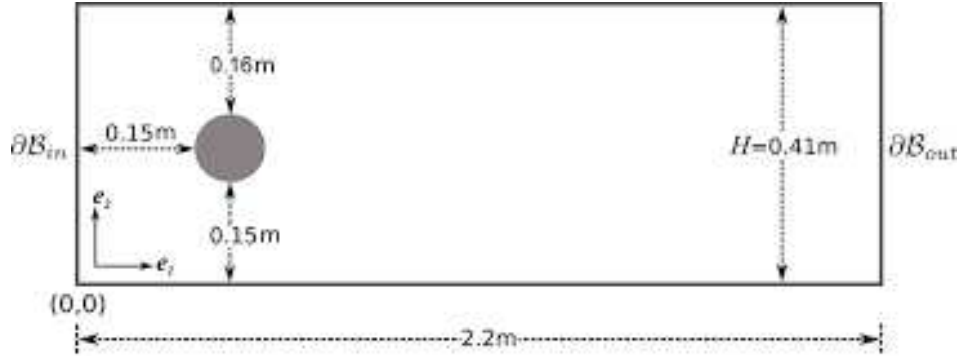


Figure 4.4: Domain  $\Omega$  of the test problem

The time dependent inflow and outflow velocity profiles are given by

$$\mathbf{u}_1(0, y, t) = \mathbf{u}_1(2.2, y, t) = \frac{6}{0.41^2} \sin\left(\frac{\pi t}{8}\right) y(0.41 - y)$$

$$\mathbf{u}_2(0, y, t) = \mathbf{u}_2(2.2, y, t) = 0$$

No-slip boundary conditions are enforced at the cylinder and walls. We take zero initial condition  $\mathbf{u}(x, y, t) = 0$  and the kinematic viscosity  $\nu = 10^{-3}$ . Moreover, there is no external force acting on the flow. We run the problem on a very coarse mesh consisting of only 10210 total degrees of freedom with an end time  $T = 8$  and time-step  $\Delta t = 0.01$ .

The plots of flow development of both BE-EMAC scheme and EMAC-FILTERED scheme at time  $t = 2, 4, 6, 8$  are presented in Figure 4.5 and Figure 4.6, respectively. We observe that although BE-EMAC solutions at  $t = 2, t = 4$  are similar to the DNS of [92, 144], solutions at  $t = 6, t = 8$  are inaccurate in which even vortices are not formed which incorrectly predicts velocity solution of turbulent-like flows. However, the plots of the EMAC-FILTERED scheme match quite well with the DNS of [92, 144] in which the formation of vortices, which are known as Von-Karman

street, are clearly observable. The results of this simulation shows the superiority of the EMAC-FILTERED scheme over the unfiltered case in terms of accuracy and prove the assertion of reducing the undesirable drawbacks of BE discretization by the application of a simple time filtering algorithm.

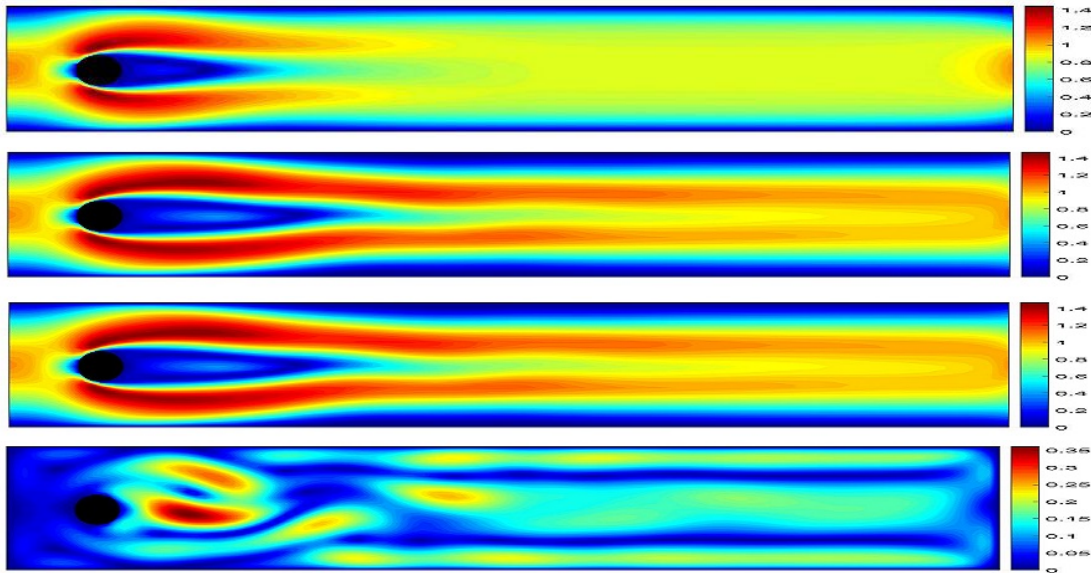


Figure 4.5: The velocity of the BE-EMAC scheme at  $t = 2, 4, 6, 8$  (from up to down).

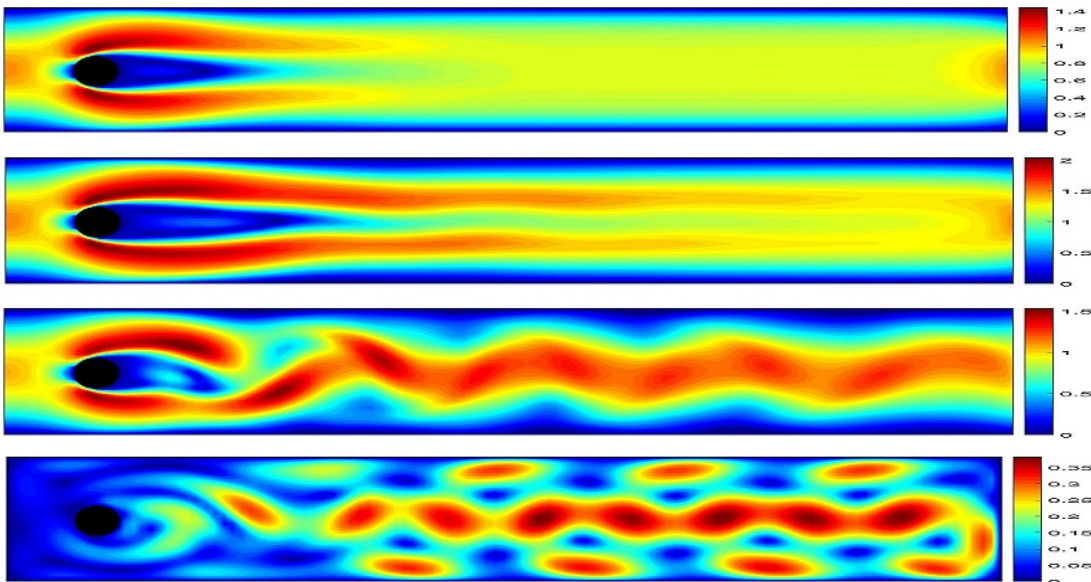


Figure 4.6: The velocity of the EMAC-FILTERED scheme at  $t = 2, 4, 6, 8$  (from up to down).

For further observation of the accuracy of our method, we compute the drag  $c_d(t)$  and lift  $c_l(t)$  coefficients at the cylinder. These values are defined in [92] as follows:

$$c_d(t) = \frac{2}{\rho L U_{max}^2} \int_S (\rho \nu \frac{\partial \mathbf{u}_{t_S}}{\partial n} n_y - p(t) n_x) dS$$

$$c_l(t) = -\frac{2}{\rho L U_{max}^2} \int_S (\rho \nu \frac{\partial \mathbf{u}_{t_S}}{\partial n} n_x + p(t) n_y) dS$$

where  $S$  is the boundary of the cylinder,  $U_{max}$  is the maximum mean flow,  $L$  is the diameter of the cylinder,  $n = (n_x, n_y)^T$  is the normal vector on the circular boundary  $S$  and  $\mathbf{u}_{t_S}$  is the tangential velocity for  $t_S = (n_y, -n_x)^T$  the tangential vector.

Table 4.3 shows the maximum drag ( $c_{d,max}$ ) and maximum lift ( $c_{l,max}$ ) values of both EMAC-FILTERED and BE-EMAC schemes behind the cylinder together with the times at which they occur. The following reference intervals are given in [92, 144]:

$$c_{d,max}^{ref} \in [2.93, 2.97], \quad c_{l,max}^{ref} \in [0.47, 0.49].$$

Comparing the reference values, we see that while both predict maximum drag coefficients correctly, the EMAC-FILTERED scheme provides the best prediction of maximum lift coefficient compared with the BE-EMAC scheme which is not even in the reference interval. Thus, this numerical test has revealed that making use of the EMAC-FILTERED scheme has notable advantages in terms of practical applications and quantitative means over the BE-EMAC scheme.

Table 4.3: Comparison of maximum drag and lift coefficients and the times at which they occur.

Method	$c_{d,max}$	$t(c_{d,max})$	$c_{l,max}$	$t(c_{l,max})$
EMAC-FILTERED	2.95281	3.94	0.468963	5.79
BE-EMAC	2.95215	3.93	0.0299554	7.13
Ref [144]	2.95092	3.93	0.47795	5.69

#### 4.5.4 Flow Over a Flat Plate

In the last experiment, we continue to test the efficiency of the EMAC-FILTERED algorithm on a channel flow over a flat plate with  $Re = 100$ , following [10, 123]. It is modeled on a  $[-7, 20] \times [-10, 10]$  rectangular channel with a  $0.125 \times 1$  flat plate placed 7 units into the channel, and vertically centered. The domain is shown in Figure 4.7 ([123]).

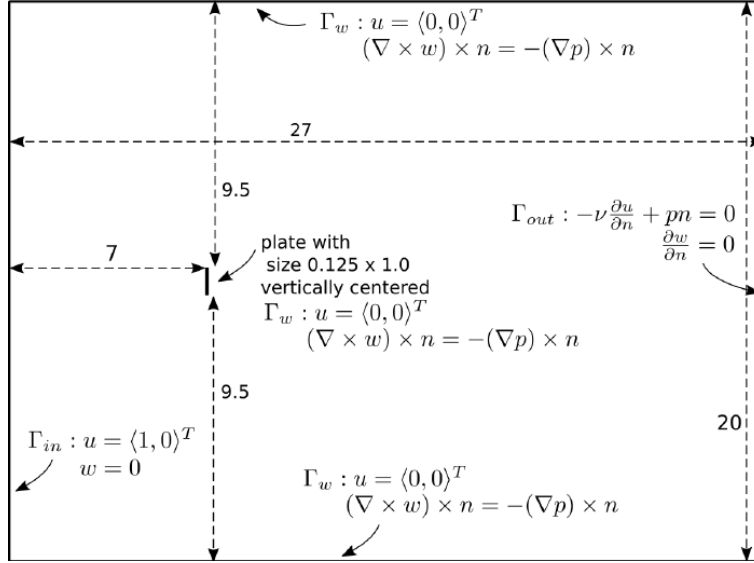


Figure 4.7: Domain  $\Omega$  of the test problem

We take inflow velocity as  $\mathbf{u}_{in} = \langle 1, 0 \rangle^T$ , zero-traction outflow and external force  $\mathbf{f} = 0$ . No-slip boundary conditions are considered on the walls and plate. The simulation is run on a very coarse mesh consisting of only 8745 total degrees of freedom with time step size  $\Delta t = 0.02$  till the end time  $T = 400$  s. The quantities of interest are the average value of the drag coefficient and Strouhal number which are defined as

$$c_d(t) = \frac{2}{\rho L U_{max}^2} \int_S \left( \rho \nu \frac{\partial \mathbf{u}_{t_S}}{\partial n} n_y - p(t) n_x \right) dS$$

$$St = \frac{fL}{U_{max}}$$

where  $S$  is the plate,  $n = (n_x, n_y)^T$  is the outward normal vector,  $\mathbf{u}_{t_S}$  is the tangential velocity for  $t_S = (n_y, -n_x)^T$  the tangential vector,  $\rho_1$  is the density,  $f$  is the frequency of vortex shedding, the maximum inlet velocity is  $U_{max} = 1$  and  $L = 1$  is the length of



the plate. Average drag values are computed using period-in-time state solutions over the time period  $100 < t < 400$ . The results are listed in Table 4.4. Our goal here is to show that, the results obtained from the EMAC-FILTERED scheme are more efficient than the unfiltered case by using coarser meshes. We observe from the simulations that this goal has been achieved. The average drag value, which is a very important quantity to define the efficiency of the considered scheme in this flow simulation, matches quite well with the values given in literature [10,123]. On the other hand, the unfiltered cases, BE-EMAC solutions, do not estimate the reference values [10,123] as closely as EMAC-FILTERED solutions. Also, the EMAC-FILTERED scheme possesses not only a dominant advantage over the unfiltered cases, but also catches the reference values with coarser mesh sizes when compared with the results given in Table 4.4. Moreover, the Strouhal numbers of both BE-EMAC and the EMAC-FILTERED solutions are quite consistent with the reference value [10]. Thus we can conclude that the EMAC-FILTERED scheme is even preferable among other well-known numerical algorithms which are considered in references.

Table 4.4: The average drag coefficients and the Strouhal number.

Method	$C_{d,avg}$	$St$
EMAC-FILTERED	2.63127	0.1900
BE-EMAC	2.577724	0.1875
Ref [123] (Very fine discretization)	2.6454	not given
Ref [10]	2.60	0.1826



## CHAPTER 5

### A FAMILY OF SECOND ORDER TIME STEPPING METHODS FOR THE DARCY-BRINKMAN EQUATIONS

In this chapter, we focus on double-diffusive convection flow in a confined porous enclosure which are given by the Darcy-Brinkman system (see [16]). Recall from Chapter 1, the Darcy-Brinkman system is given by

$$\begin{aligned}
 \mathbf{u}_t - \nu \Delta \mathbf{u} + (\mathbf{u} \cdot \nabla) \mathbf{u} + Da^{-1} \mathbf{u} + \nabla p &= (\beta_T T + \beta_S S) \mathbf{g} \quad \text{in } (0, t] \times \Omega, \\
 \nabla \cdot \mathbf{u} &= 0 \quad \text{in } (0, t] \times \Omega, \\
 \mathbf{u} &= \mathbf{0} \quad \text{on } (0, t] \times \partial\Omega, \\
 T_t - \gamma \Delta T + \mathbf{u} \cdot \nabla T &= 0 \quad \text{in } (0, t] \times \partial\Omega, \\
 S_t - D_c \Delta S + \mathbf{u} \cdot \nabla S &= 0 \quad \text{in } (0, t] \times \partial\Omega, \\
 T, S &= 0 \quad \text{on } \Gamma_D, \\
 \frac{\partial T}{\partial n} &= 0, \quad \frac{\partial S}{\partial n} = 0 \quad \text{on } \Gamma_N, \\
 \mathbf{u}(0, \mathbf{x}) = \mathbf{u}_0, \quad T(0, \mathbf{x}) = T_0, \quad S(0, \mathbf{x}) &= S_0 \quad \text{in } \Omega. \tag{5.0.1}
 \end{aligned}$$

Here  $\mathbf{u}$  is the fluid velocity,  $\mathbf{u}_0$ , the initial velocity,  $p$  the pressure,  $T$  the temperature,  $T_0$ , the initial temperature,  $S$  the concentration,  $S_0$ , the initial concentration. We also have the kinematic viscosity  $\nu > 0$ , the Darcy number  $Da$ , the thermal diffusivity  $\gamma > 0$ , the mass diffusivity  $D_c > 0$ , the gravitational acceleration vector  $\mathbf{g}$  and the thermal and solutal expansion coefficients are  $\beta_T, \beta_S$ , respectively.

In literature, there have been many numerical studies devoted to the development of efficient stabilization methods for (5.0.1) to reduce the drawbacks explained in Chapter 2 (see [23, 24, 69, 89, 126, 135, 161] and the references therein). Besides, Shao et al. [108] have used the Fourier–Galerkin spectral method to obtain a high-

accurate reference solution for the double-diffusive convection in a confined saturated porous medium. A stabilized finite element method for the solution of combined heat and mass transfer in a rectangular cavity was studied in [113]. Moreover, Cıbık and Kaya [4] have presented a projection-based stabilized finite element error analysis. In addition, Eroglu [41] has studied a reduced-order modeling using proper orthogonal decomposition to flows governed by double diffusive convection. Further, a full explicitly uncoupled variational multiscale stabilization finite element method was considered by Yang and Jiang [165]. However, there have been relatively few studies concerning the development of efficient second-order time-stepping numerical methods for investigating the Darcy-Brinkman system (5.0.1).

The common solution approach for the numerical solution of the time dependent multiphysics problems requires their discretization in space and time as well as linearization. Since linear extrapolation schemes require the solution of only one linear system per time step, they are preferable when it is compared with the fully implicit schemes that require multiple, time-consuming, nonlinear iterations at each time step. There have been a considerable number of different studies devoted to such discretizations, see e.g. [103]. One of the most popular and important linearization examples is Crank-Nicolson with linear extrapolation (CNLE) proposed by Baker [45]. CNLE is preferable in terms of stability and accuracy over the more expensive, fully implicit Crank-Nicolson (CN) method, [37, 52, 162]. Another important preferable linearization is the linearly extrapolated BDF2 (BDF2LE) time-stepping method which exhibits strong stability and damping properties that are better than those of CN for the simulation of underresolved regimes, [70, 83, 130]. In this study, we consider a family of second-order IMEX time-stepping methods for (5.0.1) which are given by

$$\begin{aligned} & \frac{(\theta + \frac{1}{2})\mathbf{u}^{n+1} - 2\theta\mathbf{u}^n + (\theta - \frac{1}{2})\mathbf{u}^{n-1}}{\Delta t} - \nu\theta\Delta\mathbf{u}^{n+1} - \nu(1-\theta)\Delta\mathbf{u}^n \\ & + ((\theta + 1)\mathbf{u}^n - \theta\mathbf{u}^{n-1}) \cdot \nabla(\theta\mathbf{u}^{n+1} + (1-\theta)\mathbf{u}^n) \end{aligned} \quad (5.0.2)$$

$$\begin{aligned} & + Da^{-1}(\theta\mathbf{u}^{n+1} + (1-\theta)\mathbf{u}^n) + \theta\nabla p^{n+1} + (1-\theta)\nabla p^n \\ & = (\beta_T((\theta + 1)T^n - \theta T^{n-1}) + \beta_S((\theta + 1)S^n - \theta S^{n-1}))\mathbf{g}, \\ & \nabla \cdot \mathbf{u}^{n+1} = 0, \end{aligned} \quad (5.0.3)$$

$$\begin{aligned} & \frac{(\theta + \frac{1}{2})T^{n+1} - 2\theta T^n + (\theta - \frac{1}{2})T^{n-1}}{\Delta t} - \gamma\theta\Delta T^{n+1} - \gamma(1-\theta)\Delta T^n \\ & + ((\theta + 1)\mathbf{u}^n - \theta\mathbf{u}^{n-1}) \cdot \nabla(\theta T^{n+1} + (1-\theta)T^n) = 0, \end{aligned} \quad (5.0.4)$$

$$\begin{aligned} & \frac{(\theta + \frac{1}{2})S^{n+1} - 2\theta S^n + (\theta - \frac{1}{2})S^{n-1}}{\Delta t} - D_c\theta\Delta S^{n+1} - D_c(1-\theta)\Delta S^n \\ & + ((\theta + 1)\mathbf{u}^n - \theta\mathbf{u}^{n-1}) \cdot \nabla(\theta S^{n+1} + (1-\theta)S^n) = 0, \end{aligned} \quad (5.0.5)$$

$$(5.0.6)$$

where  $\theta \in [\frac{1}{2}, 1]$ . The choices of  $\theta = 1$  leads to BDF2LE time stepping scheme whereas  $\theta = \frac{1}{2}$  produce CNLE time stepping scheme. Any other  $\theta \in [\frac{1}{2}, 1]$  gives also a second order method.

Besides using linearization at each time step, it is also necessary to use some successful stabilization methods for (5.0.2)-(5.0.6) to damp numerical instabilities and unphysical oscillations without compromising accuracy. A commonly preferable stabilization method for these time-stepping methods is the speed stabilization method which is obtained by adding  $-\alpha\Delta\mathbf{u}_{n+1}$  to the left-hand side and  $-\alpha\Delta\mathbf{u}_n$  to the right-hand side for a tuning parameter  $\alpha$  generally taken as the order of the mesh width  $h$ . This stabilization is relevant to techniques used in turbulence modeling [134], ocean modeling [71] as well as to the discretization of the 'Voigt term' in a turbulence model recently studied by Titi and others, e.g. [104, 160]. Some studies in the literature have used this stabilization for NSE, for more details, one can see [11, 75] and references therein. These works show the effectiveness of this stabilization for several different types of flows and the ability to increase the coefficient of the stiffness matrix, e.g. for the case of BDF2LE, from  $\nu$  to  $\nu + \alpha$  which improves the conditioning of linear systems. On the other hand, this method is  $O(\alpha\Delta t)$  shown in the analysis of [11] and so can dominate the error in second-order time-stepping methods for the usual choice of  $\alpha = O(h)$ . Choosing  $\alpha = O(\Delta t)$  creates the problem of careful readjustment of  $\alpha$  at each time the step size is changed which can make the use of adaptive time-stepping

very difficult.

The main objective of this chapter is to propose, analyze and test a new stabilization for the time-stepping methods of the form (5.0.2)-(5.0.4), by extending an earlier study of [94] for the Navier-Stokes equations (NSE) based on the pioneering work of [27, 28]. A successful stabilization method is achieved by using the idea of 'curvature stabilization' ( $\mathbf{u}^{n+1} + \mathbf{u}^n - \mathbf{u}^{n-1}$ ) instead of speed stabilization ( $\mathbf{u}^{n+1} + \mathbf{u}^n$ ) explained above. The paper's underlying ideas are to incorporate linearizations and stabilization terms such that the discrete curvature solutions in velocity, temperature, concentration, and pressure are proportional to this combination. As noted in [94], a family of the method based on curvature stabilization leads to a sufficient stabilization along with the optimal accuracy in time. Moreover, it is more accurate than speed stabilization in terms of time step  $\Delta t$  and keeping important flow quantities such as drag coefficients like speed stabilization.

The chapter is organized as follows. In Section 5.1, some mathematical preliminaries are presented which are useful in the analysis. In Section 5.2, the numerical scheme of the second-order time-stepping method for (5.0.1) is described. We give comprehensive stability analysis and a priori error analysis of the method in Section 5.3. Section 5.4 presents numerical illustrations that verify the analytical results.

## 5.1 Mathematical Preliminaries

In this chapter, we consider the standard function spaces for the continuous velocity field, pressure, temperature, and concentration spaces defined respectively by

$$\begin{aligned}
 \mathbf{X} &:= (\mathbf{H}_0^1(\Omega))^d, \\
 Q &:= L_0^2(\Omega), \\
 W &:= \{S \in H^1(\Omega) : S = 0 \text{ on } \Gamma_D\}, \\
 \Psi &:= \{\Phi \in H^1(\Omega) : \Phi = 0 \text{ on } \Gamma_D\}.
 \end{aligned} \tag{5.1.1}$$

Define the divergence-free subspace of  $\mathbf{X}$  by  $\mathbf{V}$ :

$$\mathbf{V} := \{\mathbf{v} \in \mathbf{X} : (\nabla \cdot \mathbf{v}, q) = 0, \quad \forall q \in Q\}.$$

The variational formulation of (5.0.1) reads as follows: Find  $\mathbf{u} : (0, T] \rightarrow \mathbf{X}$ ,  $p : (0, T] \rightarrow Q$ ,  $T : (0, T] \rightarrow W$ ,  $S : (0, T] \rightarrow \Psi$  satisfying

$$(\mathbf{u}_t, \mathbf{v}) + \nu(\nabla \mathbf{u}, \nabla \mathbf{v}) + b^*(\mathbf{u}, \mathbf{u}, \mathbf{v}) - (p, \nabla \cdot \mathbf{v}) = (\mathbf{f}, \mathbf{v}) \quad \forall \mathbf{v} \in \mathbf{X}, \quad (5.1.2)$$

$$(q, \nabla \cdot \mathbf{u}) = 0 \quad \forall q \in Q, \quad (5.1.3)$$

$$(T_t, \chi) + \nu(\nabla T, \nabla \chi) + c^*(\mathbf{u}, T, \chi) = 0 \quad \forall \chi \in W, \quad (5.1.4)$$

$$(S_t, \Phi) + \nu(\nabla S, \nabla \Phi) + d^*(\mathbf{u}, S, \Phi) = 0 \quad \forall \Phi \in \Psi. \quad (5.1.5)$$

For finite element approximation of (5.2.1)-(5.2.4), let  $\mathbf{X}_h \subset \mathbf{X}$ ,  $Q_h \subset Q$ ,  $W_h \subset W$ ,  $\Psi_h \subset \Psi$  be conforming finite element spaces defined on a fine mesh  $\pi_h$  for which the usual discrete inf-sup condition (3.1.4) is satisfied.

We define the discretely divergence-free subspace  $\mathbf{V}_h \subset \mathbf{X}_h$  given by

$$\mathbf{V}_h := \{\mathbf{v}_h \in \mathbf{X}_h : (q_h, \nabla \cdot \mathbf{v}_h) = 0, \forall q_h \in Q_h\}.$$

In this thesis, we use the Taylor-Hood element pair  $(\mathbf{X}_h; Q_h) = (P_k^d; P_{k-1})$  which are defined in Section 3.1 of Chapter 3. We also assume that the finite element spaces  $W_h$  and  $\Psi_h$  are composed of piecewise polynomials of degree at most  $k$ . Additionally, following [122, 143], it is assumed that the finite element spaces  $(\mathbf{X}_h, Q_h)$  satisfy the well-known approximation properties (3.1.5)-(3.1.6) and the spaces  $(W_h, \Psi_h)$  satisfy the following approximation properties

$$\inf_{\chi_h \in W_h} \|T - \chi_h\| \leq Ch^{k+1} \|T\|_{k+1} \quad T \in H^{k+1}(\Omega), \quad (5.1.6)$$

$$\inf_{\Phi_h \in \Psi_h} \|S - \Phi_h\| \leq Ch^{k+1} \|S\|_{k+1} \quad S \in H^{k+1}(\Omega), \quad (5.1.7)$$

We use the skew symmetric trilinear form (3.1.8) for the convective terms in (5.0.1) each of which satisfying the properties in (3.1.7) and Lemma 3.1.1.

**Lemma 5.1.1**

$$\|D_{n+\theta}(w) - w_t(t^{n+\theta})\|^2 \leq C\theta^6 \Delta t^3 \int_{t^{n-1}}^{t^{n+1}} \|w_{ttt}\|^2 dt. \quad (5.1.8)$$

$$\begin{aligned} \|F_{n+\theta}^{\varepsilon, \nu}(w) - w_{n+\theta}\|^2 &\leq C\theta^2(1-\theta)^2 \Delta t^3 \int_{t^n}^{t^{n+1}} \|w_{tt}\|^2 dt \\ &\quad + C\varepsilon^2 \theta^2 \nu^{-2} \Delta t^3 \int_{t^{n-1}}^{t^{n+1}} \|w_{tt}\|^2 dt. \end{aligned} \quad (5.1.9)$$

$$\|H_{n+\theta}(w) - w_{n+\theta}\|^2 \leq C\theta^2(1+\theta^2) \Delta t^3 \int_{t^{n-1}}^{t^{n+1}} \|w_{tt}\|^2 dt. \quad (5.1.10)$$

**Proof.** The first estimate is proved by expanding each term in  $D_{n+\theta}(w)$  around  $t^{n+\theta}$  by using the Taylor's theorem with integral remainders

$$w_t(t^{n+\theta}) = w_t(t^{n+\theta}) \quad (5.1.11)$$

$$\begin{aligned} w^{n+1} &= w^{n+\theta} + (1-\theta)\Delta t w_t(t^{n+\theta}) + \frac{(1-\theta)^2 \Delta t^2}{2} w_{tt}(t^{n+\theta}) \\ &\quad + \int_{t^{n+\theta}}^{t^{n+1}} w_{ttt}(t) \frac{(t^{n+1}-t)^2}{2} dt \end{aligned} \quad (5.1.12)$$

$$\begin{aligned} w^n &= w^{n+\theta} - \theta \Delta t w_t(t^{n+\theta}) + \frac{\theta^2 \Delta t^2}{2} w_{tt}(t^{n+\theta}) \\ &\quad + \int_{t^{n+\theta}}^{t^n} w_{ttt}(t) \frac{(t^n-t)^2}{2} dt \end{aligned} \quad (5.1.13)$$

$$\begin{aligned} w^{n-1} &= w^{n+\theta} - (1+\theta)\Delta t w_t(t^{n+\theta}) + \frac{(1+\theta)^2 \Delta t^2}{2} w_{tt}(t^{n+\theta}) \\ &\quad + \int_{t^{n+\theta}}^{t^{n-1}} w_{ttt}(t) \frac{(t^{n-1}-t)^2}{2} dt \end{aligned} \quad (5.1.14)$$

Then, multiplying (5.1.11) with  $-1$ , (5.1.12) with  $(\theta + \frac{1}{2})\frac{1}{\Delta t}$ , (5.1.13) with  $\frac{-2\theta}{\Delta t}$  and (5.1.14) with  $(\theta - \frac{1}{2})\frac{1}{\Delta t}$  and adding them we obtain

$$\begin{aligned} &\left( \frac{(\theta + \frac{1}{2})w^{n+1} - 2\theta w^n + (\theta - \frac{1}{2})w^{n-1}}{\Delta t} - w_t(t^{n+\theta}) \right) \\ &\leq \frac{1}{4\Delta t} \left( (2\theta + 1) \int_{t^{n+\theta}}^{t^{n+1}} \|w_{ttt}\|^2 (t^{n+1}-t)^2 dt - 4\theta \int_{t^{n+\theta}}^{t^n} \|w_{ttt}\|^2 (t^n-t)^2 dt \right. \\ &\quad \left. + (2\theta - 1) \int_{t^{n+\theta}}^{t^{n-1}} \|w_{ttt}\|^2 (t^{n-1}-t)^2 dt \right) \end{aligned} \quad (5.1.15)$$

Integrating (5.1.15) yields the estimate (5.1.8).



The proof of the second estimate follows similar lines as above. First, we write by using the Cauchy-Schwarz inequality

$$\begin{aligned} \|F_{n+\theta}^{\varepsilon,\nu}(w) - w^{n+\theta}\|^2 &\leq \|\theta w^{n+1} + (1-\theta)w^n - w^{n+\theta}\|^2 \\ &\quad + \varepsilon^2 \theta^2 \nu^{-2} \|w^{n+1} - 2w^n + w^{n-1}\|^2 \end{aligned} \quad (5.1.16)$$

Then, by using the Taylor's theorem with integral remainders, each term in  $F_{n+\theta}^{\varepsilon,\nu}(w)$  is written around  $t^{n+\theta}$

$$w^{n+\theta} = w^{n+\theta} \quad (5.1.17)$$

$$w^{n+1} = w^{n+\theta} + (1-\theta)\Delta t w_t(t^{n+\theta}) + \int_{t^{n+\theta}}^{t^{n+1}} w_{tt}(t)(t^{n+1} - t)dt \quad (5.1.18)$$

$$w^n = w^{n+\theta} - \theta\Delta t w_t(t^{n+\theta}) + \int_{t^{n+\theta}}^{t^n} w_{tt}(t)(t^n - t)dt \quad (5.1.19)$$

$$w^{n-1} = w^{n+\theta} - (1+\theta)\Delta t w_t(t^{n+\theta}) + \int_{t^{n+\theta}}^{t^{n-1}} w_{tt}(t)(t^{n-1} - t)dt \quad (5.1.20)$$

Then, for the estimation of the first term in (5.1.16), multiply (5.1.17) with  $(-1)$ , (5.1.18) with  $\theta$ , (5.1.19) with  $(1-\theta)$ . Adding them together and then integrating gives the bound. Similarly, the second term in (5.1.16) can be bounded by multiplying (5.1.18) with  $(+1)$ , (5.1.19) with  $(-2)$  and (5.1.20) with  $+1$ .

The last estimation (5.1.10) is the same as the estimation of the first term in (5.1.16).

□

## 5.2 Numerical Scheme

In this section, a family of second-order IMEX time-stepping methods for (5.0.1) is presented in detail. For this purpose, let partition the time interval  $[0, t]$  into  $N$  sub intervals with time step size  $\Delta t = T/N$  and  $T^{n+1} = (n+1)\Delta t$  with  $n = 1, 2, \dots, N-1$ . For simplicity, we consider the constant step sizes  $\Delta t = t^n - t^{n-1}$  and the quantities at time level  $t^n$  are denoted by a subscript  $n$ . A family of second-order IMEX time-stepping methods we propose for (5.0.1) reads as

$$\begin{aligned}
& \frac{(\theta + \frac{1}{2})\mathbf{u}^{n+1} - 2\theta\mathbf{u}^n + (\theta - \frac{1}{2})\mathbf{u}^{n-1}}{\Delta t} - \theta(\nu + \varepsilon)\Delta\mathbf{u}^{n+1} - (\nu - \theta(\nu + 2\varepsilon))\Delta\mathbf{u}^n \\
& - \theta\varepsilon\Delta\mathbf{u}^{n-1} + ((\theta + 1)\mathbf{u}^n - \theta\mathbf{u}^{n-1}) \cdot \nabla \left( \theta \frac{\nu + \varepsilon}{\nu} \mathbf{u}^{n+1} + \left(1 - \theta \frac{\nu + 2\varepsilon}{\nu}\right) \mathbf{u}^n + \theta \frac{\varepsilon}{\nu} \mathbf{u}^{n-1} \right) \\
& + Da^{-1} \left( \theta \frac{\nu + \varepsilon}{\nu} \mathbf{u}^{n+1} + \left(1 - \theta \frac{\nu + 2\varepsilon}{\nu}\right) \mathbf{u}^n + \theta \frac{\varepsilon}{\nu} \mathbf{u}^{n-1} \right) + \theta \frac{\nu + \varepsilon}{\nu} \nabla p^{n+1} \\
& \quad + \left(1 - \theta \frac{\nu + 2\varepsilon}{\nu}\right) \nabla p^n + \theta \frac{\varepsilon}{\nu} \nabla p^{n-1} \\
& = (\beta_T((\theta + 1)T^n - \theta T^{n-1}) + \beta_S((\theta + 1)S^n - \theta S^{n-1}))\mathbf{g}, \tag{5.2.1}
\end{aligned}$$

$$\nabla \cdot \mathbf{u}^{n+1} = 0, \tag{5.2.2}$$

$$\begin{aligned}
& \frac{(\theta + \frac{1}{2})T^{n+1} - 2\theta T^n + (\theta - \frac{1}{2})T^{n-1}}{\Delta t} - \theta(\gamma + \varepsilon_1)\Delta T^{n+1} - (\gamma - \theta(\gamma + 2\varepsilon_1))\Delta T^n \\
& - \theta\varepsilon\Delta T^{n-1} + ((\theta + 1)\mathbf{u}^n - \theta\mathbf{u}^{n-1}) \cdot \theta \frac{\gamma + \varepsilon_1}{\gamma} \nabla T^{n+1} \\
& \quad + \left(1 - \theta \frac{\gamma + 2\varepsilon_1}{\gamma} \nabla T^n\right) + \theta \frac{\varepsilon_1}{\gamma} \nabla T^{n-1} = 0, \tag{5.2.3}
\end{aligned}$$

$$\begin{aligned}
& \frac{(\theta + \frac{1}{2})S^{n+1} - 2\theta S^n + (\theta - \frac{1}{2})S^{n-1}}{\Delta t} - \theta(D_c + \varepsilon_2)\Delta S^{n+1} - (D_c - \theta(D_c + 2\varepsilon_2))\Delta S^n \\
& - \theta\varepsilon_2\Delta S^{n-1} + ((\theta + 1)\mathbf{u}^n - \theta\mathbf{u}^{n-1}) \cdot \theta \frac{D_c + \varepsilon_2}{D_c} \nabla S^{n+1} \\
& \quad + \left(1 - \theta \frac{D_c + 2\varepsilon_2}{D_c} \nabla S^n\right) + \theta \frac{\varepsilon_2}{D_c} \nabla S^{n-1} = 0, \tag{5.2.4}
\end{aligned}$$

with the parameters  $\theta \in [\frac{1}{2}, 1]$  and  $\varepsilon, \varepsilon_1, \varepsilon_2 \geq 0$ . Numerical realizations suggest that sufficient stabilizations are obtained with the choices  $\varepsilon = O(\nu)$ ,  $\varepsilon_1 = O(\gamma)$  and  $\varepsilon_2 = O(D_c)$ . There are several variants of given time step scheme. By appropriate choices of  $\theta, \varepsilon, \varepsilon_1$  and  $\varepsilon_2$  well known time stepping schemes are obtained. For instance, the choices  $\theta = 1, \varepsilon = \varepsilon_1 = \varepsilon_2 = 0$  and  $\theta = 1/2, \varepsilon = \varepsilon_1 = \varepsilon_2 = 0$  lead to just usual BDF2LE and CNLE, respectively.

To simplify the analysis, we define the following operators

$$D_{n+\theta}(w) := \frac{(\theta + \frac{1}{2})w^{n+1} - 2\theta w^n + (\theta - \frac{1}{2})w^{n-1}}{\Delta t}, \tag{5.2.5}$$

$$F_{n+\theta}^{\delta, \mu}(w) := \theta \frac{(\mu + \delta)}{\mu} w^{n+1} + \left(1 - \theta \frac{\mu + 2\delta}{\mu}\right) w^n + \theta \frac{\delta}{\mu} w^{n-1}, \tag{5.2.6}$$

$$H_{n+\theta}(w) := (\theta + 1)w^n - \theta w^{n-1}, \tag{5.2.7}$$

where  $(\delta, \mu) = (\varepsilon, \nu)$  in the case  $w = \mathbf{u}$  (for the velocity),  $(\delta, \mu) = (\varepsilon_1, \gamma)$  in the case  $w = T$  (for the temperature) and  $(\delta, \mu) = (\varepsilon_2, D_c)$  (for the concentration). By using

the operators (5.2.5)-(5.2.6) and the trilinear forms, we state a family of second order time stepping method (5.2.1)-(5.2.4) in finite dimensional spaces.

**Scheme (A family of second order time stepping schemes):** Let the initial conditions  $\mathbf{u}^0$ ,  $T^0$  and  $S^0$  be given. Define  $\mathbf{u}_h^0$ ,  $\mathbf{u}_h^{-1}$ ,  $T_h^0$ ,  $T_h^{-1}$ ,  $S_h^0$  and  $S_h^{-1}$  as the nodal interpolants of  $\mathbf{u}^0, T^0$  and  $S^0$ , respectively. Then, given time step  $\Delta t$  and  $\mathbf{u}^n$ ,  $\mathbf{u}^{n-1}$ ,  $T^n$ ,  $T^{n-1}$ ,  $S^n$  and  $S^{n-1}$ , compute  $\mathbf{u}^{n+1} \in \mathbf{X}_h, T^{n+1} \in W_h, S^{n+1} \in \Psi_h$ , and  $p^{n+1} \in Q_h$  satisfying

$$\begin{aligned} & (D_{n+\theta}(\mathbf{u}_h), \mathbf{v}_h) + \nu(F_{n+\theta}^{\varepsilon, \nu}(\nabla \mathbf{u}_h), \nabla \mathbf{v}_h) + b^*(H_{n+\theta}(\mathbf{u}_h), F_{n+\theta}^{\varepsilon, \nu}(\mathbf{u}_h), \mathbf{v}_h)) \\ & - (F_{n+\theta}^{\varepsilon, \nu}(p_h), \nabla \cdot \mathbf{v}_h) = \beta_T(\mathbf{g}H_{n+\theta}(T_h), \mathbf{v}_h) + \beta_S(\mathbf{g}H_{n+\theta}(S_h), \mathbf{v}_h), \end{aligned} \quad (5.2.8)$$

$$(\nabla \cdot \mathbf{u}_h, q_h) = 0, \quad (5.2.9)$$

$$(D_{n+\theta}(T_h), \chi_h) + \gamma(F_{n+\theta}^{\varepsilon_1, \gamma}(\nabla T_h), \nabla \chi_h) + c^*(H_{n+\theta}(\mathbf{u}_h), F_{n+\theta}^{\varepsilon_1, \gamma}(T_h), \chi_h) = 0, \quad (5.2.10)$$

$$(D_{n+\theta}(S_h), \Phi_h) + D_c(F_{n+\theta}^{\varepsilon_2, D_c}(\nabla S_h), \nabla \Phi_h) + d^*(H_{n+\theta}(\mathbf{u}_h), F_{n+\theta}^{\varepsilon_2, D_c}(S_h), \Phi_h) = 0, \quad (5.2.11)$$

for all  $(\mathbf{v}_h, \chi_h, \Phi_h, q_h) \in (\mathbf{X}_h, W_h, \Psi_h, Q_h)$ .

**Remark 5.2.1** *The studied method requires the specifications of the initial condition. The initial condition  $\mathbf{u}_h^0$  needs to be weakly divergence-free in order to achieve stability in our method.*

**Remark 5.2.2** *A family of second-order method (5.2.8)-(5.2.11) is a fully decoupled system and under the certain choices of parameters, it requires only a linear system to be solved at each time step.*

### 5.3 Numerical Analysis

In this section, the numerical analysis of a fully discrete method for solving Darcy-Brinkman system (5.0.1) is studied based on (5.2.8)-(5.2.11). We first provide the stability analysis of the method. Stability bounds are derived by using standard energy arguments. It turns out that the method (5.2.8)-(5.2.11) doesn't depend on any time step sizes.

**Lemma 5.3.1** (Unconditional Stability) *The solutions of (5.2.8)-(5.2.11) satisfy at*

$$t_n = n\Delta t$$

$$\begin{aligned} \|T_h^N\|^2 + \frac{1}{2\theta+1} \sum_{n=1}^{N-1} \|T_h^{n+1} - 2T_h^n + T_h^{n-1}\|_F^2 + \frac{4\Delta t\gamma}{2\theta+1} \sum_{n=1}^{N-1} \|F_{n+\theta}^{\varepsilon_1, \gamma}(\nabla T_h)\|^2 \\ \leq \left(\frac{2\theta-1}{2\theta+1}\right)^N \|T_h^0\|^2 + \frac{4N}{2\theta+1} \left\| \begin{bmatrix} T_h^1 \\ T_h^0 \end{bmatrix} \right\|_G^2 \end{aligned} \quad (5.3.1)$$

$$\begin{aligned} \|S_h^N\|^2 + \frac{1}{2\theta+1} \sum_{n=1}^{N-1} \|S_h^{n+1} - 2S_h^n + S_h^{n-1}\|_F^2 + \frac{4\Delta t D_c}{2\theta+1} \sum_{n=1}^{N-1} \|F_{n+\theta}^{\varepsilon_2, D_c}(\nabla S_h)\|^2 \\ \leq \left(\frac{2\theta-1}{2\theta+1}\right)^N \|S_h^0\|^2 + \frac{4N}{2\theta+1} \left\| \begin{bmatrix} S_h^1 \\ S_h^0 \end{bmatrix} \right\|_G^2 \end{aligned} \quad (5.3.2)$$

$$\begin{aligned} \|\mathbf{u}_h^N\|^2 + \frac{1}{2\theta+1} \sum_{n=1}^{N-1} \|\mathbf{u}_h^{n+1} - 2\mathbf{u}_h^n + \mathbf{u}_h^{n-1}\|_F^2 + \frac{4\Delta t D a^{-1}}{2\theta+1} \sum_{n=1}^{N-1} \|F_{n+\theta}^{\varepsilon, \nu}(\mathbf{u}_h)\|^2 \\ + \frac{2\Delta t\nu}{2\theta+1} \sum_{n=1}^{N-1} \|F_{n+\theta}^{\varepsilon, \nu}(\nabla \mathbf{u}_h)\|^2 \\ \leq \frac{C\Delta t(2\theta+1)}{\nu} \left[1 - \left(\frac{2\theta-1}{2\theta+1}\right)^N\right] (\|T_h^1\|^2 + \|T_h^0\|_2) + \frac{C\Delta t}{2\theta+1} \left\| \begin{bmatrix} T_h^1 \\ T_h^0 \end{bmatrix} \right\|_G^2 \\ + \frac{C\Delta t(2\theta+1)}{\nu} \left[1 - \left(\frac{2\theta-1}{2\theta+1}\right)^N\right] (\|S_h^1\|^2 + \|S_h^0\|^2) + \frac{C\Delta t}{2\theta+1} \left\| \begin{bmatrix} S_h^1 \\ S_h^0 \end{bmatrix} \right\|_G^2 \\ + \frac{4N}{2\theta+1} \left\| \begin{bmatrix} \mathbf{u}_h^1 \\ \mathbf{u}_h^0 \end{bmatrix} \right\|_G^2 + \left(\frac{2\theta-1}{2\theta+1}\right)^N \|\mathbf{u}_h^0\|^2. \end{aligned} \quad (5.3.3)$$

**Proof.** For stability, one needs to obtain estimation for the temperature and the concentration, then use them to estimate the velocity. So, first set  $\chi^h = F_{n+\theta}^{\varepsilon_1, \gamma}(T_h)$  in (5.2.10), then use the definition of the skew symmetric form (3.1.8) and Lemma 2.0.11 :

$$\begin{aligned} \frac{1}{\Delta t} \left\| \begin{bmatrix} T_h^{n+1} \\ T_h^n \end{bmatrix} \right\|_G^2 - \frac{1}{\Delta t} \left\| \begin{bmatrix} T_h^n \\ T_h^{n-1} \end{bmatrix} \right\|_G^2 + \frac{1}{4\Delta t} \|T_h^{n+1} - 2T_h^n + T_h^{n-1}\|_F^2 \\ + \gamma \|F_{n+\theta}^{\varepsilon_1, \gamma}(\nabla T_h)\|^2 = 0. \end{aligned} \quad (5.3.4)$$

Next, multiplying both sides of (5.3.4) by  $\Delta t$  and taking sum from  $n = 1$  to  $n = N-1$  leads to

$$\begin{aligned} \left\| \begin{bmatrix} T_h^N \\ T_h^{N-1} \end{bmatrix} \right\|_G^2 + \frac{1}{4} \sum_{n=1}^{N-1} \|T_h^{n+1} - 2T_h^n + T_h^{n-1}\|_F^2 + \Delta t \gamma \sum_{n=1}^{N-1} \|F_{n+\theta}^{\varepsilon_1, \gamma}(\nabla T_h)\|^2 \\ = \left\| \begin{bmatrix} T_h^1 \\ T_h^0 \end{bmatrix} \right\|_G^2. \end{aligned} \quad (5.3.5)$$

Using Lemma 2.0.12 yields

$$\begin{aligned} \|T_h^N\|^2 + \frac{1}{2\theta+1} \sum_{n=1}^{N-1} \|T_h^{n+1} - 2T_h^n + T_h^{n-1}\|_F^2 + \frac{4\Delta t \gamma}{2\theta+1} \sum_{n=1}^{N-1} \|F_{n+\theta}^{\varepsilon_1, \gamma}(\nabla T_h)\|^2 \\ \leq \frac{2\theta-1}{2\theta+1} \|T_h^{N-1}\|^2 + \frac{4}{2\theta+1} \left\| \begin{bmatrix} T_h^1 \\ T_h^0 \end{bmatrix} \right\|_G^2 \end{aligned} \quad (5.3.6)$$

The stability estimation (5.3.1) is now obtained by induction for  $\|T_h^{N-1}\|^2$ . For the concentration, we can obtain the stability bound by repeating the estimations of the temperature by setting  $\Phi_h = F_{n+\theta}^{\varepsilon_2, D_c}(S_h)$  in (5.2.11).

For the stability of the velocity, choose  $\mathbf{v}_h = F_{n+\theta}^{\varepsilon, \nu}(\mathbf{u}_h)$  in (5.2.8) and  $q_h = F_{n+\theta}^{\varepsilon, \nu}(p_h)$  in (5.2.9). With the definition of the skew-symmetry (3.1.8), this results

$$\begin{aligned} (D_{n+\theta}(\mathbf{u}_h), F_{n+\theta}^{\varepsilon, \nu}(\mathbf{u}_h)) + \nu \|\nabla F_{n+\theta}^{\varepsilon, \nu}(\mathbf{u}_h)\|^2 + Da^{-1} \|F_{n+\theta}^{\varepsilon, \nu}(\mathbf{u}_h)\|^2 \\ = \beta_T(\mathbf{g}H_{n+\theta}(T_h), F_{n+\theta}^{\varepsilon, \nu}(\mathbf{u}_h)) + \beta_S(\mathbf{g}H_{n+\theta}(S_h), F_{n+\theta}^{\varepsilon, \nu}(\mathbf{u}_h)). \end{aligned} \quad (5.3.7)$$

Apply Cauchy-Schwarz inequality to the right-hand side of (5.3.7) and estimate the terms as follows: the right-hand side terms in (5.3.7) are bounded with the Poincaré-Friedrichs inequality and Young's inequality

$$\begin{aligned} |\beta_T(\mathbf{g}H_{n+\theta}(T_h), F_{n+\theta}^{\varepsilon, \nu}(\mathbf{u}_h))| &\leq C\beta_T \|\mathbf{g}\|_\infty^2 \|H_{n+\theta}(T_h)\| \|F_{n+\theta}^{\varepsilon, \nu}(\nabla \mathbf{u}_h)\| \\ &\leq \frac{C(\theta+1)^2}{\nu} \|T_h^n\|^2 + \frac{C\theta^2}{\nu} \|T_h^{n-1}\|^2 \\ &\quad + \frac{\nu}{4} \|F_{n+\theta}^{\varepsilon, \nu}(\nabla \mathbf{u}_h)\|^2 \end{aligned} \quad (5.3.8)$$

and

$$\begin{aligned} |\beta_S(\mathbf{g}H_{n+\theta}(S_h), F_{n+\theta}^{\varepsilon, \nu}(\mathbf{u}_h))| &\leq C\beta_S \|\mathbf{g}\|_\infty^2 \|H_{n+\theta}(S_h)\| \|F_{n+\theta}^{\varepsilon, \nu}(\nabla \mathbf{u}_h)\| \\ &\leq \frac{C(\theta+1)^2}{\nu} \|S_h^n\|^2 + \frac{C\theta^2}{\nu} \|S_h^{n-1}\|^2 \\ &\quad + \frac{\nu}{4} \|F_{n+\theta}^{\varepsilon, \nu}(\nabla \mathbf{u}_h)\|^2 \end{aligned} \quad (5.3.9)$$

Using Lemma 2.0.11, inserting the estimations (5.3.8) and (5.3.9) and multiplying by  $\Delta t$  along with summation over the time steps, then the equation (5.3.7) becomes

$$\begin{aligned}
& \left\| \begin{bmatrix} \mathbf{u}_h^N \\ \mathbf{u}_h^{N-1} \end{bmatrix} \right\|_G^2 + \frac{1}{4} \sum_{n=1}^{N-1} \|\mathbf{u}_h^{n+1} - 2\mathbf{u}_h^n + \mathbf{u}_h^{n-1}\|_F^2 + \Delta t Da^{-1} \sum_{n=1}^{N-1} \|F_{n+\theta}^{\varepsilon, \nu}(\mathbf{u}_h)\|^2 \\
& + \frac{\Delta t \nu}{2} \sum_{n=1}^{N-1} \|F_{n+\theta}^{\varepsilon, \nu}(\nabla \mathbf{u}_h)\|^2 \\
& \leq \left\| \begin{bmatrix} \mathbf{u}_h^1 \\ \mathbf{u}_h^0 \end{bmatrix} \right\|_G^2 + \frac{C\Delta t \theta^2}{\nu} \sum_{n=1}^{N-1} (\|T_h^n\|^2 + \|T_h^{n-1}\|^2) + \frac{C\Delta t(2\theta+1)}{\nu} \sum_{n=1}^{N-1} \|T_h^n\|^2 \\
& + \frac{C\Delta t \theta^2}{\nu} \sum_{n=1}^{N-1} (\|S_h^n\|^2 + \|S_h^{n-1}\|^2) + \frac{C\Delta t(2\theta+1)}{\nu} \sum_{n=1}^{N-1} \|S_h^n\|^2. \quad (5.3.10)
\end{aligned}$$

The estimation of Lemma 2.0.12 and the use of  $\frac{\theta^2}{2\theta+1} \leq 1$  leads to

$$\begin{aligned}
& \|\mathbf{u}_h^N\|^2 + \frac{1}{2\theta+1} \sum_{n=1}^{N-1} \|\mathbf{u}_h^{n+1} - 2\mathbf{u}_h^n + \mathbf{u}_h^{n-1}\|_F^2 + \frac{4\Delta t Da^{-1}}{2\theta+1} \sum_{n=1}^{N-1} \|F_{n+\theta}^{\varepsilon, \nu}(\mathbf{u}_h)\|^2 \\
& + \frac{2\Delta t \nu}{2\theta+1} \sum_{n=1}^{N-1} \|F_{n+\theta}^{\varepsilon, \nu}(\nabla \mathbf{u}_h)\|^2 \\
& \leq \frac{2\theta-1}{2\theta+1} \|\mathbf{u}_h^{N-1}\|^2 + \frac{4}{2\theta+1} \left\| \begin{bmatrix} \mathbf{u}_h^1 \\ \mathbf{u}_h^0 \end{bmatrix} \right\|_G^2 + \frac{C\Delta t}{\nu} \sum_{n=1}^{N-1} (\|2T_h^n\|^2 + \|T_h^{n-1}\|^2) \\
& + \frac{C\Delta t}{\nu} \sum_{n=1}^{N-1} (\|2S_h^n\|^2 + \|S_h^{n-1}\|^2). \quad (5.3.11)
\end{aligned}$$

Lastly, the result follows from by using induction on  $N$  with the stability bounds (5.3.1) and (5.3.2).  $\square$

We now give an error estimation for the second-order time-stepping method of proposed algorithm which converges in space and in time if sufficiently smoothing of the solution is satisfied. The error analysis requires the true solution of the velocity, temperature, and concentration at time level  $n + \theta$  i.e.  $\mathbf{u}^{n+\theta} = \mathbf{u}(t^{n+\theta})$ ,  $T^{n+\theta} = T(t^{n+\theta})$  and  $S^{n+\theta} = S(t^{n+\theta})$ . First note that the weak formulation of (5.0.1) at time level  $(n + \theta)$  reads as follows : find  $(\mathbf{u}, T, S, p) \in (\mathbf{X}, W, \Psi, Q)$  such that

$$\begin{aligned}
& (\mathbf{u}_t(t^{n+\theta}), \mathbf{v}_h) + \nu(\nabla \mathbf{u}^{n+\theta}, \nabla \mathbf{v}_h) + b^*(\mathbf{u}^{n+\theta}, \mathbf{u}^{n+\theta}, \mathbf{v}_h) + Da^{-1}(\mathbf{u}^{n+\theta}, \mathbf{v}_h) \\
& \quad - (p^{n+\theta}, \nabla \cdot \mathbf{v}_h) = \beta_T(\mathbf{g}T^{n+\theta}, \mathbf{v}_h) + \beta_S(\mathbf{g}S^{n+\theta}, \mathbf{v}_h), \quad (5.3.12)
\end{aligned}$$

$$(\nabla \cdot \mathbf{u}^{n+\theta}, q_h) = 0, \quad (5.3.13)$$

$$(T_t(t^{n+\theta}), \chi_h) + \gamma(\nabla T^{n+\theta}, \nabla \chi_h) + c^*(\mathbf{u}^{n+\theta}, T, \chi_h) = 0, \quad (5.3.14)$$

$$(S_t(t^{n+\theta}), \Phi_h) + D_c(\nabla S^{n+\theta}, \nabla \Phi_h) + d^*(\mathbf{u}^{n+\theta}, S, \Phi_h) = 0 \quad (5.3.15)$$

for all  $(\mathbf{v}_h, \chi_h, \Phi_h, q_h) \in (\mathbf{X}_h, W_h, \Psi_h, Q_h)$ .

To obtain the optimal convergence, we assume that the following regularity assumptions hold for the true solutions:

$$\begin{aligned}
\mathbf{u}, T, S & \in L^\infty(0, T; H^1(\Omega)) \cap H^1(0, T; H^{k+1}(\Omega)) \cap H^3(0, T; L^2(\Omega)) \cap H^2(0, T; H^1(\Omega)), \\
p & \in L^2(0, T; H^{s+1}(\Omega)) \cap H^2(0, T; L^2(\Omega)).
\end{aligned} \quad (5.3.16)$$

**Theorem 5.3.1** *Let  $(\mathbf{u}, p, T, S)$  be the solution of the problems (5.0.1) such that the regularity assumptions (5.3.16) are satisfied. Then, the following bound holds for the differences  $e_{\mathbf{u}}^n = \mathbf{u}^n - \mathbf{u}_h^n$ ,  $e_T^n = T^n - T_h^n$  and  $e_S^n = S^n - S_h^n$ :*

$$\begin{aligned}
& \|e_{\mathbf{u}}^N\|^2 + \|e_T^N\|^2 + \|e_S^N\|^2 + \frac{1}{2\theta+1} \sum_{n=1}^{N-1} \|e_{\mathbf{u}}^{n+1} - 2e_{\mathbf{u}}^n + e_{\mathbf{u}}^{n-1}\|_F^2 \\
& \quad + \frac{2\Delta t\nu}{2\theta+1} \sum_{n=1}^{N-1} \|F_{n+\theta}^{\varepsilon, \nu}(\nabla e_{\mathbf{u}})\|^2 + \frac{4\Delta tDa^{-1}}{2\theta+1} \sum_{n=1}^{N-1} \|F_{n+\theta}^{\varepsilon, \nu}(e_{\mathbf{u}})\|^2 \\
& \quad + \frac{1}{2\theta+1} \sum_{n=1}^{N-1} \|e_T^{n+1} - 2e_T^n + e_T^{n-1}\|_F^2 + \frac{2\Delta t\gamma}{2\theta+1} \sum_{n=1}^{N-1} \|F_{n+\theta}^{\varepsilon_1, \gamma}(\nabla e_T)\|^2 \\
& \quad + \frac{1}{2\theta+1} \sum_{n=1}^{N-1} \|e_S^{n+1} - 2e_S^n + e_S^{n-1}\|_F^2 + \frac{2\Delta tD_c}{2\theta+1} \sum_{n=1}^{N-1} \|F_{n+\theta}^{\varepsilon_2, D_c}(\nabla e_S)\|^2 \\
& \leq \exp(\tilde{C}T) \left[ \left( \frac{2\theta-1}{2\theta+1} \right)^N \left( \|e_{\mathbf{u}}^0\|^2 + \|e_T^0\|^2 + \|e_S^0\|^2 \right) \right. \\
& \quad \left. + C \left( 1 - \left( \frac{2\theta-1}{2\theta+1} \right)^N \right) \left( \|e_{\mathbf{u}}^1\|^2 + \|e_{\mathbf{u}}^0\|^2 + \|e_T^1\|^2 + \|e_T^0\|^2 + \|e_S^1\|^2 + \|e_S^0\|^2 \right) \right] \\
& \quad + C \left( 1 - \left( \frac{2\theta-1}{2\theta+1} \right)^N \right) \left( \nu^{-1}\Delta t^4 \|p_{tt}\|_{2,0}^2 + \nu^{-1}h^{2k+2} \|p\|_{2,k+1}^2 \right. \\
& \quad \left. + \nu^{-1}\Delta t^4 \|\mathbf{u}_{ttt}\|_{2,0}^2 + \nu^{-1}h^{2k+2} \|\mathbf{u}_t\|_{2,k+1}^2 \right)
\end{aligned}$$

$$\begin{aligned}
& + (\nu + \nu^{-1} + \nu^{-1} \|\|\nabla \mathbf{u}\|_\infty^2 + \gamma^{-1} \|\|\nabla T\|_\infty^2 + D_c^{-1} \|\|\nabla S\|_\infty^2) \Delta t^4 \|\|\nabla \mathbf{u}_{tt}\|_{2,0}^2 \\
& + (\nu + \nu^{-1} + \nu^{-1} \|\|\nabla \mathbf{u}\|_\infty^2 + \gamma^{-1} \|\|\nabla T\|_\infty^2 + D_c^{-1} \|\|\nabla S\|_\infty^2) h^{2k} \|\|\mathbf{u}\|_{2,k+1}^2 \\
& + (\gamma + \gamma^{-1} + \gamma^{-1} \|\|\nabla \mathbf{u}\|_\infty^2 + \nu^{-1} \beta_T^2 \|\|\mathbf{g}\|_\infty^2) \Delta t^4 \|\|\nabla T_{tt}\|_{2,0}^2 \\
& + (\gamma + \gamma^{-1} \|\|\nabla \mathbf{u}\|_\infty^2 + \nu^{-1} \beta_T^2 \|\|\mathbf{g}\|_\infty^2) h^{2k} \|\|T\|_{2,k+1}^2 \\
& + (D_c + D_c^{-1} + D_c^{-1} \|\|\nabla \mathbf{u}\|_\infty^2 + \nu^{-1} \beta_S^2 \|\|\mathbf{g}\|_\infty^2) \Delta t^4 \|\|\nabla S_{tt}\|_{2,0}^2 \\
& + (D_c + D_c^{-1} \|\|\nabla \mathbf{u}\|_\infty^2 + \nu^{-1} \beta_S^2 \|\|\mathbf{g}\|_\infty^2) h^{2k} \|\|S\|_{2,k+1}^2 \\
& + \gamma^{-1} \Delta t^4 \|\|T_{ttt}\|_{2,0}^2 + \gamma^{-1} h^{2k+2} \|\|T_t\|_{2,k+1}^2 \\
& + \left. \begin{aligned} & D_c^{-1} \Delta t^4 \|\|S_{ttt}\|_{2,0}^2 + D_c^{-1} h^{2k+2} \|\|S_t\|_{2,k+1}^2 \end{aligned} \right].
\end{aligned}$$

**Remark 5.3.1** *Note that if one formulates Theorem 5.3.1 for the most common choice of inf-sup stable finite element spaces, like Taylor Hood element, for the velocity and pressure and piecewise quadratics polynomials for the temperature and the concentration, then the optimal errors for the velocity, temperature and concentration are obtained. Similarly, second-order accuracy in time is achieved with these finite element choices.*

**Proof.** First step is to obtain the error equations. By using the operators (5.2.5)-(5.2.7), adding and subtracting terms in (5.3.12)-(5.3.14), true solutions  $(u^{n+1}, p^{n+1}, T^{n+1}, S^{n+1})$  at time level  $n + \theta$  satisfy

$$\begin{aligned}
& (D_{n+\theta}(\mathbf{u}), \mathbf{v}_h) + \nu(F_{n+\theta}^{\varepsilon,\nu}(\nabla \mathbf{u}), \nabla \mathbf{v}_h) + b^*(H_{n+\theta}(\mathbf{u}), F_{n+\theta}^{\varepsilon,\nu}(\mathbf{u}), \mathbf{v}_h) \\
& + Da^{-1}(F_{n+\theta}^{\varepsilon,\nu}(\mathbf{u}), \mathbf{v}_h) - (p^{n+\theta}, \nabla \cdot \mathbf{v}_h) \\
& = \beta_T(\mathbf{g}H_{n+\theta}(T), \mathbf{v}_h) + \beta_S(\mathbf{g}H_{n+\theta}(S), \mathbf{v}_h) + E_1(\mathbf{u}^{n+\theta}, T^{n+\theta}, S^{n+\theta}; \mathbf{v}_h), \quad (5.3.17)
\end{aligned}$$

$$\begin{aligned}
& (D_{n+\theta}(T), \chi_h) + \gamma(F_{n+\theta}^{\varepsilon_1,\gamma}(\nabla T), \nabla \chi_h) + c^*(H_{n+\theta}(\mathbf{u}), F_{n+\theta}^{\varepsilon_1,\gamma}(T), \chi_h) \\
& = E_2(\mathbf{u}^{n+\theta}, T^{n+\theta}; \chi_h) \quad (5.3.18)
\end{aligned}$$

and

$$\begin{aligned}
& (D_{n+\theta}(S), \Phi_h) + D_c(F_{n+\theta}^{\varepsilon_2,D_c}(\nabla S), \nabla \Phi_h) + d^*(H_{n+\theta}(\mathbf{u}), F_{n+\theta}^{\varepsilon_2,D_c}(S), \Phi_h) \\
& = E_3(\mathbf{u}^{n+\theta}, S^{n+\theta}; \Phi_h) \quad (5.3.19)
\end{aligned}$$



for all  $(\mathbf{v}_h, \chi_h, \Phi_h) \in (\mathbf{X}_h, W_h, \Psi_h)$ , where

$$\begin{aligned}
E_1(\mathbf{u}^{n+\theta}, T^{n+\theta}, S^{n+\theta}; \mathbf{v}_h) &= (D_{n+\theta}(\mathbf{u}) - \mathbf{u}_t(t^{n+\theta}), \mathbf{v}_h) \\
&\quad + \nu(\nabla(F_{n+\theta}^{\varepsilon, \nu}(\mathbf{u}) - \mathbf{u}^{n+\theta}), \nabla \mathbf{v}_h) \\
&\quad + b^*(H_{n+\theta}(\mathbf{u}) - \mathbf{u}^{n+\theta}, F_{n+\theta}^{\varepsilon, \nu}(\mathbf{u}), \mathbf{v}_h) \\
&\quad + b^*(\mathbf{u}^{n+\theta}, F_{n+\theta}^{\varepsilon, \nu}(\mathbf{u}) - \mathbf{u}^{n+\theta}, \mathbf{v}_h) \\
&\quad + Da^{-1}(F_{n+\theta}^{\varepsilon, \nu}(\mathbf{u}) - \mathbf{u}^{n+\theta}, \mathbf{v}_h) \\
&\quad + \beta_T(\mathbf{g}(H_{n+\theta}(T) - T^{n+\theta}), \mathbf{v}_h) \\
&\quad + \beta_S(\mathbf{g}(H_{n+\theta}(S) - S^{n+\theta}), \mathbf{v}_h), \tag{5.3.20}
\end{aligned}$$

$$\begin{aligned}
E_2(\mathbf{u}^{n+\theta}, T^{n+\theta}; \chi_h) &= (D_{n+\theta}(T) - T_t(t^{n+\theta}), \chi_h) \\
&\quad + \gamma(\nabla(F_{n+\theta}^{\varepsilon_1, \gamma}(T) - T^{n+\theta}), \nabla \chi_h) \\
&\quad + c^*(H_{n+\theta}(\mathbf{u}) - \mathbf{u}^{n+\theta}, F_{n+\theta}^{\varepsilon_1, \gamma}(T), \chi_h) \\
&\quad + c^*(\mathbf{u}^{n+\theta}, F_{n+\theta}^{\varepsilon_1, \gamma}(T) - T^{n+\theta}, \chi_h) \tag{5.3.21}
\end{aligned}$$

and

$$\begin{aligned}
E_3(\mathbf{u}_{n+\theta}, S_{n+\theta}; \Phi_h) &= (D_{n+\theta}(S) - S_t(t^{n+\theta}), \Phi_h) \\
&\quad + D_c(\nabla(F_{n+\theta}^{\varepsilon_2, D_c}(S) - S^{n+\theta}), \nabla \Phi_h) \\
&\quad + d^*(H_{n+\theta}(\mathbf{u}) - \mathbf{u}^{n+\theta}, F_{n+\theta}^{\varepsilon_2, D_c}(S), \Phi_h) \\
&\quad + d^*(\mathbf{u}^{n+\theta}, F_{n+\theta}^{\varepsilon_2, D_c}(S) - S^{n+\theta}, \Phi_h). \tag{5.3.22}
\end{aligned}$$

Let us decompose the velocity and temperature error in the following way;

$$\begin{aligned}
e_{\mathbf{u}}^n &= \mathbf{u}^n - \mathbf{u}_h^n = (\mathbf{u}^n - I_h(\mathbf{u}^n)) + (I_h(\mathbf{u}^n) - \mathbf{u}_h^n) = \boldsymbol{\eta}_{\mathbf{u}}^n + \boldsymbol{\phi}_h^n, \\
e_T^n &= T^n - T_h^n = (T^n - I_h(T^n)) + (I_h(T^n) - T_h^n) = \eta_T^n + \xi_h^n, \\
e_S^n &= S^n - S_h^n = (S^n - I_h(S^n)) + (I_h(S^n) - S_h^n) = \eta_S^n + \zeta_h^n,
\end{aligned}$$

where  $I_h(\mathbf{u}^n) \in \mathbf{V}_h$  is the interpolant of  $\mathbf{u}^n$  in  $\mathbf{V}_h$ ,  $I_h(T^n) \in W_h$  is the interpolant of  $T^n$  in  $W_h$  and  $I_h(S^n) \in \Psi_h$  is the interpolant of  $S^n$  in  $\Psi_h$ .

The error equations for the velocity, temperature, and concentration are obtained by subtracting (5.2.8), (5.2.10), (5.2.11) from (5.3.17), (5.3.18) and (5.3.19), respectively:

$$\begin{aligned}
& (D_{n+\theta}(e_{\mathbf{u}}), \mathbf{v}_h) + \nu(F_{n+\theta}^{\varepsilon, \nu}(\nabla e_{\mathbf{u}}), \nabla \mathbf{v}_h) + b^*(H_{n+\theta}(\mathbf{u}), F_{n+\theta}^{\varepsilon, \nu}(e_{\mathbf{u}}), \mathbf{v}_h) \\
& + Da^{-1}(F_{n+\theta}^{\varepsilon, \nu}(e_{\mathbf{u}}), \mathbf{v}_h) = E_1(\mathbf{u}^{n+\theta}, T^{n+\theta}; \mathbf{v}_h) - (F_{n+\theta}^{\varepsilon, \nu}(p) - p^{n+\theta}, \nabla \cdot \mathbf{v}_h) \\
& + (F_{n+\theta}^{\varepsilon, \nu}(p) - q_h, \nabla \cdot \mathbf{v}_h) - b^*(H_{n+\theta}(e_{\mathbf{u}}), F_{n+\theta}^{\varepsilon, \nu}(\mathbf{u}_h), \mathbf{v}_h) \\
& + \beta_T(\mathbf{g}H_{n+\theta}(e_T), \mathbf{v}_h) + \beta_S(\mathbf{g}H_{n+\theta}(e_S), \mathbf{v}_h), \tag{5.3.23}
\end{aligned}$$

$$\begin{aligned}
& (D_{n+\theta}(e_T), \chi_h) + \gamma(F_{n+\theta}^{\varepsilon_1, \gamma}(\nabla e_T), \nabla \chi_h) + c^*(H_{n+\theta}(\mathbf{u}), F_{n+\theta}^{\varepsilon_1, \gamma}(e_T), \chi_h) \\
& = E_2(\mathbf{u}^{n+\theta}, T^{n+\theta}; \chi_h) - c^*(H_{n+\theta}(e_{\mathbf{u}}), F_{n+\theta}^{\varepsilon_1, \gamma}(T_h), \chi_h) \tag{5.3.24}
\end{aligned}$$

$$\begin{aligned}
& (D_{n+\theta}(e_S), \chi_h) + D_c(F_{n+\theta}^{\varepsilon_2, D_c}(\nabla e_S), \nabla \Phi_h) + d^*(H_{n+\theta}(\mathbf{u}), F_{n+\theta}^{\varepsilon_2, D_c}(e_S), \Phi_h) \\
& = E_3(\mathbf{u}^{n+\theta}, S^{n+\theta}; \Phi_h) - d^*(H_{n+\theta}(e_{\mathbf{u}}), F_{n+\theta}^{\varepsilon_2, D_c}(S_h), \Phi_h) \tag{5.3.25}
\end{aligned}$$

Taking  $\mathbf{v}_h = F_{n+\theta}^{\varepsilon, \nu}(\phi_h^n)$  in (5.3.23),  $\chi_h = F_{n+\theta}^{\varepsilon_1, \gamma}(\xi_h^n)$  in (5.3.24) and  $\Phi_h = F_{n+\theta}^{\varepsilon_2, D_c}(\zeta_h^n)$  in (5.3.25), using the error decompositions and using the skew-symmetry of the trilinear form, it follows that

$$\begin{aligned}
& \frac{1}{\Delta t} \left\| \begin{bmatrix} \phi_h^{n+1} \\ \phi_h^n \end{bmatrix} \right\|_G^2 - \frac{1}{\Delta t} \left\| \begin{bmatrix} \phi_h^n \\ \phi_h^{n-1} \end{bmatrix} \right\|_G^2 + \frac{1}{4\Delta t} \|\phi_h^{n+1} - 2\phi_h^n + \phi_h^{n-1}\|_F^2 \\
& + \nu \|F_{n+\theta}^{\varepsilon, \nu}(\nabla \phi_h^n)\|^2 + Da^{-1} \|F_{n+\theta}^{\varepsilon, \nu}(\phi_h^n)\|^2 \\
& = E_1(\mathbf{u}^{n+\theta}, T^{n+\theta}, S^{n+\theta}; F_{n+\theta}^{\varepsilon, \nu}(\phi_h)) - (F_{n+\theta}^{\varepsilon, \nu}(p) - p^{n+\theta}, \nabla \cdot F_{n+\theta}^{\varepsilon, \nu}(\phi_h)) \\
& + (F_{n+\theta}^{\varepsilon, \nu}(p) - q_h, \nabla \cdot F_{n+\theta}^{\varepsilon, \nu}(\phi_h)) - (D_{n+\theta}(\boldsymbol{\eta}_{\mathbf{u}}), F_{n+\theta}^{\varepsilon, \nu}(\phi_h)) \\
& - \nu(F_{n+\theta}^{\varepsilon, \nu}(\nabla \boldsymbol{\eta}_{\mathbf{u}}), F_{n+\theta}^{\varepsilon, \nu}(\nabla(\phi_h))) - Da^{-1}(F_{n+\theta}^{\varepsilon, \nu}(\boldsymbol{\eta}_{\mathbf{u}}), F_{n+\theta}^{\varepsilon, \nu}(\phi_h)) \\
& - b^*(H_{n+\theta}(\mathbf{u}), F_{n+\theta}^{\varepsilon, \nu}(\boldsymbol{\eta}_{\mathbf{u}}), F_{n+\theta}^{\varepsilon, \nu}(\phi_h)) - b^*(H_{n+\theta}(\phi_h), F_{n+\theta}^{\varepsilon, \nu}(\mathbf{u}_h), F_{n+\theta}^{\varepsilon, \nu}(\phi_h)) \\
& - b^*(H_{n+\theta}(\boldsymbol{\eta}_{\mathbf{u}}), F_{n+\theta}^{\varepsilon, \nu}(\mathbf{u}_h), F_{n+\theta}^{\varepsilon, \nu}(\phi_h)) + \beta_T(\mathbf{g}H_{n+\theta}(\xi_h), F_{n+\theta}^{\varepsilon, \nu}(\phi_h)) \\
& + \beta_T(\mathbf{g}H_{n+\theta}(\eta^T), F_{n+\theta}^{\varepsilon, \nu}(\phi_h)) + \beta_S(\mathbf{g}H_{n+\theta}(\xi_h), F_{n+\theta}^{\varepsilon, \nu}(\phi_h)) \\
& + \beta_S(\mathbf{g}H_{n+\theta}(\eta_S), F_{n+\theta}^{\varepsilon, \nu}(\phi_h)), \tag{5.3.26}
\end{aligned}$$

$$\begin{aligned}
& \frac{1}{\Delta t} \left\| \begin{bmatrix} \xi_h^{n+1} \\ \xi_h^n \end{bmatrix} \right\|_G^2 - \frac{1}{\Delta t} \left\| \begin{bmatrix} \xi_h^n \\ \xi_h^{n-1} \end{bmatrix} \right\|_G^2 + \frac{1}{4\Delta t} \|\xi_h^{n+1} - 2\xi_h^n + \xi_h^{n-1}\|_F^2 \\
& + \gamma \|F_{n+\theta}^{\varepsilon_1, \gamma}(\nabla \xi_h)\|^2 = E_2(\mathbf{u}^{n+\theta}, T^{n+\theta}; F_{n+\theta}^{\varepsilon_1, \gamma}(\xi_h)) - (D_{n+\theta}(\eta_T), F_{n+\theta}^{\varepsilon_1, \gamma}(\xi_h)) \\
& - \gamma(F_{n+\theta}^{\varepsilon_1, \gamma}(\nabla \eta_T), F_{n+\theta}^{\varepsilon_1, \gamma}(\nabla \xi_h)) - c^*(H_{n+\theta}(\mathbf{u}), F_{n+\theta}^{\varepsilon_1, \gamma}(\eta_T), F_{n+\theta}^{\varepsilon_1, \gamma}(\xi_h)) \\
& - c^*(H_{n+\theta}(\phi_h), F_{n+\theta}^{\varepsilon_1, \gamma}(T_h), F_{n+\theta}^{\varepsilon_1, \gamma}(\xi_h)) \\
& - c^*(H_{n+\theta}(\boldsymbol{\eta}_{\mathbf{u}}), F_{n+\theta}^{\varepsilon_1, \gamma}(T_h), F_{n+\theta}^{\varepsilon_1, \gamma}(\xi_h)) \tag{5.3.27}
\end{aligned}$$

and

$$\begin{aligned}
& \frac{1}{\Delta t} \left\| \begin{bmatrix} \zeta_h^{n+1} \\ \zeta_h^n \end{bmatrix} \right\|_G^2 - \frac{1}{\Delta t} \left\| \begin{bmatrix} \zeta_h^n \\ \zeta_h^{n-1} \end{bmatrix} \right\|_G^2 + \frac{1}{4\Delta t} \|\zeta_h^{n+1} - 2\zeta_h^n + \zeta_h^{n-1}\|_F^2 \\
& + D_c \left\| F_{n+\theta}^{\varepsilon_2, D_c}(\nabla \zeta_h) \right\|^2 = E_3(\mathbf{u}^{n+\theta}, S^{n+\theta}; F_{n+\theta}^{\varepsilon_2, D_c}(\zeta_h)) - (D_{n+\theta}(\eta_S), F_{n+\theta}^{\varepsilon_2, D_c}(\zeta_h)) \\
& - D_c(F_{n+\theta}^{\varepsilon_2, D_c}(\nabla \eta_S), F_{n+\theta}^{\varepsilon_2, D_c}(\nabla \zeta_h)) - d^*(H_{n+\theta}(\mathbf{u}), F_{n+\theta}^{\varepsilon_2, D_c}(\eta_S), F_{n+\theta}^{\varepsilon_2, D_c}(\zeta_h)) \\
& - d^*(H_{n+\theta}(\phi_h), F_{n+\theta}^{\varepsilon_2, D_c}(S_h), F_{n+\theta}^{\varepsilon_2, D_c}(\zeta_h)) \\
& - d^*(H_{n+\theta}(\boldsymbol{\eta}_{\mathbf{u}}), F_{n+\theta}^{\varepsilon_2, D_c}(T_h), F_{n+\theta}^{\varepsilon_2, D_c}(\zeta_h)). \tag{5.3.28}
\end{aligned}$$

To bound the first term in the right hand side of (5.3.26), we consider each term in (5.3.20). Using Cauchy-Schwarz, Young's, Poincaré-Friedrichs inequalities and the estimation (5.1.8), the first term in (5.3.20) is bounded by

$$\begin{aligned}
& (D_{n+\theta}(\mathbf{u}) - \mathbf{u}_t(t^{n+\theta}), F_{n+\theta}^{\varepsilon, \nu}(\phi_h)) \\
& \leq \frac{\nu}{64} \|F_{n+\theta}^{\varepsilon, \nu}(\nabla \phi_h)\|^2 + C\nu^{-1} \|D_{n+\theta}(\mathbf{u}) - \mathbf{u}_t(t^{n+\theta})\|^2 \\
& \leq \frac{\nu}{64} \|F_{n+\theta}^{\varepsilon, \nu}(\nabla \phi_h)\|^2 + C\nu^{-1} \theta^6 \Delta t^3 \int_{t^{n-1}}^{t^{n+1}} \|\mathbf{u}_{ttt}\|^2 dt.
\end{aligned}$$

Similarly, with the estimation (5.1.9) we have

$$\begin{aligned}
& \nu(\nabla(F_{n+\theta}^{\varepsilon, \nu}(\mathbf{u}) - \mathbf{u}^{n+\theta}), \nabla F_{n+\theta}^{\varepsilon, \nu}(\phi_h)) \\
& \leq \frac{\nu}{64} \|F_{n+\theta}^{\varepsilon, \nu}(\nabla \phi_h)\|^2 + C\nu \|\nabla(\theta \mathbf{u}^{n+1} + (1-\theta)\mathbf{u}^n - \mathbf{u}^{n+\theta})\|^2 \\
& \quad + C\nu^{-1} \epsilon^2 \theta^2 \|\nabla(\mathbf{u}^{n+1} - 2\mathbf{u}^n + \mathbf{u}^{n-1})\|^2 \\
& \leq \frac{\nu}{64} \|F_{n+\theta}^{\varepsilon, \nu}(\nabla \phi_h)\|^2 + C\nu \theta^2 (1-\theta)^2 \Delta t^3 \int_{t^n}^{t^{n+1}} \|\nabla \mathbf{u}_{tt}\|^2 dt \\
& \quad + C\nu^{-1} \epsilon^2 \theta^2 \Delta t^3 \int_{t^{n-1}}^{t^{n+1}} \|\nabla \mathbf{u}_{tt}\|^2 dt.
\end{aligned}$$

We use Cauchy-Schwarz, Young's inequalities, and the estimations (5.1.10) and (5.1.9) to bound the nonlinear terms

$$\begin{aligned}
& b^*(H_{n+\theta}(\mathbf{u}) - \mathbf{u}^{n+\theta}, F_{n+\theta}^{\varepsilon, \nu}(\mathbf{u}), F_{n+\theta}^{\varepsilon, \nu}(\phi_h)) \\
& \leq \frac{\nu}{64} \|F_{n+\theta}^{\varepsilon, \nu}(\nabla \phi_h)\|^2 + C\nu^{-1} \|\nabla(H_{n+\theta}(\mathbf{u}) - \mathbf{u}^{n+\theta})\|^2 \|F_{n+\theta}^{\varepsilon, \nu}(\nabla \mathbf{u})\|^2 \\
& \leq \frac{\nu}{64} \|F_{n+\theta}^{\varepsilon, \nu}(\nabla \phi_h)\|^2 + C\nu^{-1} \theta^2 (1+\theta^2) \Delta t^3 \|F_{n+\theta}^{\varepsilon, \nu}(\nabla \mathbf{u})\|^2 \int_{t^{n-1}}^{t^{n+1}} \|\nabla \mathbf{u}_{tt}\|^2 dt.
\end{aligned}$$

and

$$\begin{aligned}
& b^*(\mathbf{u}_{n+\theta}, F_{n+\theta}^{\varepsilon, \nu}(\mathbf{u}) - \mathbf{u}^{n+\theta}, F_{n+\theta}^{\varepsilon, \nu}(\phi_h)) \\
& \leq \frac{\nu}{64} \|F_{n+\theta}^{\varepsilon, \nu}(\nabla \phi_h)\|^2 + C\nu^{-1} \|\nabla \mathbf{u}^{n+\theta}\|^2 \|\nabla(F_{n+\theta}^{\varepsilon, \nu}(\mathbf{u}) - \mathbf{u}^{n+\theta})\|^2 \\
& \leq \frac{\nu}{64} \|F_{n+\theta}^{\varepsilon, \nu}(\nabla \phi_h)\|^2 + C\nu^{-1} \theta^2 (1 - \theta^2) \Delta t^3 \|\nabla \mathbf{u}^{n+\theta}\|^2 \int_{t^n}^{t^{n+1}} \|\nabla \mathbf{u}_{tt}\|^2 dt \\
& \quad + C\nu^{-3} \varepsilon^2 \theta^2 \Delta t^3 \|\nabla \mathbf{u}^{n+\theta}\|^2 \int_{t^{n-1}}^{t^{n+1}} \|\nabla \mathbf{u}_{tt}\|^2 dt,
\end{aligned}$$

Similarly, we obtain

$$\begin{aligned}
& Da^{-1}(F_{n+\theta}^{\varepsilon, \nu}(\mathbf{u}) - \mathbf{u}^{n+\theta}, F_{n+\theta}^{\varepsilon, \nu}(\phi_h)) \\
& \leq \frac{\nu}{64} \|F_{n+\theta}^{\varepsilon, \nu}(\nabla \phi_h)\|^2 + C\nu^{-1} \|\nabla(F_{n+\theta}^{\varepsilon, \nu}(\mathbf{u}) - \mathbf{u}^{n+\theta})\|^2 \\
& \leq \frac{\nu}{64} \|F_{n+\theta}^{\varepsilon, \nu}(\nabla \phi_h)\|^2 + C\nu^{-1} \theta^2 (1 - \theta^2) \Delta t^3 \int_{t^n}^{t^{n+1}} \|\nabla \mathbf{u}_{tt}\|^2 dt \\
& \quad + C\nu^{-3} \varepsilon^2 \theta^2 \Delta t^3 \int_{t^{n-1}}^{t^{n+1}} \|\nabla \mathbf{u}_{tt}\|^2 dt,
\end{aligned}$$

We proceed to bound the last two terms in (5.3.20) in a similar manner

$$\begin{aligned}
& \beta_T((\mathbf{g}H_{n+\theta}(T) - T^{n+\theta}), F_{n+\theta}^{\varepsilon, \nu}(\phi_h)) \\
& \leq \frac{\nu}{64} \|F_{n+\theta}^{\varepsilon, \nu}(\nabla \phi_h)\|^2 + C\beta_T^2 \|\mathbf{g}\|_\infty^2 \nu^{-1} \theta^2 (1 + \theta)^2 \Delta t^3 \int_{t^{n-1}}^{t^{n+1}} \|\nabla T_{tt}\|^2 dt.
\end{aligned}$$

and

$$\begin{aligned}
& \beta_S((\mathbf{g}H_{n+\theta}(S) - S^{n+\theta}), F_{n+\theta}^{\varepsilon, \nu}(\phi_h)) \\
& \leq \frac{\nu}{64} \|F_{n+\theta}^{\varepsilon, \nu}(\nabla \phi_h)\|^2 + C\beta_S^2 \|\mathbf{g}\|_\infty^2 \nu^{-1} \theta^2 (1 + \theta)^2 \Delta t^3 \int_{t^{n-1}}^{t^{n+1}} \|\nabla S_{tt}\|^2 dt.
\end{aligned}$$

We have completed to bound the terms in (5.3.20). To bound the remaining terms on right-hand side of (5.3.26), we use Cauchy-Schwarz and Young's inequalities along with (5.1.9)

$$\begin{aligned}
& (F_{n+\theta}^{\varepsilon, \nu}(p) - p^{n+\theta}, \nabla \cdot F_{n+\theta}^{\varepsilon, \nu}(\phi_h)) \\
& \leq \frac{\nu}{64} \|F_{n+\theta}^{\varepsilon, \nu}(\nabla \phi_h)\|^2 + C\nu^{-1} \|\theta p^{n+1} + (1 - \theta)p^n - p^{n+\theta}\|^2 \\
& \quad + C\nu^{-3} \varepsilon^2 \theta^2 \|p^{n+1} - 2p^n + p^{n-1}\|^2 \\
& \leq \frac{\nu}{64} \|F_{n+\theta}^{\varepsilon, \nu}(\nabla \phi_h)\|^2 + C\nu^{-1} \theta^2 (1 - \theta)^2 \Delta t^3 \int_{t^n}^{t^{n+1}} \|p_{tt}\|^2 dt \\
& \quad + C\nu^{-3} \varepsilon^2 \theta^2 \Delta t^3 \int_{t^{n-1}}^{t^{n+1}} \|p_{tt}\|^2 dt,
\end{aligned}$$

$$\begin{aligned}
& (F_{n+\theta}^{\varepsilon,\nu}(p) - q_h, \nabla \cdot F_{n+\theta}^{\varepsilon,\nu}(\nabla \phi_h)) \\
& \leq \frac{\nu}{64} \|F_{n+\theta}^{\varepsilon,\nu}(\nabla \phi_h)\|^2 + C\nu^{-1} \left( \|F_{n+\theta}^{\varepsilon,\nu}(p) - p^{n+\theta}\|^2 + \|p^{n+\theta} - q_h\|^2 \right) \\
& \leq \frac{\nu}{64} \|F_{n+\theta}^{\varepsilon,\nu}(\nabla \phi_h)\|^2 + C\nu^{-1} \theta^2 (1-\theta)^2 \Delta t^3 \int_{t^n}^{t^{n+1}} \|p_{tt}\|^2 dt \\
& \quad + C\nu^{-3} \varepsilon^2 \theta^2 \Delta t^3 \int_{t^{n-1}}^{t^{n+1}} \|p_{tt}\|^2 dt + C\nu^{-1} \|p^{n+\theta} - q_h\|^2,
\end{aligned}$$

and

$$\begin{aligned}
& (D_{n+\theta}(\boldsymbol{\eta}_{\mathbf{u}}), F_{n+\theta}^{\varepsilon,\nu}(\phi_h)) \\
& \leq C \left\| \frac{\frac{1}{2}(\boldsymbol{\eta}_{\mathbf{u}}^{n+1} - \boldsymbol{\eta}_{\mathbf{u}}^{n-1}) + \theta(\boldsymbol{\eta}_{\mathbf{u}}^{n+1} - \boldsymbol{\eta}_{\mathbf{u}}^n) - \theta(\boldsymbol{\eta}_{\mathbf{u}}^n - \boldsymbol{\eta}_{\mathbf{u}}^{n-1})}{\Delta t} \right\| \|F_{n+\theta}^{\varepsilon,\nu}(\nabla \phi_h)\| \\
& \leq C \left( \left\| \frac{1}{2\Delta t} \int_{t^{n-1}}^{t^{n+1}} \boldsymbol{\eta}_t^{\mathbf{u}} dt \right\| \right. \\
& \quad \left. + \left\| \frac{\theta}{\Delta t} \int_{t^n}^{t^{n+1}} \boldsymbol{\eta}_t^{\mathbf{u}} dt \right\| + \left\| \frac{\theta}{\Delta t} \int_{t^{n-1}}^{t^n} \boldsymbol{\eta}_t^{\mathbf{u}} dt \right\| \right) \|F_{n+\theta}^{\varepsilon,\nu}(\nabla \phi_h)\| \\
& \leq \frac{C\nu^{-1}(\theta^2 + 4)}{\Delta t} \int_{t^{n-1}}^{t^{n+1}} \|\boldsymbol{\eta}_t^{\mathbf{u}}\|^2 dt + \frac{\nu}{64} \|F_{n+\theta}^{\varepsilon,\nu}(\nabla \phi_h)\|^2.
\end{aligned}$$

The next term in (5.3.26) is bounded by using Cauchy-Schwarz and Young's inequalities, taking into account the expansion of  $F_{n+\theta}^{\varepsilon,\nu}$ . It follows that

$$\begin{aligned}
& \nu(F_{n+\theta}^{\varepsilon,\nu}(\nabla \boldsymbol{\eta}_{\mathbf{u}}), F_{n+\theta}^{\varepsilon,\nu}(\nabla \phi_h)) \\
& \leq \nu \|F_{n+\theta}^{\varepsilon,\nu}(\nabla \boldsymbol{\eta}_{\mathbf{u}})\| \|F_{n+\theta}^{\varepsilon,\nu}(\nabla \phi_h)\| \\
& \leq C\nu^{-1} \left( (\theta + \varepsilon\theta\nu^{-1})^2 \|\nabla \boldsymbol{\eta}_{\mathbf{u}}^{n+1}\|^2 + (1 - \theta - 2\varepsilon\theta\nu^{-1})^2 \|\nabla \boldsymbol{\eta}_{\mathbf{u}}^n\|^2 \right. \\
& \quad \left. + \varepsilon^2 \theta^2 \nu^{-2} \|\nabla \boldsymbol{\eta}_{\mathbf{u}}^{n-1}\|^2 \right) + \frac{\nu}{64} \|F_{n+\theta}^{\varepsilon,\nu}(\nabla \phi_h)\|^2.
\end{aligned}$$

Similarly, we have

$$\begin{aligned}
& Da^{-1}(F_{n+\theta}^{\varepsilon,\nu}(\boldsymbol{\eta}_{\mathbf{u}}), F_{n+\theta}^{\varepsilon,\nu}(\phi_h)) \\
& \leq CDa^{-1} \|F_{n+\theta}^{\varepsilon,\nu}(\nabla \boldsymbol{\eta}_{\mathbf{u}})\| \|F_{n+\theta}^{\varepsilon,\nu}(\nabla \phi_h)\| \\
& \leq C\nu^{-1} \left( (\theta + \varepsilon\theta\nu^{-1})^2 \|\nabla \boldsymbol{\eta}_{\mathbf{u}}^{n+1}\|^2 + (1 - \theta - 2\varepsilon\theta\nu^{-1})^2 \|\nabla \boldsymbol{\eta}_{\mathbf{u}}^n\|^2 \right. \\
& \quad \left. + \varepsilon^2 \theta^2 \nu^{-2} \|\nabla \boldsymbol{\eta}_{\mathbf{u}}^{n-1}\|^2 \right) + \frac{\nu}{64} \|F_{n+\theta}^{\varepsilon,\nu}(\nabla \phi_h)\|^2.
\end{aligned}$$

Applying estimation (3.1.9) for the nonlinear terms and expansion of the operators along with Cauchy-Schwarz and Young's inequalities leads to

$$\begin{aligned}
& b^*(H_{n+\theta}(\mathbf{u}), F_{n+\theta}^{\varepsilon, \nu}(\boldsymbol{\eta}_{\mathbf{u}}), F_{n+\theta}^{\varepsilon, \nu}(\boldsymbol{\phi}_h)) \\
& \leq C \|H_{n+\theta}(\nabla \mathbf{u})\| \|F_{n+\theta}^{\varepsilon, \nu}(\nabla \boldsymbol{\eta}_{\mathbf{u}})\| \|F_{n+\theta}^{\varepsilon, \nu}(\nabla \boldsymbol{\phi}_h)\| \\
& \leq C \nu^{-1} \left( (\theta + 1)^2 \|\nabla \mathbf{u}^n\|^2 + \theta^2 \|\nabla \mathbf{u}^{n-1}\|^2 \right) \left( (\theta + \varepsilon \theta \nu^{-1})^2 \|\nabla \boldsymbol{\eta}_{\mathbf{u}}^{n+1}\|^2 \right. \\
& \quad \left. + (1 - \theta - 2\varepsilon \theta \nu^{-1})^2 \|\nabla \boldsymbol{\eta}_{\mathbf{u}}^n\|^2 + \varepsilon^2 \theta^2 \nu^{-2} \|\nabla \mathbf{u}^{n-1}\|^2 \right) + \frac{\nu}{64} \|F_{n+\theta}^{\varepsilon, \nu}(\nabla \boldsymbol{\phi}_h)\|^2
\end{aligned}$$

and

$$\begin{aligned}
& b^*(H_{n+\theta}(\boldsymbol{\eta}_{\mathbf{u}}), F_{n+\theta}^{\varepsilon, \nu}(\mathbf{u}_h), F_{n+\theta}^{\varepsilon, \nu}(\boldsymbol{\phi}_h)) \\
& \leq C \nu^{-1} \|F_{n+\theta}^{\varepsilon, \nu}(\nabla \mathbf{u}_h)\|^2 \|H_{n+\theta}(\nabla \boldsymbol{\eta}_{\mathbf{u}})\|^2 + \frac{\nu}{64} \|F_{n+\theta}^{\varepsilon, \nu}(\nabla \boldsymbol{\phi}_h)\|^2 \\
& \leq C \nu^{-1} \left( (\theta + \varepsilon \theta \nu^{-1})^2 \|\nabla \mathbf{u}_h^{n+1}\|^2 + (1 - \theta - 2\varepsilon \theta \nu^{-1})^2 \|\nabla \mathbf{u}_h^n\|^2 \right. \\
& \quad \left. + \varepsilon^2 \theta^2 \nu^{-2} \|\nabla \mathbf{u}_h^{n-1}\|^2 \right) \\
& \quad \times \left( (\theta + 1)^2 \|\nabla \boldsymbol{\eta}_{\mathbf{u}}^n\|^2 + \theta^2 \|\nabla \boldsymbol{\eta}_{\mathbf{u}}^{n-1}\|^2 \right) + \frac{\nu}{64} \|F_{n+\theta}^{\varepsilon, \nu}(\nabla \boldsymbol{\phi}_h)\|^2.
\end{aligned}$$

Similarly, to bound the next nonlinear term, with the help of (3.1.10), one gets

$$\begin{aligned}
& b^*(H_{n+\theta}(\boldsymbol{\phi}_h), F_{n+\theta}^{\varepsilon, \nu}(\mathbf{u}_h), F_{n+\theta}^{\varepsilon, \nu}(\boldsymbol{\phi}_h)) \\
& \leq C \|F_{n+\theta}^{\varepsilon, \nu}(\nabla \mathbf{u}_h)\|_{\infty} \|H_{n+\theta}(\boldsymbol{\phi}_h)\| \|F_{n+\theta}^{\varepsilon, \nu}(\nabla \boldsymbol{\phi}_h)\| \\
& \quad + C \|F_{n+\theta}^{\varepsilon, \nu}(\mathbf{u}_h)\|_{\infty} \|H_{n+\theta}(\boldsymbol{\phi}_h)\| \|F_{n+\theta}^{\varepsilon, \nu}(\nabla \boldsymbol{\phi}_h)\| \\
& \leq C \nu^{-1} \left( \|F_{n+\theta}^{\varepsilon, \nu}(\nabla \mathbf{u}_h)\|_{\infty}^2 + \|F_{n+\theta}^{\varepsilon, \nu}(\mathbf{u}_h)\|_{\infty}^2 \right) \left( (\theta + 1)^2 \|\boldsymbol{\phi}_h^n\|^2 + \theta^2 \|\boldsymbol{\phi}_h^{n-1}\|^2 \right) \\
& \quad + \frac{\nu}{64} \|F_{n+\theta}^{\varepsilon, \nu}(\nabla \boldsymbol{\phi}_h)\|^2.
\end{aligned}$$

Similarly, the last four terms in (5.3.26) are bounded by

$$\begin{aligned}
& \beta_T(\mathbf{g}H_{n+\theta}(\boldsymbol{\xi}_h), F_{n+\theta}^{\varepsilon, \nu}(\boldsymbol{\phi}_h)) \\
& \leq \frac{\nu}{64} \|F_{n+\theta}^{\varepsilon, \nu}(\nabla \boldsymbol{\phi}_h)\|^2 + C \beta_T^2 \|\mathbf{g}\|_{\infty}^2 \nu^{-1} \left( (\theta + 1)^2 \|\boldsymbol{\xi}_h^n\|^2 + \theta^2 \|\boldsymbol{\xi}_h^{n-1}\|^2 \right),
\end{aligned}$$

$$\begin{aligned}
& \beta_T(\mathbf{g}H_{n+\theta}(\boldsymbol{\eta}_T), F_{n+\theta}^{\varepsilon, \nu}(\boldsymbol{\phi}_h)) \\
& \leq \frac{\nu}{64} \|F_{n+\theta}^{\varepsilon, \nu}(\nabla \boldsymbol{\phi}_h)\|^2 + C \beta_T^2 \|\mathbf{g}\|_{\infty}^2 \nu^{-1} \left( (\theta + 1)^2 \|\nabla \boldsymbol{\eta}_T^n\|^2 + \theta^2 \|\nabla \boldsymbol{\eta}_T^{n-1}\|^2 \right),
\end{aligned}$$

$$\begin{aligned} & \beta_S(\mathbf{g}H_{n+\theta}(\zeta_h), F_{n+\theta}^{\varepsilon, \nu}(\phi_h)) \\ & \leq \frac{\nu}{64} \|F_{n+\theta}^{\varepsilon, \nu}(\nabla \phi_h)\|^2 + C\beta_S^2 \|\mathbf{g}\|_\infty^2 \nu^{-1} \left( (\theta + 1)^2 \|\zeta_h^n\|^2 + \theta^2 \|\zeta_h^{n-1}\|^2 \right), \end{aligned}$$

$$\begin{aligned} & \beta_S(\mathbf{g}H_{n+\theta}(\eta_S), F_{n+\theta}^{\varepsilon, \nu}(\phi_h)) \\ & \leq \frac{\nu}{64} \|F_{n+\theta}^{\varepsilon, \nu}(\nabla \phi_h)\|^2 + C\beta_S^2 \|\mathbf{g}\|_\infty^2 \nu^{-1} \left( (\theta + 1)^2 \|\nabla \eta_S^n\|^2 + \theta^2 \|\nabla \eta_S^{n-1}\|^2 \right). \end{aligned}$$

Next insert the above bounds into the (5.3.23), use the approximation property (3.1.6), multiply by  $\Delta t$  and take the sum from  $n = 1$  to  $n = N - 1$ ;

$$\begin{aligned} & \left\| \begin{bmatrix} \phi_h^N \\ \phi_h^{N-1} \end{bmatrix} \right\|_G^2 + \frac{1}{4} \sum_{n=1}^{N-1} \|\phi_h^{n+1} - 2\phi_h^n + \phi_h^{n-1}\|_F^2 + \frac{\Delta t \nu}{2} \sum_{n=1}^{N-1} \|F_{n+\theta}^{\varepsilon, \nu}(\nabla \phi_h)\|^2 \\ & + \Delta t D a^{-1} \sum_{n=1}^{N-1} \|F_{n+\theta}^{\varepsilon, \nu}(\phi_h)\|^2 \\ & \leq \left\| \begin{bmatrix} \phi_h^1 \\ \phi_h^0 \end{bmatrix} \right\|_G^2 + C \Delta t \sum_{n=1}^{N-1} \left[ \nu^{-1} \theta^2 (1 - \theta)^2 \Delta t^3 \int_{t^n}^{t^{n+1}} \|p_{tt}\|^2 dt \right. \\ & + \nu^{-3} \epsilon^2 \theta^2 \Delta t^3 \int_{t^{n-1}}^{t^{n+1}} \|p_{tt}\|^2 dt + \nu^{-1} h^{2k+2} \|p^{n+\theta}\|_{k+1}^2 \\ & + \nu^{-1} \theta^6 \Delta t^3 \int_{t^{n-1}}^{t^{n+1}} \|\mathbf{u}_{ttt}\|^2 dt + C \nu \theta^2 (1 - \theta)^2 \Delta t^3 \int_{t^n}^{t^{n+1}} \|\nabla \mathbf{u}_{tt}\|^2 dt \\ & + C \nu^{-1} \epsilon^2 \theta^2 \Delta t^3 \int_{t^{n-1}}^{t^{n+1}} \|\nabla \mathbf{u}_{tt}\|^2 dt \\ & + C \nu^{-1} \theta^3 (1 + \theta)^2 \Delta t^3 \|F_{n+\theta}^{\varepsilon, \nu}(\nabla \mathbf{u})\|^2 \int_{t^{n-1}}^{t^{n+1}} \|\nabla \mathbf{u}_{tt}\|^2 dt \\ & + C \nu^{-1} \theta^2 (1 - \theta)^2 \Delta t^3 \|\nabla \mathbf{u}^{n+\theta}\|^2 \int_{t^n}^{t^{n+1}} \|\nabla \mathbf{u}_{tt}\|^2 dt \\ & + C \nu^{-3} \epsilon^2 \theta^2 \Delta t^3 \|\nabla \mathbf{u}^{n+\theta}\|^2 \int_{t^{n-1}}^{t^{n+1}} \|\nabla \mathbf{u}_{tt}\|^2 dt \\ & + C \nu^{-1} \theta^2 (1 - \theta^2) \Delta t^3 \int_{t^n}^{t^{n+1}} \|\nabla \mathbf{u}_{tt}\|^2 dt + C \nu^{-3} \epsilon^2 \theta^2 \Delta t^3 \int_{t^{n-1}}^{t^{n+1}} \|\nabla \mathbf{u}_{tt}\|^2 dt \\ & + C \beta_T^2 \|\mathbf{g}\|_\infty^2 \nu^{-1} \theta^2 (1 + \theta)^2 \Delta t^3 \int_{t^{n-1}}^{t^{n+1}} \|\nabla T_{tt}\|^2 dt \\ & + C \beta_S^2 \|\mathbf{g}\|_\infty^2 \nu^{-1} \theta^2 (1 + \theta)^2 \Delta t^3 \int_{t^{n-1}}^{t^{n+1}} \|\nabla S_{tt}\|^2 dt + \frac{(\theta^2 + 4) \nu^{-1}}{\Delta t} \int_{t^{n-1}}^{t^{n+1}} \|\boldsymbol{\eta}_t^{\mathbf{u}}\|^2 dt \\ & + C \nu \left( (\theta + \varepsilon \theta \nu^{-1})^2 \|\nabla \boldsymbol{\eta}_{\mathbf{u}}^{n+1}\|^2 + (1 - \theta - 2\epsilon \theta \nu^{-1})^2 \|\nabla \boldsymbol{\eta}_{\mathbf{u}}^n\|^2 \right) \end{aligned}$$

$$\begin{aligned}
& +\epsilon^2\theta^2\nu^{-2}\|\nabla\boldsymbol{\eta}_{\mathbf{u}}^{n-1}\|^2) + \nu^{-1}\left((\theta + \epsilon\theta\nu^{-1})^2\|\nabla\boldsymbol{\eta}_{\mathbf{u}}^{n+1}\|^2\right. \\
& + (1 - \theta - 2\epsilon\theta\nu^{-1})^2\|\nabla\boldsymbol{\eta}_{\mathbf{u}}^n\|^2 + \epsilon^2\theta^2\nu^{-2}\|\nabla\boldsymbol{\eta}_{\mathbf{u}}^{n-1}\|^2) + \nu^{-1}\left((\theta + 1)^2\|\nabla\mathbf{u}^n\|^2\right. \\
& + \theta^2\|\nabla\mathbf{u}^{n-1}\|^2) \left. \left((\theta + \epsilon\theta\nu^{-1})^2\|\nabla\boldsymbol{\eta}_{\mathbf{u}}^{n+1}\|^2 + (1 - \theta - 2\epsilon\theta\nu^{-1})^2\|\nabla\boldsymbol{\eta}_{\mathbf{u}}^n\|^2\right.\right. \\
& + \epsilon^2\theta^2\nu^{-2}\|\nabla\boldsymbol{\eta}_{\mathbf{u}}^{n-1}\|^2) + \nu^{-1}\left((\theta + \epsilon\theta\nu^{-1})^2\|\nabla\mathbf{u}_h^{n+1}\|^2\right. \\
& + (1 - \theta - 2\epsilon\theta\nu^{-1})^2\|\nabla\mathbf{u}_h^n\|^2 + \epsilon^2\theta^2\nu^{-2}\|\nabla\mathbf{u}_h^{n-1}\|^2) \left. \left((\theta + 1)^2\|\nabla\boldsymbol{\eta}_{\mathbf{u}}^n\|^2\right.\right. \\
& + \theta^2\|\nabla\boldsymbol{\eta}_{\mathbf{u}}^{n-1}\|^2) + C\beta_T^2\|\mathbf{g}\|_\infty^2\nu^{-1}\left((\theta + 1)^2\|\nabla\eta_T^n\|^2 + \theta^2\|\nabla\eta_T^{n-1}\|^2\right) \\
& + C\beta_S^2\|\mathbf{g}\|_\infty^2\nu^{-1}\left((\theta + 1)^2\|\nabla\eta_S^n\|^2 + \theta^2\|\nabla\eta_S^{n-1}\|^2\right) \\
& + \nu^{-1}\left(\|F_{n+\theta}^{\epsilon,\nu}(\nabla\mathbf{u}_h)\|_\infty^2 + \|F_{n+\theta}^{\epsilon,\nu}(\mathbf{u}_h)\|_\infty^2\right)\left((\theta + 1)^2\|\phi_h^n\|^2 + \theta^2\|\phi_h^{n-1}\|^2\right) \\
& + C\beta_T^2\|\mathbf{g}\|_\infty^2\nu^{-1}\left((\theta + 1)^2\|\xi_h^n\|^2 + \theta^2\|\xi_h^{n-1}\|^2\right) \\
& + C\beta_S^2\|\mathbf{g}\|_\infty^2\nu^{-1}\left((\theta + 1)^2\|\zeta_h^n\|^2 + \theta^2\|\zeta_h^{n-1}\|^2\right)].
\end{aligned}$$

Next we observe that due to Lemma 2.0.12 and approximation results (3.1.5), (5.1.6) and (5.1.7) we have;

$$\begin{aligned}
& \|\phi_h^N\|^2 + \frac{1}{2\theta + 1}\sum_{n=1}^{N-1}\|\phi_h^{n+1} - 2\phi_h^n + \phi_h^{n-1}\|_F^2 + \frac{2\Delta t\nu}{2\theta + 1}\sum_{n=1}^{N-1}\|F_{n+\theta}^{\epsilon,\nu}(\nabla\phi_h)\|^2 \\
& + \frac{4Da^{-1}\Delta t}{2\theta + 1}\sum_{n=1}^{N-1}\|F_{n+\theta}^{\epsilon,\nu}(\phi_h)\|^2 \\
& \leq \left(\frac{2\theta - 1}{2\theta + 1}\right)^N\|\phi_h^0\|^2 + 2\left(1 - \left(\frac{2\theta - 1}{2\theta + 1}\right)^N\right)\left[\left\|\begin{bmatrix} \phi_h^1 \\ \phi_h^0 \end{bmatrix}\right\|_G^2\right. \\
& + C\left(\nu^{-1}\Delta t^4\|p_{tt}\|_{2,0}^2 + \nu^{-1}h^{2k+2}\|p\|_{2,k+1}^2 + \nu^{-1}\Delta t^4\|\mathbf{u}_{ttt}\|_{2,0}^2\right. \\
& + \nu\Delta t^4\|\nabla\mathbf{u}_{tt}\|_{2,0}^2 + \nu^{-1}\Delta t^4\|\nabla\mathbf{u}_{tt}\|_{2,0}^2 + \nu^{-1}\Delta t^4\|\nabla\mathbf{u}\|_{\infty,0}^2\|\nabla\mathbf{u}_{tt}\|_{2,0}^2 \\
& + \nu^{-1}\beta_T^2\|\mathbf{g}\|_\infty^2\Delta t^4\|\nabla T_{tt}\|_{2,0}^2 + \nu^{-1}\beta_S^2\|\mathbf{g}\|_\infty^2\Delta t^4\|\nabla S_{tt}\|_{2,0}^2 \\
& + \nu^{-1}h^{2k+2}\|\mathbf{u}_t\|_{2,k+1}^2 + \nu h^{2k}\|\mathbf{u}\|_{2,k+1}^2 + \nu^{-1}h^{2k}\|\mathbf{u}\|_{2,k+1}^2 \\
& + \nu^{-1}h^{2k}\|\nabla\mathbf{u}\|_\infty^2\|\mathbf{u}\|_{2,k+1}^2 + \nu^{-1}h^{2k}\beta_T^2\|\mathbf{g}\|_\infty^2\|T\|_{2,k+1}^2 \\
& \left. + \nu^{-1}h^{2k}\beta_S^2\|\mathbf{g}\|_\infty^2\|S\|_{2,k+1}^2\right) + C\nu^{-1}\Delta t\sum_{n=0}^{N-1}\|\phi_h^n\|^2
\end{aligned}$$



$$+C\nu^{-1}\beta_T^2\|\mathbf{g}\|_\infty^2\Delta t\sum_{n=0}^{N-1}\|\xi_h^n\|^2+C\nu^{-1}\beta_S^2\|\mathbf{g}\|_\infty^2\Delta t\sum_{n=0}^{N-1}\|\zeta_h^n\|^2\Big].\quad (5.3.29)$$

The proof of temperature proceeds along the lines of the velocity error estimation. The first term  $E_2(\mathbf{u}_{n+\theta}, T_{n+\theta}; F_{n+\theta}^{\varepsilon_1, \gamma}(\xi_h))$  in (5.3.27) is bounded by using Cauchy-Schwarz, Young's inequalities, expansion of operators and Taylor's theorem. Then, one gets

$$\begin{aligned} & (D_{n+\theta}(T) - T_t(t^{n+\theta}), F_{n+\theta}^{\varepsilon_1, \gamma}(\xi_h)) \\ & \leq \frac{\gamma}{64} \|F_{n+\theta}^{\varepsilon, \gamma}(\nabla \xi_h)\|^2 + C\kappa^{-1} \|D_{n+\theta}(T) - T_t(t^{n+\theta})\|^2 \\ & \leq \frac{\gamma}{64} \|F_{n+\theta}^{\varepsilon_1, \gamma}(\nabla \xi_h)\|^2 + C\gamma^{-1}\theta^6\Delta t^3 \int_{t^{n-1}}^{t^{n+1}} \|T_{ttt}\|^2 dt \end{aligned}$$

and

$$\begin{aligned} & \gamma(\nabla(F_{n+\theta}^{\varepsilon_1, \gamma}(T) - T^{n+\theta}), \nabla F_{n+\theta}^{\varepsilon_1, \gamma}(\xi_h)) \\ & \leq \frac{\gamma}{64} \|F_{n+\theta}^{\varepsilon, \gamma}(\nabla \xi_h)\|^2 + C\kappa \|\nabla(F_{n+\theta}^{\varepsilon, \gamma}(T) - T^{n+\theta})\|^2 \\ & \leq \frac{\gamma}{64} \|F_{n+\theta}^{\varepsilon, \gamma}(\nabla \xi_h)\|^2 + C\kappa \|\nabla(\theta T^{n+1} + (1-\theta)T^n - T^{n+\theta})\|^2 \\ & \quad + C\kappa^{-1}\varepsilon^2\theta^2 \|\nabla(T^{n+1} - 2T^n + T^{n-1})\|^2 \\ & \leq \frac{\gamma}{64} \|F_{n+\theta}^{\varepsilon_1, \gamma}(\nabla \xi_h)\|^2 + C\gamma\theta^2(1-\theta)^2\Delta t^3 \int_{t^n}^{t^{n+1}} \|\nabla T_{tt}\|^2 dt \\ & \quad + C\gamma^{-1}\varepsilon_1^2\theta^2\Delta t^3 \int_{t^{n-1}}^{t^{n+1}} \|\nabla T_{tt}\|^2 dt. \end{aligned}$$

The trilinear terms are bounded similar as in the velocity case

$$\begin{aligned} & c^*(H_{n+\theta}(\mathbf{u}) - \mathbf{u}^{n+\theta}, F_{n+\theta}^{\varepsilon_1, \gamma}(T), F_{n+\theta}^{\varepsilon_1, \gamma}(\xi_h)) \\ & \leq C \|\nabla(H_{n+\theta}(\mathbf{u}) - \mathbf{u}^{n+\theta})\| \|F_{n+\theta}^{\varepsilon, \gamma}(\nabla T)\| \|F_{n+\theta}^{\varepsilon, \gamma}(\nabla \xi_h)\| \\ & \leq \frac{\gamma}{64} \|F_{n+\theta}^{\varepsilon, \gamma}(\nabla \xi_h)\|^2 + C\kappa^{-1} \|\nabla(H_{n+\theta}(\mathbf{u}) - \mathbf{u}^{n+\theta})\|^2 \|F_{n+\theta}^{\varepsilon, \gamma}(\nabla T)\|^2 \\ & \leq \frac{\gamma}{64} \|F_{n+\theta}^{\varepsilon_1, \gamma}(\nabla \xi_h)\|^2 + C\gamma^{-1}\theta^2(1+\theta)^2\Delta t^3 \|F_{n+\theta}^{\varepsilon_1, \gamma}(\nabla T)\|^2 \int_{t^{n-1}}^{t^{n+1}} \|\nabla \mathbf{u}_{tt}\|^2 dt \end{aligned}$$

and

$$\begin{aligned}
& c^*(\mathbf{u}^{n+\theta}, F_{n+\theta}^{\varepsilon_1, \gamma}(T) - T^{n+\theta}, F_{n+\theta}^{\varepsilon_1, \gamma}(\xi_h)) \\
& \leq C \|\nabla \mathbf{u}^{n+\theta}\| \|\nabla(F_{n+\theta}^{\varepsilon, \gamma}(T) - T^{n+\theta})\| \|F_{n+\theta}^{\varepsilon, \gamma}(\nabla \phi_T)\| \\
& \leq \frac{\gamma}{64} \|F_{n+\theta}^{\varepsilon, \gamma}(\nabla \xi_h)\|^2 + C\kappa^{-1} \|\nabla \mathbf{u}^{n+\theta}\|^2 \|\nabla(F_{n+\theta}^{\varepsilon, \gamma}(T) - T^{n+\theta})\|^2 \\
& \leq \frac{\gamma}{64} \|F_{n+\theta}^{\varepsilon_1, \gamma}(\nabla \xi_h)\|^2 + C\gamma^{-1}\theta^2(1-\theta)^2\Delta t^3 \|\nabla \mathbf{u}^{n+\theta}\|^2 \int_{t^n}^{t^{n+1}} \|\nabla T_{tt}\|^2 dt \\
& \quad + C\gamma^{-3}\varepsilon_1^2\Delta t^3 \|\nabla \mathbf{u}^{n+\theta}\|^2 \int_{t^{n-1}}^{t^{n+1}} \|\nabla T_{tt}\|^2 dt.
\end{aligned}$$

Similarly, the remaining terms in (5.3.27) follow analogously the proof of the velocity.

One gets the bound

$$\begin{aligned}
& (D_{n+\theta}(\eta_T), F_{n+\theta}^{\varepsilon_1, \gamma}(\xi_h)) \\
& \leq \|D_{n+\theta}(\eta_T)\| \|F_{n+\theta}^{\varepsilon, \gamma}(\xi_h)\| \\
& \leq C \left\| \frac{\frac{1}{2}(\eta_T^{n+1} - \eta_T^{n-1}) + \theta(\eta_T^{n+1} - \eta_T^n) - \theta(\eta_T^n - \eta_T^{n-1})}{\Delta t} \right\| \|F_{n+\theta}^{\varepsilon, \gamma}(\nabla \xi_h)\| \\
& \leq C \left\| \frac{1}{\Delta t} \left( \frac{1}{2} \int_{t^{n-1}}^{t^{n+1}} \eta_t^T dt + \theta \int_{t^n}^{t^{n+1}} \eta_t^T dt - \theta \int_{t^{n-1}}^{t^n} \eta_t^T dt \right) \right\| \|F_{n+\theta}^{\varepsilon, \gamma}(\nabla \xi_h)\| \\
& \leq C \left( \left\| \frac{1}{2\Delta t} \int_{t^{n-1}}^{t^{n+1}} \eta_t^t dt \right\| + \left\| \frac{\theta}{\Delta t} \int_{t^n}^{t^{n+1}} \eta_t^t dt \right\| + \left\| \frac{\theta}{\Delta t} \int_{t^{n-1}}^{t^n} \eta_t^t dt \right\| \right) \|F_{n+\theta}^{\varepsilon, \gamma}(\nabla \xi_h)\| \\
& \leq C\kappa^{-1}(\theta^2 + 4) \left\| \frac{1}{\Delta t} \int_{t^{n+1}}^{t^{n-1}} \eta_t^T dt \right\|^2 + \frac{\gamma}{64} \|F_{n+\theta}^{\varepsilon, \gamma}(\nabla \xi_h)\|^2 \\
& \leq \frac{C\gamma^{-1}(\theta^2 + 4)}{\Delta t} \int_{t^{n-1}}^{t^{n+1}} \|\eta_t^T\|^2 dt + \frac{\gamma}{64} \|F_{n+\theta}^{\varepsilon_1, \gamma}(\nabla \xi_h)\|^2
\end{aligned}$$

and the following bound for the viscous term

$$\begin{aligned}
& \gamma(F_{n+\theta}^{\varepsilon_1, \gamma}(\nabla \eta_T), F_{n+\theta}^{\varepsilon_1, \gamma}(\nabla \xi_h)) \\
& \leq \gamma \|F_{n+\theta}^{\varepsilon, \gamma}(\nabla \eta_T)\| \|F_{n+\theta}^{\varepsilon, \gamma}(\nabla \xi_h)\| \\
& \leq C\gamma \left( \left( \theta + \frac{\varepsilon_1\theta}{\gamma} \right)^2 \|\nabla \eta_T^{n+1}\|^2 + \left( 1 - \theta - \frac{2\varepsilon_1\theta}{\gamma} \right)^2 \|\nabla \eta_T^n\|^2 + \frac{\varepsilon_1^2\theta^2}{\gamma^2} \|\nabla \eta_T^{n-1}\|^2 \right) \\
& \quad + \frac{\gamma}{64} \|F_{n+\theta}^{\varepsilon_1, \gamma}(\nabla \xi_h)\|^2.
\end{aligned}$$

Applying Cauchy-Schwarz, expansion of the operators along with the Young's inequality yields

$$\begin{aligned}
& c^*(H_{n+\theta}(\mathbf{u}), F_{n+\theta}^{\varepsilon_1, \gamma}(\eta_T), F_{n+\theta}^{\varepsilon_1, \gamma}(\xi_h)) \\
& \leq C \|H_{n+\theta}(\nabla \mathbf{u})\| \|F_{n+\theta}^{\varepsilon, \gamma}(\nabla \eta_T)\| \|F_{n+\theta}^{\varepsilon, \gamma}(\nabla \phi_T)\| \\
& \leq C \gamma^{-1} \left( (\theta + 1)^2 \|\nabla \mathbf{u}^n\|^2 + \theta^2 \|\nabla \mathbf{u}^{n-1}\|^2 \right) \left( \left( \theta + \frac{\varepsilon_1 \theta}{\gamma} \right)^2 \|\nabla \eta_T^{n+1}\|^2 \right. \\
& \quad \left. + \left( 1 - \theta - \frac{2\varepsilon_1 \theta}{\gamma} \right)^2 \|\nabla \eta_T^n\|^2 + \frac{\varepsilon_1^2 \theta^2}{\gamma^2} \|\nabla \eta_T^{n-1}\|^2 \right) + \frac{\gamma}{64} \|F_{n+\theta}^{\varepsilon_1, \gamma}(\nabla \xi_h)\|^2
\end{aligned}$$

and

$$\begin{aligned}
& c^*(H_{n+\theta}(\boldsymbol{\eta}_{\mathbf{u}}), F_{n+\theta}^{\varepsilon_1, \gamma}(T_h), F_{n+\theta}^{\varepsilon_1, \gamma}(\phi_T)) \\
& \leq C \|H_{n+\theta}(\nabla \boldsymbol{\eta}_{\mathbf{u}})\| \|F_{n+\theta}^{\varepsilon, \gamma}(\nabla T_h)\| \|F_{n+\theta}^{\varepsilon, \gamma}(\nabla \phi_T)\| \\
& \leq C \kappa^{-1} \|F_{n+\theta}^{\varepsilon, \gamma}(\nabla T_h)\|^2 \|H_{n+\theta}(\nabla \boldsymbol{\eta}_{\mathbf{u}})\|^2 + \frac{\gamma}{64} \|F_{n+\theta}^{\varepsilon, \gamma}(\nabla \phi_T)\|^2 \\
& \leq C \gamma^{-1} \left( (\theta + \varepsilon_1 \theta \kappa^{-1})^2 \|\nabla T_h^{n+1}\|^2 + (1 - \theta - 2\varepsilon_1 \theta \gamma^{-1})^2 \|\nabla T_h^n\|^2 \right. \\
& \quad \left. + \varepsilon_1^2 \theta^2 \gamma^{-2} \|\nabla T_h^{n-1}\|^2 \right) \times ((\theta + 1)^2 \|\nabla \boldsymbol{\eta}_{\mathbf{u}}^n\|^2 + \theta^2 \|\nabla \boldsymbol{\eta}_{\mathbf{u}}^{n-1}\|^2) \\
& \quad + \frac{\gamma}{64} \|F_{n+\theta}^{\varepsilon_1, \gamma}(\nabla \phi_T)\|^2.
\end{aligned}$$

Finally, the last trilinear term is bounded by Lemma 3.1.1:

$$\begin{aligned}
& c^*(H_{n+\theta}(\phi_h), F_{n+\theta}^{\varepsilon_1, \gamma}(T_h), F_{n+\theta}^{\varepsilon_1, \gamma}(\xi_h)) \\
& \leq C \|F_{n+\theta}^{\varepsilon, \gamma}(\nabla T_h)\|_{\infty} \|H_{n+\theta}(\phi_h)\| \|F_{n+\theta}^{\varepsilon, \gamma}(\nabla \phi_h)\| \\
& \quad + C \|F_{n+\theta}^{\varepsilon, \gamma}(T_h)\|_{\infty} \|H_{n+\theta}(\phi_h)\| \|F_{n+\theta}^{\varepsilon, \gamma}(\nabla \phi_h)\| \\
& \leq C \gamma^{-1} \left( \|F_{n+\theta}^{\varepsilon_1, \gamma}(\nabla T_h)\|_{\infty}^2 + \|F_{n+\theta}^{\varepsilon_1, \gamma}(T_h)\|_{\infty}^2 \right) \left( (\theta + 1)^2 \|\phi_h^n\|^2 + \theta^2 \|\phi_h^{n-1}\|^2 \right) \\
& \quad + \frac{\gamma}{64} \|F_{n+\theta}^{\varepsilon_1, \gamma}(\nabla \phi_h)\|^2.
\end{aligned}$$

Next, insert the above bounds into the (5.3.24) and take the sum from  $n = 1$  to  $n = N - 1$ :

$$\begin{aligned}
& \left\| \begin{bmatrix} \xi_h^N \\ \xi_h^{N-1} \end{bmatrix} \right\|_G^2 + \frac{1}{4} \sum_{n=1}^{N-1} \|\xi_h^{n+1} - 2\xi_h^n + \xi_h^{n-1}\|_F^2 + \frac{\Delta t \gamma}{2} \sum_{n=1}^{N-1} \|F_{n+\theta}^{\varepsilon_1, \gamma}(\nabla \xi_h)\|^2 \\
& \leq \left\| \begin{bmatrix} \xi_h^1 \\ \xi_h^0 \end{bmatrix} \right\|_G^2 + C \Delta t \sum_{n=1}^{N-1} \left[ \gamma^{-1} \theta^6 \Delta t^3 \int_{t^{n-1}}^{t^{n+1}} \|T_{ttt}\|^2 dt \right. \\
& \quad + \gamma \theta^2 (1-\theta)^2 \Delta t^3 \int_{t^n}^{t^{n+1}} \|\nabla T_{tt}\|^2 dt + \gamma^{-1} \varepsilon_1^2 \theta^2 \Delta t^3 \int_{t^{n-1}}^{t^{n+1}} \|\nabla T_{tt}\|^2 dt \\
& \quad + C \gamma^{-1} \theta^2 (1+\theta)^2 \Delta t^3 \|F_{n+\theta}^{\varepsilon_1, \gamma}(\nabla T)\|^2 \int_{t^{n-1}}^{t^{n+1}} \|\nabla \mathbf{u}_{tt}\|^2 dt \\
& \quad + C \gamma^{-1} \theta^2 (1-\theta)^2 \Delta t^3 \|\nabla \mathbf{u}_{n+\theta}\|^2 \int_{t^n}^{t^{n+1}} \|\nabla T_{tt}\|^2 dt \\
& \quad + C \gamma^{-3} \varepsilon_1^2 \theta^2 \Delta t^2 \|\nabla \mathbf{u}^{n+\theta}\|^2 \int_{t^{n-1}}^{t^{n+1}} \|\nabla T_{tt}\|^2 dt + \frac{(\theta^2 + 4) \gamma^{-1}}{\Delta t} \int_{t^{n-1}}^{t^{n+1}} \|\eta_t^T\|^2 dt \\
& \quad + \gamma \left( (\theta + \varepsilon_1 \theta \gamma^{-1})^2 \|\nabla \eta_T^{n+1}\|^2 + (1 - \theta - 2\varepsilon_1 \theta \gamma^{-1})^2 \|\nabla \eta_T^n\|^2 \right. \\
& \quad \left. + \varepsilon_1^2 \theta^2 \gamma^{-2} \|\nabla \eta_T^{n-1}\|^2 \right) + \gamma^{-1} \left( (\theta + 1)^2 \|\nabla \mathbf{u}^n\|^2 + \theta^2 \|\nabla \mathbf{u}^{n-1}\|^2 \right) \\
& \quad \left( (\theta + \varepsilon_1 \theta \gamma^{-1})^2 \|\nabla \eta_T^{n+1}\|^2 + (1 - \theta - 2\varepsilon_1 \theta \gamma^{-1})^2 \|\nabla \eta_T^n\|^2 \right. \\
& \quad \left. + \varepsilon_1^2 \theta^2 \gamma^{-2} \|\nabla \eta_T^{n-1}\|^2 \right) + \gamma^{-1} \left( (\theta + \varepsilon_1 \theta \gamma^{-1})^2 \|\nabla T_h^{n+1}\|^2 \right. \\
& \quad \left. + (1 - \theta - 2\varepsilon_1 \theta \gamma^{-1})^2 \|\nabla T_h^n\|^2 + \varepsilon_1^2 \theta^2 \gamma^{-2} \|\nabla T_h^{n-1}\|^2 \right) \\
& \quad + \left( (\theta + 1)^2 \|\nabla \eta_{\mathbf{u}}^n\|^2 + \theta^2 \|\nabla \eta_{\mathbf{u}}^{n-1}\|^2 \right) + \gamma^{-1} \left( \|F_{n+\theta}^{\varepsilon_1, \gamma}(\nabla T_h)\|_\infty^2 + \|F_{n+\theta}^{\varepsilon_1, \gamma}(T_h)\|_\infty^2 \right) \\
& \quad \left. + \left( (\theta + 1)^2 \|\phi_{\mathbf{u}}^n\|^2 + \theta^2 \|\phi_{\mathbf{u}}^{n-1}\|^2 \right) \right].
\end{aligned}$$

Applying the stability bound Lemma 2.0.12 in the last estimation yields;

$$\begin{aligned}
& \|\xi_h^N\|^2 + \frac{1}{2\theta + 1} \sum_{n=1}^{N-1} \|\xi_h^{n+1} - 2\xi_h^n + \xi_h^{n-1}\|_F^2 + \frac{2\Delta t \gamma}{2\theta + 1} \sum_{n=1}^{N-1} \|F_{n+\theta}^{\varepsilon_1, \gamma}(\nabla \xi_h)\|^2 \\
& \leq \left( \frac{2\theta - 1}{2\theta + 1} \right)^N \|\xi_h^0\|^2 + 2 \left( 1 - \left( \frac{2\theta - 1}{2\theta + 1} \right)^N \right) \left[ \left\| \begin{bmatrix} \xi_h^1 \\ \xi_h^0 \end{bmatrix} \right\|_G^2 \right. \\
& \quad + C \left( \gamma^{-1} \Delta t^4 \|T_{ttt}\|_{2,0}^2 + \gamma \Delta t^4 \|\nabla T_{tt}\|_{2,0}^2 + \gamma^{-1} \Delta t^4 \|\nabla T_{tt}\|_{2,0}^2 \right. \\
& \quad \left. + \gamma^{-1} \Delta t^4 \|\nabla T\|_\infty^2 \|\nabla \mathbf{u}_{tt}\|_{2,0}^2 + \gamma^{-1} \Delta t^4 \|\nabla \mathbf{u}\|_\infty^2 \|\nabla T_{tt}\|_{2,0}^2 \right. \\
& \quad \left. + \gamma^{-1} h^{2k+2} \|T_t\|_{2,k+1}^2 + \gamma h^{2k} \|T\|_{2,k+1}^2 \right]
\end{aligned}$$

$$\begin{aligned}
& +\gamma^{-1}h^{2k} \left( \|\nabla \mathbf{u}\|_\infty^2 \|T\|_{2,k+1}^2 + \gamma^{-1}h^{2k} \|\nabla T\|_\infty^2 \|\mathbf{u}\|_{2,k+1}^2 \right) \\
& + C\gamma^{-1}\Delta t \sum_{n=0}^{N-1} \|\phi_h^n\|^2 \Big]. \tag{5.3.30}
\end{aligned}$$

Repeating the similar arguments of the temperature error, the concentration error equation (5.3.28) is estimated by

$$\begin{aligned}
& \|\zeta_h^N\|^2 + \frac{1}{2\theta+1} \sum_{n=1}^{N-1} \|\zeta_h^{n+1} - 2\zeta_h^n + \zeta_h^{n-1}\|_F^2 + \frac{2\Delta t D_c}{2\theta+1} \sum_{n=1}^{N-1} \|F_{n+\theta}^{\varepsilon_2, D_c}(\nabla \zeta_h)\|^2 \\
& \leq \left( \frac{2\theta-1}{2\theta+1} \right)^N \|\zeta_h^0\|^2 + 2 \left( 1 - \left( \frac{2\theta-1}{2\theta+1} \right)^N \right) \left[ \left\| \begin{bmatrix} \zeta_h^1 \\ \zeta_h^0 \end{bmatrix} \right\|_G^2 \right. \\
& + C \left( D_c^{-1} \Delta t^4 \|S_{ttt}\|_{2,0}^2 + D_c \Delta t^4 \|\nabla S_{tt}\|_{2,0}^2 + D_c^{-1} \Delta t^4 \|\nabla S_{tt}\|_{2,0}^2 \right. \\
& + D_c^{-1} \Delta t^4 \|\nabla S\|_\infty^2 \|\nabla \mathbf{u}_{tt}\|_{2,0}^2 + D_c^{-1} \Delta t^4 \|\nabla \mathbf{u}\|_\infty^2 \|\nabla S_{tt}\|_{2,0}^2 \\
& + D_c^{-1} h^{2k+2} \|S_t\|_{2,k+1}^2 + D_c h^{2k} \|S\|_{2,k+1}^2 + D_c^{-1} h^{2k} \|\nabla \mathbf{u}\|_\infty^2 \|S\|_{2,k+1}^2 \Big) \\
& \left. + D_c^{-1} h^{2k} \|\nabla S\|_\infty^2 \|\mathbf{u}\|_{2,k+1}^2 + C D_c^{-1} \Delta t \sum_{n=0}^{N-1} \|\phi_h^n\|^2 \right]. \tag{5.3.31}
\end{aligned}$$

Now, summing (5.3.29), (5.3.30) and (5.3.31) we obtain

$$\begin{aligned}
& \|\phi_h^N\|^2 + \|\xi_h^N\|^2 + \|\zeta_h^N\|^2 + \frac{1}{2\theta+1} \sum_{n=1}^{N-1} \|\phi_h^{n+1} - 2\phi_h^n + \phi_h^{n-1}\|_F^2 \\
& + \frac{2\Delta t \nu}{2\theta+1} \sum_{n=1}^{N-1} \|F_{n+\theta}^{\varepsilon, \nu}(\nabla \phi_h)\|^2 + \frac{4\Delta t D a^{-1}}{2\theta+1} \sum_{n=1}^{N-1} \|F_{n+\theta}^{\varepsilon, \nu}(\phi_h)\|^2 \\
& + \frac{1}{2\theta+1} \sum_{n=1}^{N-1} \|\xi_h^{n+1} - 2\xi_h^n + \xi_h^{n-1}\|_F^2 + \frac{2\Delta t \gamma}{2\theta+1} \sum_{n=1}^{N-1} \|F_{n+\theta}^{\varepsilon, \gamma}(\nabla \xi_h)\|^2 \\
& + \frac{1}{2\theta+1} \sum_{n=1}^{N-1} \|\zeta_h^{n+1} - 2\zeta_h^n + \zeta_h^{n-1}\|_F^2 + \frac{2\Delta t D_c}{2\theta+1} \sum_{n=1}^{N-1} \|F_{n+\theta}^{\varepsilon, D_c}(\nabla \zeta_h)\|^2 \\
& \leq \left( \frac{2\theta-1}{2\theta+1} \right)^N \left( \|\phi_h^0\|^2 + \|\xi_h^0\|^2 + \|\zeta_h^0\|^2 \right) \\
& + 2 \left( 1 - \left( \frac{2\theta-1}{2\theta+1} \right)^N \right) \left[ \left\| \begin{bmatrix} \phi_h^1 \\ \phi_h^0 \end{bmatrix} \right\|_G^2 + \left\| \begin{bmatrix} \xi_h^1 \\ \xi_h^0 \end{bmatrix} \right\|_G^2 + \left\| \begin{bmatrix} \zeta_h^1 \\ \zeta_h^0 \end{bmatrix} \right\|_G^2 \right. \\
& \left. + C \left( \nu^{-1} \Delta t^4 \|p_{tt}\|_{2,0}^2 + \nu^{-1} h^{2k+2} \|p\|_{2,k+1}^2 + \nu^{-1} \Delta t^4 \|\mathbf{u}_{ttt}\|_{2,0}^2 \right) \right]
\end{aligned}$$

$$\begin{aligned}
& +\nu\Delta t^4 \|\nabla \mathbf{u}_{tt}\|_{2,0}^2 + \nu^{-1}\Delta t^4 \|\nabla \mathbf{u}_{tt}\|_{2,0}^2 + \nu^{-1}\Delta t^4 \|\nabla \mathbf{u}\|_{\infty,0}^2 \|\nabla \mathbf{u}_{tt}\|_{2,0}^2 \\
& +\nu^{-1}\beta_T^2 \|\mathbf{g}\|_{\infty}^2 \Delta t^4 \|\nabla T_{tt}\|_{2,0}^2 + \nu^{-1}\beta_S^2 \|\mathbf{g}\|_{\infty}^2 \Delta t^4 \|\nabla S_{tt}\|_{2,0}^2 \\
& +\nu^{-1}h^{2k+2} \|\mathbf{u}_t\|_{2,k+1}^2 + \nu h^{2k} \|\mathbf{u}\|_{2,k+1}^2 + \nu^{-1}h^{2k} \|\mathbf{u}\|_{2,k+1}^2 \\
& +\nu^{-1}h^{2k} \|\nabla \mathbf{u}\|_{\infty}^2 \|\mathbf{u}\|_{2,k+1}^2 + \nu^{-1}h^{2k}\beta_T^2 \|\mathbf{g}\|_{\infty}^2 \|T\|_{2,k+1}^2 \\
& +\nu^{-1}h^{2k}\beta_S^2 \|\mathbf{g}\|_{\infty}^2 \|S\|_{2,k+1}^2 + \gamma^{-1}\Delta t^4 \|T_{ttt}\|_{2,0}^2 + \gamma\Delta t^4 \|\nabla T_{tt}\|_{2,0}^2 \\
& +D_c\Delta t^4 \|\nabla S_{tt}\|_{2,0}^2 + D_c^{-1}\Delta t^4 \|\nabla S_{tt}\|_{2,0}^2 + D_c^{-1}\Delta t^4 \|\nabla S\|_{\infty}^2 \|\nabla \mathbf{u}_t\|_{2,0}^2 \\
& +D_c^{-1}\Delta t^4 \|\nabla \mathbf{u}\|_{\infty}^2 \|\nabla S_{tt}\|_{2,0}^2 + D_c^{-1}h^{2k+2} \|S_t\|_{2,k+1}^2 + D_ch^{2k} \|S\|_{2,k+1}^2 \\
& +D_c^{-1}h^{2k} \|\nabla \mathbf{u}\|_{\infty}^2 \|S\|_{2,k+1}^2 + D_c^{-1}h^{2k} \|\nabla S\|_{\infty}^2 \|\mathbf{u}\|_{2,k+1}^2 \Big) \\
& +\tilde{C}\Delta t \sum_{n=0}^{N-1} (\|\phi_h^n\|^2 + \|\xi_h^n\|^2 + \|\zeta_h^n\|^2) \Big] \tag{5.3.32}
\end{aligned}$$

where  $\tilde{C} := \tilde{C}(\nu^{-1}, \gamma^{-1}, D_S^{-1}, \beta_T^2, \beta_S^2, \|\mathbf{g}\|_{\infty}^2)$ .

We next apply the Lemma 2.0.13 and use the following inequality in (5.3.32),

$$0 \leq \left(\frac{2\theta - 1}{2\theta + 1}\right)^N \leq 1 \quad \text{for any } N \geq 0.$$

The final result follows from the triangle inequality and Lemma 2.0.12.  $\square$

**Corollary 5.3.1** *Under the assumptions of Theorem 5.3.1, let  $(\mathbf{X}_h, W_h, \Psi_h, Q_h) = (P_2, P_2, P_2, P_1)$  be the finite element spaces given by Remark 5.3.1. Then the asymptotic error estimation satisfies*

$$\begin{aligned}
& \|e_{\mathbf{u}}^N\|^2 + \|e_T^N\|^2 + \|e_S^N\|^2 + \frac{1}{2\theta + 1} \sum_{n=1}^{N-1} \|e_{\mathbf{u}}^{n+1} - 2e_{\mathbf{u}}^n + e_{\mathbf{u}}^{n-1}\|_F^2 \\
& + \frac{2\Delta t\nu}{2\theta + 1} \sum_{n=1}^{N-1} \|F_{n+\theta}^{\varepsilon,\nu}(\nabla e_{\mathbf{u}})\|^2 + \frac{4\Delta tDa^{-1}}{2\theta + 1} \sum_{n=1}^{N-1} \|F_{n+\theta}^{\varepsilon,\nu}(e_{\mathbf{u}})\|^2 \\
& + \frac{1}{2\theta + 1} \sum_{n=1}^{N-1} \|e_T^{n+1} - 2e_T^n + e_T^{n-1}\|_F^2 + \frac{2\Delta t\gamma}{2\theta + 1} \sum_{n=1}^{N-1} \|F_{n+\theta}^{\varepsilon,\gamma}(\nabla e_T)\|^2 \\
& + \frac{1}{2\theta + 1} \sum_{n=1}^{N-1} \|e_S^{n+1} - 2e_S^n + e_S^{n-1}\|_F^2 + \frac{2\Delta tD_S}{2\theta + 1} \sum_{n=1}^{N-1} \|F_{n+\theta}^{\varepsilon,D_c}(\nabla e_S)\|^2 \\
& \leq C((\Delta t)^4 + h^4 + \|e_{\mathbf{u}}^0\|^2 + \|e_{\mathbf{u}}^1\|^2 + \|e_T^0\|^2 + \|e_T^1\|^2 + \|e_S^0\|^2 + \|e_S^1\|^2).
\end{aligned}$$

**Proof.** The result follows immediately from the regularity assumptions (5.3.16).  $\square$

## 5.4 Numerical Experiments

In this section, we perform two numerical tests to show the efficiency of the proposed method and validate the theoretical findings. The first example is the verification of the numerical convergence rates for an analytic test problem with a known solution. The second example is of more practical interest; it is a buoyancy-driven cavity flow example in a tall rectangular cavity.

The simulations are performed with the finite element software package FreeFem++ [42]. In all computations, the Taylor-Hood finite element for velocity and pressure, and piecewise quadratics for temperature and concentration are used on triangular grids. The Darcy flow regime ( $Da = \infty$ ) is assumed for all tests. In order to see the effect of stabilization parameters, the results are also compared with the usual BDF2LE method, which is obtained through picking  $\epsilon = \epsilon_1 = \epsilon_2 = 0$  and  $\theta = 1$  (unstabilized case) in (5.2.1)-(5.2.4), which gives

$$\begin{aligned} & \frac{(\theta + \frac{1}{2})\mathbf{u}^{n+1} - 2\theta\mathbf{u}^n + (\theta - \frac{1}{2})\mathbf{u}^{n-1}}{\Delta t} - \theta\nu\Delta\mathbf{u}^{n+1} - (\nu - \theta\nu)\Delta\mathbf{u}^n \\ & + ((\theta + 1)\mathbf{u}^n - \theta\mathbf{u}^{n-1}) \cdot \nabla(\theta\mathbf{u}^{n+1} + (1 - \theta\mathbf{u}^n)) + \theta\nabla p^{n+1} + (1 - \theta)\nabla p^n \\ & = \left( \beta_T((\theta + 1)T^n - \theta T^{n-1}) + \beta_S((\theta + 1)S^n - \theta S^{n-1}) \right) \mathbf{g} + \mathbf{f}^{n+\theta} \end{aligned} \quad (5.4.1)$$

$$\nabla \cdot \mathbf{u}^{n+1} = 0 \quad (5.4.2)$$

$$\begin{aligned} & \frac{(\theta + \frac{1}{2})T^{n+1} - 2\theta T^n + (\theta - \frac{1}{2})T^{n-1}}{\Delta t} - \theta\gamma\Delta T^{n+1} - (\gamma - \theta\gamma)\Delta T^n \\ & + ((\theta + 1)\mathbf{u}^n - \theta\mathbf{u}^{n-1}) \cdot \nabla(\theta T^{n+1} + (1 - \theta T^n)) = \varphi^{n+\theta} \end{aligned} \quad (5.4.3)$$

$$\begin{aligned} & \frac{(\theta + \frac{1}{2})S^{n+1} - 2\theta S^n + (\theta - \frac{1}{2})S^{n-1}}{\Delta t} - \theta D_c \Delta S^{n+1} - (D_c - \theta D_c) \Delta S^n \\ & + ((\theta + 1)\mathbf{u}^n - \theta\mathbf{u}^{n-1}) \cdot \nabla(\theta S^{n+1} + (1 - \theta S^n)) = \psi^{n+\theta}. \end{aligned} \quad (5.4.4)$$

Here, the forcing functions  $\mathbf{f}^{n+\theta}$ ,  $\varphi^{n+\theta}$  and  $\psi^{n+\theta}$  are included in (5.4.1)-(5.4.4). We also note that the similar results are also obtained with the CNLE with the choices of parameters  $\epsilon = \epsilon_1 = \epsilon_2 = 0$  and  $\theta = 1/2$ .

### 5.4.1 Numerical convergence study

In this subsection, we show that the theoretical orders of the errors are also obtained through a numerical simulation. To do so, we pick the known-solution

$$\begin{aligned} \mathbf{u} &= \begin{pmatrix} \cos(y) \\ \sin(x) \end{pmatrix} e^t, \quad p = (x - y)(1 + t), \\ T &= \sin(x + y)e^{1-t}, \quad S = \cos(x + y)e^{1-t}. \end{aligned} \quad (5.4.5)$$

with the parameters  $Pr = D_c = \gamma = \beta_T = \beta_S = 1$  and the right-hand side functions  $\mathbf{f}$ ,  $\varphi$  and  $\psi$  are chosen such that (5.4.5) satisfies (5.0.1).

We will present computational results with  $\epsilon = \epsilon_1 = \epsilon_2 = 0$ ,  $\theta = 1$  and  $\epsilon = \epsilon_1 = \epsilon_2 = 1$  (with stabilization) in a unit square. The final time and the time step size are chosen as  $T = 10^{-1}$  and  $\Delta t = T/16$ . To test the spatial convergence, we fix the time step size and calculate the errors for varying  $h$  and consider the velocity errors in the discrete norm  $L^2(0, T; \mathbf{H}^1(\Omega))$

$$\|\mathbf{u} - \mathbf{u}_h\|_{2,1} = \left\{ \Delta t \sum_{n=1}^N \|\mathbf{u}(t^n) - \mathbf{u}_h^n\|^2 \right\}^{1/2}.$$

The results of different  $\epsilon$ ,  $\epsilon_1$  and  $\epsilon_2$  values for the spatial errors and error rates are given in Table 5.1 and Table 5.2. One can see that the orders of convergence of  $\|\mathbf{u} - \mathbf{u}_h\|_{2,1}$ ,  $\|T - T_h\|_{2,1}$  are quadratic, which is an optimal order for both BDF2LE and for the proposed method. We note that because of the parameter choices of this numerical test, the errors for  $\|S - S_h\|_{2,1}$  are similar. We also fix the mesh size to  $h = 1/128$  to see the temporal errors and the convergence rates by using different time steps with an end time of  $T = 1$ . The results are given in Table 5.3 and Table 5.4. As expected, we observe a second-order convergence in time. However, the velocity error rates becomes better for the stabilized case as  $\Delta t$  decreases. In addition, the rates for the temperature errors are far better than the unstabilized case when they are compared with the proposed method. In summary, the observations of convergence orders of (5.2.8)-(5.2.10) are in accordance with the discussion in Corollary 5.3.1.



Table 5.1: Spatial errors and rates of convergence for  $\epsilon = \epsilon_1 = \epsilon_2 = 0$ .

$h$	$\ \mathbf{u} - \mathbf{u}_h\ _{2,1}$	Rate	$\ T - T_h\ _{2,1}$	Rate
1/4	1.606e-3	–	3.99e-3	–
1/8	4.357e-4	1.88	1.00e-3	1.99
1/16	1.124e-4	1.95	2.527e-4	1.98
1/32	2.848e-5	1.98	6.318e-5	2.00
1/64	7.171e-6	1.98	1.592e-5	1.98

Table 5.2: Spatial errors and rates of convergence for  $\epsilon = \epsilon_1 = \epsilon_2 = 1$ .

$h$	$\ \mathbf{u} - \mathbf{u}_h\ _{2,1}$	Rate	$\ T - T_h\ _{2,1}$	Rate
1/4	1.621e-3	–	4.003e-3	–
1/8	4.403e-4	1.88	1.01e-3	1.98
1/16	1.136e-4	1.95	2.531e-4	2.00
1/32	2.879e-5	1.98	6.365e-5	1.99
1/64	7.244e-6	1.98	1.740e-5	1.88

Table 5.3: Temporal errors and rates of convergence for  $\epsilon = \epsilon_1 = \epsilon_2 = 0$ .

$\Delta t$	$\ \mathbf{u} - \mathbf{u}_h\ _{2,1}$	Rate	$\ T - T_h\ _{2,1} = \ S - S_h\ _{2,1}$	Rate
1	3.093e-2	–	6.572e-2	–
1/2	6.662e-3	2.21	3.415e-2	1.01
1/4	1.568e-3	2.08	1.220e-2	1.49
1/8	3.842e-4	2.02	3.617e-3	1.75
1/16	1.007e-4	1.93	9.841e-4	1.88

Table 5.4: Temporal errors and rates of convergence for  $\epsilon = \epsilon_1 = \epsilon_2 = 1$ .

$\Delta t$	$\ \mathbf{u} - \mathbf{u}_h\ _{2,1}$	Rate	$\ T - T_h\ _{2,1} = \ S - S_h\ _{2,1}$	Rate
1	6.203e-3	–	7.005e-1	–
1/2	2.880e-3	1.10	1.991e-1	1.81
1/4	1.293e-3	1.15	5.233e-2	1.92
1/8	3.921e-4	1.72	1.151e-2	2.18
1/16	1.058e-4	1.90	2.610e-3	2.14

### 5.4.2 Buoyancy Driven Cavity Test

As another numerical test, we apply the proposed method to so-called buoyancy-driven cavity flow in a tall rectangular enclosure. It is a well-known benchmark problem for testing fluid flows driven solely by a density difference due to a temperature gradient. This problem forms a prototype of many applications such as thermal insulation, cooling of electronic devices, nuclear reactors etc. Buoyancy-driven flows are complex flows due to coupling between the transport properties of flow and thermal fields.

The purpose of this example is to capture correct flow patterns on coarse mesh and to get the correct solution where the unstabilized case fails. In this test, the effects of several dimensionless problem parameters on the solution are considered. We also calculate the Nusselt numbers and Sherwood numbers for this cavity test and compare our results with those reported previously. The computational domain we use is a rectangular cavity of height 2 and width 1 with different temperature and concentration values at vertical walls, which are regarded as hot and cold walls, see Figure 5.1 ([4]). The horizontal walls are insulated and assumed to allow no heat and species transfer through. The boundary conditions are no-slip boundary conditions for the velocity and Dirichlet boundary conditions for the temperature and concentration at vertical walls as well. The horizontal walls accept the boundary conditions,  $\frac{\partial T}{\partial n} = \frac{\partial S}{\partial n} = 0$ .

At the initial stage, the fluid has no motion. According to the variation of temperature and concentration at vertical walls, the motion will be started due to the buoyancy

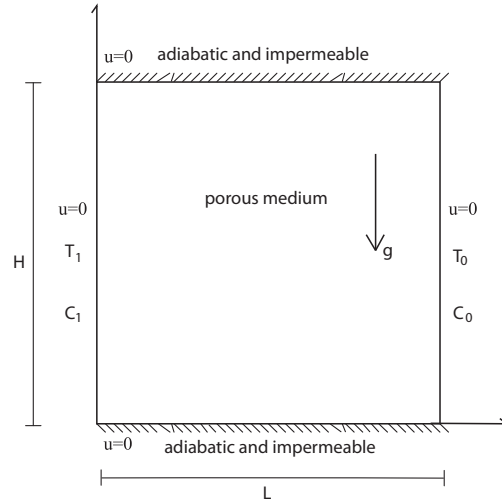


Figure 5.1: The physical domain with its boundary conditions

forces as density varies. The final time is chosen to be  $T = 1$  and the time interval is divided into equidistant time steps of length  $10^{-4}$ . The stabilization parameters are taken as  $\epsilon = O(\nu)$ ,  $\epsilon_1 = O(\gamma)$ ,  $\epsilon_2 = O(D_c)$ .

Before we present our results, we remark that the correct patterns are captured for all different parameter cases for a very coarse mesh consisting of only 8262 velocity d.o.f, 4131 temperature d.o.f, and concentration d.o.f.

In general, the proposed method and the unstabilized case produce very similar results for the tests with  $Ra \leq 10^5$ . However, the unstabilized case gave no result and the solution diverges for  $Ra = 10^6$ . This might be noted as the greatest superiority of our method against the unstabilized case.

#### 5.4.2.1 The effect of buoyancy ratio $N$

In this test, the effect of buoyancy ratio  $N$  is considered for  $N = 0.8$  and  $N = 1.3$ , by fixing  $Pr = 1$ ,  $Ra = 10^5$  and  $Le = 2$ . The results are shown in Figure 5.2. It can be observed that the variation of density in concentration is larger than the variation in temperature for  $N > 1$ . As it is expected, due to the increase in the buoyancy ratio, the

concentration stratification increases. Thus, the force pushing the low concentration fluid up becomes greater, [113].

For  $N < 1$ , this time density variations are due to the temperature gradients mostly and the situation turns out for temperature. These graphics perfectly agree with the benchmark studies of [113] and [126].

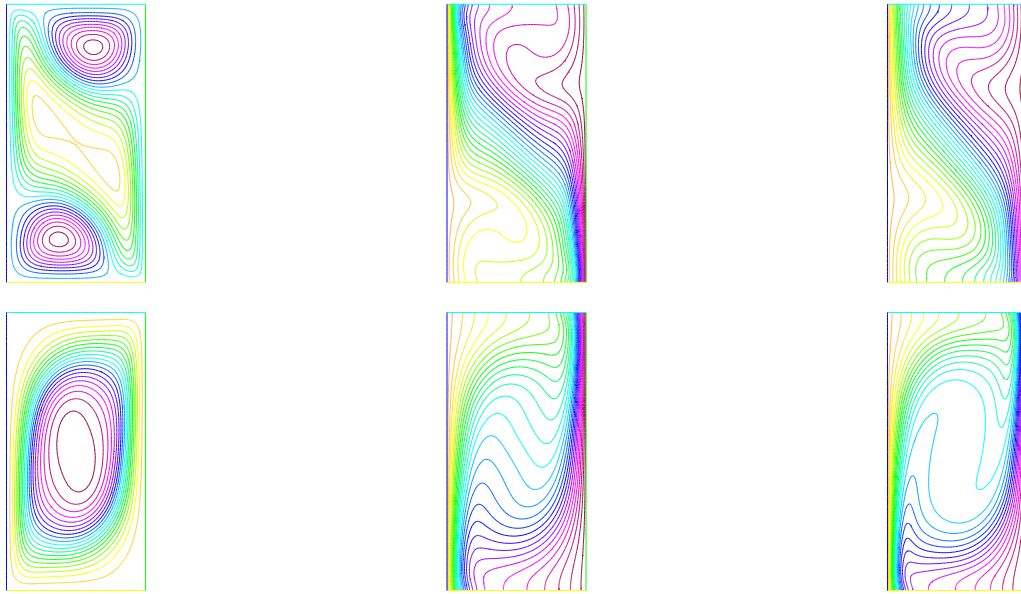


Figure 5.2: Velocity streamlines, Temperature contours and Concentration contours (from left to right) for  $Pr = 1, Ra = 10^5, Le = 2$  with  $N = 1.3$  (up) and  $N = 0.8$  (down)

#### 5.4.2.2 The effect of Lewis number $Le$

The effect of the Lewis number is considered with the choices of  $Le = 0.2$  and  $Le = 1.0$ . The values of  $Pr = 1, Ra = 10^5$  and  $N = 1$  are fixed in all computations. Due to the definition of Lewis number,  $Le \leq 1.0$  means the mass diffusivity is greater than the thermal diffusivity. In this case, the concentration becomes dominant because of its better capability of spreading higher concentration values. The value of  $Le = 1.0$  means equal diffusivity case. When temperature and concentration behave in the same way, the forces made by the temperature and concentration cancel each other in both walls initially. Thus, the fields diffuse exactly in the same way and these

forces always are balanced equally. The final solution is just the diffusion of the fields through the domain as is noted in [113]. The mentioned situations above could be observed directly from Figure 5.3.

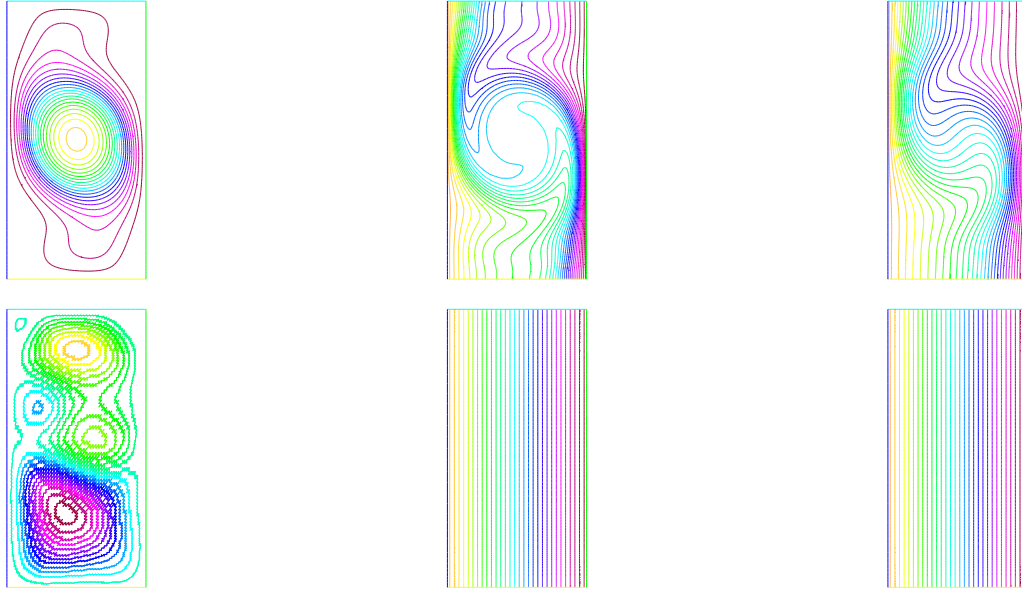


Figure 5.3: Velocity streamlines, Temperature contours and Concentration contours (from left to right) for  $Pr = 1$ ,  $Ra = 10^5$ ,  $N = 1$  with  $Le = 0.2$  (up) and  $Le = 1.0$  (down)

#### 5.4.2.3 The effect of Rayleigh number $Ra$

For natural convection type problems, increasing the Rayleigh number and keeping the thermal and mass diffusivity parameters constant will increase the characteristic velocity of the flow. This can cause the flow to behave turbulently. Since the transition to turbulent case means richness of the flow scales, dealing with a very challenging numerical problem is inevitable as the Rayleigh number increases. The test is carried out for three different Rayleigh numbers,  $Ra = 10^4, 10^5, 10^6$  with the coarse mesh discretization. The results are presented in Figure 5.4 only for the case  $Ra = 10^6$ . For other  $Ra$  values, the figures are similar and we do not depict them. All the results are comparable with [41], which uses a POD-ROM scheme and an extra VMS stabilization for  $Ra = 10^6$  for finer meshes.

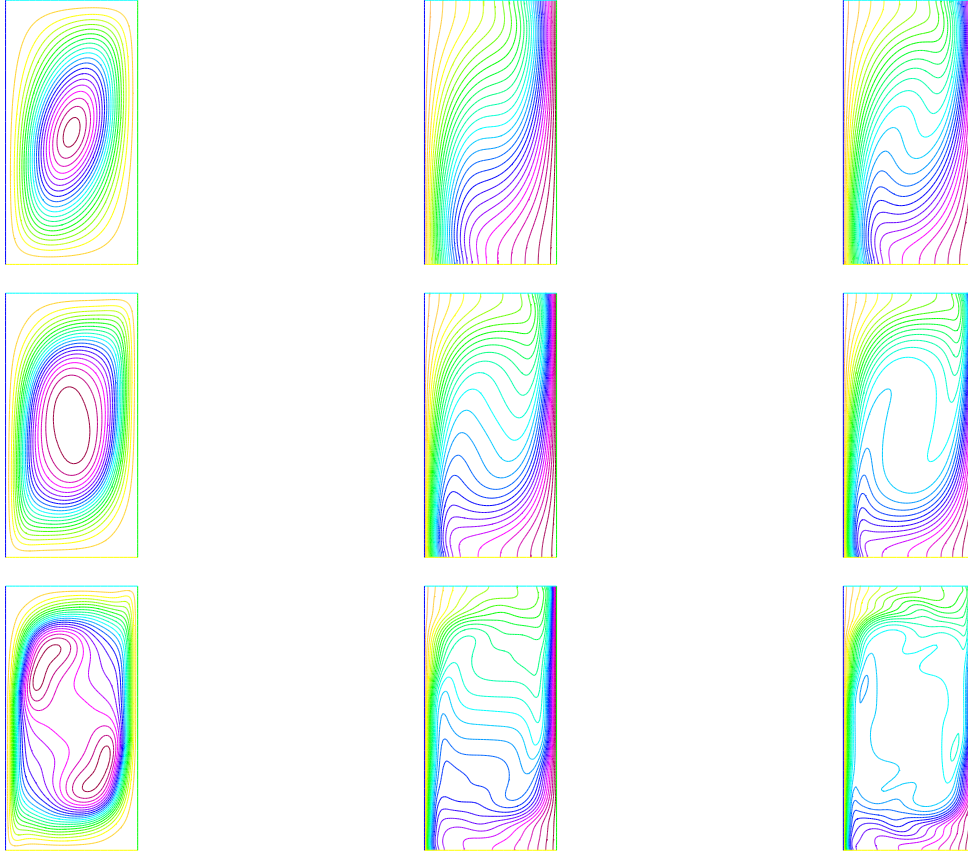


Figure 5.4: Velocity streamlines, Temperature contours and Concentration contours (from left to right) for  $Pr = 1, Le = 2, N = 0.8$  with  $Ra = 10^4$  (up),  $Ra = 10^5$  (middle) and  $Ra = 10^6$  (down)

#### 5.4.2.4 Thermal and Mass Distributions in Buoyancy Driven Cavity

In terms of engineering, calculation of thermal and mass distributions along with different boundaries which are kept at different temperatures and concentrations are of vital importance for convective flows inside enclosures. There are physical parameters called the Nusselt number (Nu) and Sherwood number (Sh) for measuring these distributions. Local and average Nusselt and Sherwood numbers are given with the following formulas

$$\begin{aligned} \text{Nu}_{loc} &= \pm \left\{ \frac{\partial T}{\partial x} \right\}_{wall}, \text{Nu}_{av} = \int_{\Omega} \text{Nu}_{loc} dy. \\ \text{Sh}_{loc} &= \pm \left\{ \frac{\partial S}{\partial x} \right\}_{wall}, \text{Sh}_{av} = \int_{\Omega} \text{Sh}_{loc} dy. \end{aligned}$$

Calculation of  $Nu_{av}$  and  $Sh_{av}$  at a buoyancy driven cavity test example has been widely used in order to verify and validate proposed numerical schemes on produced codes. The flow parameters are taken as  $Pr = 1, Le = 2, N = 0.8$  for  $Ra = 10^4$  and  $Ra = 10^5$  in this test. Well-known numerical simulations in literature are known to obtain such results for a  $100 \times 200$  rectangle, which is regarded as a coarse mesh [126]. Table 5.5 and Table 5.6 gives a comparison of the results of both presented method and results of [7, 126]. As it is seen, acceptable results for Nu and Sh are obtained with the proposed scheme.

Table 5.5: Comparison of average Nusselt numbers on the vertical boundary of the cavity at  $x = 0$  (hot wall) for  $Pr = 1, Le = 2, N = 0.8$  with mesh size used in computation for varying Rayleigh Numbers

Ra	Proposed Method	Ref. [7]	Ref. [126]
$10^4$	3.65(25×40)	3.67(31×41)	3.68(100×200)
$10^5$	6.78(25×40)	6.82(31×41)	6.84(100×200)

Table 5.6: Comparison of average Sherwood numbers on the vertical boundary of the cavity at  $x = 0$  (hot wall) for  $Pr = 1, Le = 2, N = 0.8$  with mesh size used in computation for varying Rayleigh Numbers

Ra	Proposed Method	Ref. [7]	Ref. [126]
$10^4$	4.78(25×40)	4.89(31×41)	4.91(100×200)
$10^5$	8.75(25×40)	6.82(31×41)	8.70(100×200)





## CHAPTER 6

### CONCLUSION

This thesis presented the finite element analysis of second-order and reliable methods for the incompressible fluid-flow driven by the NSE and the Darcy-Brinkman equations with double-diffusive convection.

In the first part (Chapter 3) of the thesis, we introduced and analyzed an efficient, fully discrete SAV regularization method for approximating solutions to NSE with BDF2LE time discretization. The proposed stabilization method is effective only for small scales in fluid flow. We have found that the solutions of the proposed algorithm preserve both energy and helicity identities. We have obtained smooth and regular bounded solutions without time step restriction. We also proved optimally convergent of the method with suitable choices of the artificial viscosity and the grad-div stabilization parameter. Several numerical tests were performed to verify the theoretical findings and show that the superiority of the method over the CN-SAV and unstabilized NSE.

In the second part (Chapter 4) of the thesis, we proposed and analyzed the backward Euler based modular time filter method for the EMAC formulation of NSE. The approach increases numerical accuracy from first order to second order without requiring any additional computational effort. We provided unconditional stability and optimally convergent results of the method. A rich blend of numerical experiments verified the theoretical expectations and demonstrated reliability and efficiency of the proposed method. The numerical results clearly exposed that the EMAC-FILTERED scheme produces more accurate results and better quality solutions over the unfiltered case. Thus, the simplicity of BE discretization is combined with desirable accuracy and efficiency properties which we aim to arrive. We also showed that the EMAC-

FILTERED scheme conserves important physical quantities as good, or better than the BE-EMAC scheme.

In the last part (Chapter 5) of the thesis, we studied a new optimally accurate numerical regularization based on the idea of curvature stabilization for (a family of) second order time-stepping methods for the double-diffusive convection system. The proposed algorithm has the advantage of requiring the solution of only one linear system per time step and thus it is efficient in terms of computational effort. We performed the unconditional stability and optimal convergence results of the method. Several numerical tests were presented to prove the efficiency of the proposed method.

There are several research directions that could be inspired from this thesis. One possible direction is to extend the SAV method and the EMAC-FILTERED method to different kind of fluid flow problems like natural convection, MHD and Darcy-Brinkman equations.

Another direction is to study the SAV method, the EMAC-FILTERED and the curvature stabilization idea to optimal control problems.

## REFERENCES

- [1] A. Arakawa. Computational design for long-term numerical integration of the equations of fluid motion: Two dimensional incompressible flow, Part I. *J. Comput. Phys.*, 1, 119–143, 1966.
- [2] A. Arakawa and V. Lamb. A potential enstrophy and energy conserving scheme for the shallow water equations. *Monthly Weather Rev.*, 109, 18–36, 1981.
- [3] A. Cibik, S. Kaya, and F. G. Eroglu. Analysis of Second Order Time Filtered Backward Euler Method for MHD Equations. *J. Sci. Comput.*, 82(2), 696–713, 2020.
- [4] A. Cibik and S. Kaya. Finite element analysis of a projection-based stabilization method for the Darcy–Brinkman equations in double-diffusive convection. *Appl. Numer. Math.*, 64, 35–49, 2013.
- [5] A. Cibik and S. Kaya. A projection based stabilized finite element method for steady-state natural convection problems. *J. Math. Anal. Appl.*, 381, 469–484, 2011.
- [6] A. Guzel and W. Layton. Time filters increase accuracy of the fully implicit method. *BIT*, 58(2), 301–315, 2018.
- [7] A. J. Chamkha and H. Al-Naser. Hydromagnetic double-diffusive convection in a rectangular enclosure with opposing temperature and concentration gradients. *Int. J. of Heat and Mass Transfer*, 45, 2465–2483, 2002.
- [8] A. J. Chorin and J. E. Marsden. *A Mathematical Introduction to Fluid Mechanics*, Springer-Verlag, New-York, 1993.
- [9] A. Komiya, K. Tsubaki, S. Maruyama, and H. Mitsugashira. Continuous measurement of an artificial upwelling of deep sea water induced by the perpetual salt fountain. *Deep Sea Res. Part I Oceanogr. Res. Pap.*, 54:75–84, 2007.

- [10] A. K. Saha. Direct numerical simulation of two-dimensional flow past a normal flat plate. *J. Eng. Mechanics*, 139(2):1894-1901, 2013.
- [11] A. Labovsky, W. Layton, C. Manica, M. Neda, and L. Rebholz, The Stabilized Extrapolated Trapezoidal Finite-Element Method for the Navier-Stokes Equations. *Comput. Methods. Appl. Mech. Engrg.*, 198, 958–974, 2009.
- [12] A. Masud and R. Calderer. Residual based turbulence models for moving boundary flows: hierarchial application of vms and three level scale separation. *Int. J. Numer. Methods Fluids*, 73, 284–305, 2013.
- [13] A. Mojtabi and M. C. Charrier-Mojtabi. Double-diffusive convection, in: Handbook of Porous media Part III, Taylor and Francis, 2005.
- [14] A. Palha and M. Gerritsma. A mass, energy, enstrophy and vorticity conserving(MEEVC) mimetic spectral element discretization for the 2D incompressible Navier–Stokes equations. *J. Comput. Phys.*, 328, 200–220, 2017.
- [15] A. Shapiro. The use of an exact solution of the Navier–Stokes equations in a validation test of a three-dimensional nonhydrostatic numerical model. *Mon. Wea. Rew.*, 121(8), 2420–2425, 1993.
- [16] B. Goyeau, J. P. Songbe, and D. Gobin. Numerical study of double-diffusive natural convection in a porous cavity using the Darcy-Brinkman formulation. *Int. J. Heat Mass Transfer*, 39, 1363-1378, 1995.
- [17] B. J. Geurts. Elements of direct and large-eddy simulation. Edwards, 2004.
- [18] C. Canuto, M. Y. Hussaini, A. Quarteroni, and T. A. Zang. Spectral methods, evolution to complex geometries and applications to fluid dynamics. *Sci. Comput.*, 2007.
- [19] C. F. Chen and D. H. Johnson. Double-Diffusive Convection: A report on an Engineering Foundation Conference. *J. Fluid Mec.*, 138, 405-416, 1984.
- [20] C. Kılıçaslan. *Modelling and Simulation of Metal Cutting by Finite Element Method*. Master thesis, İzmir Institute of Technology, 2009.
- [21] C. L. Fefferman. Existence and smoothness of the Navier-Stokes equation. The Millennium Prize Problems, *Clay Math. Inst.*, Cambridge, 57-67, 2006.

- [22] C. L. M. H. Navier. Mémoire sur les lois du mouvement des fluides. *Mém. Acad. Royal Society*, 6, 389–440, 1823.
- [23] C. Liao and P. Z. Huang. The modified characteristics finite element method for time dependent Darcy-Brinkman problem. *Eng. Comput.* 36, 356–376, 2019.
- [24] C. Liao, P. Z. Huang, and Y. N. He. A decoupled finite element method with different time steps for the nonstationary Darcy-Brinkman problem. *J. Numer. Math.*, 2019.
- [25] C. S. Peskin. Numerical analysis of blood flow in the heart. *J. Comput. Phys.*, 25(3), 220–252, 1977.
- [26] C. Sargentone, S. La Cognata, and J. Nordstrom. A new high order energy and enstrophy conserving Arakawa-like Jacobian differential operator. *J. Comput. Phys.*, 301, 167–177, 2015.
- [27] C. Trenchea. Second order implicit for local effects and explicit for nonlocal effects is unconditionally stable. *ROMAI J.*, 1, 163-178, 2016.
- [28] C. Trenchea. Stability of partitioned imex methods for systems of evolution equations with skew-symmetric coupling. *ROMAI J.* ,10, 175-189, 2014.
- [29] D. A. Nield and A. Bejan. Convection in Porous Media. *Springer, Berlin*, 1992.
- [30] D. Arnold and J. Qin. Quadratic velocity/linear pressure Stokes elements. In R. Vichnevetsky, D. Knight, and G. Richter, editors. *Advances in Computer Methods for Partial Differential Equations VII*, 28–34, 1992.
- [31] D. Braess. *Finite Elements: Theory, fast solvers and applications in elasticity theory*. Cambridge University Press, 2007.
- [32] D. D. Holm, E. Olson, E. S. Titi, S. Chen, C. Foias, and S. Wynne. Camassa-Holm equations as a closure model for turbulent channel and pipe flow. *Phys. Rev. Lett.*, 81, 5338–5341, 1998.
- [33] D. D. Holm, E. Olson, E. S. Titi, S. Chen, C. Foias, and S. Wynne. The Camassa-Holm equations and turbulence. *Phys D*, 133, 49–65, 1999, Predictability: quantifying uncertainty in models of complex phenomena (Los Alamos, NM, 1998).

- [34] D. D. Padova, L. Calvo, P. M. Carbone, D. Maraglino, and M. Mossa. Comparison between the Lagrangian and Eulerian Approach for Simulating Regular and Solitary Waves Propagation, Breaking and Run-Up. *Appl. Sci.*, 11(20), 2021.
- [35] D. Pastrana, J. C. Cajas, O. Lehmkuhl, I. Rodriguez, and G. Houzeaux. Large-eddy simulations of the vortex-induced vibration of a low mass ratio two-degree-of-freedom circular cylinder at subcritical Reynolds numbers. *Comput. Fluids*, 173, 118–132, 2018.
- [36] E. Hairer and G. Wanner. Solving ordinary differential equations 11 : stiff and differential algebraic problems. *Springer-Verlag*, 2002.
- [37] F. Armero and J. C. Simo. Long-term dissipativity of time-stepping algorithms for an abstract evolution equation with applications to the incompressible MHD and Navier-Stokes equations. *Comput. Methods Appl. Mech. Engrg.*, 131, 41–90, 1996.
- [38] F. Brezzi and M. Fortin. Mixed and Hybrid Finite Element Methods. *volume 15 of Springer Series in Computational Mathematics*, Springer-Verlag, 1991.
- [39] F. D. Deffenbaugh and F. J. Marshall. Time development of the flow about an impulsively started cylinder. *AIAA Journal*, 14(7), 908–913, 1976.
- [40] F. Fleissner, T. Gaugele, and P. Eberhard. Applications of the Discrete Element Method in Mechanical Engineering. *Multibody Syst. Dyn.*, 18, 81-94, 2007.
- [41] F. G. Eroglu, S. Kaya, and L. G. Rebholz. POD-ROM for the Darcy-Brinkman equations with double-diffusive convection. *J. Numer. Math.*, 27, 123–139, 2019.
- [42] F. Hecht, New development in freefem++. *J. Numer. Math.*, 20, 251-265, 2012.
- [43] F. Tone, X. M. Wang, and D. Wirosoetisno. Long-time dynamics of 2d double-diffusive convection: analysis and/of numerics. *Numer. Math.*, 10, 541–566, 2015.
- [44] G. A. Baker, V. A. Dougalis, and O. Karakashian. On a higher order accurate fully discrete Galerkin approximation to the Navier-Stokes equations. *Math. Comput.*, 39, 339-375, 1982.

- [45] G. Baker. Galerkin approximations for the Navier-Stokes equations. *Tech. report*, Harvard University.
- [46] G. Fix. Finite element models for ocean circulation problems. *SIAM J. Appl. Math.*, 29(3), 371–387, 1975.
- [47] G. G. Stokes. On the theories of the internal friction of fluids in motion and of the equilibrium and motion of elastic solids. *Trans. Cambridge Philos. Soc.*, 8, 287–319, 1845.
- [48] G. J. Das. Finite element solution to engineering problems. *Jurnal Akademik*, 1(1), 1-12.
- [49] G. M. Mirouh, P. Garaud, S. Stellmach, A. L. Traxler, and T. S. Wood. A new model for mixing by double-diffusive convection (semi-convection). I. The conditions for layer formation. *Astrophys. J.*, 750(1), 2012.
- [50] H. Owen, G. Chrysokentis, M. Avila, D. Mira, G. Houzeaux, R. Borrell, J. C. Cajas, and O. Lehmkuhl. Wall-modeled large-eddy simulation in a finite element framework. *Int. J. Numer. Methods Fluids*, 92(1), 20–37, 2020.
- [51] J. Boussinesq. *Théorie Analytique de la Chaleur*. vol. 2. Gauthier-Villars, Paris, 1903.
- [52] J. C. Simo, F. Armero, and C. A. Taylor. Stable and time-dissipative finite element methods for the incompressible Navier-Stokes equations in advection dominated flows. *Internat. J. Numer. Methods Engrg.*, 38, 1475–1506, 1995.
- [53] J. Evans and T. J. R. Hughes. Isogeometric divergence-conforming B-splines for the steady Navier–Stokes equations. *Math. Model Meth. Appl. Sci.*, 23(08), 1421–1478, 2013.
- [54] J. Frutos, B. Garcia-Archilla, and J. Novo. The post-processed mixed finite-element method for the Navier-Stokes equations: refined error bounds. *SIAM J. Numer. Anal.*, 46(1), 201-230, 2008.
- [55] J. G. Liu and W. Wang. Energy and helicity preserving schemes for hydro and magnetohydro-dynamics flows with symmetry. *J. Comput. Phys.*, 200, 8–33, 2004.

- [56] J. Guzman and M. Neilan. Conforming and divergence-free Stokes elements in threedimensions. *IMA J. Numer. Anal.*, 34(4), 1489–1508, 2014.
- [57] J. Heywood and R. Rannacher. Finite element approximation of the nonstationary Navier-Stokes equations, Part II: Stability of solutions and error estimates uniform in time. *SIAM J. Numer. Anal.*, 23:750-777, 1986.
- [58] J. L. Guermond, Stabilization of Galerkin approximations of transport equations by subgrid modeling. *M2AN*, 33, 1293-1316, 1999.
- [59] J. Kramer, J. Ravnik, R. Jecl, and L. Škerget. Three-dimensional doublediffusive natural convection with opposing buoyancy effects in porous enclosure by boundary element method. *Int. J. Comp. Meth. and Exp. Meas.*, 1:103–115, 2013.
- [60] J. Kramer, R. Jecl, and L. Škerget. Boundary domain integral method for double diffusive natural convection in porous media saturated with compressible fluid. *AIP Conference Proceedings*, 1048:332–335, 2008.
- [61] J. L. Guermond, J. T. Oden, and S. Prudhomme. Mathematical perspectives on large eddy simulation models for turbulent flows. *J. Math. Fluid Mech.*, 6, 194–248, 2004.
- [62] J. Leray. Sur le mouvement d’un liquide visqueux emplissant l’espace. *Acta Mathematica*, 63, 193-248, 1934.
- [63] J. Löwe and G. Lube. A projection based variational multiscale method for Large-Eddy simulation with application to non-isothermal free convection problems. *Math. Models Methods Appl. Sci.*, 22, 1–31, 2012.
- [64] J. Marshall, A. Adcroft, C. Hill, L. Perelman, and C. Heisey. A finite-volume, incompressible navier–stokes model for studies of the ocean on parallel computers. *J. Geophys. Res.*, 102:5733-5752, 1997.
- [65] J. M. Varah. Stability restrictions on second order, three level finite difference schemes for parabolic equations. *SIAM J. Numer. Anal.*, 17, 300-309, 1980.
- [66] J. Nichele and D. A. Teixeira. Evaluation of Darcy-Brinkman equation for simulations of oil flows in rocks. *J. Petrol Sci. Eng*, 134, 76-78, 2015.



- [67] J. P. Kelliher, R. Temam, and X. Wang. Boundary layer associated with the Darcy-Brinkman-Boussinesq model for convection in porous media. *Physica D.*, 240:619–628, 2011.
- [68] J. P. Songbe, B. Goyeau, and D. Gobin. Numerical study of double-diffusive natural convection in a porous cavity using the Darcy-Brinkman formulation. *Int. J. Heat. Mass Tran.*, 39(7):1363-1378, 1996.
- [69] J. Serrano-Arellano, M. Gijn-Rivera, J. M. Riesco-vila, and F. Elizalde-Blancas. Numerical study of the double diffusive convection phenomena in a closed cavity with internal CO<sub>2</sub> point sources. *Int. J. Heat Mass Transfer*, 71, 664-674, 2014.
- [70] C. Xu, Y. Zhang, and J. Zhou. Convergence of a linearly extrapolated BDF2 finite element scheme for viscoelastic fluid flow. *Bound. Value Probl.*, 140, 2017.
- [71] K. Bryan. Accelerating the convergence to equilibrium of ocean-climate models. *Journal of Physical Oceanography*, 14, 666–673, 1984.
- [72] K. Ghorayeb and A. Mojtabi. Double diffusive convection in a vertical rectangular cavity. *Phys. Fluids*, 9 (8):2339–2348, 1997.
- [73] K. J. Galvin, New subgrid artificial viscosity Galerkin methods for the Navier-Stokes equations. *Comput. Methods Appl. Mech. Engrg.* , 200, 242-250, 2011.
- [74] L. Berselli, T. Illiescu, and W. Layton. *Mathematics of Large Eddy Simulation of Turbulent Flows*. Springer, 2005.
- [75] L. Davis and F. Pahlevani. Semi-implicit schemes for transient Navier-Stokes equations and eddy viscosity models. *Numer. Methods for Partial Differential Equations*, 25, 212–231, 2009.
- [76] L. P. Franca and T. J. R. Hughes. Two classes of mixed finite element methods. *Comput. Methods Appl. Mech. Engrg.*, 69 (1), 189–129, 1988.
- [77] L. Rebholz. An Energy and Helicity conserving finite element scheme for the Navier-Stokes equations. *SIAM J. Numer. Anal.*, 45(4), 1622–1638, 2007.

- [78] L. Rebholz. Helicity and physical fidelity in turbulence modeling. *Ph.D. thesis*, University of Pittsburgh, 2006.
- [79] M. Akbas. An Adaptive Time Filter Based Finite Element Method for the Velocity-Vorticity-Temperature Model of the Incompressible Non-Isothermal Fluid Flows. *Gazi University Journal of Science*, 33, 696-713, 2020.
- [80] M. Akın, A. F. Çabalar, and H. Yalçın. Evaluation of the performance of geotextiles using Finite Element Analysis in the settlement results: A case study in Kayseri, Turkey. *11th International Conference on Geosynthetics (IIICG)*, Seoul, Güney Kore, 1-7, 2018.
- [81] M. A. Belenli, S. Kaya, L. Rebholz, and N. Wilson. A subgrid stabilization finite element method for incompressible magnetohydrodynamics. *Int. J. Comput. Math.*, 90(7), 1506–1523, 2013.
- [82] M. A. Medebber and N. Retiel. Numerical study of double diffusive convection within the annular region of two concentric vertical cylinders. *In Defect and Diffusion Forum*, 374:1-17, 2017.
- [83] M. Akbas, S. Kaya, and L. G. Rebholz. On the stability at all times of linearly extrapolated BDF2 timestepping for multiphysics incompressible flow problems. *Numer. Methods Partial Differ. Equ.*, 33, 999-1017, 2017.
- [84] M. A. Olshanskii and L. G. Rebholz. A note on helicity balance of the Galerkin method for the 3D Navier-Stokes equations. *Comput. Methods Appl. Mech. Eng.*, 199, 1032-1035, 2010.
- [85] M. B. Liu and G. R. Liu. Smoothed Particle Hydrodynamics (SPH): An Overview and Recent Developments. *Arch. Comput. Methods Eng.*, 17, 25-76, 2010.
- [86] M. E. Stern. The "salt-fountain" and thermohaline convection. *Tellus*, 12:172-175, 1960.
- [87] M. Gunzburger. *Finite element methods for viscous incompressible flows 1st edition: A guide to theory, practice, and algorithms*. Academic Press, New York, 1989.

- [88] M. Karimi-Fard, M. C. Charrier-Mojtabi, and K. Vafai. Non-Darcian effects on double-diffusive convection within a porous medium. *Numer. Heat Transfer, Part A: Appl.*, 31 (8):837–852, 1997.
- [89] M. Mamou, P. Vasseur, and E. Bilgen. A Galerkin finite-element study of the onset of double-diffusive convection in an inclined porous enclosure. *Int. J. Heat Mass Transf.*, 41, 1513–1529, 1998.
- [90] M. Müller, S. Schirm, and M. Teschner. Interactive blood simulation for virtual surgery based on smoothed particle hydrodynamics. *Technol. Health Care*, 12(1), 25–31, 2004.
- [91] M. Olshanskii and L. Rebholz. Longer time accuracy for incompressible Navier-Stokes simulations with the EMAC formulation. *Comput. Methods Appl. Mech. Engrg.*, 372, 1-12, 2020.
- [92] M. Shafer and S. Turek. Benchmark Computations of Laminar Flow Around Cylinder, E.H. Hirschel ed., *Flow Simulation with High-Performance Computers II. Notes Numer. Fluid Mech.*, Vieweg, 52, 547-566, 1996.
- [93] N. Jiang and W. Layton. An algorithm for fast calculation of flow ensembles. *Int. J. Uncertain. Quan.*, 4, 273-301, 2004.
- [94] N. Jiang, M. Mohebbujaman, L. G. Rebholz, and C. Trechea. An optimally accurate discrete regularization for second order time stepping methods for Navier-Stokes equations. *Comput. Methods Appl. Mech. Engrg.*, 310, 388-405, 2016.
- [95] O. Ladyzhenskaya. *The Mathematical Theory of Viscous Incompressible Flow*. Gordon and Breach, New York, 1969.
- [96] O. Lehmkuhl, U. Piomelli, and G. Houzeaux. On the extension of the integral length-scale approximation model to complex geometries. *Int. J. Heat Fluid Flow*, 78, 1–12, 2019.
- [97] O. Lehmkuhl, G. Houzeaux, H. Owen, G. Chrysokentis, and I. Rodriguezb. A low-dissipation nite element scheme for scale resolving simulations of turbulent ows. *J. Comput. Phys.*, 390, 51–65, 2019.

- [98] O. Lehmkuhl, F. Sacco, B. Paun, T. Iles, P. Iaizzo, G. Houzeaux, M. Vzaquex, C. Butakff, and J. Aguado-Sierra. Left ventricular trabeculations decrease the wall shearstress and increase the intraventricular pressure drop in CFD simulations. *Front. Physiol.*, 9, 1–15, 2018.
- [99] O. Lehmkuhl, F. Sacco, B. Paun, T. Iles, P. Iaizzo, G. Houzeaux, M. Vzaquex, C. Butakoff, and J. Aguado-Sierra. Evaluating the roles of detailed endocardial structures on right ventricular haemodynamics by means of CFD simulations. *Int. J. Numer. Methods Biomed. Eng.*, 34, 1–14, 2018.
- [100] P. Ciarlet. *The Finite Element Method for Elliptic Problems*. North-Holland, Amsterdam, 1978.
- [101] P. Fischer and T. Iliescu. Large eddy simulation of turbulent channel flows by the rational LES model. *Phys. Fluids*, 15, 3036–3047, 2003.
- [102] P. Gresho. On the theory of semi-implicit projection methods for viscous incompressible flow and its implementation via a finite element method that also introduces a nearly consistent mass matrix. part 2: Applications. *Int. J. Numer. Meth. Fluids*, 11, 621-659, 1990.
- [103] P. Gresho and R. Sani. *Incompressible flow and the finite element method vol. 1: Advection-diffusion and isothermal laminar flow*. Wiley., New York, 2000.
- [104] P. Kuberry, A. Larios, L. Rebholz, and N. Wilson. Numerical approximation of the Voigt regularization for incompressible Navier-Stokes and magnetohydrodynamic flows, *Computers and Mathematics with Applications*, 64, 2647–2662, 2012.
- [105] P. Sagaut. *Large Eddy Simulation for Incompressible Flows (2nd ed)*. Springer: Berlin, 2002.
- [106] P. Solin. *Partial Differential Equations and the Finite Element Method*. John Wiley and Sons, Inc., Hoboken, NJ, USA, 2005.
- [107] Q. Cao, D. Y. H. Pui, and W. Lipiński. A concept of a novel solar-assisted largescale cleaning system (SALSCS) for urban air remediation. *Aerosol Air Qual. Res.*, 15, 1–10, 2015.

- [108] Q. Shao, M. Fahs, A. Younes, and A. Makradi. A high accurate solution for Darcy-Brinkman double-diffusive convection in saturated porous media. *Numer. Heat Transf. B-Fund.*, 69, 26–47, 2016.
- [109] R. Adams. Sobolev spaces. *Academic Press, New York*, 1975.
- [110] R. Aubry, S. R. Idelsohn, and E. Oñate. Particle Finite Element Method in Fluid-Mechanics Including Thermal Convection-Diffusion. *Comput. Struct.*, 83, 1459-1475, 2005.
- [111] R. A. Khurram and A. Masud. A multiscale stabilized formulation of the incompressible Navier-Stokes equations for moving boundary flows and fluid-structure interaction. *Comput. Mech.*, 38, 403–416, 2006.
- [112] R. Liska and B. Wendroff. Comparison of several difference schemes on 1D and 2D test problems for the Euler equations. *SIAM J. Sci. Comput.*, 25, 995-1017, 2003.
- [113] R. March, A. Coutinho, and R. Elias. Stabilized finite element simulation of double-diffusive natural convection. *Mecanica Computacional*, 29, 7985-8000, 2010.
- [114] R. Martin, M. Soria, O. Lehmkuhl, A. Gorobets, and A. Duben. Noise radiated by an open cavity at low Mach number: Effect of the cavity oscillation mode. *Int. J. Aeroacoustics*, 2019.
- [115] P. M. Gresho and R. L. Sani. Incompressible flow and the finite element method. 2, Isothermal Laminar Flow, Wiley, 1998.
- [116] R. Salmon and L. D. Talley. Generalizations of Arakawa’s Jacobian. *J. Comput. Phys.*, 83, 247–259, 1989.
- [117] R. S. Rogallo and P. Moin. Numerical simulation of turbulent flows. *Annu. Rev. Fluid Mech.*, 16, 99–137, 1984.
- [118] R. Temam. Navier-Stokes equations and nonlinear functional analysis. *SIAM*, 1995.
- [119] R. Temam. Navier-Stokes equations. Elsevier, North-Holland, 1991.

- [120] R. V. Abramov and A. J. Majda. Discrete approximations with additional conserved quantities: deterministic and statistical behavior. *Methods Appl. Anal.*, 10(2), 151–190, 2003.
- [121] R. W. Schmitt. Double Diffusion in Oceanography. *Ann. Rev. of Fluid Mech.*, 26, 255-285, 1994.
- [122] S. C. Brenner and L. R. Scott. The Mathematical Theory of Finite Element Methods. *Texts in Applied Mathematics*, 15, Springer-Verlag, New York, 1994.
- [123] S. Charnyi, T. Heister, M. Olshanskii, and L. Rebholz. On conservation laws of Navier-Stokes Galerkin discretizations. *J. Comput. Phys.*, 337, 289-308, 2017.
- [124] S. Charnyi, T. Heister, M. Olshanskii, and L. Rebholz. Efficient discretizations for the emac formulation of the incompressible Navier-Stokes equations. *Appl. Numer. Math.*, 141, 220-233, 2019.
- [125] S. Chen, C. Foias, D. D. Holm, E. Olson, E. S. Titi, and S. Wynne. A connection between the Camassa-Holm equations and turbulent flows in channels and pipes. *Phys Fluids*, 11, 2343–2353, 1999.
- [126] S. Chen, J. Tölke, and M. Krafczyk. Numerical investigation of double-diffusive (natural) convection in vertical annuluses with opposing temperature and concentration gradients. *Int. J. Heat Fluid Flow*, 31, 217-226, 2010.
- [127] S. H. Xin, P. L. Quéré, and L. S. Tuckerman. Bifurcation analysis of double-diffusive convection with opposing horizontal thermal and solutal gradients. *Phys. Fluids*, 10, 850, 1998.
- [128] S. Kaya, M. Aggul, and A. E. Labovsky. Two approaches to creating a turbulence model with increased temporal accuracy. *Appl. Math. Comput.*, 358, 25-36, 2019.
- [129] S. S. Collis. Monitoring unresolved scales in multiscale turbulence modeling. *Phys. Fluids*, 13, 1800-1806, 2001.
- [130] S. S. Ravindran. Convergence of extrapolated BDF2 finite element schemes for unsteady penetrative convection model, *Numer. Funct. Anal. Optim.*, 33, 48-79, 2012.

- [131] S. S. Ravindran. An extrapolated second order backward difference time-stepping scheme for the Magnetohydrodynamics system. *Numer. Funct. Anal. Optim.*, 37, 990-1020, 2006.
- [132] S. S. Ravindran. A second-order backward difference time-stepping scheme for penalized Navier-Stokes equations modeling filtration through porous media. *Numer. Methods Partial Differ. Equ.*, 32, 681-705, 2016.
- [133] S. Zhang. A new family of stable mixed nite elements for the 3d Stokes equations. *Math. Comput.*, 74, 543–554, 2005.
- [134] T. Hughes, L. Mazzei, and K. Jansen. Large eddy simulation and the variational multiscale method. *Comput. Vis. Sci.*, 3, 47-59, 2000.
- [135] T. L. Bergman and R. Srinivasan. Numerical simulation of Soret-induced double diffusion in an initially uniform concentration binary liquid. *Int. J. Heat Mass Transf.*, 32, 679-687, 1989.
- [136] T. N. Palmer. Towards the probabilistic earth-system simulator: a vision for the future of climate and weather prediction. *Q. J. Royal Meteorol. Soc.*, 138(665), 841–861, 2012.
- [137] T. Rabczuk, R. Gracie, J. H. Song, and T. Belytschko. Immersed Particle Method for Fluid-Structure Interaction: Particle method for fluid-structure interaction. *Int. J. Numer. Meth. Eng.*, 81, 48-71, 2010.
- [138] V. DeCaria and M. Schneier. An embedded variable step IMEX scheme for the incompressible Navier-Stokes equations. *Comput. Methods Appl. Mech. Engrg.*, 376(9), 2021.
- [139] V. DeCaria, S. Gottlieb, Z. J. Grant, and W. Layton. A general linear method approach to the design and optimization of efficient, accurate, and easily implemented time-stepping methods in CFD. *J. Comput. Phys.*, 455, 2022.
- [140] V. Decaria, W. Layton, and H. Zhao. A time-accurate, adaptive discretization for fluid flow problems. *Int. J. Numer. Anal. Model.*, 17(2), 254-280, 2000.
- [141] V. Girault and P. A. Raviart. *Finite element approximation of the Navier-Stokes equations*, Lecture Notes in Mathematics 749, Springer-Verlag, Berlin, 1979.

- [142] V. Girault and P. A. Raviart. *Finite element methods for the Navier-Stokes equations theory and algorithms*, Springer-Verlag, 1986.
- [143] V. John. *Finite Element Methods for Incompressible Flow Problems. Springer Series in Computational Mathematics 51*, Springer-Verlag: Berlin, 2016.
- [144] V. John. Reference values for drag and lift of a two-dimensional time-dependent flow around the cylinder. *Int. Numer. Meth. Fl.*, 44, 777-788, 2004.
- [145] V. John. Large eddy simulation of turbulent incompressible flows. analytical and numerical results for a class of LES models. *LN in CSE*, 34, Springer-Verlag, Berlin, 2004.
- [146] V. John, A. Linke, C. Merdon, M. Neilan, and L. G. Rebholz. On the divergence constraint in mixed finite element methods for incompressible flows. *SIAM Rev.*, 59(3), 492-544, 2017.
- [147] V. John, G. Matthies and J. A. Rang, Comparison of time-discretization/linearization approaches for the incompressible Navier-Stokes equation. *Comput. Methods Appl. Mech. Engrg.*, 195, 5995-6010, 2006.
- [148] V. John and W. Layton. Analysis of numerical errors in large eddy simulation. *SIAM J. Numer. Anal.*, 40, 995-1020, 2002.
- [149] V. John, N. Ahmed, T. C. Rebollo, and S. Rubino. A review of variational multiscale methods for the simulation of turbulent incompressible flows. *Arch. Comput. Methods Engrg.*, 24, 115-164, 2017.
- [150] V. John and S. Kaya. Finite element error analysis of a variational multiscale method for the Navier-Stokes equations. *Adv. Comput. Math.*, 28, 43-61, 2008.
- [151] V. John and S. Kaya. A finite element variational multiscale method for the Navier-Stokes equations. *SIAM J. Sci. Comp.*, 26, 1485-1503, 2005.
- [152] V. John, S. Kaya, and W. Layton. A two-level variational multiscale method for convection-dominated convection-diffusion equations. *Comput. Methods Appl. Mech. Engrg.*, 195, 4594-4603, 2006.



- [153] W. Bangerth, D. Davydov, T. Heister, L. Heltai, G. Kanschat, M. Kronbichler, M. Maier, B. Turcksin, and D. Wells. The deal.II library, version 8.4. *J. Numer. Math.*, 2016.
- [154] W. Hundsdorfer. Partially implicit BDF2 blends for convection dominated flows. *SIAM J. Numer. Anal.*, 38, 1763-1783, 2001.
- [155] W. Layton. Introduction to the Numerical Analysis of Incompressible Viscous Flows. *SIAM*, 2008.
- [156] W. Layton. A connection between subgrid scale eddy viscosity and mixed methods. *Appl. Math. Comput.*, 133, 147-157, 2002.
- [157] W. Layton, H. Tran, and C. Trechea. Numerical analysis of two partitioned methods for uncoupling evolutionary MHD flows. *Numer. Methods Partial Differ. Equ.*, 30, 1083-1102, 2014.
- [158] Y. Bazilevs, V. M. Calo, T. J. R. Hughes, A. Reali, and G. Scovazzi. Variational multiscale residual-based turbulence modeling for large eddy simulation of incompressible flows. *Comput. Methods Appl. Mech. Eng.*, 197, 173–201, 2007.
- [159] Y. Bazilevs, V. M. Calo, T. J. R. Hughes, and Y. Zhang. Isogeometric fluid-structure interaction: theory, algorithms, and computations. *Comput. Mech.*, 43, 3–37, 2008.
- [160] Y. Cao, E. Lunasin, and E. Titi. Global well-posedness of the three-dimensional viscous and inviscid simplified Bardina turbulence models. *Commun. Math. Sci.*, 4, 823–848, 2006.
- [161] Y. H. Zeng and P. Z. Huang. A grad-div stabilized projection finite element method for a double-diffusive natural convection model. *Numer. Heat Transf. B-Fund.*, 78, 110–123, 2020.
- [162] Y. He. Two-level method based on finite element and Crank-Nicolson extrapolation for the time-dependent Navier-Stokes equations. *SIAM J. Numer. Anal.*, 41, 1263–1285, 2003.

- [163] Y. Liu, L. Zhang, X. Wang, and W. K. Liu. Coupling of Navier–Stokes equations with protein molecular dynamics and its application to hemodynamics. *Int. J. Numer. Methods Fluids*, 46(12), 1237–1252, 2004.
- [164] Y. N. He and W. W. Sun. Stability and convergence of the Crank-Nicolson/Adams-Bashforth scheme for the Time-Dependent Navier-Stokes equations. *SIAM J. Numer. Anal.*, 45, 837-869, 2007.
- [165] Y. Yang and Y. Jiang. An explicitly uncoupled VMS stabilization finite element method for the time-dependent Darcy-Brinkman equations in double-diffusive convection. *Numer. Algor.*, 78, 569-597, 2018.

## CURRICULUM VITAE

### PERSONAL INFORMATION

**Surname, Name:** Demir, Medine

**Nationality:** Turkish (TC)

**E-mail:** mdndmr3406@gmail.com

### EDUCATION

Degree	Institution	Year of Graduation
B.S.	Middle East Technical University	2014
High School	Avcılar Lisesi	2009

### FOREIGN LANGUAGES

English (Advanced), Spanish (Elementary)

### COMPUTER SKILLS

Freefem++ (Advanced), Matlab (Elementary), LaTeX, Microsoft Office Packages

### PROFESSIONAL EXPERIENCE

Year	Place	Enrollment
2014-2022	Middle East Technical University	Research Assistant

### PUBLICATIONS

1. A. Çıbık, M. Demir, and S. Kaya Merdan, "A family of second order time stepping methods for the Darcy-Brinkman equations", *Journal of Mathematical Analysis and Applications*, 472, 148-175, 2019.
2. M. Demir, and S. Kaya Merdan, "An analysis of a linearly extrapolated BDF2

subgrid artificial viscosity method for incompressible flows", *Applied Numerical Mathematics*, 156, 140-157, 2020.

3. A. Çıbık, M. Demir, and S. Kaya Merdan, "On the Analysis of the Second Order Time Filtered Backward Euler Method for the EMAC formulation of Navier-Stokes Equations", *Journal of Mathematical Analysis and Applications* (submitted).

## PROCEEDINGS

1. Medine Demir, Aytekin Çıbık, and Songul Kaya Merdan, "Numerical analysis of a Family of Second Order Time Stepping Methods for Boussinesq Equations", Proceedings of the World Congress on Engineering, Vol. 1, pp. 56-59, July 4-6, 2018, London, UK.
2. Medine Demir, and Songul Kaya Merdan, "A Numerical Study of a Modular Sparse Grad-Div Stabilization Method for Boussinesq Equations", Proceedings of 8th International Conference on Mathematical Modeling in Physical Science, J. Phys.: Conf. Ser., Vol. 1391, August 26-29, 2019, Bratislava, Slovakia.
3. Medine Demir, and Songul Kaya Merdan, "Numerical Investigation of the Boussinesq equations through a Subgrid Artificial Viscosity Method", The European Conference on Numerical Mathematics and Advanced Applications (ENUMATH 2019), pp. 293-301, September 30- October 4, 2019, Egmond aan Zee, Netherlands.

## SCIENTIFIC MEETINGS

### Presentations in International Scientific Meetings

1. Medine Demir, Aytekin Çıbık, and Songul Kaya Merdan, "Numerical analysis of a Family of Second Order Time Stepping Methods for Boussinesq Equations", WCE 2018, July 4-6, 2018, London, UK.

2. Medine Demir, and Songul Kaya Merdan, "A Numerical Study of a Modular Sparse Grad-Div Stabilization Method for Boussinesq Equations", IC-MSQUARE 2019, August 26-29, 2019, Bratislava, Slovakia.
3. Medine Demir, and Songul Kaya Merdan, "Numerical Investigation of the Boussinesq equations through a Subgrid Artificial Viscosity Method", ENUMATH 2019, September 30-4, 2019, Egmond aan Zee, Netherlands.

### **Presentations in National Scientific Meetings**

1. Medine Demir, Aytekin ıbık, and Songul Kaya Merdan, "Dođal Konveksiyon Problemleri iin İkinici Mertebeden Zaman Adımlaması Yöntemleri Ailesinin Sayısal Analizi", 13. Ankara Matematik Günleri, 27-28 Nisan, 2018, TOBB ETÜ, Ankara, Türkiye.
2. Medine Demir, Aytekin ıbık, and Songul Kaya Merdan, "A Numerical Study of Second Order Time Stepping Methods for the Boussinesq Equations.", BEYOND: Workshop on Computational Science and Engineering, 20-21 Ekim, 2018, METU, Ankara, Türkiye.
3. Medine Demir, Aytekin ıbık, and Songul Kaya Merdan, "Numerical Analysis of Second Order Time Stepping Methods for the Natural Convection Problems", ICAME 2018, 27-29 June, 2018, Balıkesir, Turkey.